University of Strathclyde

Department of Electrical Engineering

HYSTERESIS EFFECTS IN TRANSFORMERS

Being a study of the influence of the magnetic properties of the core on the transient and steady-state performance of transformers, including ferroresonance.

by

John W. Teape, B.Sc.

Thesis presented for the degree of Doctor of Philosophy in Electrical Engineering of the University of Strathclyde.

March 1976.

CONTENTS

SUMMARY

The mathematical analysis of static electromagnetic devices such as transformers, voltage stabilisers, etc., is complicated by the nonlinear, multi-valued relationship between flux density and field strength in the ferromagnetic core. Initially, various methods of analysis are discussed, with emphasis on the importance of incorporating a means of adequately representing the influence of the magnetisation characteristic, and the physical structure of the core.

The single-valued exponential series representation of the flux density / field strength relationship which was developed in an earlier investigation into transient currents in transformers due to switching of the supply, is modified and extended to cater for the non-unique nature of the B/H relationship. This new representation is then incorporated into the mathematical models of single-phase and three-limb, three-phase transformers, which are utilised in the study of residual core conditions in these devices.

The ways in which residual conditions are established, and the influence of such factors as load and primary circuit configuration are examined, both experimentally and theoretically, and the results used in devising a simple graphical technique for estimating the magnitude and polarity of remanent flux and m.m.f. A study is also made of the effect of residual conditions on the transient currents which occur on reapplication of the supply.

An example of the extension of the range of application of the transformer model is demonstrated in a brief study of ferroresonance in single- and three-phase systems. The

processes involved in the initiation of a stable resonant condition are considered, and a comparison of computed and recorded steady-state current, voltage and flux density waveforms is made.

Finally, general conclusions are drawn, and some suggestions are made as to how the transformer model might be improved, together with examples of other areas of interest in which the analytical techniques developed for the transformer may be applied.

List of Principal Symbols

A - area

B - flux density

C - capacitance

E - rms e.m.f

e - instantaneous e.m.f

H - magnetic field strength

I - rms current

i - instantaneous current

K - coefficient, constant

L - length

l - leakage inductance

M - inductance

N - turns

p - d/dt

q - instantaneous charge

R - resistance

t - time

V - rms voltage

v - instantaneous voltage

X - reactance

Z - impedance

α - initial switching angle

β - first delay angle

δ - second delay angle

θ - phase angle

ϕ - flux

ψ - flux linkages

μ - permeability

Subscripts

A, B, C	-	primary winding quantities
a, b, c	-	secondary circuit quantities
i	-	1, 2, 3, ... n
j	-	n+1, n+2, n+3, ... m
L	-	Load
m	-	magnetising, integer
n	-	integer
p	-	phase leakage
X, Y, Z	-	supply quantities (delta primary)
d	-	differential

-CHAPTER 1-

INTRODUCTION

The use of iron and other highly permeable materials is almost universal as the basic constituent of the core of electromagnetic machines. The magnetic properties of these materials can be extensively modified to suit almost any application, by combining them with other elements in alloys. There are, however, two aspects of magnetic behaviour which characterise these materials, in any form, and which cannot be completely eliminated without destroying the ferromagnetic properties. Magnetic nonlinearity and hysteresis are well-documented phenomena which present considerable problems in the analysis of electromagnetic devices incorporating ferromagnetic materials.

One means of avoiding these problems is simply to neglect the effects of saturation and hysteresis, and results produced from this type of analysis are reasonably accurate in many cases. There are instances, however, where linear theory fails to yield reliable solutions, and it becomes necessary to make allowance for the magnetic properties of the core in the analysis. For example, the transient performance of transformers and other static electromagnetic devices is determined almost entirely by the magnetisation characteristic of the core material. Certain aspects of steady-state behaviour are also greatly influenced by the effects of saturation and hysteresis, such as in the case of ferroresonance.

An investigation into the the effects of magnetic nonlinearity in static electromagnetic devices was initiated in the Department in 1968, aimed at establishing a method of accurately computing the transient currents due to switching of

the supply. This was a direct result of the significant discrepancies between theory and practice, found when linear methods were used in the transient analysis of induction motors rotating at sub- and super-synchronous speeds[15]. The initial investigation[1] was concentrated on static devices in general, and single- and three-phase transformers in particular, and was intended as a preliminary study of magnetic nonlinearity, the results of which would ultimately be applied to rotating machines such as a.c. commutator and slip-ring motors. Instead, it has formed the basis of an extensive investigation into the more fundamental aspects of the electromagnetic behaviour of transformers.

1.1 Project History.

At the time of the start of this work in 1968, the techniques available for the analysis of static nonlinear electromagnetic devices had not been sufficiently developed to enable the various quantities (current, flux, etc.) to be calculated to within a reasonably consistent degree of accuracy, both in terms of the amplitude and shape of the waveforms. This latter requirement is a consequence of the methods used in power system protection where it is necessary to distinguish between transient inrush currents, and those due to faults in the transformer.

The reasons for these weaknesses in the available techniques of analysis were twofold;

(i) The difficulty in taking full account of the actual magnetic circuit arrangement in polyphase systems, and hence the effect this may have on the performance.

(ii) The errors introduced by neglecting the nonlinear properties of the magnetisation characteristic of the core, or

by using an inaccurate method of representation.

A solution to the first of these problems was found by deriving a series of nonlinear differential and algebraic equations to describe the electric and magnetic circuit relationships of a general, static, electromagnetic system. Similar work was later published by Nakra and Barton[2] which served to reinforce the validity of this approach.

MacFadyen[1] also examined in detail the various ways in which the magnetisation characteristic could be represented mathematically for use in solving the system equations. The existing methods using linear approximations, Fourier series, power series, etc., failed to provide a convenient means of accurately representing the B/H curve over the complete range of field strength, i.e. $0 \leq H < \infty$. The method of analysis also requires that the differential permeability (dB/dH) or the slope of the B/H characteristic be accurately represented. A simple, yet highly accurate method of expressing the flux density as a function of field strength using an exponential series was devised which, although neglecting the non-unique nature of the B/H relationship, nevertheless provided the means whereby transient currents in single-phase and three-phase transformers could be accurately computed.

The results of this investigation showed the effects which inter-phase magnetic coupling can have on the transient performance of polyphase transformers, and the influence which this effect has, together with the magnetisation characteristic, on the shape of the transient waveforms.

1.2 Aims of the Present Investigation.

Over the past five to eight years there have been significant advances in the field of electromagnetic analysis, for example references 3, 4 and 5, as a result of the ever-increasing capability of digital computers to perform large amounts of arithmetic. Finite difference and finite element techniques can now be applied to a wide range of problems to produce solutions of great accuracy. In the light of these recent developments it is necessary to reappraise the type of transformer model proposed by MacFadyen, and Nakra and Barton, and to consider whether there are, as yet, any realistic alternative methods of analysis.

The single-valued function representation of the B/H relationship has been shown to be adequate when considering cases of zero initial flux in the transformer core, and simultaneous switching of the supply in a polyphase system. However, as reference 2 indicates, the level of residual flux, when present, is a very important factor in determining peak transient current due to switching the supply. It is therefore considered necessary to incorporate a representation of the complete magnetisation characteristic in the transformer model, and to examine in detail the establishment of remanent core conditions, and the effect which these have on subsequent transformer behaviour.

The use of the transformer model need not be limited to the study of transients due to switching of the supply. As an example of the possible range of application, practical cases of ferroresonance in single-phase and three-phase systems are analysed, and results compared with laboratory test measurements.

-CHAPTER 2-

TRANSFORMER MODEL

In any investigation which involves the analysis of systems incorporating electromagnetic devices such as transformers, the first requirement is to select or devise a suitable method of representing mathematically the device and the associated external circuit (supply, load, etc.). There are several factors which must be considered when choosing the method of representation, or model, to be used. These factors are,

(a) The type of application, e.g. transient, steady-state, linear, nonlinear, etc.

(b) The accuracy required.

(c) The complexity of the model.

(d) The flexibility of the model for application to other situations.

(e) The fidelity of the model compared with the real system.

The facilities available for computational work will normally fix the limits on factors (b) and (c), although it may not be necessary to work at those limits. Factors (d) and (e) are often limited only by the ingenuity of the investigator.

For the purposes of the present investigation into the performance of static, nonlinear electromagnetic devices, it is essential that the model used is valid for both steady-state and transient applications, and that magnetic nonlinearity and

hysteresis can, if necessary, be incorporated in the representation.

Many of the phenomena associated with transformer behaviour such as ferroresonance, transient currents, residual conditions, etc., are very dependent on system conditions, and for this reason it is desirable that maximum accuracy in computation is achieved, commensurate with the facilities available. Thus the number of approximations made should be kept to a minimum, while not unduly increasing the complexity of the representation and consequently requiring large amounts of computer run time for relatively little output. Since it is envisaged that the techniques used here will be extended to cover other aspects of transformer behaviour, beyond the scope of the present investigation, the model chosen should ideally correspond as closely as possible to the actual device and incorporate maximum flexibility for further application.

2.1 Approaches to Transformer Modelling.

There are basically three ways in which the problem of mathematical representation of electromagnetic devices may be tackled,

1. Equivalent circuit methods.
2. Magnetic field analysis.
3. Combined magnetic and electric circuit model.

and the choice of which approach to take in any particular investigation can be made by considering the factors discussed above.

The equivalent circuit method of transformer analysis is a well established technique for use in steady-state

applications, and as such is an invaluable tool. However, a model of this type lacks the flexibility, fidelity and accuracy required in the present investigation. The equivalent circuit of a single- phase, two winding transformer, shown in Fig. 2.1.1 can be adapted to cater for transient as well as steady-state conditions by allowing M, the mutual inductance between the two coils, to vary as a function of the coil currents. This version of the equivalent circuit model, while no longer suitable for producing algebraic solutions to the steady-state performance, is nevertheless adequate in most applications where a complete solution is required, as long as the relationship between M and the coil currents can be accurately represented.

Extending this equivalent circuit of the single-phase transformer to the poly-phase case, where each phase of the transformer is represented by a circuit identical to that of Fig. 2.1.1, does not give a sufficiently accurate representation of the real system since magnetic coupling between individual phases is not catered for except for the conditions under which the transformer parameters are measured. While such a representation can often give good results in terms of the peak transient current and steady-state performance, it is unlikely that close correlation between computed and recorded waveshape will be achieved, which could be a critical factor in protection systems applications.

Another factor which will be very dependent on magnetic linking between phases is the condition of the core following supply interruption, i.e. residual conditions. A transformer which has been energised and then disconnected from the supply will almost invariably have residual flux in the core. Since disconnection does not normally occur simultaneously in

all phases, inter-phase magnetic coupling can affect the residual flux levels in the de-energised phases during the disconnection procedure. It is therefore improbable that a method of analysis based on an equivalent circuit model of the transformer would produce sufficiently accurate results for the purposes of the present study.

The second type of approach to transformer analysis, which relies almost completely on the direct solution of the magnetic field equations, will almost certainly produce the most accurate results and be most flexible in its application. This is due to the close correlation between this method of representation and the actual device. A full solution would in this case require that the problem be treated as 3-dimensional (e.g. reference 3), and account taken of the distribution of the flux in the magnetic core and in the air, or other insulating material, around the transformer. The steel tank which invariably encases large power transformers can greatly increase the complexity of the problem.

As with all complex problems, there are various approximations which may be made to reduce the amount of work required to produce a solution. For example, by splitting the analysis into two parts, the air flux distribution[4,5] and the core flux[6], a degree of simplification can be achieved. Little error is introduced, and the problem greatly simplified if a 2-dimensional solution is sought[4-7], and a degree of symmetry assumed.

Irrespective of the number of simplifying assumptions made, the problem requires the use of numerical methods to solve the nonlinear field equations; usually finite difference or finite element methods are employed. Solutions of this type

tend to involve large amounts of computer time, and this factor alone virtually excludes the use of this method of representation for all but the most specialised of applications requiring the solution to a strictly limited number of situations, such as the examination of the leakage fields in a power transformer or saturation effects at corners in the core. For more general problems, such as transient analysis, which require a large number of calculations to be carried out, the complete utilisation of field analysis techniques becomes, for the present, an impractical proposition.

As computer systems develop, and faster, more powerful machines become available, the use of field analysis to solve time-varying problems involving nonlinear electromagnetic devices should become feasible. As a first step towards this aim, methods of representing the transformer mathematically have been developed which incorporate aspects of both circuit and field theory, without becoming over-complex and therefore limited in their application. This type of approach, while making certain simplifying assumptions regarding the fields and fluxes in the system, takes account of the relationship between the electric circuit and magnetic circuit quantities, and has been shown to give reasonably accurate results[1,2]. The amount of computing time required is considerably less than that to produce the solution to a given problem using field analysis alone,[4] and is only slightly more than the time taken using equivalent circuit techniques.

This latter method of transformer modelling therefore appears to offer the best compromise between the two other methods described above, and is the method which has been adopted for use in the present investigation. A short description of the technique and examples of the application to

transformers is given below.

2.2 General Electromagnetic System.

MacFadyen[1] has proposed a method of representing mathematically a general static electromagnetic system based on a physical model of the magnetic circuit. A similar approach has been taken by Nakra and Barton[2] in that the equations describing the system are divided into two categories, viz., the electric circuit equations and the magnetic circuit equations.

2.2.1 Electric circuit equations.

The voltage equations for the coils on any limb of the general polyphase system shown in Fig. 2.2.1 can be written as,

$$v_n = i_n.R_n + l_n.pi_n + N_n.p\emptyset_j$$

where, $\emptyset_j$ is the component of flux linking all coils on the j th. limb. Thus for the case of two windings per phase, referring all quantities to N turns,

$$v_A = i_A.R_A + l_A.pi_A + N.p\emptyset_j \qquad \ldots\ldots 2.2.1$$

$$v_a = i_a.R_a + l_a.pi_a + N.p\emptyset_j$$

$\emptyset_j$ will be mainly confined to the magnetic core. The expression for the corresponding e.m.f., $N.p\emptyset_j$ can therefore be expanded in terms of the magnetisation characteristic of the core. Assuming uniform flux distribution over the cross-sectional area of the limb, then,

$$\dot{\emptyset}_j = B_j.A_j$$

thus,

$$N.p\emptyset_j = N.A_j.pB_j$$
$$= N.A_j.(dB_j/dH_j).pH_j \qquad \ldots\ldots 2.2.2$$

where dB_j/dH_j is the differential permeability or slope of the magnetisation characteristic.

A magnetisation current for the limb, i_j, is defined by,

$$i_j = H_j.L_j/N$$

where L_j is the mean flux path length in the limb. Substituting for H_j in eqn. 2.2.2,

$$N.p\emptyset_j = M_j.pi_j$$

where, $M_j = N^2.A_j./\mu_d/L_j$

which has the dimensions of inductance. Eqn. 2.2.1 can now be written as,

$$v_A = i_A.R_A + l_A.pi_A + M_j.pi_j$$
$$v_a = i_a.R_a + l_a.pi_a + M_j.pi_j \qquad \ldots\ldots 2.2.3$$

A series of equations of this type can be derived for each limb in the system. In order to solve the equations it is necessary to establish further relationships since for each limb in the system there is one unknown quantity more than the number of equations.

2.2.2 Magnetic circuit equations.

The additional equations required are obtained by consideration of the magnetic circuit relationships. Magnetic flux will be present in the core and in the air between any two points on the core provided an m.m.f. exists between the points. In the general system with n-coils per phase, any component of flux may link with one or more coils on the same limb. Flux may also link with all coils on the same limb but fail to link with coils on other limbs. This component of flux, which has a path mainly in air, is defined as the phase-leakage flux, and the corresponding phase-leakage inductance is taken as being constant. For convenience, the phase-leakage flux associated with each limb is assumed to be concentrated in a single phase-leakage path, as shown in Fig. 2.2.2, which also shows the other assumed flux paths in the system.

Applying Ampere's Magnetic Circuital Law,

$$\sum i.N = \oint H.dl$$

round any closed path in the system will result in an equation such as,

$$N.i_A + N.i_a = H_1.L_1 + H_{p1}.L_{p1} \quad \ldots\ldots 2.2.4$$

which is obtained by taking a path comprising limb 1 and the phase-leakage path for that limb, (Fig. 2.2.2). Substituting for H_1 and H_{p1} in eqn. 2.2.4, and dividing throughout by N,

$$i_A + i_a = i_1 + i_{p1} \quad \ldots\ldots 2.2.5$$

where i_1 and i_{p1} are the magnetising currents associated with the main flux in limb 1 and the phase-leakage flux for that limb respectively.

Further equations may be derived by summing the fluxes at a junction, since,

$$\oint B.dS = 0$$

then for the junction of limb 1 and the upper yoke,

$$\phi_1 + \phi_{21} + \phi_{31} - \phi_{p1} = 0$$

Substituting for ϕ in terms of B, and differentiating with respect to time gives,

$$A_1 \cdot \mu_{d1} \cdot pH_1 + A_{21} \mu_{d21} \cdot pH_{21} + A_{31} \cdot \mu_{d31} \cdot pH_{31} - A_{p1} \cdot \mu_o \cdot pH_{p1} = 0$$

$$\text{i.e.} \quad M_1 \cdot pi_1 + M_{21} \cdot pi_{21} + M_{31} \cdot pi_{31} - M_{p1} \cdot pi_{p1} = 0 \quad ..2.2.6$$

The complete system can therefore be represented by a combination of simultaneous differential and algebraic equations of the type given in eqns. 2.2.3, 2.2.5 and 2.2.6. Two specific examples are given below which are relevent to the present investigation, viz., the single-phase, two winding transformer, and the three-phase, three-limb, two winding per phase transformer.

2.3 Single-Phase Transformer.

The voltage equations for the two winding, single-phase transformer, shown in Fig. 2.3.1 are,

$$v_A = i_A.R_A + l_A.pi_A + M.pi_m \qquad \ldots\ldots 2.3.1$$

$$v_a = i_a.R_a + l_a.pi_a + M.pi_m$$

where all quantities are referred to N_1 (primary) turns. The magnetic circuit equation is,

$$i_A + i_a = i_m \qquad \ldots\ldots 2.3.2$$

and substituting for i_m in eqn. 2.3.1 gives,

$$v_A = i_A.R_A + l_A.pi_A + M.p(i_A + i_a) \qquad \ldots\ldots 2.3.3$$

$$v_a = i_a.R_a + l_a.pi_a + M.p(i_A + i_a)$$

which are the equations for the simple equivalent circuit shown in Fig. 2.1.1. Allowance can be made for eddy-current loss by the conventional method of loading a secondary winding with a resistance which produces losses equal to the total eddy-current effect.

2.4 Three-Phase Transformer.

Fig. 2.4.1 shows a three-limb, three-phase transformer with two windings per phase. The voltage equations for this system comprise three primary-circuit equations and three for the secondary circuit, giving a total of six. For the

primary circuit,

$$v_A = i_A.R_A + l_A.pi_A + M_1.pi_1$$

$$v_B = i_B.R_B + l_B.pi_B + M_2.pi_2 \qquad \ldots\ldots 2.4.1a$$

$$v_C = i_C.R_C + l_C.pi_C + M_3.pi_3$$

and for the secondary circuit,

$$v_a = i_a.R_a + l_a.pi_a + M_1.pi_1$$

$$v_b = i_b.R_b + l_b.pi_b + M_2.pi_2 \qquad \ldots\ldots 2.4.1b$$

$$v_c = i_c.R_c + l_c.pi_c + M_3.pi_3$$

There are, in this case, nine unknown currents, i.e. three more than the number of equations. By summation of the fluxes at the junctions of each of the limbs with the upper yoke, a further three equations for the system can be derived,

$$0 = \phi_1 - \phi_4 - \phi_7$$

$$0 = \phi_2 - \phi_5 + \phi_7 + \phi_8$$

$$0 = \phi_3 - \phi_6 - \phi_8$$

Substituting and differentiating as in eqn. 2.2.6, the following three equations are obtained,

$$0 = M_1.pi_1 - M_4.pi_4 - M_7.pi_7$$

$$0 = M_2.pi_2 - M_5.pi_5 + M_7.pi_7 + M_8.pi_8 \ldots 2.4.2$$

$$0 = M_3.pi_3 - M_6.pi_6 - M_8.pi_8 \qquad \ldots\ldots 2.4.2$$

These equations, however, introduce a further five unknowns into the system, requiring another five equations in order to make the solution possible. The additional equations can be obtained as in section 2.2.2 by applying Ampere's Law around a series of closed paths, such as that comprising limb 1, the upper yoke, limb 2, and the lower yoke, which gives,

$$i_A + i_a - i_B - i_b = i_1 + i_7 - i_2 + i_7 \qquad \ldots\ldots 2.4.3$$

Since, by symmetry, i_7 (upper yoke) = i_7 (lower yoke), the two yoke paths may be considered as a single unit, and eqn. 2.4.3 re-written as,

$$i_7 = i_A + i_a - i_B - i_b - i_1 + i_2$$

Similarly,

$$i_8 = i_C + i_c - i_B - i_b - i_3 + i_2$$

$$i_4 = i_A + i_a - i_1 \qquad \ldots\ldots 2.4.4$$

$$i_5 = i_B + i_b - i_2$$

$$i_6 = i_C + i_c - i_3$$

These five algebraic equations complete the system of fourteen simultaneous equations required to represent the three-limb transformer of Fig. 2.4.1. The equations may be reduced by substituting for i_4 to i_8 from eqn. 2.4.4 into the nine differential equations.

Further modifications may be necessary according to the winding configuration and type of load, if any, and also to take account of switching conditions. This procedure is described in chapter 4, together with a description of the method used to solve the equations. The transformer model derived above is also utilised in ferroresonance applications in chapter 5, which also contains details of the actual form of the equations for this case.

2.5 Representation of the Magnetisation Characteristic.

An integral part of the solution of the transformer equations is the value of the differential permeability, u_d, for the transformer core sections. If the differential permeability is constant, i.e. there is a straight-line relationship between the flux density and the field strength, then the equations can be solved directly in terms of the rates of change of the currents, and the currents found by a process of numerical integration.

Magnetic materials do not exhibit this type of B/H relationship, although for the sake of simplicity the mutual inductance is often assumed to be constant. A typical magnetisation characteristic for a magnetic material is shown in Fig. 2.5.1, which is obviously far from linear. This is the curve obtained when the magnetic field is slowly increased from zero, the material having been initially demagnetised (i.e. there is no initial value of flux density).

There are a number of ways in which this characteristic may be represented mathematically, apart from assuming linearity. The effects of saturation can be crudely modelled

by the use of a second linear region as illustrated in Fig. 2.5.1. A more sophisticated method of representation, although not necessarily more accurate, is to use some form of mathematical function to represent the curve. Trutt, Erdélyi and Hopkins[8] examine and assign a 'figure of merit' to a number of possible functions, including hyperbolic, trigonometric and exponential functions, as well as power series. They conclude that, due to the difficulty encountered in satisfactorily representing the curve over its entire range using such functions, the curve can be best represented by a large number of small regions over which the characteristic can be taken as linear (see Fig. 2.5.2).

MacFadyen[1] has compared a number of well-known methods, including Fourier series and rational-fraction approximation[9], but finds that no method gives an accurate representation of the B/H curve over the range $0<H<\infty$, in terms of the differential permeability/field strength relationship as well as in B and H. Many methods, while apparently giving a reasonable representation of the B/H relationship, gave values of differential permeability which were totally erroneous, even to the extent of giving negative values. MacFadyen then presents a method of representing the magnetisation curve over the entire range of H by using an exponential series of the form shown below,

$$B = u_o.H + \sum_{i=1}^{n} K_{2i-1}.(1 - \exp(-K_{2i}.H)) \quad \ldots 2.5.1$$

which has the general shape shown in Fig. 2.5.3. The coefficients of the n-terms are found by graphical means or by iteration. This method gives a very accurate representation

of the u_d/H and B/H relationships over the range of H from near the origin to infinity. The values of u_d and B for $H<0$ are obtained by using the absolute value of H in eqn. 2.5.1. Allowance for the region of reverse curvature near the origin can be made by the addition of a term to represent the curve of the difference between the actual characteristic and the curve from eqn. 2.5.1. This difference curve can be represented by an equation such as[1],

$$\Delta B = K_{2n+1} \cdot \exp(-K_{2n+2} \cdot H^{K_{2n+3}}) \quad \ldots\ldots 2.5.2$$

Alternatively, the ratio of B from eqn. 2.5.1 to the actual value of B for a given field strength may be plotted over the region near the origin, to give the curve shown in Fig. 2.5.4. This curve may be represented in turn by an equation,

$$B' = 1 + \sum_{j+1}^{m} C_{2j-1} \cdot \exp(-C_{2j} \cdot H) \quad \ldots\ldots 2.5.3$$

the coefficients of which can be found using iteration techniques.

2.6 Representation of the Complete Magnetisation Characteristic.

No matter how accurately the magnetisation curve of Fig. 2.5.1 can be represented by mathematical functions of the type described above, the complex, multi-valued nature of the B/H relationship has not been taken into consideration. The phenomenon of magnetic hysteresis was first recognised during the nineteenth century, and attempts to represent the

complete magnetisation characteristic date back to 1887 when Lord Rayleigh[10] proposed a method of representing small, steady-state B/H loops.

Since then there have been several methods postulated by various authors of representing the complex B/H relationship mathematically, particularly since the advent of digital computers. For example, Potter and Schmulian[11] suggest the following equation as being suitable for representing the magnetisation characteristic of magnetic tape,

$$B(H, \alpha) = B_s . \mathrm{sgn}(\alpha) - (1 + \tanh(\frac{H_c - \mathrm{sgn}(\alpha).H}{H_c} \tanh^{-1} S))$$

where, α is a variable which is dependent on the magnetic history (see Fig. 2.6.1).

$\mathrm{sgn}(\alpha) = 1$ for $\alpha \geq 0$, and -1 for $\alpha < 0$.

H_c = major loop coercive field strength.

B_s = saturated flux density.

$S = B_r/B_s$ (squareness).

It is very unlikely, however, that the four loop parameters chosen, H_c, B_s, B_r and H_m will be sufficient to achieve a reasonable degree of accuracy in the representation. Manly[12] suggests the use of an additional parameter, w, which is 'the half-height width of the differentiated loop', i.e. the width in terms of H, of the u_d/H curve for the major hysteresis loop at $u_d = u_{dmax}/2$, as shown in Fig. 2.6.2. Results obtained for various function representations - hyperbolic tangent, arctangent, normal curve, etc., are presented, but the author concludes that 'the models fall short

in representing most materials of interest.'

2.6.1 General method of representation.

The non-unique B/H relationship for magnetic materials may be considered as an infinite number of single-valued trajectories, or curves, which are bounded in the B/H plane by the limit cycle or outer hyteresis loop as shown in Fig. 2.6.3. It is only necessary to represent the curves for H increasing positively, since in general, decreasing curves may be obtained by rotating the corresponding increasing characteristic by 180^{o} about the origin. Trajectories (e) and (f) in Fig. 2.6.3 are examples of increasing characteristics, all of which originate on the boundary curve (b) and pass through the positive saturation point, (H_s, B_s). It is assumed that the increasing trajectories, and consequently the decreasing curves, do not intersect.

In order to be able to represent all increasing curves, expressions must initially be obtained for at least two curves in the plane, preferably curves (a) and (d). Any other curve can then be generated by assuming a constant ratio, which can be evaluated knowing one point on the required trajectory defined by initial conditions or turning points in the B/H plane. Thus curve (c) may be expressed as,

$$B_c = (B_d - B_a)/2$$

Greater accuracy may be achieved by obtaining expressions for intermediate curves such as curve (c). Thus if trajectories (a), (c) and (d) are explicitly defined, the the expressions for characteristics (e) and (f) become,

$$B_e = B_c + (B_d - B_c).\frac{Y}{X+Y} \qquad \ldots\ldots 2.6.1$$

$$B_f = B_a + (B_c - B_a).\frac{Y'}{X'+Y'} \qquad \ldots\ldots 2.6.2$$

The expression for B_e will apply to curves which originate on the limit cycle at values of $B > B_R$ such as curve (g) in Fig. 2.6.3, since in this case,

$$\frac{B_g - B_c}{B_d - B_c} > 1$$

i.e., the curve will lie above curve (d) at all points. It is therefore possible to represent all curves in the B/H plane using eqn. 2.6.1 to obtain characteristics lying above (c), and eqn. 2.6.2 for those below (c).

In order to generate trajectories which originate at large values of H ($|H| > H_c$), e.g. curves lying close to (a) in Fig. 2.6.3, then it is necessary to extrapolate curves (c) and (d) beyond the limit cycle curve (b). The expressions for these curves and the boundary curve (a) must therefore be capable of representing magnetisation characteristics over the range $-\infty < H < +\infty$.

2.6.2 Representation of single magnetisation curve.

It has already been stated that there are several ways in which a B/H curve may be represented mathematically and almost any one of these methods could be modified for use in

the representation of the complete characteristic. Only two of the methods described above appear to give a reasonable representation of the curve over an extensive range of H, viz, the exponential series and piecewise-linear methods. The piecewise-linear method of representation, while easily modified to give the correct shape required for the complete characteristic, suffers from the drawbacks of requiring a large amount of computer storage, and being less accurate in representing the u_d/H relationship than the exponential series.

The exponential series is less easily modified to give the required overall shape, but is potentially a more accurate and more easily handled method. A complete B/H curve will have a shape similar to that shown in Fig. 2.6.4. If the point of maximum slope, (H_o, B_o), is located, it is possible to derive coefficients for two independent exponential series, one to represent the curve for values of H greater than H_o, and a second series to represent the curve in the region $H<H_o$. This technique will give a curve with the correct shape, and will be highly accurate in terms of the u_d/H relationship, except at $H=H_o$ where there may exist a discontinuity. It is therefore desireable to further modify the expression for the curve to eliminate the discontinuity at (H_o, B_o).

Consider the expression for the hyperbolic tangent function,

$$\tanh\left(\frac{x}{2}\right) = \frac{1 - e^{-x}}{1 + e^{-x}}$$

which has the correct general shape required, but is not suitable for the representation of the magnetisation curves due to the symmetrical shape of the function. If coefficients are introduced into the expression, and the variable changed to H,

then an expression for the flux density is obtained,

$$B = K_1 \cdot \frac{1 - \exp(-K_2 \cdot H)}{1 + \exp(-K_3 \cdot H)} \qquad \ldots\ldots 2.6.3$$

Fig. 2.6.5 illustrates the effect which the variation of the relative magnitudes of K_2 and K_3 has on the shape of the function. For $K_3 = K_2$, the shape is similar to that for the hyperbolic tangent, i.e. symmetrical. If $K_3 < K_2$, then the flux density will tend towards $-\infty$ as H increases negatively. By making K_3 larger than K_2 than as $H \rightarrow -\infty$, $B \rightarrow 0$. It is therefore impossible to produce an asymmetric function of this type which retains the correct shape required for the representation. However, if $K_3 \gg K_2$, then for all values of H less than zero, B is effectively zero, and it becomes possible to produce a function to represent the curve which has the correct asymmetric shape and is continuous at all points in the range $-\infty < H < +\infty$, i.e.,

$$B = K_1 \cdot \frac{1 - \exp(-K_2 \cdot H)}{1 + \exp(-K_0 \cdot H)} + K_3 \cdot \frac{1 - \exp(-K_4 \cdot H)}{1 + \exp(+K_0 \cdot H)} \qquad \ldots\ldots 2.6.4$$

where the two terms, one representing the curve for values of $H > 0$, and the second in the region $H < 0$, are virtually independent if K_0 is very large compared with K_2 and K_4. By allowing for the air line and shifting the origin of the expression to the point of maximum slope, (H_0, B_0), then the complete expression becomes,

$$B = B_o + u_o \cdot (H-H_o)$$

$$+ \sum_{i=1}^{n} K_{2i-1} \cdot \left[1 - \exp(-K_{2i} \cdot (H-H_o))\right] / \left[1 + \exp(-K_o \cdot (H-H_o))\right]$$

$$+ \sum_{j=n+1}^{m} K_{2j-1} \cdot \left[1 - \exp(-K_{2j} \cdot (H-H_o))\right] / \left[1 + \exp(K_o \cdot (H-H_o))\right]$$

.....2.6.5

This expression has been used to represent single curves which are then utilised in the representation of the complete magnetisation characteristic. An example is given in Fig. 2.6.6 which shows the recorded magnetisation characteristic of a single-phase, 1-kVA, 250v. transformer, together with the curves obtained using eqn. 2.6.5. The coefficients for this characteristic and those for the other transformers used in this investigation are given in appendix A1.

The method used to obtain the coefficients is described in appendix A2 which also contains a brief description of the computer program used in the determination of the coefficients.

2.6.3 General observations on method of representation.

Although the method of representing the complete B/H characteristic of a magnetic material, presented in section 2.6.1, requires that a minimum of two, and preferably three curves are initially represented, using for example eqn. 2.6.5, the information given by steel and transformer manufacturers does not always specify the amount of detail necessary to do this. A method, which is described in detail in appendix A3, has therefore been devised which allows the complete representation to be achieved with the minimum of information, i.e. the

B/H curve (B_r=0), and a knowledge of B_R and H_c. This method, while being less accurate than that described above, is very useful where it is impractical to measure the transformer characteristics directly.

It should be noted, however, that the characteristics of the completed transformer may differ considerably from that of the steel itself, due to air gaps in the core caused by the methods used in the construction. The characteristics of the steel also vary according to the angle at which the flux crosses the grain direction. This problem is dealt with in greater detail in chapter 3.

For the purposes of representing the B/H characteristics of magnetic materials, it was assumed in section 2.6.1 that, in general, increasing curves do not intersect. Examination of the oscilloscope traces shown in Fig. 2.6.7 indicate that, under certain circumstances, curves of this type will in fact cross. The occurrence of these crossovers can be explained by considering the process of magnetisation as proposed by Preisach[13] which is given in appendix A4. It is unlikely that errors due to this imperfection in the representation will in themselves be significant, and in any case will be much less than if hysteresis is neglected. This is therefore not considered a serious fault in the representation, but if necessary, it should be possible to modify the method given to incorporate this type of behaviour.

2.7 Summary.

The various ways in which a static, nonlinear, electromagnetic device may be modelled mathematically have been described and a method of achieving this by a combined

electric-circuit and magnetic-circuit approach is given. Examples of the application of this method are presented for the single-phase transformer, and the three-limb, core type three-phase transformer with two windings perphase.

A method of representing the complete magnetisation characteristic of a ferromagnetic material has been proposed together with a suitable expression for representing the B/H relationship of a single curve which is accurate over the complete range of H. A discrepancy between the method of representation proposed and the observed behaviour of ferromagnetic materials is discussed and the conclusion reached that this will have little effect on results obtained using this method.

-CHAPTER 3-

EXPERIMENTAL REQUIREMENTS

It is generally agreed that the various factors which may affect the performance of transformers include the transformer parameters (winding resistance, leakage inductance, etc.), the magnetisation characteristic of the core, the supply voltage and impedance, and the point on the voltage waveform at which the supply is connected (transient performance). The magnitude and direction of residual core flux can also have a considerable effect on the transient behaviour of transformers. The way in which values for these factors are obtained are described in the first part of this chapter.

The second part of the chapter is devoted to the techniques used in the control and monitoring of transformer conditions.

3.1 Transformer Parameters.

The parameters required for the solution of the transformer equations are the winding resistances, coil-leakage inductances (one or two windings per phase), and in the case of a polyphase transformer, the phase-leakage inductances. All the above parameters are assumed to be constant.

The d.c. resistance and coil-leakage inductance values were measured using standard d.c. and short-circuit tests. The conventional method of dividing the total leakage inductance obtained from the short-circuit test equally between the two

coils used (all parameters referred to N turns) was employed, which gave reasonable results when used in subsequent computations.

A test to measure the phase-leakage inductances has been devised by MacFadyen[1]. This test involves the measurement of the flux linking search coils sited on each branch of the magnetic core at the limb under consideration, as shown in Fig. 3.1.1. Thus knowing ϕ_1, ϕ_2 and ϕ_3, ϕ_p, the phase-leakage flux can be determined. The corresponding phase-leakage inductance is given approximately by,

$$M_p = N.\phi_p/i_A$$

where, M_p is the phase-leakage inductance, and i_A is the limb coil current.

An alternative method of estimating the phase-leakage inductance is simply to divide the single value of zero-sequence inductance obtainable for the three-limb transformer equally among the three phase-leakage paths. In the case of a fivelimb transformer, the zero-sequence inductance will be highly nonlinear unless the outer limbs are excited at the same time as the three wound limbs, forcing the flux to return in the air instead of via the low reluctance paths provided by the outer limbs. Since it may not be practicable to measure phase-leakage inductance directly, this method could prove a convenient alternative. MacFadyen has shown that large errors may be introduced by allowing for only a single phase-leakage path, or by neglecting the effects of phase-leakage flux entirely but has presented no comparison of results obtained using phase-leakage inductances and those for zero-sequence induct-

ance. A comparison of this type will be made in chapter 4.

One transformer parameter which will normally only apply to transformers with high voltage windings (e.g. transmission and distribution transformers) is the h.v. winding self-capacitance. This capacitance is distributed throughout the winding, but for simplicity can be considered as a single, lumped value. A simple way of measuring this capacitance is to charge the winding capacitance using a d.c. source and to measure the frequency of the oscillation which occurs when the supply is suddenly removed. If L, the winding self-inductance is constant, i.e. nonlinearity can be neglected, then the frequency of oscillation is given by,

$$\omega = \left[\frac{1}{L.C} - \frac{R^2}{4.L^2}\right]^{\frac{1}{2}}$$

Since, for virtually all transformers, $(1/L.C) \gg (R^2/4.L^2)$, the frequency will be close to the undamped natural frequency,

$$\omega = 1/(L.C)^{\frac{1}{2}}$$

In order to assure reasonable linearity the voltages and currents are kept very small. Both L and C are assumed unknown so that it is necessary to measure two values of frequency; one for the winding self-capacitance alone, and one with a known capacitance, C_1, connected in parallel with the winding so that,

$$\omega_1 = 1/(L.C)^{\frac{1}{2}}$$

$$\omega_2 = 1/(L.(C + C_1))^{\frac{1}{2}}$$

which gives,

$$C = \frac{C_1}{(\omega_1/\omega_2)^2 - 1}$$

The value of C obtained can be checked by repeating this procedure using several different values of C_1. This method of measuring capacitance, while being approximate, should be sufficiently accurate for use in the present investigation. A complete list of the parameters, including winding capacitance where relevent, is given in appendix A1.

3.2 Magnetisation Characteristic.

It may often be necessary to obtain the magnetisation characteristic of a transformer experimentally, even where information on the characteristic is available, since the methods of construction used in power transformers introduce small air gaps between core sections, which can cause the magnetic properties of the completed transformer to differ considerably from that of the steel alone. In addition, components of flux are forced to cross the steel normal to the grain at the junctions as shown in Fig. 3.2.1 which may also affect the B/H characteristic of the transformer. By obtaining the magnetisation characteristic directly, and assuming that the core is magnetically homogenous, the effect of core air gaps and cross-grain flux may be taken into account without introducing additional equations into the transformer model described in chapter 2.

The measurement of the B/H characteristic involves obtaining a value of magnetic flux density for a corresponding value of applied field strength. As the B/H relationship is

non-unique, the flux density for a given value of field strength is only meaningful if the magnetic history of the core is known. While the measurement of absolute flux density in the core is virtually impossible, it is possible to measure changes in the flux density by integrating the e.m.f. induced in a search coil wound round the section of core to be examined. The signal from the integrator is calibrated by applying the following equations,

$$\Psi = -\int e.dt$$

$$\Psi = B.A.N_s$$

where, Ψ is the flux linkages in the search coil
e is the e.m.f. induced in the search coil
A is the effective cross-sectional area of the core
N_s is the number of turns in the search coil

If a sinusoidally varying voltage is applied to the primary winding of the transformer, the e.m.f. induced in the search coil is given by,

$$e = \hat{E}.\sin(\omega t)$$

so that,

$$\Psi = -\hat{E}/\omega \,.\cos(\omega t)$$

and,

$$\hat{B} = \hat{E}/(N_s.A.\omega) \qquad \ldots\ldots 3.2.1$$

It is therefore possible to calibrate the integrated e.m.f signal in terms of flux density if the peak value of the sinusoidal voltage induced in the search coil is known.

Ampere's Magnetic Circuital Law,

$$\oint H.dl = N.i$$

can be applied round any closed path in the core. If the flux density is assumed to be constant in all parts of the flux path, then the magnetic circuit equation becomes,

$$N.i = H.L$$

i.e. $$H = N.i/L \qquad \text{.....3.2.2}$$

where, i is the current in the primary winding.
L is the mean flux path length.

The voltage drop across a low resistance shunt connected in series with the primary winding will be directly proportional to the current in the winding. This voltage signal can therefore be calibrated in terms of the magnetic field strength, H, using eqn. 3.2.2.

The magnetisation characteristic is obtained by applying a slowly varying direct voltage to the primary winding of the transformer. The signal from the integrator is applied to the Y-plates of an oscilloscope, and the signal from the series shunt to the X-plates as shown in Fig. 3.2.2. An oscillogram of the B/H characteristic is produced in this way and two examples obtained from an 8-kVA, three-phase transformer are shown in Fig. 3.2.3. D.c. excitation is used to eliminate as far as possible the effects of eddy-currents. This method is also used to record flux density and current during transient and steady-state a.c. conditions.

In order to calibrate the B/H characteristic in terms of the absolute value of flux density, rather than the change in flux density, all measurements were taken with the transformer core initially de-magnetised.

In the case of a three-limb, three-phase transformer core, the B/H characteristic is measured by energising the two outer limbs in series so that the resultant fluxes are in the same direction round the core. If the coils are identical and the core is symmetrical about the centre limb, then very little flux will be set up in the centre limb. As with the single-phase transformer, the B/H characteristic is obtained in this way assuming that the flux density is constant in all parts of the core flux path, i.e. that the cross-sectional areas of the limbs and yokes are all the same.

To check the magnetic isotropy of the core, i.e. to ensure that the effect of core air gaps and cross-grain flux does not lead to appreciable variation in the magnetic properties from section to section in the core, the measurement of the B/H characteristic was also carried out using first the coil on one outer limb in series with that on the centre limb, and then the other limb and centre limb together. No measurable difference could be detected in any of the three magnetisation characteristics thus obtained.

The characteristics of the single-phase and two three-phase transformers which were used in the study of transformer behaviour are given in Figs. 2.6.6, 3.2.4 and 3.2.5 res., together with the corresponding exponential series curves. The series coefficients are given in appendix A1. Fig. 3.2.6 shows the magnetisation characteristic of the steel used in the construction of the 50-kVA distribution transformer as supplied

by the steel manufacturer. The experimentally-obtained characteristic in Fig. 3.2.5 departs considerably from this and serves to illustrate the effects of constructional methods on the magnetic properties of the core.

3.3 Supply Impedance.

Fig. 3.3.1 shows the circuit used to control and record transient and steady-state conditions in a single-phase transformer. The mains supply, the auto-transformer and other external circuit elements will all have a certain impedance, and the total impedance, which is assumed constant for a given frquency is given by,

$$\bar{Z}_s = R_s + jX_s$$

To protect the switching angle selector from the high steady-state currents used in the measurement of R_s and X_s the impedance of this device is measured separately.

The Thevinin equivalent circuit of the supply, which is used in the computation of transformer performance, consists of an open-circuit e.m.f., $\bar{E}$, and the effective supply impedance, $R_s + jX_s$. E can be measured directly. If this circuit is used to supply a unity power-factor load then, taking the voltage across the load as reference,

$$E\angle\delta = V\angle 0^o + I\angle 0^o . Z_s\angle\phi \qquad \ldots\ldots 3.3.1$$

where, $\bar{V}$ is the load voltage.
$\bar{I}$ is the load current.

δ, the phase angle between E and V (see Fig. 3.3.2) was measured using a digital phase meter, allowing R_s, X_s and l_s to be evaluated from eqn. 3.3.1.

For auto-transformer turns ratios other than 1:1, the leakage inductance of the auto-transformer, which has a degree of nonlinearity dependent on the turns ratio, causes the supply inductance to vary with current. However, since l_s is very small compared with the self inductance of the test transformer primary winding for rated steady-state conditions, its value will only become significant when the test transformer saturates, i.e. during transient conditions. For this reason the value of l_s used in the calculation of transformer performance was that obtained for large values of current. Appendix A1 lists the values of R_s and l_s used in the investigation and the effect of varying the supply impedance is examined and discussed in chapter 4.

3.4 Switching angle selector.

The double-pole switching angle selectors[14] which were available in the department had been used successfully in the study of switching transients for a number of years. In the study of transients in three-phase transformers with four-wire supplies it is necessary to control the switching in all three lines. The units available could not be readily connected together to give non-simultaneous switching in three lines, and unreliable operation was experienced, due to pick-up problems in the pulse transformers, when this was attempted. It was decided to try to improve the design of the switching angle selectors with a view to constructing a single-pole unit which could be readily connected in series with a number of similar

units to provide n-pole operation.

Several sucessful designs were produced, but the circuit shown in Fig. 3.4.1 was chosen as the final version owing to its compact size when constructed, and its capability to supply several watts of power to the thyristor gate, if required. The operation of the unit is described below.

3.4.1 Description of circuit.

The variable phase (with respect to the mains supply), sine-wave output from the magslip, M, is reduced to a low voltage, square-wave signal by resistor R1 and zener diode Z1. The square-wave signal is fed to the base of transistor T1 via a current limiting resistor R2. This causes T1 to switch 'on' and 'off' producing a large square-wave voltage at the collector of T1 as shown in Fig. 3.4.1. Capacitor C1 and resistor R5 form a differentiating arrangement which forms a train of negative and positive pulses at the lagging and leading edges of the square-wave, i.e. at the zero-voltage points on the magslip output. Diode D1 prevents the negative pulses from reaching transistor T2 which forms an emitter-follower arrangement with R7 . The magnitude of the pulses appearing across R7 while SCR1 is in the non-conducting state is limited by the large resistor R3.

When the 'Reset' switch is closed, SCR1 is gated 'on' by push-button PB1 and held in this condition by hold-on resistor R8 when PB1 is released. This action raises the collector of T2 to the d.c. supply level, +9v., thus bringing the emitter follower into operation. This in turn causes large positive pulses to appear across R7. The first positive pulse reaching T2 once SCR1 has been switched 'on' will

cause SCR2 to start conducting, which provides the supply to a multivibrator as shown. SCR2 is held-on by resistor R10.

The high frequency (about 20kHz) output from the collectors of T3 and T4 is used to switch alternately the two darlingto pairs, T5 and T7, and, T6 and T8. The output from PT1 is a high frequency square-wave with no d.c. component. A full-wave rectifier (D2-D5) and a small smoothing capacitor C4 provide a spike-free d.c. signal to the gate of the main thyristor via a current limiting resistor R19, the value of which can be adjusted to cater for the gate requirements of the thyristor.

The main thyristor used in the new units was an 800v. 30A rms triac which required a gate current of 200mA. at a voltage of 3v. The unit is capable of providing up to 10 watts of power to the thyristor gate which is sufficient for most, if not all, applications.

The interconnection of single-pole units to provide n-pole operation is achieved by connecting the output from the emitter-follower of one unit to the gate of either SCR1 or SCR2 in a second unit to give non-simultaneous or simultaneous switching respectively. In order that all connected devices may be operated from a single 'master' unit, only the d.c. supply in the master unit is used, thus making it possible to reset all units by the operation of a single switch.

3.4.2 Advantages over previous design.

The large pulses produced by the pulse unit and the low output impedance makes the units less prone to the pick-up problems experienced with the original devices, the circuit for which is shown in Fig. 3.4.2. Previously a d.c. supply had

to be provided on the secondary side of the pulse transformers for each pole, in addition to the d.c. supply required on the primary side - a total of three supplies for each double-pole unit. This arrangement could prove problematic if the unit was required to operate in h.v. systems. Only one d.c. supply is required in the new design, irrespective of the number of interconnected poles, although the number may be limited in practice by the output capacity of a single supply. The insulation level is governed only by the pulse transformers which can be chosen to suit the particular application.

The compact nature of the electronic circuit makes it possible, using 2" magslips, to assemble a complete double-pole unit, including triacs and heatsinks, into a box much smaller than was previously possible (see Fig. 3.4.3). Finally, apart from the increased flexibility of the new design, the saving in cost achieved through no longer requiring the number of isolated d.c. supplies, and the use of smaller boxes etc., more than compensates for the additional cost of the electronic components.

3.4.3 Impedance of switching angle selector.

The recorded voltage/current characteristic for the switching angle selector is shown in Fig. 3.4.4. The voltage drop across the pole can be expressed as,

$$V_{pole} = a.\ (i/|i|) + b.i$$

where a and b are constants, and i is the instantaneous current through the pole. Thus the impedance for any given value of current is given by,

$$R_{pole} = b + a/|i|$$

3.5 Recording and Measuring Methods.

There are three quantities which are of interest in the study of transformer behaviour under transient and steady-state conditions, viz., voltage, current and flux or flux density. The transformer m.m.f.'s may also be of considerable interest but it is not possible to measure these except under special circumstances.

The basic recording device used in the investigation was a Tektronix 5013 storage oscilloscope. In previous work in the department[15-17], ultra-violet recorders were utilised, but this method lacked the flexibility of the storage oscilloscope in that it takes several seconds before the recording becomes discernible, and it is not possible to superimpose two or more traces unless taken at the same time. In addition, since a permanent record was not always required, wastage of large amounts of the special u.v. sensitive paper was eliminated.

Voltage recording on the oscilloscope was invariably carried out using high resistance voltage dividers, while flux density was monitored using the method described in section 3.2.

A signal proportional to the current can be obtained in two ways, i.e. by the use of low resistance shunts in the current paths, or from current transformers. Wherever possible, the former method was adopted, usually when the shunts could be sited at the star point of a three-phase transformer winding, or invariably in the single-phase case.

Current transformers were used where it was necessary to isolate the current signals, either because the star point of the winding was not accessible, or the winding was delta connected. Results obtained in this way were indistinguishable from those obtained using shunts, indicating that little or no distortion in the current waveform had been introduced through the use of current transformers.

The equipment used in the experimental work is shown in Fig. 3.5.1.

-CHAPTER 4-

MAGNETIC NONLINEARITY AND HYSTERESIS IN TRANSFORMERS

The characteristic nonlinearity and hysteresis which is exhibited by magnetic materials such as iron, cobalt, etc., play a significant role in determining the performance of devices incorporating these materials. These effects can, in some instances, be employed to advantage. Permanent magnets, hysteresis motors and the magnetic core storage used in computers are all examples of the useful application of the phenomenon of magnetic hysteresis. Saturable reactors and static voltage stabilisers depend upon saturation of the magnetic core for their operation.

The effects of magnetic nonlinearity and hysteresis can, however, create problems in the operation of the more conventional electromagnetic machines such as transformers and induction motors. These problems, which are mainly associated with the transient performance and efficiency of operation, have been the subject of a vast amount of literature dating back over several decades.

Both phenomena cause losses in these types of machines, either directly or indirectly. Losses due to hysteresis which result in heating of the magnetic core can be minimized by the selection of a suitable core material such as grain-orientated silicon steel which is widely used in transformer laminations. Magnetic nonlinearity, while not a direct source of losses, effectively limits the level of flux density at which a machine with a steel or iron core can be operated, since higher levels of flux density would

require disproportionately larger magnetising currents, which in turn result in large losses in the machine windings.

While much attention has been given in the past to the effect of magnetic nonlinearity on the transient performance of transformers[18,19,20,21], the part played by hysteresis has been largely neglected. This is probably due to the problems involved in satisfactorily representing the complete magnetisation characteristic of the core, and subsequently utilising the method of representation in the analysis of the complete device. Yet as will be shown, residual core flux, which is a direct consequence of hysteresis, can have a very significant effect on transients due to switching operations.

In order to study the ways in which the transient behaviour of transformers can be affected by a combination of magnetic nonlinearity and hysteresis, the performance equations for the single-phase transformer and a three-limb, three-phase transformer, derived in chapter 2, are used in conjunction with the representation of the complete magnetisation characteristic for magnetic materials, which was also presented in that chapter.

4.1 Single-Phase Transformer.

In chapter 2, the performance equations for the single-phase transformer were given as,

$$v_A = i_A.R_A + l_A.pi_A + M.pi_m$$

$$v_a = i_a.R_a + l_a.pi_a + M.pi_m$$

where all quantities are referred to N_1 (primary) turns.

In order to solve the above equations, the secondary voltage, v_a, must be expressed in terms of the load quantities. Thus for a series combination of resistance, capacitance and inductance as the load, the secondary circuit equation becomes,

$$i_L.R_L + l_L.pi_L + q_c/C_L = i_a.R_a + l_a.pi_a + M.pi_m \quad \ldots\ldots 4.1.1$$

where, q_c is the instantaneous charge on C_L

Also, $i_a = -i_L$

$$pq_c = i_L$$

The above equations can be solved by means of a numerical integration technique such as the Runge-Kutta method. The computation of the transformer transients using this method of solution is relatively straightforward, if a single-valued function representation of the B/H characteristic is used. If, however, the complete magnetisation characteristic is represented using the method described in chapter 2, then it becomes necessary to monitor the magnetising current, i_m, in order to detect turning points in the B/H plane. When a positive or negative peak value of i_m (or the flux) is detected, then all quantities must be reset to their values at the beginning of the step, i.e. at the turning point, and the new trajectory for the magnetisation characteristic generated.

An example of the resultant computed transient B/H pattern is shown in Fig. 4.1.1. The apparent discrepancy between the computed and recorded patterns is due to the

effects of eddy currents, for which no allowance has been made in the transformer model. If the conventional method of incorporating eddy current losses in the transformer model is used i.e. by shunting the input terminals of the transformer by a resistor which produces losses equal to those due to eddy currents, the resultant steady-state B/i pattern corresponds very closely to the recorded pattern as shown in Fig. 4.1.2. This method of allowing for eddy current effects is only valid for steady-state conditions.

4.2 Residual Flux in Single-Phase Transformers.

In single-phase transformers, with only one nonlinear magnetic path to consider, the incorporation of residual conditions in the calculations is a relatively simple matter. In the de-energised state, (no currents in the coils of the transformer), the equation for the magnetic path in the core is,

$$\oint H.dl = 0$$

i.e. there is no residual value of magnetising current associated with the core path, even though residual flux may be present.

A single-phase transformer operating at or near its rated voltage has a steady-state B/H characteristic similar to that shown in Fig. 4.2.1. The characteristic will cross the zero-H axis at a point close to the limit cycle values, $\pm B_R$. Supply disconnection will normally occur when the input current falls to zero, i.e.,

$$i_1 = i_m + i_L = 0$$

Thus at this point,

$$i_m = -i_L \qquad \ldots\ldots 4.2.1$$

The point on the steady-state B/H characteristic at which this condition will occur will depend largely on two factors, viz., the size of the load, if any, and the load power factor.

In the unloaded transformer, since no load current flows, the residual conditions will be established at the instant of supply interruption,[33] i.e. at the point $(0, B_r)$ in Fig. 4.2.1, provided eddy current effects can be neglected. In a large unity power factor load, the load current will be virtually in phase with the supply voltage, and the flux will lag the load current by approximately 90^o, as shown in Fig. 4.2.2(a). Thus when the input voltage phase angle is zero, $v_a = i_L = 0$, and $\emptyset$ and i_m are at their negative maxima, (point A in Fig. 4.2.2(b)). If the load resistance is very small, then the input current will fall to zero when the phase angle of the input voltage is very small, i.e. when $i_L = -i_m$. This corresponds to point B in Fig. 4.2.2 (b). As the size of the load is reduced, the point on the B/H characteristic corresponding to input current zero will be displaced towards the point $(0, -B_r)$, which is the no-load point.

Following supply interruption, the magnetisation current will decay to zero along with the load current, and the final value of residual flux density for a unity power factor load will be $\pm B_r$, depending on the polarity of the input current immediately before disconnection.

A large inductive load will cause the load current to lag the supply voltage by θ as shown in Fig. 4.2.3(a). As θ increases, the point on the B/H characteristic at which supply interruption occurs will shift along the lower or upper curve in the direction of the arrows, as shown in Fig. 4.2.3(b). When the load is purely inductive, disconnection will occur just as the load current falls to zero, i.e. at point C or C' in Fig. 4.2.3(b). As with a unity power factor load, this point will move toward the zero load point, as the size of the load is reduced. The final residual flux level for points lying between $(0, -B_r)$ and $(H_c, 0)$ and those lying between $(0, +B_r)$ and $(-H_c, 0)$ will depend on the actual point of disconnection, since the magnetisation current will decay to zero along a trajectory determined by that point, as shown in Fig. 4.2.3(b).

A similar argument can be applied to leading power factor loads to show that the disconnection point lies between point A, the unity power factor point, and point D, or A' and D', for a large purely capacitive load, in Fig. 4.2.4. Thus the size or kVA of the load determines the range over which the residual flux value can vary, and the power factor of the load determines the final value of B_r. Fig. 4.2.5 shows the variation of residual flux with kVA and power factor.

The curves for leading power factor loads are shown broken since the capacitance in the system, due to winding self-capacitance or a leading p.f. load element, may cause 'ringing' between the nonlinear inductance of the transformer and the capacitance, on supply interruption. These damped oscillations cause field reversals, which tend to

de-magnetise the core. The extent to which de-magnetisation will take place depends on the magnitude and frequency of the oscillations and the amount of natural damping in the system. It is therefore difficult to predict the final state of the core following supply interruption, for this condition.

Where the value of capacitance is small, the tendancy will be for high frequency oscillations of low amplitude to occur which will decay rapidly due to high eddy current and hysteresis losses. De-magnetisation will not usually be great in this case. Large values of capacitance will cause low frequency, high amplitude oscillations to be initiated, with longer time constants. This will result in a greater degree of de-magnetisation.

This behaviour introduces a frequency-dependent factor into the analysis, i.e. eddy current loss. Since no allowance has been made for the effects of eddy currents in the analysis, the results of attempts to compute residual flux density, where capacitance is significant, will be subject to a degree of error. The conventional method of catering for eddy current losses by shunting the input terminals of the transformer with a constant value of resistance will only be valid for frequencies about 50 Hz. - the frequency at which the losses are measured.

4.2.1 Effects of hysteresis on transient performance.

Fig. 4.2.6 shows the recorded transient current pattern for a single-phase transformer for a switching angle of 0^{o}, together with the computed results using the complete representation of the magnetisation characteristic and those for a single-valued function representation. The transformer

is unloaded and initially de-magnetised. From these results and those given in Fig. 4.2.7, which illustrate the variation of peak transient current with switching angle, it can be seen that hysteresis does not significantly affect the peak transient current due to switching in an unloaded, de-magnetised single-phase transformer. Both sets of computed results were also found to be virtually identical for the case of a loaded transformer, (for example see Fig. 4.2.8).

The reason for the similarity between computed results using the complete B/H representation and those for a single-valued function, is that the initial magnetisation trajectory and residual flux level (zero) is identical in both cases, which will tend to produce similar results.

In the general case, however, where residual flux is present in the core when the supply is connected, the initial magnetisation trajectory may differ considerably from that for zero remanence, as will the level of peak flux density for a given switching angle. An example of the effect which different residual flux levels in an unloaded single-phase transformer have on the transient current is given in Fig. 4.2.9, while Fig. 4.2.10 shows how the peak transient current varies with the value of residual flux density.

A comparison of the curves of peak transient current versus switching angle for residual flux density values of 0, +0.9 Tesla and -0.9 Tesla, given in Fig. 4.2.11, shows the considerable influence of B_r on the transient performance of an unloaded single-phase transformer, for any given switching angle. Results for various loaded conditions, which are given in Figs. 4.2.12, 4.2.13 and 4.2.14 show a similar dependance on residual flux density.

It should be noted, however, that the damped oscillations observed in the initial stages of the transient current pattern for a leading power factor load (Fig. 4.2.14(a)) which are due to the interaction of the leakage inductance of the transformer and the load, may in fact produce larger current peaks than the transient magnetising current. This region of the transient current will not be greatly influenced by residual flux, and, depending on the switching angle, little or no variation in the peak value of current will take place as the level of residual flux density is varied. Normally this initial oscillation has a very short time constant compared with the magnetising current transient, and should not cause spurious operation of protection equipment in power systems. The peak current following this initial 'ringing' may therefore still be of considerable interest.

4.3 Three-Phase Transformer.

The nine differential and five algebraic simultaneous equations for the three-limb, three-phase transformer with two windings per phase, which were derived from the performance equations of the general, static electromagnetic system in chapter 2, do not take account of the transformer winding configuration or the type of load. The primary circuit equations (eqn. 2.4.1(a)) can be used in the given form as long as the phase voltages can be precisely defined, which is the case for a delta or four-wire star connection, but not for a star connected winding with floating star point.

The secondary circuit equations (eqn. 2.4.1(b)) must be modified to allow for both winding configuration and the type of load, if any, as in the case of the single-phase

transformer. Additional differential or algebraic equations may be required, depending on the load arrangement. For example, if the load is delta connected an additional, zero-sequence, equation is required, i.e. since,

$$v_a + v_b + v_c = 0$$

then,
$$0 = i_{aL}.R_{aL} + l_{aL}.pi_{aL} + q_{ca}/C_{aL}$$
$$+ i_{bL}.R_{bL} + l_{bL}.pi_{bL} + q_{cb}/C_{bL}$$
$$+ i_{cL}.R_{cL} + l_{cL}.pi_{cL} + q_{cc}/C_{cL} \quad \ldots\ldots 4.3.1$$

assuming a series R,l,C load per phase. This equation is required since in the secondary circuit there are four independent variables (currents) for this arrangement, but only three equations in the original set. The presence of capacitance in the system gives rise to further simple differential equations,

$$pq_{ca} = i_{aL}$$
$$pq_{cb} = i_{bL}$$
$$pq_{cc} = i_{cL}$$

which apply to any arrangement of an R,l,C series connected load.

The magnetic circuit equations (eqns. 2.4.2 and 2.4.4) are only affected by changes in the magnetic circuit and thus only apply to the three-limb core-type transformer.

4.3.1 Method of calculation.

In a three-phase, two-winding transformer, there are three possible primary winding configurations as well as three for the secondary winding and three for the load (considering the load as three lumped impedances arranged in delta or star). Not all combinations of secondary winding and load connections are possible; for example a delta connected secondary winding cannot be considered along with a four-wire star connected load. In addition there are two no-load secondary connections, star and delta, giving a total of seven secondary circuit configurations, which are summarised in tabulated form below.

Sec. \ Load	No-load	3-wire star	4-wire star	Delta
3-wire star	x*	x		x
4-wire star	x*		x	
Delta	x	x		x

x - indicates possible combination

* - 3- and 4-wire star identical for no-load

Since any combination of primary winding and secondary circuit configuration is possible, then a total of twenty-one permutations of the three circuit configurations are feasible.

A general computer program was developed which would allow any one of the twenty-one permutations to be chosen. The number of differential equations required to describe any particular system is dependent on the type and

configuration of the load. There are a maximum of ten differential equations which will form the major system of equations, i.e. three each for the primary circuit, the magnetic circuit, and the secondary winding, plus a zero-sequence equation in the case of a delta connected load. The other differential equations, which are dependent on the type of load, will be of a trivial nature, e.g. for a capacitive load,

$$pq_c = i_c$$

The major differential equations are arranged in matrix form, having first substituted for i_4 to i_8 from the algebraic magnetic circuit equations (eqn. 2.4.4),

$$\left[V\right] = \left[M\right].\left[P\right]$$

where V is the voltage vector, M is the inductance matrix, and P is the solution vector. If all switching operations are confined to the input side of the transformer, then the three magnetic circuit differential equations and the four possible secondary circuit equations remain unaltered throughout the computation. It is therefore possible to define the first seven elements of the voltage vector, and the first 7x7 elements of the inductance matrix, independently of the primary winding connection.

The remaining elements of the voltage vector and inductance matrix will depend on the primary winding connection and switching conditions. An example of the complete matrix equation for an arrangement comprising delta connected primary, secondary and load circuits is given overleaf.

$$
\begin{bmatrix} 0 \\ 0 \\ 0 \\ V_4 \\ V_5 \\ V_6 \\ V_7 \\ V_8 \\ V_9 \\ V_{10} \end{bmatrix}
=
\begin{bmatrix}
M_1+M_4+M_7 & -M_7 & & -M-M_4 7 & M_7 & & & -M_4/3 & M_4/3+M_7 & -M_4/3 \\
-M_7 & M_2+M_5+M_7+M_8 & -M_8 & M_7 & -M-M_5 7-M_8 & M_8 & & -M_5/3 & -2M/3_5-M_7-M_8 & -M/3_5-M_8 \\
 & -M_8 & M_3+M_6+M_8 & & M_8 & -M-M_6 8 & & -M_6/3 & M_6/3+M_8 & 2M_6/3+M_8 \\
M_1 & M_2 & M_3 & l_a & l_b & l_c & & & & \\
 & M_2 & & -l'_{bL} & l_b+2l'_{bL} & -l'_{bL} & -l'_{bL} & & & \\
 & & M_3 & -l'_{cL} & -l'_{cL} & l_c+2l'_{cL} & -l'_{cL} & & & \\
 & & & 2l'_{aL}-l'_{aL}-l'_{cL} & 2l'_{bL}-l'_{aL}-l'_{cL} & 2l'_{cL}-l'_{aL}-l'_{bL} & l'_{aL}+l'_{bL}+l'_{cL} & & & \\
M_1 & M_2 & M_3 & & & & & l'_A+l'_B+l'_C & 2l'_B-l'_A-l'_C & l'_A+l'_B-2l'_C \\
 & M_2 & & & & & & l'_B & 2l'_B+2l_s & l'_B+l_s \\
M_1 & & & & & & & l'_A & -l'_A-l_s & l'_A+l_s
\end{bmatrix}
\cdot
\begin{bmatrix} pi_1 \\ pi_2 \\ pi_3 \\ pi_a \\ pi_b \\ pi_c \\ pi_o \\ pi_Z \\ pi_B \\ pi_A \end{bmatrix}
$$

'÷ INDICATES DIVISION BY 3

Matrix equation for delta connected primary, secondary and load.

The voltage vector quantities are given by,

$$v_4 = -i_a.R_a - i_b.R_b - i_c.R_c$$

$$v_5 = (i_o + i_a - 2.i_b + i_c).R_{bL}/3 - i_b.R_b + q_b/C_b$$

$$v_6 = (i_o + i_a + i_b - 2.i_c).R_{cL}/3 - i_c.R_c + q_c/C_c$$

$$v_7 = -(i_o - 2.i_a + i_b + i_c).R_{aL}/3 - q_a/C_a$$
$$-(i_o + i_a - 2.i_b + i_c).R_{bL}/3 - q_b/C_b$$
$$-(i_o + i_a + i_b - 2.i_c).R_{cL}/3 - q_c/C_c$$

$$v_8 = -i_A.R_A - i_B.R_B - i_C.R_C$$

$$v_9 = v_B - (2.i_B - i_A - i_C).R_s - i_B.R_B$$

$$v_{10} = v_A - (2.i_A - i_B - i_C).R_s - i_A.R_A$$

Each phase of the load is taken, as before, as a series combination of resistance, inductance and capacitance. The first 7x7 elements of the inductance matrix depend only on the secondary circuit configuration.

The solution vector, P, can be obtained by matrix inversion or, as is done in the computer program, by elimination. Since the differential equations are nonlinear, the values of inductance must be recalculated, and the new solution vector found, at each stage of the computation.

As with the single-phase transformer, the use of the method of representing the complete B/H relationship described in chapter 2 requires that the magnetising currents are monitored in order to detect turning points in the B/H plane. In the case of a three-limb transformer there are a total of five nonlinear magnetic paths, i.e. the three limb and two yoke paths. A turning point detected in any one or more of the core sections will necessitate the resetting of all quantities to their respective values at the time the turning point occurred, and new magnetisation trajectories generated for those sections. Occasionally, the effect which the new magnetisation curves have on the overall system will subsequently cause turning points in the B/H characteristics of other sections. It may therefore be necessary to reset the transformer quantities several times before a stable situation is established.

A flow diagram for the computer program used to compute three-phase transformer performance is shown in Fig. 4.3.1. The program also includes provision for the computation of residual conditions in three-phase transformers, which will be explained in the following sections.

4.4 Zero Residual Flux Conditions.

Although, in general, residual flux is present to some extent in transformer cores at the instant of connection of the supply, the particular case where the core is magnetically neutral immediately prior to switch-on provides a convenient means whereby the effects of hysteresis on transformer transients can be examined. This examination cannot be undertaken through experiment alone, since there is no means

of eliminating the effects of hysteresis from recorded transients in order to compare these with the results for the actual transformer.

A theoretical comparison of this type can, however, be achieved through calculation, by obtaining results for identical conditions of voltage, switching angles, etc., using a single-valued function representation of the B/H characteristic, and the complete representation. The effect of hysteresis on the transient currents and fluxes in a three-phase transformer was investigated by initially varying the switching conditions to find where large discrepancies between results for the two methods of representing the magnetisation characteristic were evident. The influence of such factors as winding configuration, switching sequence and load on these discrepancies were subsequently examined.

4.4.1 Switching conditions.

The two sets of results obtained for the transient currents due to simultaneous switching of the supply to a three-phase transformer show a marked similarity, irrespective of switching angle, load, etc., so long as the transformer is initially de-magnetised. An example of this is given in Fig. 4.4.1. At no point do the two computed results differ by more than 2%, which is better than the accuracy of the illustration. As in the case of the single-phase transformer, the reason for the similarity is that the initial magnetisation trajectories and residual flux density (zero) are identical in all cases.

The condition where one or more, but not all, phases in a poly-phase transformer are energised, as occurs during

non-simultaneous switching of the supply, can be visualised as effectively setting up 'residual' conditions in the core members which may influence the subsequent transients when the remaining lines are connected. Since the transformer equations take account of magnetic coupling between phases, then for short delays between the switching of all lines, i.e. until a turning point in the B/H characteristic of one or more of the core sections has been reached, the conditions in the core will be the same for both methods of representation. Little difference would therefore be expected between the two sets of results, at least in the first transient peaks, for short switching delays.

The occurrence of a turning point in the B/H plane causes the magnetisation trajectories for the two methods of representation employed, to diverge, resulting in possibly differing conditions in the core when the remaining supply lines are connected. This in turn would be expected to result in discrepancies in the transient current patterns. The time taken to reach the first significant turning point in the B/H plane will be largely governed by the initial switching angle. For example, in a three-wire star connected transformer, for an initial switching angle of 90^{o}, the first turning point will occur after approximately 5 ms (90^{o}) for a 50 Hz. supply, unless the third line is connected before this. For other switching angles this time will vary up to a maximum of about 10 ms when the initial switching angle is 0^{o} or 180^{o}.

In practice, discrepancies were only found in cases where the unloaded transformer had been energised asymmetrically, i.e. the centre limb and an outer limb energised first in the case of a three-wire star connected

primary winding (Fig. 4.4.2), or an outer limb energised first in the case of a four-wire star, or delta, connected primary (Fig. 4.4.3). Where the transformer had been energised symmetrically, i.e. the centre limb first followed by the two outer limb together, or vice-versa, results for the two methods of representing the B/H relationship were practically indistinguishable. The only exception to this was the four-wire star connected primary which gave the same results for both methods of representation when any two phases were energised simultaneously, followed by the third.

The reason for this behaviour can be established by considering the transient flux density distribution during the switching operations. For the three-wire star connection, Fig. 4.4.4, if phases A and C are energised first, the core being initially de-magnetised, then the reluctance of the flux paths for $\emptyset_A$ and $\emptyset_C$ will be the same at any point in time, and thus the instantaneous impedance of both phases will be nominally the same. The voltage and flux for each phase will be equal and opposite for the two outer limbs, and practically no flux will take a path through the centre limb, which will therefore remain de-magnetised until the third line is connected. This will be the case irrespective of the B/H characteristic, but only applies to transformers which are symmetrical about the centre limb.

Therefore, assuming that the effects of regulation are small, the flux density distribution at any point in time for a symmetrically energised transformer will be effectively independent of the magnetisation characteristic, so that there will be little difference between results computed using a single-valued curve to represent the magnetisation character-

istic and those using the complete representation. Fig. 4.4.5 shows the transient B/t and i/t patterns for the symmetrical energisation of an unloaded transformer with a three-wire star connected primary winding. No significant difference between the two computed results for this condition could be discerned.

The discrepancies arise when, as a result of the dissimilar flux path reluctances which occur during asymmetrical energisation, the flux distribution becomes dependent upon the magnetisation characteristic. If phases B and C in Fig. 4.4.4 are energised first, then although the B/t patterns are identical up to the first peak, as shown in Fig. 4.4.6, differences begin to appear in the region of zero flux as a result of the change in the B/H trajectories, which affect the flux (and voltage) distribution. Transients initiated by switching the third line at a point where the flux density curves diverge will be different in the two cases, as illustrated in Fig. 4.4.2, since even a small change in initial flux conditions can cause large changes in the currents due to the nonlinear nature of the magnetisation characteristic.

Similar arguements can be used to explain the results obtained for four-wire star and delta connected windings. Although a four-wire star connected primary appears to be asymmetrically energised when one outer limb and the centre limb are switched together before the third line is connected, since the voltages, and hence the fluxes, are effectively independent in each limb, the flux in the third limb will not be significantly affected by the B/H characteristic, and no major differences between the transients computed using the two methods of representation will be detected.

4.4.2 Secondary configuration and load.

An unloaded delta connected secondary winding will have an effect on the transient currents since it provides a low impedance path for zero-sequence components of current, but will have only a marginal effect on the transient flux distribution. A relatively large load, however, whether balanced or unbalanced will effectively determine the transient e.m.f distribution in the transformer, for a three-wire star or delta connected primary, and so maintain a flux distribution which is largely independent of the magnetisation characteristic.

Fig. 4.4.7 shows the results obtained from both methods of representing the B/H relationship for a loaded transformer with a delta connected primary, energised asymmetrically. Where the load is small, the influence of the load on the flux distribution will diminish, which may give rise to differing results as found in the no-load case.

In general, therefore, magnetic hysteresis will have an effect on the transient behaviour of poly-phase transformers, even when the core is initially de-magnetised. This effect is only evident after long delays in the switching operation, and can be largely eliminated if the transformer is energised while loaded.

4.5 Residual Conditions in Three-Phase Transformers.

Unlike the single-phase transformer, there is no simple way to predict the values of residual flux in a three-phase transformer, even if unloaded. This is mainly due to the effects of magnetic coupling between energised and de-energised

phases during non-simultaneous disconnection of the supply lines. In attempting to overcome this problem, Nakra and Barton[2] have established residual flux artificially by exciting the outer limbs of a three-limb transformer in series-aiding so that the centre limb remains de-magnetised. This method, while providing a convenient means of testing the method of analysis, does not, in general, result in residual conditions which occur in practice as will be shown.

The situation is further complicated by the effects of load. Although, as with the single-phase transformer, it is evident that capacitance either in the load or appearing as winding self-capacitance, may tend to de-magnetise the core following supply interruption, the effect of a lagging or unity power factor load is less obvious. It is possible, however, by making a few simplifications to the transformer model, to make a qualitative study of the behaviour of the fields and fluxes in the core of the transformer during disconnection, and to deduce from this the relative values of the residual conditions once all currents have decayed to zero. In order to confirm these deductions, a means of obtaining numerical values for the remanent fields and fluxes is essential. There are basically two ways in which these conditions can be ascertained, i.e. by measurement or by calculation. The measurement of residual flux is relatively easily achieved by continuous monitoring using the system described in chapter 3.

The magnitude of the residual magnetic field in a particular core member may have an effect on reclosure transients, since the values of residual flux density and field strength effectively define the initial magnetisation trajectory for that core member. No means of directly measuring the magnetic field in the core has yet been devised, and, due to

the nature of the B/H characteristic, H cannot be inferred from the value of flux density. It is therefore only possible to obtain values for the residual field strength by calculation, which can be done using the transformer model described in chapter 2.

The section following describes the method used to establish residual conditions experimentally, and by calculation, the results of which are used to confirm the findings of the subsequent qualitative analysis. Also presented is a means whereby numerical values for the residual conditions may be obtained graphically, which is based on the results of the qualitative analysis.

4.5.1 Establishing residual conditions.

For the purposes of this investigation, residual conditions in the core were created by initially energising the transformer and allowing the currents, fluxes, etc., to reach steady-state before disconnecting the supply by removing, simultaneously, the gate signals to the thyristors used in controlling the switch-on conditions. The thyristors will cease to conduct only when the current falls to a value close to zero, (typically less than 50mA.). Thus for a given steady-state condition there will be a finite number of residual conditions, depending on the harmonic content of the line currents. For example, if the line currents are predominantly of fundamental frequency, then the residual conditions will depend only on the first line to be disconnected, and the polarity of the current in that line immediately before interruption, giving a total of six possible residual conditions, (3 lines x 2 polarities = 6).

Where the harmonic content causes the line current to fall to zero more than once per half-cycle of the fundamental,

the number of possible residual conditions will be correspondingly increased. This may occur, for example, in the case of a small leading power factor load.

This procedure can be simulated in the calculation of residual conditions by allowing the current in a given line to fall to zero, and adjusting the transformer equations to allow for that line being disconnected. This is repeated for each line in turn as the currents fall to zero, until the supply has been completely disconnected. At this stage in the computation there may still be circulating coil currents due to winding configuration or load, which can continue to affect flux density and field levels. The computation must therefore be continued until these currents have decayed to insignificant levels.

The accuracy to which residual conditions can be computed will depend largely on how well the transformer conditions immediately prior to, and during, supply interruption can be represented mathematically. Fig. 4.5.1 shows the recorded and computed traces for the line currents and limb flux densities in a three-limb, unloaded 8-kVA transformer with a three-wire star connected primary winding before and during a disconnection procedure in which the current in line A was the first to fall to zero after the thyristor gate signals had been removed. The computed steady-state performance prior to disconnection is obtained by allowing any transients to decay to zero following switch-on. The transient region can be minimised by selection of suitable switching conditions. Computed residual conditions are tabulted below, together with the measured values of residual flux density in each limb.

Core Member	Computed		Measured
	B (T)	H (A/m)	B (T)
Limb 1	0.09	-1.7	0.06
Limb 2	-0.61	-3.9	-0.59
Limb 3	0.52	-1.6	0.48
Yoke 1-2	0.11	-1.5	-
Yoke 2-3	0.52	-1.6	-

Although recorded and computed values of remanent flux density compare well in this case, a complete comparison of all residual conditions is not possible. A convenient indirect method is to compare recorded and computed reconnection transient currents. The transient current patterns obtained when the transformer, with the residual conditions as given above, is reconnected to the supply, is shown in Fig. 4.5.2, together with the computed pattern. The close correlation indicates that the computed residual conditions do in fact compare well with the actual values of B and H.

No attempt has been made here to compute or measure the effects of current 'chopping' or the voltage drop due to arcing in circuit breakers on the residual conditions. While it is quite possible to carry out the computation, it is extremely difficult to achieve any control over such switching conditions experimentally, and therefore no reasonable comparison of computed and experimental results could be made.

4.5.2 Qualitative analysis.

Before attempting to analyse qualitatively the establishment of residual conditions in a three-limb transformer, it is necessary to make some simplifying approximations without which the analysis would be impossibly cumbersome.

It is assumed that leakage fluxes (both coil- and phase-leakage) are negligible compared with the mutual fluxes and can be neglected. It is also assumed that coil resistance is insignificant during disconnection so that the coil e.m.f. equals the voltage, i.e. the effects of regulation can be neglected. Thus for the transformer shown in Fig. 2.4.1,

$$\phi_7 = \phi_1$$

$$\phi_8 = \phi_3$$

$$\phi_1 + \phi_2 + \phi_3 = 0 \qquad \ldots\ldots 4.5.1$$

Also, two new quantities are defined,

$$i_1^0 = i_1 + i_7$$

$$i_3' = i_3 + i_8$$

In effect, the yokes and outer limbs are considered as single sections, and values of flux are assumed to be the same in adjacent yoke and limb. Thus, since $i_4 = i_5 = i_6 = 0$, the magnetic circuit equations given in chapter 2 (eqn. 2.4.4) become,

It is evident from the symmetry of the transformer that the residual conditions created when the first line is disconnected when the current falls to zero while going positive, will be equal in magnitude but opposite in polarity to those for the same line disconnected first when the current is zero, going negative. Thus there will be only three absolute sets of residual conditions which have to be considered in this case. This does not apply to cases where the line currents have a significant even harmonic content, or where the line current falls to zero more than once per half-cycle of the fundamental.

Fig. 4.5.4 shows an example of the recorded B/t and i/t patterns taken during the disconnection of the transformer, in which the current in line X is the first to fall to zero following the removal of the thyristor gate signals. Also shown are the corresponding computed patterns. At the instant the current in line X becomes zero,

$$i_X = 0$$

$$i_A = i_C$$

and eqn. 4.5.3 reduces to,

$$i'_1 = i'_3 \qquad \text{.....4.5.4}$$

Since the flux path lengths of the two outer sections are the same, the values of field strength will be identical assuming constant cross-sectional area. If the current in line X falls to zero while going positive, then from the phasor diagram of Fig. 4.5.3 the following relationships at this point can be established,

(P71 overleaf)

$$i_1' - i_A - i_a - i_2 + i_B + i_b = 0$$

$$i_3' - i_C - i_c - i_2 + i_B + i_b = 0 \qquad \ldots\ldots 4.5.2$$

i.e. $$i_1' - i_A - i_a = i_3' - i_C - i_c \qquad \ldots\ldots 4.5.3$$

These equations can now be applied to particular cases. Since the same techniques are applied throughout, only two examples are presented here, viz., unloaded delta connected transformer, and delta connected primary with resistive load. Other selected examples including star connection and inductive and capacitive load conditions are given in Appendix A5.

(1) Delta connected primary, no load.

In this case, the magnetic circuit equations (eqn. 4.5.2) reduce to,

$$i_1' - i_A - i_2 + i_B = 0$$

$$i_3' - i_C - i_2 + i_B = 0$$

and for the electric circuit,

$$i_X + i_Y + i_Z = 0$$

Fig. 4.5.3 shows the approximate phase relationships between the steady-state currents, voltages and fluxes. These relationships are used only as a guide as to the conditions in the core and coils immediately before the disconnection procedure begins, and not for actual numerical values at this stage.

i_1' and $\emptyset_1$ are positive and increasing positively.

i_3' and $\emptyset_3$ are positive and decreasing.

i_2 and $\emptyset_2$ are near their negative maxima.

$$\emptyset_1 + \emptyset_2 + \emptyset_3 = 0$$

The general magnetic state of the core at the instant i_X becomes zero can be summarised as in Fig. 4.5.5. Here it is assumed that all sections operate in the steady-state on the same B/H characteristic, which lies near the limit cycle at rated voltage. It should be noted that the magnitude of $\emptyset_1$ is less than that of $\emptyset_3$ at this point since H_1' and H_2' are restricted to have the same value. The measured and computed core conditions at this stage are tabulated below.

Core Member	Computed		Measured
	B (T)	H (A/m)	B (T)
Limb 1	0.64	29.8	0.65
Limb 2	-1.50	-715.3	-1.50
Limb 3	0.86	29.4	0.85

The coil currents and core fluxes will begin to decay following the disconnection of line X. During this period the values of field strength in the two outer sections will remain equal, and the three main fluxes will sum to zero at all points in time. The magnitude of $\emptyset$ in the centre limb will be larger than in either of the two outer sections until the two remaining lines have been disconnected, which occurs approximately 90^o after line X, since the main component of the line current i_Y (and i_Z) is i_B with line X removed.

When all lines have been disconnected,

$$i_A = i_B = i_C \qquad \ldots\ldots 4.5.5$$

therfore,

$$i_1^{\circ} = i_3^{\circ} = i_2 \qquad \ldots\ldots 4.5.6$$

Note that all final values of magnetising current have the same polarity. The value of field strength for the centre limb will be larger than H_1° and H_3° since the flux path length is shorter. Therefore, in order to maintain $\sum \emptyset = 0$, the m.m.f.°s in the outer limb and yoke sections have become negative. The final state of the core is established at the instant the last two lines are removed since eqns. 4.5.1 and 4.5.6 cannot be satisfied simultaneously unless all core conditions are stable. This is not necessarily the case if phase-leakage flux is allowed for, but is found to be very close to the practical case.

Thus for the disconnection sequence considered, $\emptyset_1$ will, in general, be smaller than $\emptyset_3$ and have approximately the same remanent field strength. $\emptyset_2$ will be larger than, and opposite in polarity to both $\emptyset_1$ and $\emptyset_3$, while H_2 will have the same polarity as H_1° and H_3°, but will be larger in magnitude. These final conditions are illustrated in Fig. 4.5.5. The computed and measured values tabulated below confirm these general conclusions.

Core Member	Computed		Measured
	B (T)	H (A/m)	B (T)
Limb 1	0.27	-3.9	0.19
Limb 2	-0.69	-9.6	-0.70
Limb 3	0.42	-4.0	0.45

The residual conditions which are established when either of the other two lines is disconnected first can be deduced in exactly the same manner, as demonstrated in appendix A5. Computed and measured values for these conditions are tabulated below.

(a)

Core Member	Computed		Measured
	B (T)	H (A/m)	B (T)
Limb 1	0.50	-2.1	0.50
Limb 2	0.11	-5.6	0.05
Limb 3	-0.59	-1.9	-0.60

(b)

Core Member	Computed		Measured
	B (T)	H (A/m)	B (T)
Limb 1	-0.58	-1.8	-0.65
Limb 2	0.30	-5.1	0.30
Limb 3	0.31	-2.0	0.30

(a) - line Y disconnected first.

(b) - line Z disconnected first.

In each case the residual conditions are those for the current in the first line to be disconnected falling to zero while going positive. Residual conditions for the first line removed when the current in that line is zero, going negative, will be equal in magnitude, but opposite in polarity to the corresponding case considered above.

Residual conditions show a similar pattern for all disconnection sequences in an unloaded transformer with a delta connected primary winding. There are, however,

variations in the relative values of flux and m.m.f. depending on which line is first to be disconnected. It would not be valid, therefore, to attempt to define a general set of residual conditions which could be adapted to fit all disconnection sequences.

A delta connected secondary winding will have very little effect on the residual conditions, since the basic relationships remain unchanged. The two other primary winding connections, i.e. three- and four-wire star, can be treated in a similar way to the delta connected winding, as shown in appendix A5.

(2) Delta connected primary, four-wire star connected secondary with resistive load — line X disconnected first.

In the phasor diagram for this configuaration, given in Fig. 4.5.6, it is assumed that the load is sufficiently large so that the steady-state primary phase currents are approximately in phase with their respective voltage, i.e. steady-state magnetising current is small compared with the load current. The magnetic circuit equations in this case are,

$$i_1^{\circ} - i_A - i_a - i_2 + i_B + i_b = 0$$

$$i_3^{\circ} - i_C - i_c - i_2 + i_B + i_b = 0 \qquad \ldots\ldots 4.5.7$$

and, $\quad \phi_1 + \phi_2 + \phi_3 = 0$

When $i_X = 0$, while going positive,

i_1° and ϕ_1 are large negative and falling.

i_2 and ϕ_2 are small (near zero), increasing negatively.

i_3° and $\emptyset_3$ are large positive and increasing.

as illustrated in Fig. 4.5.7. Also,

$$i_A = i_C$$

$$i_Y = -i_Z$$

$$\emptyset_1 \doteq -\emptyset_3$$

As v_B falls to zero from its negative maximum, $\emptyset_2$ will become increasingly negative. v_C and v_A will also reduce with v_B from their positive values towards zero. Thus $\emptyset_1$ and $\emptyset_3$ will both increase positively since,

$$\Delta\emptyset = -\frac{1}{N}.\int e.dt$$

so that the change in $\emptyset$ will be approximately the same for $\emptyset_1$ and $\emptyset_3$ since, neglecting the effects of regulation, for a large balanced resistive load, $e_A = e_C$ when line X is removed. Thus $\emptyset_1$ will fall from its negative value towards zero, while $\emptyset_3$ and $i_3^{'}$ become larger.

All line currents will become zero when v_B is near zero, and,

i_3° and $\emptyset_3$ are very large and positive

i_2 and $\emptyset_2$ are large and negative.

i_1° and $\emptyset_1$ are small, ($\emptyset_1$ negative; i_1° positive).

as shown in Fig. 4.5.7. As circulating currents decay to zero, $\emptyset_3$ and $\emptyset_2$ will fall, and finally, as before, $i_1^{\circ} = i_2 = i_3^{\circ}$,

giving rise to the residual conditions shown in Fig. 4.5.7, which are confirmed by the computed and measured conditions tabluated below.

Core Member	Computed		Measured
	B (T)	H (A/m)	B (T)
Limb 1	-0.06	0.97	-0.10
Limb 2	-0.52	1.20	-0.55
Limb 3	0.58	1.20	0.65

Other primary winding configurations will naturally give different residual conditions to the delta connected primary considered above. These other cases can be analysed using basically the same techniques (see appendix A5). The table below lists the computed residual conditions for the three primary winding connections, with the secondary connected in star and unloaded. Results for an unloaded delta connected secondary winding were found to be virtually identical to the corresponding cases given below.

Core Member	4-wire star		3-wire star		Delta	
	B (T)	H (A/m)	B (T)	H (A/m)	B (T)	H (A/m)
Limb 1	0.27	-4.0	0.09	-1.7	0.27	-3.9
Limb 2	-0.69	-9.4	-0.61	-3.9	-0.69	-9.6
Limb 3	0.43	-3.9	0.52	-1.6	0.42	-4.0

line A (X) disconnected first when i_A zero, going positive.

It can be seen from the example given in appendix A5 that the magnetic state of the transformer core when lines A and C have been disconnected from the four-wire star

connected primary, is very similar to the delta case illustrated in Fig. 4.5.5 when i_X is zero. The subsequent decay of the fluxes and m.m.f.'s to their final residual values is the same in both instances, giving rise to the near identical conditions listed above. The examples given in appendix A5 show that the residual conditions for 4-wire star and delta primary winding connections are in fact, effectively the same for any particular disconnection sequence, for the same value of phase voltage.

In addition to the winding configuration, the size or impedance of the load, if any, on the transformer, will have an effect on remanent flux density and field strength, as was demonstrated by the unity power factor loaded case examined above. Computed results, which are shown in Fig. 4.5.8 illustrate the variation in residual flux density with load kVA for a three-wire star connected primary winding. As the load is reduced, residual flux levels tend towards those found for the unloaded case, as would be expected. Changes in residual flux density are also found as the power factor is varied, while maintaining the load impedance constant, as shown in Fig. 4.5.9(a) and (b). As in the no-load case, the same residual conditions are obtained for four-wire star and delta connected primary windings (Fig. 4.5.9(b)).

The results given above, and in appendix A5, for the residual conditions established when the supply to a three-phase transformer is interrupted, show the same general trends as in the single-phase case, i.e. that resistive loads tend to ensure large residual flux levels, while low power factor inductive loads will produce conditions close to the de-magnetised state. Residual conditions for a capacitive load on the transformer are difficult to predict in either type of

transformer, but the damped oscillations which can occur following disconnection of the supply will tend to de-magnetise the core in both cases, and the final residual flux levels will be critically dependent on the frequency and amplitude of these oscillations.

Results for the limb fluxes during interruption of the supply to a three-phase transformer, which has a large leading power factor load, given in Fig. 4.5.10, show that the rate of damping of the oscillations is larger in practice than predicted using the transformer model described in chapter 2. The reason for the discrepancy is, as indicated previously, almost certainly the effect of eddy current losses in the core. The rapid decay of the oscillations will tend to maintain the levels of residual flux, and thus, in practice, the values of remanent flux density will be larger than those computed.

Although the load power factor for a power transformer will usually be close to unity, the case where winding self-capacitance in an h.v. winding is significant can be approximated by loading the transformer in the computer program with a leading power factor load. Tests on an 11kV/433v, 50-kVA distribution transformer, details of which are given in appendix A1, were carried out in order to confirm that the transformer model was valid for larger transformers than had previously been used in the department. Results were taken for various conditions of switching angles and residual conditions, using a value of winding self capacitance which was estimated from results of the test described in chapter 3. No attempt was made to load the transformer for reasons of safety.

Figs. 4.5.11 and 4.5.12 show examples of the computed and recorded transient currents for this transformer, which were taken at reduced voltage in order to prevent damage to

the switching thyristors which had a peak current rating of 180 A. The results for zero residual conditions show that the accuracy achieved is similar to that for the smaller, 8-kVA transformer. However, attempts to compute residual conditions following supply interruption were not successful, as can be seen from the results in Fig. 4.5.12. Again, this is due to the effects of eddy currents limiting the extent of de-magnetisation.

4.5.3 Graphical estimation of residual conditions.

The values of remanent flux density obtained by computation correspond closely with measured values (except where capacitance is significant), demonstrating that this is a valid method of evaluating residual conditions to within reasonably close limits. The computation time (and cost) may be saved by utilising the findings of the qualitative analysis to produce numerical values for the various residual quantities. A graphical method has therefore been devised which should allow residual conditions to be estimated to within perhaps ±20% of the actual values.

The method utilises the recorded B/H characteristic which is modified to produce intermediate trajectories using the interpolation technique for the mathematical representation presented in chapter 2. It is assumed that all sections of the core operate on the same steady-state B/H cycle, which is the case if the core has the same cross-sectional area at all points, and the transformer is energised from a balanced three-phase supply.

The no-load case considered above, i.e. delta connected primary winding, is used as an example of the technique. Consider the phasor diagram of Fig. 4.5.3. When the current in line X falls to zero while going positive, $\emptyset_1$ and $\emptyset_3$ are

both positive and sum to the peak value of $\emptyset$ since $\emptyset_2$ is near the negative peak, and $\sum \emptyset = 0$. Neglecting the effects of regulation, the limb flux is given by,

$$\emptyset = \emptyset_o - \frac{1}{N}.\int v_{ph}.dt$$

where, $v_{ph} = \hat{V}_{ph}.\sin(\omega.t)$

The peak value of the steady-state flux is therefore given by,

$$\hat{\emptyset} = \frac{\hat{V}_{ph}}{\omega.N}$$

and,

$$\hat{B} = \frac{\hat{V}_{ph}}{N.A.\omega}$$

since all core sections have the same cross-sectional area. Substituting numerical values for $\hat{V}_{ph}$, N, A and ω from appendix A1 gives,

$$\hat{B} = 1.51 \text{ Tesla}$$

This information allows the steady-state B/H loop of Fig. 4.5.13 to be derived from the magnetisation characteristic of the transformer given in Fig. 3.2.4(a). Since flux paths 1 and 3 are operating on different parts of the B/H cycle at this point in time (see Fig. 4.5.5), and from eqn. 4.5.4, $i_1' = i_3'$, it is necessary to search for a value of H which will give $B_1 + B_3 = 1.51$ Tesla. This can be done by inspection, and leads to the following conditions,

$$H_1' = H_3' = 26 \text{ A/m.}$$

$$B_1 = 0.61 \text{ T.}$$

$$B_3 = 0.90 \text{ T.}$$

as shown in Fig. 4.5.13.

As before, the flux in limb 3 will continue to decay along the upper boundary curve, while B_2 follows the lower boundary curve. It is necessary to generate a new trajectory for the flux in limb 1, which can be done knowing the point at which the new curve originates, as shown in Fig. 4.5.13. The final relationships, which apply when all coil currents are zero are,

$$\phi_1 + \phi_2 + \phi_3 = 0$$

$$i_1' = i_2 = i_3'$$

and, taking into account the flux path lengths and cross-sectional are of the core members,

$$B_1 + B_2 + B_3 = 0$$

$$H_1^o = H_3' = 0.41.H_2$$

The residual conditions, which are obtained by finding points on the B/H trajectories which satisfy these equations, by trial and error methods, are listed below, together with computed and measured values. Very close correlation between computed and estimated residual conditions has been achieved in this case, with the maximum difference in flux density values being about 5%, and a maximum difference of 7% in the field strength.

Core Member	Estimated		Computed		Measured
	B (T)	H (A/m)	B (T)	H (A/m)	B (T)
Limb 1	0.28	-3.7	0.27	-3.9	0.19
Limb 2	-0.72	-9.0	-0.69	-9.6	-0.70
Limb 3	0.44	-3.7	0.42	-4.0	0.45

The residual conditions obtained above are sufficiently accurate to allow reconnection transient currents to be computed to within a few per cent of recorded values, as shown in the example given in Fig. 4.5.14.

4.6 Effect of Residual Conditions on Reclosure Transients.

The maximum level of flux in any section of the core is very dependent on the initial value since,

$$\phi = \phi_o - \frac{1}{N} \cdot \int e \cdot dt$$

As it is the peak flux which determines the magnitude of the transient magnetising currents, this initial value of flux will have a considerable effect on the transient current peak, particularly in the case of a highly nonlinear magnetisation characteristic. A small value of ϕ_o can result in a large increase in the magnitude of the peak transient current over the case where ϕ_o is zero.

Conversely, as has been shown in the single-phase transformer (Fig. 4.2.9), residual flux can also reduce the peak transient current, depending on whether the direction of ϕ_o tends to reduce or enhance the value of maximum flux. For example see Fig. 4.6.1. Since switching conditions are usually random, the precise effect which residual flux will

have on reclosure transients is impossible to predict. However, knowing the winding configuration, type of load, transformer parameters, etc., it is possible to compute the range within which the transient current peaks will lie. This range will inevitably be much wider than for zero residual conditions only considered.

In a study of this type there is an infinite variety of combinations of winding configuration, switching angles, load, switching sequence, etc., all of which will have some effect on the residual conditions or subsequent reclosure transients. It is not possible, therefore, to present a comprehensive set of computed and experimental results which covers all possible conditions. The accuracy of the computed transients using the transformer model given in chapter 2 has already been demonstrated in this chapter, as well as in reference 1. The examples given below, which are used to illustrate the major influences of the various factors affecting transient behaviour, are predominantly computed results, with occasional recorded results presented to validate certain observations.

4.6.1 Significance of residual phase-leakage flux and m.m.f.

MacFadyen[1] has demonstrated the importance of incorporating phase-leakage flux in the transient calculations, and so allowance for this was invariably made. It was found that the use of the zero-sequence inductance in place of measured values of phase-leakage inductance did not give rise to significant changes in the computation of switching transients. In the qualitative analysis of the establishment of residual conditions, however, it was assumed that phase-leakage flux was negligible compared with the main core fluxes. In order to examine the effect of neglecting residual phase-leakage flux,

the values associated with each phase-leakage path were set to zero by making outer limb and adjacent yoke flux densities and field strengths equal. Several computer runs were made which, as the example given in Fig. 4.6.2 shows, indicated that this does not have a serious effect on the reclosure transients.

If the values of residual field strength in all core sections are also set to zero, then for the case considered above, the difference between results computed using the complete set of residual conditions, and those using the basic information only (i.e. residual flux density in the three limbs) is no greater than about 1% at the peak current value. It should therefore be possible to predict, within a reasonable degree of accuracy, the reclosure transients for a transformer of this type, knowing only the level of remanent flux in each limb, which may be obtained experimentally, or by graphical means (see Fig. 4.5.14).

4.6.2 Switching conditions.

It has already been stated that the residual conditions which result when the current in the first line to be disconnected from the transformer is zero, going positive, will be equal in magnitude, but opposite in polarity to those which are established when the current is zero, going negative. In a de-magnetised transformer, the inrush currents for a particular set of switching conditions will be equal and opposite to those obtained when the first switching angle is altered by 180^{o}, as shown in Fig. 4.6.3. This is not the case when residual conditions are present. If the initial switching angle is changed by 180^{o}, the resulting transient currents will differ considerably in magnitude from the original values, as shown in

Fig. 4.6.4. A change in the polarity of the residual conditions is also required before the transient currents will have the same magnitude, as illustrated by the two examples given in Fig. 4.6.4.

In Fig. 4.6.5, the variation in peak transient current with simultaneous switching angle is shown, for an unloaded transformer with a delta connected primary winding. These results demonstrate the considerable effect which residual conditions have over the entire switching range, causing increases of more than 50% in the largest value of peak current in lines Y and Z. Residual conditions will have a similar effect for other primary winding connections, as in the case of a three-wire star connection, shown in Fig. 4.6.6.

For a de-magnetised transformer, the largest transient currents are usually found when the transformer is energised non-simultaneously ($\alpha = 0^{o}$ or 180^{o}; $\beta = 90^{o}$), as the curves in Fig. 4.6.7 indicate. When residual conditions are present, it is found that the same switching conditions can also produce maximum peak transient current, depending on the nature of the residual conditions, i.e. whether the polarity of residual flux tends to enhance or diminish the peak level of transient flux. For the switching sequence considered, the results in Fig. 4.6.7 show that residual conditions established when line X is disconnected first cause a 35% increase in the largest current peak (line Y) over the de-magnetised case. Fig. 4.6.7 also shows that, for non-zero residual flux, the switching conditions which result in minimum transient current are, in general, $\alpha = 90^{o}$ or 270^{o}; $\beta = 90^{o}$ or 270^{o}, as for a de-magnetised transformer.

It is also necessary to consider the reconnection transient currents obtained when the transformer is loaded,

since, as has been demonstrated, the size and power factor of the load has considerable influence on the residual conditions established for a given disconnection sequence. The transient currents for a unity power factor load show a marked dependence on residual conditions, as would be expected. Fig. 4.6.8 illustrates the considerable effect which residual conditions can have on the transient current patterns, for this type of load. The effect of remanent flux on the variation, with switching conditions, of peak transient current in each line, for simultaneous and non-simultaneous switching is shown in Figs. 4.6.9 and 4.6.10 respectively. The range over which the peak currents vary is not as great in this case as for the unloaded transformer. This is due to the large steady-state current level which restricts the minimum transient current values.

For a low power factor inductive load, however, the range over which the peak transient currents vary will not be as great as in either the no-load or unity power factor load cases. This is a consequence of the de-magnetising effect of the load, which, if purely inductive, will effectively result in zero residual conditions when the supply is disconnected, and all reconnection transient current patterns for a given set of switching conditions will be virtually the same, irrespective of disconnection sequence. An example of the transient current patterns obtained for this type of load is given in Fig. 4.6.11. Fig. 4.6.12 shows the expected variation in peak transient current with simultaneous and non-simultaneous switching conditions for a hypothetical zero power factor inductive load.

No results for a capacitively-loaded transformer are presented here owing to the problems associated with evaluating residual conditions (see Figs. 4.5.10 and 4.5.12).

Where no residual flux is present, if the switching conditions are specified with respect to the voltage of the first phase or line to be connected, the variation in the transient current patterns of the first and subsequent lines to be connected is small as shown in Fig. 4.6.13. The maximum difference in the magnitude of the current peaks for corresponding lines is about 3% for the example given, although variations of up to 12% were found where the transient peaks were very large. This figure is small compared to the 125% variation found when residual conditions are present, as the example in Fig. 4.6.14 shows.

These large differences are due to the relative variation of remanent flux from limb to limb as the connection sequence is changed. It is therefore important to specify the switching sequence together with the other parameters when considering reconnection transients.

-CHAPTER 5-

FERRORESONANCE

The solution to ferroresonance problems has usually been sought in one of two forms,

1. Analytical solution[22,23,28], where the various quantities are obtained as explicit functions of the system parameters. These functions normally take the form of a power series.

2. Topological or phase-plane solution[22,23,25], which, in general, gives more qualitative information about ferroresonant conditions rather than the currents, voltages, etc., as explicit functions of time.

Both techniques are extremely valuable in the study of the phenomenon of ferroresonance and have been extensively applied to this end. While these methods will undoubtedly continue to be utilised and developed, there exists presently serious limitations as to their application in higher order systems such as those incorporating three-phase transformers[27]. Since topological and analytical solutions are highly desireable from the point of view of obtaining the maximum amount of information for the minimum effort, ferroresonance in a three-phase system may be reduced to the equivalent single-phase case[26] for ease of solution. This treatment is only valid for a limited number of situations, for example, where resonance occurs in one phase only[24].

The case where a three-phase ferroresonant condition is treated strictly as such appears to have been almost

totally neglected. Numerical methods of solution (for example see reference 22) do not suffer from the limitations of phase-plane or analytical techniques in that it is quite possible to obtain a solution to highly complex problems without sacrificing accuracy or over-simplifying the situation to a point where results are highly questionable. The main disadvantage of this type of approach is that each single set of initial conditions and system parameters must be analysed individually in order to build up a complete picture of the phenomenon. This naturally requires a large amount of computational effort which may be prohibitive in a general study of ferroresonance. It is also less valuable than topological methods in leading to a better understanding of the subject of ferroresonance.

When applied to specific systems, however, the amount of computer time necessary to obtain the solution to a given problem will be relatively small, and a more accurate and true analysis of system behaviour may be derived.

5.1 Single-Phase Ferroresonance.

Fig. 5.1.1(a) shows the simplest practical ferroresonant circuit which is usually the basis for a study of the subject. Swift[25] uses a parallel L-C arrangement as shown in Fig. 5.1.1(b) which is a crude representation of an unloaded single-phase transformer energised through a long feeder line. Since the present investigation is not concerned with specific applications, rather than validating a method of numerical analysis, the former circuit was chosen owing to its simplicity.

The differential equation for the circuit may be written,

$$v = i.R + N.p\emptyset + \frac{1}{C}.\int i.dt \qquad \ldots\ldots 5.1.1$$

This equation may be differentiated with respect to time, i.e.,

$$pv = R.pi + N.p^2\emptyset + i/C \qquad .....5.1.2$$

If the relationship between the current and flux is obtained from the magnetisation characteristic of the nonlinear inductor and expressed as,

$$i = f(\emptyset)$$

then by substituting for i in eqn. 5.1.2 the following equation is obtained which may be solved using one of the methods indicated,

$$pv = R.p[f(\emptyset)] + f(\emptyset)/C + N.p^2\emptyset \qquad ..5.1.3$$

Owing to the highly complex nature of the magnetisation characteristic of an iron-cored coil, the function $f(\emptyset)$ cannot be written explicitly in terms of flux. The function is almost invariably approximated by a single-valued power series which usually has the form,

$$i = a.\emptyset + b.\emptyset^3 \qquad .....5.1.4$$

The cubic term is sometimes replaced by one of fifth or seventh order, depending on the shape of the magnetisation characteristic and the type of solution sought.

Combining eqns. 5.1.3 and 5.1.4, assuming sinusoidal excitation, and neglecting losses (i.e. R=0), then the following equation is obtained,

$$\omega E\cos\omega t = N.p^2\emptyset + \frac{a}{C}.\emptyset + \frac{b}{C}.\emptyset^3 \qquad \ldots.5.1.5$$

which is the classical differential equation known as 'Duffing's Equation'.

Alternatively, the equations for the circuit shown in Fig. 5.1.1(a) can be written as,

$$v = i.R + l.pi + M.pi + q/C \qquad \ldots\ldots.5.1.6$$

and, $$pq = i \qquad \ldots\ldots.5.1.7$$

Equations 5.1.6 and 5.1.7 may be solved simultaneously using a method of numerical integration to give the system voltages and currents directly. It is possible in this case to use a highly accurate representation of the magnetisation characteristic without unduly increasing the complexity of the method of solution.

5.1.1 Modes of ferroresonance.

There are basically two types of resonance which may occur, viz., subharmonic in which the voltages and currents contain components of frequencies which are integral submultiples (predominantly 1/3 or 1/5) of the supply frequency, and fundamental resonance in which the only significant harmonics are of a higher frequency than the supply. In general, the conditions associated with subharmonic resonance are much less severe in terms of voltage and current than with fundamental resonance.

The single-phase transformer which was used to produce the results given in chapter 4 was connected in series

with a 6.8μF capacitor to give the circuit shown in Fig. 5.1.1(a). Fig. 5.1.2 shows the computed and recorded steady-state current, voltage and B/H patterns obtained for the initial conditions indicated. It can be seen that the fundamental component of frequency of the current and voltage waveforms has a period of 60ms, i.e. a frequency of $16\frac{2}{3}$ Hz. This condition is therefore one of subharmonic ferroresonance. It was found experimentally that this condition was stable only over a relatively small range of applied voltage, i.e. from about V=90v to V=160v. An interesting aspect of this condition was that as the applied voltage was increased, the value of peak current fell, so that at 140v the B/H pattern shown in Fig. 5.1.3 was obtained, which has a lower peak current (and flux density) than that shown in Fig. 5.1.2.

Reduction in the applied voltage below 115v gave rise to the current waveform shown in Fig. 5.1.4. The asymmetrical nature of the waveform indicates the presence of a component of frequency twice that of the fundamental. Since the apparent fundamental frequency is $16\frac{2}{3}$ Hz. - 1/3 that of the supply, then this component has a frequency of $33\frac{1}{3}$ Hz. or 2/3 the supply frequency. The computed results also exhibt the asymmetrical form found experimentally.

In order to demonstrate the significance of hysteresis in estabishing subharmonic ferroresonance, an attempt was made to compute this condition using a single-valued representation of the transformer magnetisation characteristic. The results of this computation are presented in Fig. 5.1.5(b) along with recorded and computed current waveforms obtained from the ferroresonant condition shown in Fig. 5.1.3. This appears to confirm the view expressed by Swift[28] that - 'subharmonic stability is critically dependent on losses in the

circuit[9]. While there are certainly subharmonic components of frequency in the current waveform illustrated, a prolonged computation failed to stabilise. Although it is not valid to draw concrete conclusions from a single result such as this, it is nevertheless difficult to accept the possibility of an analytical solution giving reasonable results in this case, since numerical methods properly applied are inherently more accurate in solving a problem of this type. The fact that analytical methods often lead to sucess must be due in part to the fact, demonstrated by Hayashi[22], that the method of representation of the magnetisation characteristic and the form of the solution can be chosen to give acceptable results in cases such as this.

An increase in applied voltage results in a spontaneous jump from a non-resonant condition to one of fundamental ferro-resonance at approximately 230v. Once in this condition the applied voltage can be reduced to a value of about 65v before resonance failed to be sustained. Fig. 5.1.6 shows the value of peak current obtained experimentally as the r.m.s applied voltage was varied together with some computed results. Also shown is the region in which subharmonic ferroresonance is sustained, which has a negative slope in the stable portion of the curve.

An example of recorded and computed results for a fundamental resonant condition (V=200v) is given in Fig. 5.1.7. This illustrates the statement made above that this condition is more severe that that of subharmonic resonance. Character-istic of this mode of ferroresonance is the high third harmonic content of the current and voltage waveforms which gives rise to current spikes as shown.

In practice, three modes of single-phase ferroresonance could be distinguished. On increasing the applied voltage

beyond that required to establish fundamental resonance, a third type becomes evident which is characterised by a large second harmonic component of frequency in the steady-state current and voltage waveforms, which results in an unsymmetrical B/H pattern as illustrated in Fig. 5.1.8. The discrepancy between computed and recorded B/H patterns in this case, and in Fig. 5.1.7, is due to the effect of eddy currents, which is not incorporated in the computed results. This mode of ferroresonance has been observed previously[29] and it was proposed that the condition might be utilised in computer logic or memory circuits. This application would appear impractical today due to the relatively large power losses and bulk involved in such a system, compared with modern integrated circuit devices.

5.2 Ferroresonance in Three-Phase Systems.

Ferroresonance has been observed in three-phase systems under a variety of conditions[30,31,32]. The system may appear to resonate in one phase only, or a true three-phase condition may occur. In all cases of ferroresonance found in practice, the condition is initiated by some form of system disturbance. This disturbance may take the form of switching transients (connection or disconnection), load-shedding or a fault causing disconnection of one or two lines only.

Perhaps the most interesting occurrence of ferro-resonance in a three-phase system is that which takes place when the supply to an unloaded or lightly loaded transformer which is fed from one side of a double-circuit line (Fig. 5.2.1) is interrupted. The second circuit is used to supply

a remote load. In practice, when the two circuits are energised, the voltage between lines of the same phase at any distance from the busbars is effectively zero, and capacitive coupling between lines will have relatively little effect on the steady-state performance of the system.

If the supply to the transformer is interrupted at a point remote from the transformer, the capacitive coupling between the lines of the feeder circuits may cause ferro-resonance to be initiated, even though there is no direct connection between the transformer and the busbar. This will be a true three-phase condition, usually associated with systems with floating neutral. As will be shown, it is possible for resonance to occur in a system with the star point of the transformer earthed. One phase of a crude model of this situation is shown in Fig. 5.2.1(b). This simplified version of the conditions described above was used to obtain experimental results in the laboratory.

Obviously, to reliably predict the initiation of ferro-resonance, rather than the conditions required to sustain resonance, once initiated, the system conditions immediately prior to the disturbance which precedes the resonant condition must be accurately specified. Since the system will usually be operating in steady-state before the disturbance takes place, a means of establishing these conditions was adopted, which was similar to that used to compute residual conditions in chapter 4. The series capacitor shown in Fig. 5.2.2 was initially short-circuited and the system allowed to settle into a non-resonant steady-state condition, after connecting the supply. At a predetermined point on the supply voltage waveform, the switches across the series capacitors were

opened simultaneously in all three lines, and the system again allowed to settled into steady-state.

5.2.1 Three-phase system equations.

The mathematical model used in the computation of three-phase ferroresonant conditions was that described in chapter 2, with suitable modifications to take account of series and parallel capacitance. For the case described above (i.e. earthed neutral), the primary voltage equations may be written,

$$v_A = i_{sA}.R_s + l_s.pi_{sA} + q_{sA}/C_{sA} + q_{pA}/C_{pA}$$

$$v_B = i_{sB}.R_s + l_s.pi_{sB} + q_{sB}/C_{sB} + q_{pB}/C_{pB}$$

$$v_C = i_{sC}.R_s + l_s.pi_{sC} + q_{sC}/C_{sC} + q_{pC}/C_{pC}$$

Also,

$$q_{pA}/C_{pA} = i_A.R_A + l_A.pi_A + M_1.pi_1$$

$$q_{pB}/C_{pB} = i_B.R_B + l_B.pi_B + M_2.pi_2$$

$$q_{pC}/C_{pC} = i_C.R_C + l_C.pi_C + M_3.pi_3$$

Incorporating these equations into the transformer model, the following matrix equation is obtained,

$$
\begin{bmatrix} 0 \\ \hline 0 \\ \hline 0 \\ \hline V_4 \\ \hline V_5 \\ \hline V_6 \\ \hline V_7 \end{bmatrix} =
\begin{bmatrix}
M_1+M_4+M_7 & -M_7 & & -M_4 & -M_4-M_7 & M_7 & \\ \hline
-M_7 & M_2+M_5+M_7+M_8 & -M_8 & -M_5 & M_7 & -M_5-M_7-M_8 & M_8 \\ \hline
 & -M_8 & M_3+M_6+M_8 & -M_6 & & M_8 & -M_6-M_8 \\ \hline
M_1 & M_2 & M_3 & l_a+l_b+l_c & & & \\ \hline
M_1 & & & & l_A & & \\ \hline
 & M_2 & & & & l_B & \\ \hline
 & & M_3 & & & & l_C
\end{bmatrix}
\cdot
\begin{bmatrix} pi_1 \\ \hline pi_2 \\ \hline pi_3 \\ \hline pi_a \\ \hline pi_A \\ \hline pi_B \\ \hline pi_C \end{bmatrix}
$$

where,

$$v_5 = q_{pA}/C_{pA} - i_A.R_A$$

$$v_6 = q_{pB}/C_{pB} - i_B.R_B$$

$$v_7 = q_{pC}/C_{pC} - i_C.R_C$$

The zero-sequence equation, for which,

$$v_4 = -i_a.(R_a + R_b + R_c)$$

caters for a delta-connected secondary winding.

The remainder of the system quantities are found from the following additional differential equations,

$$pi_{sA} = (v_A - i_{sA} \cdot R_A - q_{sA}/C_{sA} + q_{pA}/C_{pA})/l_s$$

$$pi_{sB} = (v_B - i_{sB} \cdot R_B - q_{sB}/C_{sB} + q_{pB}/C_{pB})/l_s$$

$$pi_{sC} = (v_C - i_{sC} \cdot R_C - q_{sC}/C_{sC} + q_{sC}/C_{sC})/l_s$$

$$pq_{sA} = i_{sA} \quad : \quad pq_{pA} = i_{sA} - i_A$$

$$pq_{sB} = i_{sB} \quad : \quad pq_{pB} = i_{sB} - i_B$$

$$pq_{sC} = i_{sC} \quad : \quad pq_{pC} = i_{sC} - i_C$$

The equations for any other circuit configuration may be derived in the same manner as the example given above. Solution of the equations is carried out as before using a numerical integration technique.

The opening of the switches across the series capacitors is simulated in the computer program by restricting the capacitor charges to zero at each step in the computation until the point corresponding to the opening of the switches, where the values of q for the series capacitors are allowed to vary according to the differential equations given above.

5.2.2 Results.

Initially, a series of experimental tests were carried out in order to establish the conditions required for subharmonic and fundamental resonance. It was found that, for the laboratory model, the conditions required for the initiation of subharmonic resonance were very critical indeed. A slight variation in the nominal supply voltage of 107v rms/phase, and/or the switching conditions for the series capacitors (opened when V_A at 137^o or 317^o) prevented a stable resonant state from being established.

The steady-state current and voltage waveforms for this condition are shown in Fig. 5.2.2. As can be seen, very close agreement between computed and recorded results was achieved. A similar correlation between experimental and computed results was found in terms of the critical influence of the system conditions on the establishment of stable subharmonic resonance. A change of one step length (0.0002s = 3.6^o at 50Hz.) in the point in the computation at which the series capacitor switches were opened resulted in a non-resonant condition, even though the transient voltages and currents immediately following the opening of the switches were virtually indistinguishable from those leading to a stable resonant condition. Computed and recorded results for the transient voltage in phase B of the transformer following the switching operation are shown in Fig. 5.2.3. These results highlight the importance of the transient region between non-resonant and resonant states.

An attempt to compute subharmonic ferroresonance using a single-valued function representation of the B/H characteristic of the transformer was, as in the single-phase

case, completely unsuccessful. It was not possible, despite prolonged computation and reduced step length, to establish a recognisable steady-state condition, thus further emphasising the necessity of incorporating the non-unique nature of the B/H relationship in calculations of this type.

Further experimental investigation led to the discovery of a second subharmonic condition, for which the predominant subharmonic frequency was 10Hz., i.e. 1/5 of the supply frequency. The steady-state current and voltage waveforms are shown in Fig. 5.2.4, together with the system parameters. This condition is much more severe in terms of the voltage and current magnitudes than the 1/3 subharmonic condition above. Although several attempts were made to compute the 1/5 subharmonic resonant condition, using various step lengths in the numerical integration, the computed transients caused by the opening of the switches very rapidly deviated from the experimental values, thus failing to initiate a stable resonant condition.

Fundamental resonance normally involves higher voltages and currents than subharmonic resonance, for the same system parameters, as was shown in the single-phase case. It was observed in the experimental work that fundamental resonance in the three-phase system was readily initiated, and variations in voltage and switching were far less significant than for subharmonic resonance. Despite this apparantly reduced requirement for accuracy in specifying the system conditions, computed results were much less satisfactory than in the 1/3 subharmonic case, although recognisable steady-state voltage and current waveforms could be obtained which had the same general form as the

recorded waveforms, as the example in Fig. 5.2.5 shows. The computed results appear to contain a component of frequency which is 1/2 that of the supply, and which is absent from the recorded waveforms.

Fig. 5.2.6 shows the voltage across phase B of the transformer immediately prior to, and following the opening of the series capacitor switches. The computed and recorded waveshapes correspond reasonably well up to about 40ms after the switches are opened, but subsequently diverge. The large voltages which appear across the transformer terminals indicate high rates of change of flux density in the core. This in turn leads to large eddy current losses and possible changes in the magnetisation characteristic of the core due to skin effect in the laminations. It is therefore not surprising to find a lack of correlation between computed and experimental results in this case, since eddy currents are not catered for in the computation.

This deduction is supported by the fact that the highly accurate computed results which were obtained for the 1/3 subharmonic resonant condition, were produced by the identical computer program used to produce the waveforms given in Figs. 5.2.5 and 5.2.6, the only difference being the magnitude of the applied voltage (V_{ph} = 107v and 270v). Since eddy current losses are unlikely to be significant in the low voltage, subharmonic resonance case, compared with the effects of hysteresis, it seems reasonable to conclude that the discrepancies found between computed and recorded results when the voltage is increased, are due to the damping effect of eddy current losses.

The possibility that these discrepancies are due to

rounding errors in the computation was investigated by running the same program on two different computers (ICL 1904S and GE415) with different rounding errors. The results produced corresponded to within 0.1% even after several thousands of steps. Since the rounding errors for the two computers differ by a factor of 2 (1 byte) this source of error can be discounted.

It should be noted, however, that while it was not possible to compute accurately the waveshapes of the currents and voltages for fundamental resonance, it was nevertheless possible to show that ferroresonance had been established.

-CHAPTER 6-

CONCLUSIONS AND SUGGESTIONS FOR FURTHER WORK

The advantages and disadvantages of the various approaches to transformer analysis have been discussed in chapter 2, which indicate that an accurate representation of the electromagnetic relationships can be achieved using the techniques developed in references 1 and 2, without recourse to complex and time-consuming magnetic field analysis. It has been shown that assuming the transformer core to be magnetically isotropic does not lead to significant discrepancies between theory and practice, although variations in the magnetic properties from point to point in the core due mainly to corner effects, can have a large effect on the form of the measured B/H characteristic.

A preliminary examination of corner effects has shown that these may be catered for directly in the transformer model using similar equations as for the rest of the magnetic circuit, and assuming a discretely variable magnetisation characteristic. Thus the necessity to carry out flux and field measurements on the completed transformer may be avoided.

The transformer model can also be extended to cater for multi-winding transformers, using the concept of mutual leakage inductance. For a transformer with more than two windings per phase, as shown in Fig. 6.1(a), flux may link with two or more coils on the same limb, but fail to link all coils. Allowance can be made in the transformer equations for the mutual components of leakage flux by incorporating

a mutual leakage inductance term in the voltage equations.

The use of an exponential series to represent the complete, multi-valued B/H relationship for the transformer core is a logical extension to the single-valued representation used by MacFadyen[1]. The high degree of accuracy achieved in the representation of magnetisation characteristics has been demonstrated in two ways,

(i) By comparison of the series representation of the B/H characteristics of several transformers with recorded curves.

(ii) By the degree of correlation between computed and recorded patterns of transient and steady-state current, voltage and flux.

Generation of intermediate B/H trajectories by interpolation between curves which are explicitly represented, does not allow for the intersection of increasing curves, which has been shown to take place under certain circumstances (see Fig. 2.6.7 and appendix A4). Considering the accuracy achieved in using the simple interpolation technique, it is unlikely that significant errors are introduced by failing to allow curves of the same type to intersect.

Throughout the investigation, eddy currents in the core have been deliberately neglected. This was done in order to highlight the areas where eddy currents have the greatest influence. If, as is assumed in the transformer analysis, the flux in any core member is evenly distributed over the cross-sectional area of the iron, then the conventional method of representing the effects of eddy currents in the analysis, by a resistive load on a secondary winding, is valid, as long as there is one such arrangement for each core member.

Alternatively, for uniform flux density, the magnitude of the eddy current in a lamination is proportional to the rate of change of flux density, which is evaluated for each core section at every stage of the analysis, and which could therefore be used to obtain a value for the eddy current. Many of the instances where eddy currents have been found to have a significant effect on transformer behaviour involve large rates of change of flux (e.g. ferroresonance and supply disconnection), which can cause the flux distribution in the core laminations to vary due to skin effect. It may be necessary therefore to investigate this phenomenon in detail before eddy currents can be adequately represented.

In chapter 4, the processes involved in the establishment of residual core conditions following supply interruption were examined, and it was shown that for a given system operating in steady-state, there are only a finite number of residual conditions which can occur, if disconnection takes place at a natural current zero. The effect which these residual conditions have on subsequent reclosure transients has been shown to be considerable in the case of a transformer which is unloaded, or has a near-unity power factor load. Large, low power factor loads (inductive or capacitive), tend to produce near-zero residual conditions following supply disconnection, so that relatively little variation in the reclosure transients will occur, for any given switching conditions.

There is little doubt that the large discrepancies found between computed and recorded disconnection and reclosure transients, where system capacitance was significant, were due to eddy current losses in the core. Since, in M.V. and H.V. systems, capacitance is generally present in the form of transformer winding self-capacitance, as in the case of the 50-kVA distribution transformer considered in chapter 4, and

line-to-earth and line-to-line capacitance, it will be necessary to incorporate some means of allowing for eddy current loss in distribution and transmission transformers when computing residual conditions.

A simple series resonant circuit has been used in chapter 5 to demonstrate the three modes of ferroresonance which can be distinguished in single-phase systems, i.e. subharmonic, normal or fundamental, and asymmetric or superharmonic resonance. The accuracy achieved in computing the steady-state conditions for each of these modes shows that the method of analysis, based on the transformer model of chapter 2, is valid in this case.

Although one case of subharmonic resonance in a three-phase system was sucessfully computed, attempts to compute fundamental resonance failed to achieve a reasonable degree of correlation with experimental results - again due eddy current effects. It has been shown, however, that ferroresonance is not necessarily restricted to single-phase conditions, and since analytical techniques are unlikely to yield useful results in polyphase cases, numerical methods of analysis such as that used in the present investigation, appear to offer the best alternative. Further development of the transformer model is essential, particularly with regard to iron losses, in order to produce reliable and accurate solutions.

The study of ferroresonance is only one example of the possible extension of the range of application of the transformer model. The use of vacuum circuit breakers in distribution systems creates problems in transformer protection due to the high voltages induced in the windings, caused by the current-chopping properties of these devices. The method of

analysis used in the computation of residual conditions can be readily adapted to provide a means of determining transient overvoltages due to current-chopping, and ways in which these may be minimised to avoid damage to transformers which are switched using v.c.b's.

A further application is in the study of transformer performance under various secondary circuit conditions, including unbalanced, single-phase, two-phase and nonlinear loads, as well as short-circuits etc. Other static electro-magnetic devices may also be modelled, and their transient and steady-state performance determined, using the same techniques as for the transformer. For example, of interest to power system protection engineers is the performance of current transformers during transient conditions. The behaviour of voltage stabilisation equipment and short-circuit limiting couplings during sudden load changes are other areas where this type of approach could prove valuable.

REFERENCES

1. MacFadyen, W.K: ' Transient Currents in Nonlinear Electromagnetic Devices ', Ph.D. Thesis, University of Strathclyde, 1973.

2. Nakra, H.L., and Barton, T.H: ' Three-Phase Transformer Transients ', IEEE Trans.,1974, PAS-93, pp. 1810-1819.

3. Carpenter, C.J., and Djurovic, M: ' 3-Dimensional Computation of Transformer Leakage Fields and Associated Losses ', IEEE Trans., MAG-11, 1975, pp. 1535-1537.

4. Andersen, O.W: ' Transformer Leakage Flux Program Based on the Finite Element Method ', IEEE Trans., 1973, PAS-92, pp. 682-689.

5. Monaco, A.D., Giuseppetti, G., and Tontini, G: ' Studio di Campi Elettrici e Magnetici Stanzionari con il Metodo Degli Elementi Finiti - Applicazione ai Trasformatori ', Elettrotechnica, 1975, Vol. 62, No. 7, pp. 585-598.

6. Sabir, S.A.Y., and Shepherd, W: ' Magnetic properties of Alcomax III with dynamic excitation ', Proc. IEE, 1974, 121, (8), pp. 907-912.

7. Silvester, P., and Chari, M.V.K: ' Finite Element Solution of Saturable Magnetic Field Problems ', IEEE Trans., 1970, PAS-89, pp. 1642-1651.

8. Trutt, F.C., Erdelyi, E.A., and Hopkins, R.E: 'Representation of the Magnetisation Characteristic of D.C. Machines for Computer Use', IEEE Trans., 1968, PAS-87, pp. 665-669.

9. Widger, G.F.T: 'Representation of magnetisation curves over extensive range by rational-fraction approximations', Proc. IEE, 1969, 116, (1), pp. 156-160.

10. Lord Rayleigh; 'On the Behaviour of Iron and Steel under the Operation of Feeble Magnetic Forces', Phil. Mag., 1887, Vol. 23, No. 142, pp. 225-245.

11. Potter, R.I., and Schmulian, R.J: 'Self-Consistently Computed Magnetization Patterns in Thin Magnetic Recording Media', IEEE Trans., 1971, MAG-7, pp. 873-880.

12. Manly, W.A: 'An Appraisal of Several Nonlinear Hysteresis Loop Models', IEEE Trans., 1973, MAG-9, pp. 256-260.

13. Preisach, F: 'On Magnetic After-Effect', Zeitschrift für Physik, 1935, Vol. 94, p. 277.

14. Simpson, R.R.S., Slater, R.D: 'Heavy-duty switching angle selector', Proc. IEE, 1967, 114, (1), pp. 115-116.

15. Slater, R.D: 'Transients in Electrical Machines', Ph.D. Thesis, University of Strathclyde, 1966.

16. Simpson, R.R.S: 'Transient Torques in a Salient-Pole Machine', Ph.D. Thesis, University of Strathclyde, 1967.

17. Flynn, F: ' Transients in Electrical Machines ', Ph.D. Thesis, University of Strathclyde, 1970.

18. Specht, T.R: ' Transformer Magnetizing Inrush Current ', AIEE Trans., 1951, Vol. 70, pp. 323-327.

19. Holcomb, J.E: ' Distribution Transformer Magnetising Inrush Current ', AIEE Trans., 1961, Vol. 80, pp. 697-702.

20. Coratenalu, V., and Murgu, Z: ' Transient Energizing Phenomena on Three-Phase Transformers ', Electrotechnica, 1963, 11, No. 9, pp. 321-328.

21. Hudson, A.A: ' Transformer Magnetising Inrush Current - A Resume of Published Information ', ERA Report No. 5152, 1966.

22. Hayashi, C: ' Nonlinear Oscillations in Physical Systems ', McGraw-Hill, New York, 1964.

23. Cunningham, W.J: ' Introduction to Nonlinear Analysis ', McGraw-Hill, New York, 1958.

24. Wale, G.D: ' Ferroresonance in a disconnected e.h.v. power system ', GEC Journal, 1973, Vol. 40, No. 2, pp. 79-86.

25. Swift, G.W: ' An Analytical Approach to Ferroresonance', IEEE Trans., 1969, PAS-88, pp. 42-46.

26. Rusck, S: ' Ferroresonance in Voltage Transformers ', ASEA Journal, 1957, Vol. 30, pp. 20-22.

27. Wright, I.A: ' Three-Phase Subharmonic Oscillations in Symmetrical Power Systems ', IEEE Trans., 1971, PAS-90, pp. 1295-1304.

28. Wright, I.A., and Morsztyn, K: ' Subharmonic Oscillations in Power Systems - Theory and Practice', IEEE Trans., 1970, PAS-89, pp. 1805-1815.

29. Baycura, O.M., and Donovan, J.C: ' An Unsymmetrical Mode of Ferroresonance ', IEEE Trans., 1971, MAG-7, pp. 890-895.

30. Pickett, M.J., Manning, H.L., and Van Geem, H.N: ' Near Resonant Coupling on EHV Circuits: I - Field Investigation ', IEEE Trans., 1968, PAS-87, pp. 322-325.

31. Clerici, A., and Didriksen, C.H: ' Dynamic Overvoltages and Ferroresonance found in Switching Surge Studies for Iran 400 kV System ', IEEE Trans., 1972, PAS-91, pp. 195-203.

32. Dolan, E.J., Gillies, D.A., and Kimbark, E.W: ' Ferroresonance in a Transformer Switched with an EHV Line ', IEEE Trans., 1972, PAS-91, pp. 1273-1280.

33. Blume, L.F., et al: ' Transformer Engineering ', Wiley, New York, 2nd. edition, 1951, pp. 32-34.

ACKNOWLEDGEMENTS

The author wishes to express his thanks to Professor E. S. Fairley for his encouragement and for providing the facilities for carrying out the investigation.

The advice and constant encouragement of Dr. W. S. Wood is gratefully acknowledged. Thanks are due to Dr. R. Simpson and Dr. R. Slater for the invaluable discussions and advice throughout the course of the investigation, and to Dr. F. Flynn and other collegues in the Department for their assistance in the experimental work, and for helpful criticism during the preparation of this thesis.

Appreciation is also expressed to Mr. J. Dickson and his staff in the Departmental Workshop for their services.

APPENDICES

APPENDIX A1

Transformer Parameters.

(1) Single-Phase Transformer.

Nominal rating:	1 kVA.	
Rated voltage:	250 v.	
Winding resistances:	$R_A = 1.06\Omega$	$R_a = 1.70\Omega$
Leakage inductances:	$l_A = 0.00157$ H.	$l_a = 0.0054$ H.
External primary resistance:	$R_s = 0.85\Omega$	
External primary inductance:	$l_s = 0.0012$ H.	
Flux path lengths (Fig. A1.1):	$L_1 = 0.1396$ m.	$L_2 = 0.293$ m.
Core C.S.A.'s (Fig. A1.1):	$A_1 = 0.0026\ m^2$	$A_2 = 0.0013\ m^2$
Coil turns:	$N_1 = 240$	$N_2 = 446$

Series coefficients:- ($K_o = 1.0$)

K_{2i-1}			K_{2i}
Top curve	$B_r = 0$ curve	Lower curve	All curves
0.012249	0.316506	0.68076	$5.90124.10^{-2}$
0.584281	0.867873	0.855769	$3.14299.10^{-3}$
0.630603	0.632325	0.639468	$7.98744.10^{-5}$
-0.03797	-0.316762	-0.836004	$-8.27501.10^{-2}$
-0.10073	-0.428730	-0.736386	$-3.77088.10^{-3}$
-0.064357	-0.088836	-0.611022	$-7.39063.10^{-5}$

$B_o = 0.95$ T. $B_o = 0.36$ T. $B_o = 0.0$ T. $H_o = 38.0\ A.m^{-1}$

(2) Small Three-Phase Transformer.

Nominal rating:	8 kVA.
Rated phase voltages:	240 v. / 415 v.
Primary resistance:	0.764 Ω /phase.
Secondary resistance:	0.69 Ω /phase.
Primary leakage inductance:	0.00123 H. /phase.
Sec. leakage inductance:	0.00369 H. /phase.
Ext. primary resistance:	0.45 Ω /line (3-wire star) 0.6 Ω /line (4-wire star) 0.3 Ω /line (delta)
Ext. primary inductance:	0.00055 H. /line (3-wire star) 0.00075 H. /line (4-wire star) 0.0014 H. /line (delta)
Phase leakage inductances:	M_4 = 0.00844 H. M_5 = 0.00694 H. M_6 = 0.01124 H.
Flux path lengths (Fig. A1.2):	L_1 = 0.285 m L_2 = 0.41 m
Core C.S.A.'s (Fig. A1.2):	A_1 = 0.0054 m^2 A_2 = 0.0054 m^2
Coil turns:	N_1 = 132 N_2 = 228

Series coefficients:- (K_o = 100.0)

K_{2i-1}			K_{2i}
Top curve	B_r = 0 curve	Lower curve	All curves
0.011847	0.163231	0.466535	$4.63878.10^{-1}$
0.308789	0.5369	0.576735	$3.10537.10^{-2}$
0.798201	0.818619	0.825121	$1.78794.10^{-3}$
0.350698	0.354836	0.35823	$8.76442.10^{-5}$
-0.009995	-0.137274	-0.308138	$-7.31445.10^{-1}$
-0.069472	-0.271919	-0.492279	$-3.87953.10^{-2}$
-0.062	-0.263484	-0.758486	$-1.82854.10^{-3}$
-0.046206	-0.1613	-0.352237	$-8.95966.10^{-5}$
B_o = 0.6 T.	B_o = 0.195 T.	B_o = -0.16 T.	H_o = 6.0 A.m^{-1}

(3) Three-Phase Distribution Transformer.

Nominal rating:	50 kVA.
Phase voltages:	433 v. / 11 kV.
Primary (l.v.) resistance:	0.03 Ω /phase.
Secondary (h.v.) resistance:	55.7 Ω /phase.
Primary leakage inductance:	0.00025 H. /phase.
Secondary leakage induct.:	0.446 H. /phase.
External primary resistance:	as for 8 kVA. transformer.
External primary inductance:	as for 8 kVA. transformer.
Zero-sequence inductance:	0.0072 H. /phase.
Winding self-capacitance:	5nF /phase

Flux path lengths (Fig. A1.2): $L_1 = 0.47$ m $L_2 = 0.9$ m

Core C.S.A.'s (Fig. A1.2): $A_1 = 0.00942\ m^2$ $A_2 = 0.0096\ m^2$

Coil turns: $N_1 = 89$ $N_2 = 3916$

Series coefficients:- ($K_o = 100.0$)

K_{2i-1}			K_{2i}
Top curve	$B_r = 0$ curve	Lower curve	All curves
0.0	0.172219	0.712219	$2.89655.10^{-1}$
0.141471	0.479252	0.479252	$3.17890.10^{-2}$
0.905669	0.905669	0.905669	$1.40383.10^{-3}$
0.255633	0.255633	0.255633	$1.10795.10^{-4}$
-0.355051	-0.204053	-0.028567	$-4.31881.10^{-1}$
-0.398103	-0.228795	-0.032031	$-2.90272.10^{-2}$
-0.771141	-0.443184	-0.062046	$-1.37281.10^{-3}$
-0.249764	-0.143542	-0.020096	$-1.16644.10^{-4}$

$B_o = 0.76$ T. $B_o = 0.25$ T. $B_o = -0.29$ T. $H_o = 8.0\ A.m^{-1}$

APPENDIX A2

Evaluation of Exponential Series Coefficients.

The method used to evaluate the coefficients of the exponential series given in eqn. 2.6.5 is virtually identical to that given in reference 1 for calculating the coefficients of eqn. 2.5.1. One point on the curve must be specified for each coefficient, i.e. a total of 2.(i + j) points. Initially the origin is shifted to the point (H_o, B_o), and the air-line contribution subtracted from each value of B, so that,

$$B'_n = B_n - B_o - \mu_o.(H_n - H_o)$$

$$H'_n = H_n - H_o$$

Points are then taken in pairs, as shown in Fig. A2.1. The contribution from all terms, except the term containing the coefficients to be evaluated, is deducted from the two values of B' under consideration to give,

$$\Delta B'_n = B'_n - \sum(\text{all terms except term containing } K_n) \text{ at } H = H'_n$$

$$\Delta B'_{n+1} = B'_{n+1} - \sum(\text{all terms except term containing } K_n) \text{ at } H = H'_{n+1}$$

An initial value of zero is assigned to all coefficients, so that for the first two points, on the first iteration,

$$\Delta B'_1 = B'_1 = K_1.[1-\exp(-K_2.H'_1)]/[1+\exp(-K_o.H'_1)]$$

$$\Delta B'_2 = B'_2 = K_1.[1-\exp(-K_2.H'_2)]/[1+\exp(-K_o.H'_2)]$$

and, in general,

$$\Delta B_n^{\circ} = K_n.[1 - \exp(-K_{n+1}.H_n^{\circ})]/[1 + \exp(-K_o.H_n^{\circ})] \quad \ldots 1$$

$$\Delta B_{n+1}^{\circ} = K_n.[1 - \exp(-K_{n+1}.H_{n+1}^{\circ})]/[1 + \exp(-K_o.H_{n+1}^{\circ})] \ldots 2$$

Dividing eqn. 1 by eqn. 2,

$$\Delta B_n^{\circ}/\Delta B_{n+1}^{\circ} = Y_n = Z_n.[1-\exp(-K_{n+1}.H_n^{\circ})]/[1-\exp(-K_{n+1}.H_{n+1}^{\circ})] \ldots 3$$

where,

$$Z_n = [1+\exp(-K_o.H_{n+1}^{\circ})]/[1+\exp(-K_o.H_n^{\circ})] \doteq 1$$

A value of K_{n+1} which satisfies eqn. 3 is found by an iteration process in the computer program. Alternatively, K_{n+1} may be evaluated manually by plotting Y_n over a range of values for K_{n+1}, and interpolating to find the value which satisfies eqn. 3. K_n is then found from either eqn. 1 or eqn. 2.

In this way values for all coefficients can be obtained. However, it is only possible to fit the series exactly to two points in this way, and so the process must be repeated until the error at all points falls to an acceptable level. It was found that, for each of the three magnetisation characteristics represented for the purposes of the investigation, all points chosen in the evaluation of the series coefficients could be fitted to within 0.001% after twenty or so iterations.

Under certain circumstances it is not possible to obtain correct values for K_n and K_{n+1} for a given pair of points. This occurs when $|\Delta B_n^{\circ}| > |\Delta B_{n+1}^{\circ}|$ ($|H_n^{\circ}| < |H_{n+1}^{\circ}|$), or

PAGE NUMBERING AS ORIGINAL

when either or both $\Delta B'_n$ and $\Delta B'_{n+1}$ have the wrong sign - $\Delta B'$ should have the same sign as H'. If any of these conditions occur during the evaluation of the coefficients it is usually a result of attempting to incorporate too many terms in the series, or is due to the points chosen being badly distributed. As a general rule, pairs of points should be selected with the order of magnitude of H, and with relatively much larger gaps between successive pairs, i.e. on a logarithmic basis.

The computer program written to evaluate the series coefficients also contains provision for calculating coefficients for other curves using the same values of K_{n+1} as for the first curve represented. For these other curves, therefore, it is only necessary to specify one point for each term in the series, in order to evaluate the new values of K_n.

APPENDIX A3

Derivation of the Complete Magnetisation Characteristic Representation from a Single Curve.

The method of obtaining a representation of the complete magnetisation characteristic from a knowledge of the B/H curve for $B_r = 0$, and the values of B_R and H_c, is based on a system of modifying the coefficients of the series representation of the known curve to produce new coefficients for series to represent the limit cycle or boundary curve, and the curve for which $B_r = B_R$.

Initially an exponential series is obtained to represent the known curve for values of $H > H_o$. This is done assuming negligible influence in this region of the terms representing the curve for $H < H_o$, so that,

$$B_{H>H_o} = B_1 + \mu_o.(H-H_o) + \sum_{i=1}^{n} K_{2i-1}.[1-\exp(-K_{2i}.(H-H_o))]/D(H) \quad \ldots\ldots 1$$

where,

$$D(H) = 1 + \exp(-K_o.(H-H_o))$$

This assumption is valid if K_o is very large. Certain other assumptions must also be made in order to complete the representation, i.e. that the boundary curve has its point of maximum slope at $H = H_o$. Experience has shown this to be approximately true in practice. Also, in general, $H_c > H_o$, which is the case considered here.

Eqn. 1 can be modified to represent the lower boundary curve by initially shifting the origin from (H_o, B_1) to

(H_o, B_2) as shown in Fig. A3.1. The value of B_2 is obtained by adjusting the coefficients of eqn. 1 so that the curve passes through the point $(H_c, 0)$. As stated in section 2.6.1, increasing curves do not intersect, but become infinitely close as $H \to \infty$. The ultimate level of B in eqn.1 as $H \to \infty$, neglecting the $\mu_o.(H-H_o)$ term is,

$$B_{max} = B_1 + \sum_{i=1}^{n} K_{2i-1}$$

and the displaced curve must also reach this ultimate level, without intersecting the original curve, so that,

$$B_2 + \sum_{i=1}^{n} K'_{2i-1} = B_1 + \sum_{i=1}^{n} K_{2i-1} \quad \ldots\ldots 2$$

where K'_{2i-1} are the required modified coefficients. For simplicity, only K_1 is adjusted, the rest of the K_{2i-1} values being left unaltered. This allows for the case of n = 1, and is shown to be justified when the coefficients derived using this method are compared with those obtained using the method described in chapter 2. Eqn. 2 therefore reduces to,

$$B_2 + K'_1 = B_1 + K_1 \quad \ldots\ldots 3$$

The value of flux density at $H = H_c$ is zero on the lower boundary curve, therefore,

$$0 = B_2 + \mu_o.(H_c-H_o) + K'_1.E_2/D(H_c) + S/D(H_c) \quad \ldots\ldots 4$$

where,

$$E_2 = 1 - \exp(-K_2.(H_c - H_o)$$

$$S = \sum_{i=1}^{n} K_{2i-1} \cdot [1 - \exp(-K_{2i} \cdot (H_c - H_o))]$$

Substituting for K_1' from eqn. 3 in eqn. 4, gives,

$$B_2 = -[\mu_o \cdot (H_c - H_o) \cdot D(H_c) + E_2 \cdot (B_1 + K_1) + S] / [E_2 + D(H_c)]$$

.....5

B_2 and K_1' can therefore be found from eqns. 5 and 3. The equation used to represent the lower boundary curve (curve (b) in Fig. A3.1) in the region $H > H_o$,

$$B_{b_{H>H_o}} = B_2 + \mu_o \cdot (H - H_o) + \sum_{i=1}^{n} K'_{2i-1} \cdot [1 - \exp(-K_{2i} \cdot (H - H_o))] / D(H)$$

cannot intersect curve (a) in Fig. A3.1, since the difference between the two curves is given by,

$$\Delta B = (B_1 - B_2) \cdot [1 - [1 - \exp(-K_2 \cdot (H - H_o))] / D(H)]$$

which is positive for all values of $H > H_o$, if $B_1 > B_2$.

The equation for the lower boundary curve in the region $H < H_o$ is,

$$B_{b_{H<H_o}} = B_2 + \mu_o \cdot (H - H_o) + \sum_{j=n+1}^{m} K_{2j-1} \cdot (1 - \exp(-K_{2j} \cdot (H - H_o))) / D'(H)$$

.....6

where,

$$D'(H) = 1 + \exp(+K_o \cdot (H - H_o))$$

Since this part of the curve is used to represent the upper boundary curve in the region $H > -H_o$, the final value of B as

$H \to -\infty$, neglecting the air-line term, will be,

$$B_{max} = -\left[B_1 + \sum_{i=1}^{n} K_{2i-1}\right]$$

Therefore,

$$B_2 + \sum_{j=n+1}^{m} K_{2j-1} = -B_1 - \sum_{i=1}^{n} K_{2i-1} \qquad \ldots\ldots 7$$

By defining,

$$K_j\Big|_{j=2n+1 \to 2m} = -K_i\Big|_{i=1 \to 2n}$$

and, $$B_o = B_2$$

this section of the lower boundary curve is then represented by eqn. 1 with the origin moved from (H_o, B_1) to (H_o, B_2) and the whole curve rotated by 180^o about the new origin. In order to satisfy eqn. 7, the value of K_{2n+1} is adjusted so that,

$$K'_{2n+1} = -B_1 - K_1 - B_2$$

The lower boundary curve now has the correct shape, but does not necessarily pass through the $(0, -B_R)$ point. This is achieved by modifying the coefficient K_{2n+2} in the term,

$$K'_{2n+1} \cdot (1 - \exp(-K_{2n+2} \cdot (H - H_o)))/D'(H)$$

Eqn. 6 reduces to the following form at $(0, -B_R)$,

$$-B_R = B_2 + \mu_o \cdot (-H_o) + K_{2n+1} \cdot (1 - \exp(-K_{2n+2} \cdot (-H_o)))/D'(0) + S_1/D'(0) \qquad \ldots\ldots 8$$

where,

$$S_1 = \sum_{j=n+2}^{m} K_{2j-1} \cdot [1 - \exp(K_{2j} \cdot H_o)]$$

and solving eqn. 8 for K_{2n+2} gives,

$$K_{2n+2} = \log_e \{1 + [D'(0) \cdot (B_R + B_2 - \mu_o \cdot H_o) + S_1] / K'_{2n+1}\} / H_o \quad \ldots\ldots 9$$

In cases where,

$$B_R + B_2 - \mu_o \cdot H_o + S_1 < 0$$

it is not possible to find a value for K_{2n+2} using the above method. If this occurs, then an alternative method is to modify the relative values of K_{2n+1} and K_{2n+3}, while keeping the sum of the two coefficients constant, so that,

$$K''_{2n+1} + K'_{2n+3} = K'_{2n+1} + K_{2n+3} \quad \ldots\ldots 10$$

and,

$$-B_R = B_2 - \mu_o + K''_{2n+1} \cdot X/D'(0) + K'_{2n+3} \cdot Y/D'(0) + S_2/D'(0) \quad \ldots\ldots 11$$

where,

$$X = 1 - \exp(K_{2n+2} \cdot H_o)$$

$$Y = 1 - \exp(K_{2n+4} \cdot H_o)$$

$$S_2 = \sum_{j=n+3}^{m} K_{2j-1} \cdot (1 - \exp(K_{2j} \cdot H_o))$$

From eqn. 11,

$$K''_{2n+1} \cdot X + K'_{2n+3} \cdot Y = Z \quad \ldots\ldots 12$$

where,

$$Z = -D'(0).(B_R + B_2 - \mu_o.H_o) + S_2$$

Solving eqns. 10 and 12 for K''_{2n+1} and K'_{2n+3} gives,

$$K''_{2n+1} = (Z - W.Y)/(X-Y)$$

$$K'_{2n+3} = W - K''_{2n+1}$$

The original curve, (a) in Fig. A3.1 is represented in the region, $H<H_o$, by a modified version of eqn. 6. This modification can be done in two ways,

(i) Eqn. 6 can be shifted so that its origin lies at (H_o, B_1), and the sum of the exponential terms multiplied by a factor, C, to cause the curve to pass through the (0, 0) point, i.e.,

$$0 = B_1 - u_o.H_o + C.\sum terms\Big|_{H=0}$$

which gives,

$$C = (u_o.H_o - B_1)/\left\{\sum terms\Big|_{H=0}\right\}$$

(ii) Again shifting the origin of eqn. 6 from (H_o, B_2) to (H_o, B_1), the coefficient K_{2n+1} can be altered to cause the curve to pass through the (0, 0) point such that,

$$0 = B_1 - \mu_o.H_o + K'_{2n+1}.[1-\exp(K_{2n+2}.H_o)]/D'(0) + S_1/D'(0)$$

Rearranging the above equation gives,

$$K'_{2n+1} = [(u_o.H_o - B_1).D'(0) - S_1]/[1+\exp(K_{2n+2}.H_o)]$$

Either method will give a reasonable representation of this part of the curve.

The coefficients for any other curve in the B/H plane can be derived in a similar way to the lower boundary curve, if two points on the curve are known. To complete the representation, coefficients for the $B_r=B_R$ curve must be obtained. Since only one point on this curve is known precisely, i.e. $(0, B_R)$, a second point must be estimated in order that the coefficients can be evaluated. It is expedient to estimate the value of B at the point of maximum slope of the curve, i.e. the point (H_o, B_3) in Fig. A3.1. B_3 can be taken arbitrarily at a point half way between B_R and the value of B at $H=H_o$ on the upper boundary curve.

The coefficients given below for the magnetisation characteristic representation of the single-phase transformer which have been derived using the above method compare favourably with those given in appendix A1.

Top curve	$B_r=0$ curve	Lower curve	All curves
0.0	0.316506	0.676506	$5.90124.10^{-2}$
0.569379	0.867873	0.867873	$3.14299.10^{-3}$
0.632325	0.632325	0.632325	$7.98744.10^{-5}$
-0.072480	-0.370790	-0.926976	$-5.90124.10^{-2}$
-0.051450	-0.246961	-0.617403	$-3.14299.10^{-3}$
-0.052694	-0.252930	-0.632325	$-7.98744.10^{-5}$
B_3=0.975 T.	B_1=0.36 T.	B_2=0.0 T.	H_o=38.0 A.m^{-1}

Fig. A3.2 shows that the curves produced using the above method do not deviate greatly from those derived using the method presented in chapter 2. Note that in this instance it has not been possible to cause the lower boundary curve to pass through the $(0, -B_R)$ point by adjusting K_8 as in eqn. 9. Instead, the relative values of K_7 and K_9 have been altered in order to achieve this, and K_8 set equal to $-K_2$.

APPENDIX A4

Preisach Theory[13]

Preisach assumes that the magnetic material consists of a large number of elementary dipoles, each of which can be represented by a rectangular hysteresis loop, of variable width, $2H_c$, and displaced along the H-axis by an amount, H_m, as shown in Fig. A4.1. The displacement, H_m, is caused by the action of the other dipoles, and varies from dipole to dipole, and also with the overall magnetic state of the material. A probability density function, $\gamma(H_c, H_m)$ is used to define the distribution of the dipoles in terms of their magnetisation parameters, so that the number of dipoles within the range, $H_m \rightarrow H_m + dH_m$ and $H_c \rightarrow H_c + dH_c$ is, $\gamma(H_c, H_m).dH_c.dH_m$.

When the material is magnetically neutral, there are as many dipoles in the state $+B_s$ as there are at $-B_s$ as shown in Fig. A4.2(a). If an external field, $H > 0$, is applied, all dipoles in the $-B_s$ state will switch to the $+B_s$ state where the applied field is greater than the corresponding value of $H_c + H_m$. Thus all dipoles lying below the line of state defined by the equation,

$$H = H_m + H_c$$

will be in the $+B_s$ state, as shown in Fig. A4.2(b). As the field is reduced from its peak positive value, H_{max}, which corresponds to the line Q-Q in Fig. A4.2(c), reverse switching from $+B_s$ to $-B_s$ will occur in those dipoles for which H (the applied field) is less than $H_m - H_c$, i.e. all dipoles lying above the line of state defined by,

$$H = H_m - H_c$$

as shown in Fig. A4.2(c).

The resultant value of flux density in the material will be given by the difference of the total number of dipoles in the $+B_s$ state and the total number in the $-B_s$ state, multiplied by the contribution to the net flux density from each dipole, B_s. This difference is represented by the area enclosed by the lines Q-Q and R-R in Fig. A4.2(c), and the H_c and H_m axes. Thus the net flux density is given by,

$$B = 2.B_s \iint \gamma(H_c, H_m).dH_c.dH_m$$

Although it is not possible to carry out a full analysis of the magnetic state of the material under consideration, without knowledge of the distribution function, $\gamma(H_c, H_m)$, a qualitative study of the magnetic behaviour can still be made using the concepts developed for the H_c/H_m diagram, and relating these to the B/H plane. In this way it is possible to explain the appearance of the observed crossovers of increasing B/H trajectories, and to derive the criteria for these to occur.

Consider the case where a piece of magnetic material is initially in the neutral state, as shown in Fig. A4.3(a). A positive field, H, is applied which slowly increases from zero to a value, H_1, so that all dipoles below the line H_1-H_1 in Fig. A4.3(b) are in the $+B_s$ state. The field is then slowly reduced to a value, $H_2 > 0$. The number of dipoles switched from their original $-B_s$ state to $+B_s$ is therefore represented by the area, A, shown shaded in Fig. A4.3(c). The B/H

trajectory corresponding to these two operations is shown in Fig. A4.4(a). As the applied field is again increased, this time from H_2 to $H_3 < H_1$, the difference in the number of switched dipoles, and hence the net flux density, for any value of H during this third operation, and the same value of H during the initial magnetisation ($0 \rightarrow H_1$), is represented by the shaded area, B, in Fig. A4.3(d). Thus as H increases from H_2 to H_3 the net flux density is greater at all points, than that for the initial magnetisation, and the B/H trajectory for this operation lies above the initial curve. If $H_3 = H_2$, then the material is in exactly the same magnetic state as at the end of the first excursion in H, and further increase in H will cause the B/H curve to follow the initial trajectory, shown as a broken line in Fig. A4.4(b).

If, instead of the field reducing to a value of H_2 which is greater than zero, from H_1, a minimum value of H is reached such that, $-H_1 < H < 0$, then as the field is slowly increased from this minimum value, the net difference in flux density between this operation and the initial magnetisation is represented by the difference of the shaded areas, C and D, in Fig. A4.3(e). At H=0, if the net magnetisation is negative, then the B/H trajectory will lie below the initial curve. At $H = -H_2$, all dipoles for which $H_m < 0$ have reverted to their original $+B_s$ state, and the net magnetisation is given by area D only. Thus at this point, since the difference is positive, the trajectory must lie above the initial magnetisation curve, i.e. the curves have crossed, as shown in Fig. A4.4(c). The crossover will occur when, the net difference in magnetisation between the two curves is zero, i.e. the number of dipoles represented by area C in Fig. A4.3(e) is equal to that represented by area D. The conditions required for the cross-over of other curves can be derived in the same way.

APPENDIX A5

Establishment of Residual Conditions in Three-Phase Transformers.

(a) Delta connected primary, no load.

i) Line Y disconnected first:-

$$i_Y = 0$$

$$i_B = i_A$$

$$i_2 = i_1'$$

Referring to the phasor diagram of Fig. 4.5.3, when $i_Y = 0$, the following information regarding the magnetic state of the core can be derived,

i_2 and $\emptyset_2$ are positive and increasing positively.

i_1' and $\emptyset_1$ are positive and decreasing.

i_3' and $\emptyset_3$ are near their negative maxima.

These conditions are similar to those found for i_X disconnected first. However, since the flux path lengths of sections 1 and 2 are different, $H_2 > H_1'$. The ratio H_1'/H_2 will be constant following the disconnection of line Y, and will be equal to $L_2/(L_1 + L_7)$. Consequently $\emptyset_1$ and $\emptyset_2$ will be closer at this stage than the corresponding fluxes in the case considered in chapter 4, while H_3' will have a value about the same as H_2 previously, assuming that the peak flux levels are similar. Fig. A5.1 illustrates this situation, and the behaviour of the fields and fluxes as i_X and i_Z fall to zero.

The ratio H_1'/H_2 is maintained as i_C and the fluxes decay. When all line currents are zero, then eqn. 4.5.1 and eqn. 4.5.6 will hold as before, and i_1' and i_2 will have become negative. Also, $H_1' = H_3' > H_2$, which results in the conditions shown in Fig. A5.1, i.e. $\emptyset_2$ has become very small, while $\emptyset_1$ is only slightly smaller in magnitude than $\emptyset_3$. Computed and measured residual conditions for this case which are given in section 4.5.2 confirm these deductions.

ii) Line Z disconnected first:-

Using the same arguements as above, it can be shown that the condition of the core as i_Z falls to zero, while going positive, will be as illustrated in Fig. A5.1(b). In this case the two positive fluxes, $\emptyset_2$ and $\emptyset_3$ have very different values at this stage, although as the ratio of H_2/H_3' is maintained constant during the subsequent decay of i_X and i_Y, the final value of H_2 will be larger than H_3, causing the two fluxes to assume final levels which will be closer together than the corresponding fluxes in previous cases, as shown in Fig. A5.2.

(b) Three-wire Star connected primary, no load.

i) Line A disconnected first:-

The magnetic circuit equations for this case are,

$$i_1' - i_A - i_2 + i_B = 0$$

$$i_3' - i_C - i_2 + i_B = 0$$

$$\emptyset_1 + \emptyset_2 + \emptyset_3 = 0$$

also, for the electric circuit,

$$i_A + i_B + i_C = 0$$

The approximate phase relationships are given in Fig. A5.2(a). When the current in line A falls to zero while going positive,

$$i_A = 0$$

$$i_B = -i_C$$

and,

$$i_1' - i_2 + i_B = 0$$

$$i_3' - i_2 + 2.i_B = 0 \qquad \ldots\ldots 1$$

i_1' and $\emptyset_1$ are near zero and increasing positively.

i_3' and $\emptyset_3$ are large positive and decreasing.

i_2 and $\emptyset_2$ are large negative, increasing negatively.

Since i_1' is very small, then from eqn. 1 above, $i_2 \doteqdot -i_3'$. Therefore $|H_2| > |H_3'|$, and since both values of H are large, $|\emptyset_2| > |\emptyset_3|$. $\emptyset_1$ will therefore have a small positive value, as shown in Fig. A5.2(b), in order that $\sum\emptyset = 0$.

As the currents in the remaining two lines fall to zero, i_2 and i_3' will decay at about the same rate, and the difference between $|\emptyset_2|$ and $|\emptyset_3|$ will reduce. Thus $\emptyset_1$ follows the trajectory shown in Fig. A5.2(b). Finally, when all coil currents are zero, the magnetic circuit equations again reduce to,

$$i_1' = i_2 = i_3'$$

The condition of the core when all coil currents are zero will therefore be as shown in Fig. A5.2(b). $\emptyset_1$ will be small and have the same polarity as $\emptyset_3$ which is large. $\emptyset_2$ will be opposite in polarity to $\emptyset_1$ and $\emptyset_3$, and be larger than either. Computed results for this condition are given in section 4.5.2.

Fig. A5.3 illustrates the magnetic behaviour of the core for lines B and C disconnected first when the respective currents are zero, going positive. The behaviour under these conditions is deduced in the same way as above.

(c) Four-wire Star connected primary, no load.

The magnetic circuit equations for all lines connected are identical to the three-wire case, as are the steady-state phase relationships as given in Fig. A5.2(a). When the current in line A falls to zero, $i_B \doteqdot -i_C$, and the other conditions will be very similar to those for a three-wire star connection at this point as shown in Fig. A5.4(a).

In the four-wire case, however, $\emptyset_2$ and i_2 will continue to increase negatively, since the e.m.f. for the centre limb, and hence the flux, is virtually independent of the other phases. $\emptyset_3$ and i_3' will decrease, forcing $\emptyset_1$ to increase positively. The next line current to fall to zero will be i_C, and when this occurs, $i_1' = i_3'$, i.e. $H_1' = H_3'$. At this stage $\emptyset_2$ and i_2 will be large, negative and decreasing in magnitude as shown in Fig. A5.4(a). All m.m.f.'s will now decay, maintaining $i_1' = i_3'$ and $\sum\emptyset = 0$ at all points. Finally when i_B becomes zero, and $i_1' = i_2 = i_3'$ the residual conditions shown in Fig. A5.4(a) are established, which correspond with

the computed conditions given in section 4.5.2.

Also given in Fig. A5.4 are the residual conditions for the two other disconnection sequences which can be derived in the same way as above.

(d) Delta connected primary, inductive load.

Fig. A5.5(a) shows the approximate phase relationships for a large, purely inductive load on the transformer. As in the case of a resistive load, it is assumed the load currents are much larger than the steady-state magnetising currents, and therefore the phase currents will lag the phase coltages by 90^{o} as shown. The magnetic circuit equations are as for the resistive load (eqn. 4.5.7).

For $i_X = 0$, going positive,

$$i_Y = -i_Z$$

$$i_A = i_C$$

$$\phi_1 \doteqdot \phi_3$$

$$v_{BC} \doteqdot 0$$

i_1' and ϕ_1 are positive and increasing.

i_3' and ϕ_3 are positive and decreasing.

i_2 and ϕ_2 are near their negative maxima.

This condition is summarised in Fig. A5.5(b). Since $i_A = i_C$ (which will be primarily the load component of the input current) then for a balanced load, $i_a \doteqdot i_c$.

Therefore,

$$di_a/dt \doteqdot di_c/dt$$

and,

$$v_a \doteqdot v_c$$

$$v_{AB} \doteqdot v_{CA}$$

However, since di_a/dt and di_c/dt were opposite in sign immediately before line X was removed, the only way in which the above equations can be satisfied is if the phase voltages fall immediately to zero, also satisfying the voltage equation for the delta connected primary,

$$v_{AB} + v_{BC} + v_{CA} = 0$$

Thus all phase voltages are zero, and all currents are at a turning point at this stage.

The change in flux in the two outer sections following the disconnection of line X will be approximately the same since $v_{AB} \doteqdot v_{CA}$, and this change will be given by,

$$\Delta\phi = -\frac{1}{N}.\int e.dt$$

so that $\phi_1 \doteqdot \phi_3$ during this period. $\Delta\phi$ will be negative in this case, causing ϕ_1 and ϕ_3 to decrease. The flux in the centre limb will fall from its negative maximum to a value near zero when the remaining lines are disconnected. Since $\sum\phi = 0$, and $\phi_1 \doteqdot \phi_3$, it follows that at this stage all fluxes will be very small. Fig. A5.5(b) which illustrates this condition shows the same flux and field distribution as the computed results given in section 4.5.2.

(e) Delta connected primary, capacitive load.

The steady-state phasor diagram, shown in Fig. A5.6 is used to establish the basic relationships between each of the various quantities. At the instant that $i_X = 0$, going positive,

$$i_Y = -i_Z$$

$$i_A = i_C$$

$$\varnothing_1 \doteqdot \varnothing_3$$

$$v_{BC} \doteqdot 0$$

i'_1 and $\varnothing_1$ are negative and increasing negatively.

i'_3 and $\varnothing_3$ are negative and decreasing in magnitude.

i_2 and $\varnothing_2$ are near their positive maxima.

i.e. the conditions in the core are very similar to those for the transformer load being purely inductive, and line X disconnected first when $i_X = 0$, going negative.

Since the input currents are predominantly load current, and $i_A = i_C$, then for a balanced load,

$$i_a \doteqdot i_c \doteqdot C_L.(dv_a/dt) \doteqdot C_L.(dv_c/dt)$$

and thus,

$$v_a \doteq -v_o + \frac{1}{C}.\int i_a.dt$$

$$v_c \doteqdot v_o + \frac{1}{C}.\int i_c.dt$$

since $v_c \doteqdot -v_a = v_o$ when $i_X = 0$, going positive. Δv is the same in both phases, and is positive in this case, since i_a and i_c are initially positive and will fall to zero during the

disconnection procedure. Also, since,

$$v_{AB} + v_{BC} + v_{CA} = 0$$

then, $\Delta v_{BC} = -\Delta v_{AB} - \Delta v_{CA} = -2.\Delta v$

Thus the maximum change in v_{AB} and v_{CA} will be $0.5.\hat{v}_{line}$.
At the instant line X is disconnected,

$$v_{AB} \doteqdot -v_{CA} \doteqdot -(1/\sqrt{3}).\sqrt{2}.\ V_{line}$$

so that the fluxes in sections 1 and 3 of the core will be given by,

$$\phi_1 \doteqdot \phi_o - \frac{1}{N}.\int [-v_o + \frac{1}{C}.\int i_a.dt\ ]\ dt$$

$$\phi_3 \doteqdot \phi_o - \frac{1}{N}.\int [+v_o + \frac{1}{C}.\int i_c.dt\ ]\ dt$$

v_{AB} changes from $-(\sqrt{2}/\sqrt{3}).V_{line}$ to $(1/\sqrt{2} - \sqrt{2}/\sqrt{3}).V_{line}$, so that $\Delta\phi_1$ is negative. Similarly, $\Delta\phi_3$ is positive. ϕ_2 will fall to a value near zero, so that when disconnection of the last two lines takes place, $\phi_3 \doteqdot -\phi_1$ and $\phi_2 \doteqdot 0$, as shown in Fig. A5.6(b).

If no oscillations took place following the disconnection of the last two lines, the final residual conditions would be as shown in Fig. A5.6(b). However, as the computed results given in section 4.5.2 indicate, a degree of de-magnetisation takes place as would be expected.

DIAGRAMS

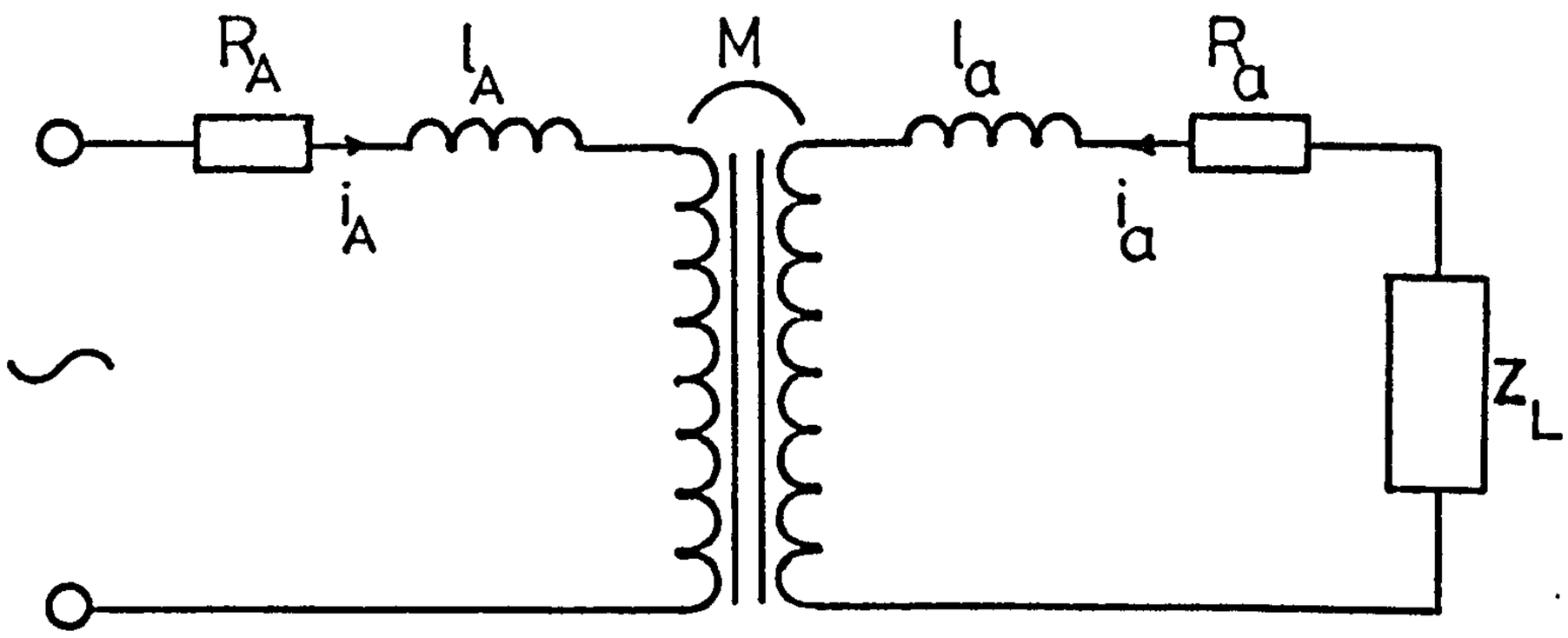

Fig. 2.1.1 Equivalent circuit for single-phase, two winding transformer.

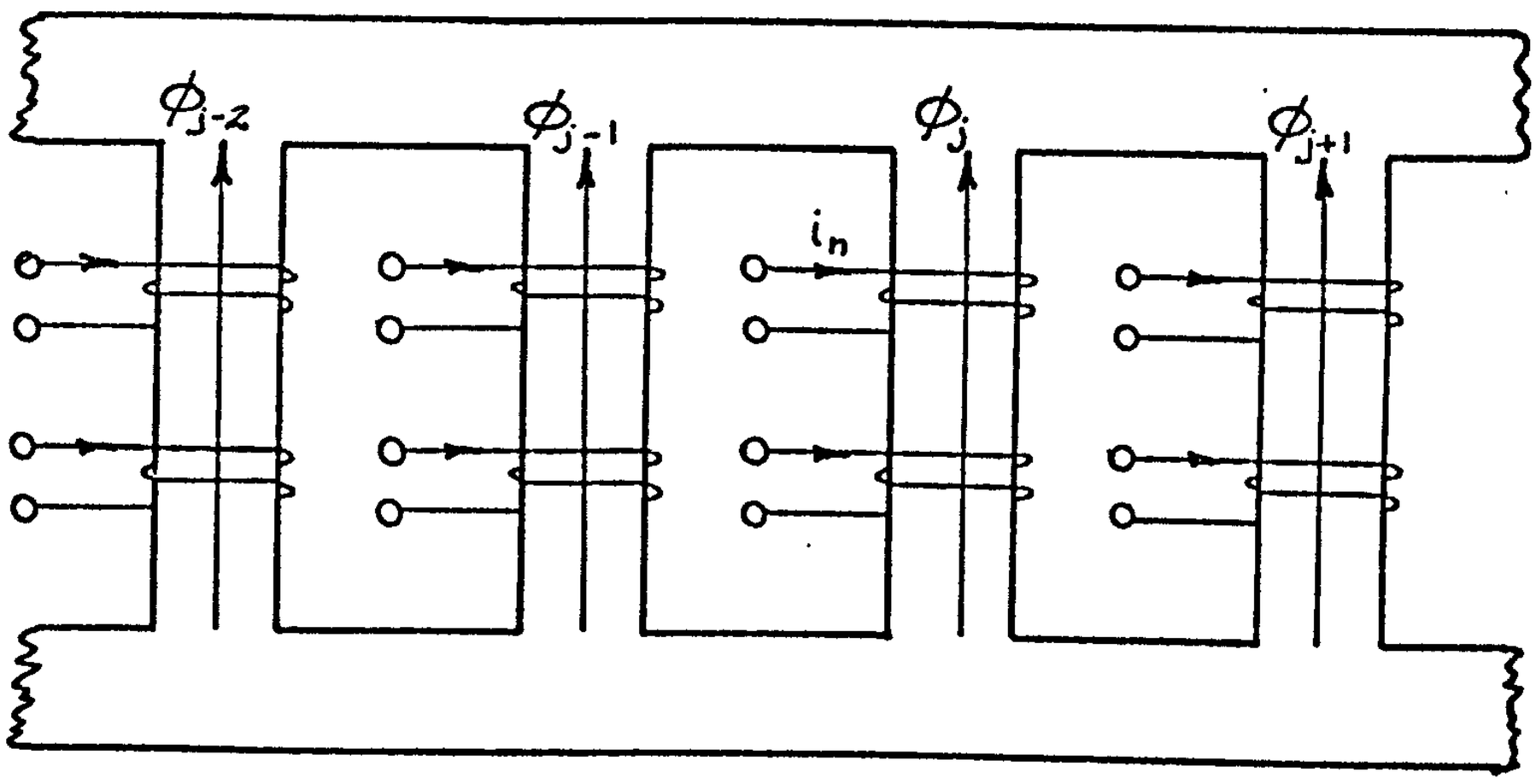

Fig. 2.2.1 General static, polyphase system.

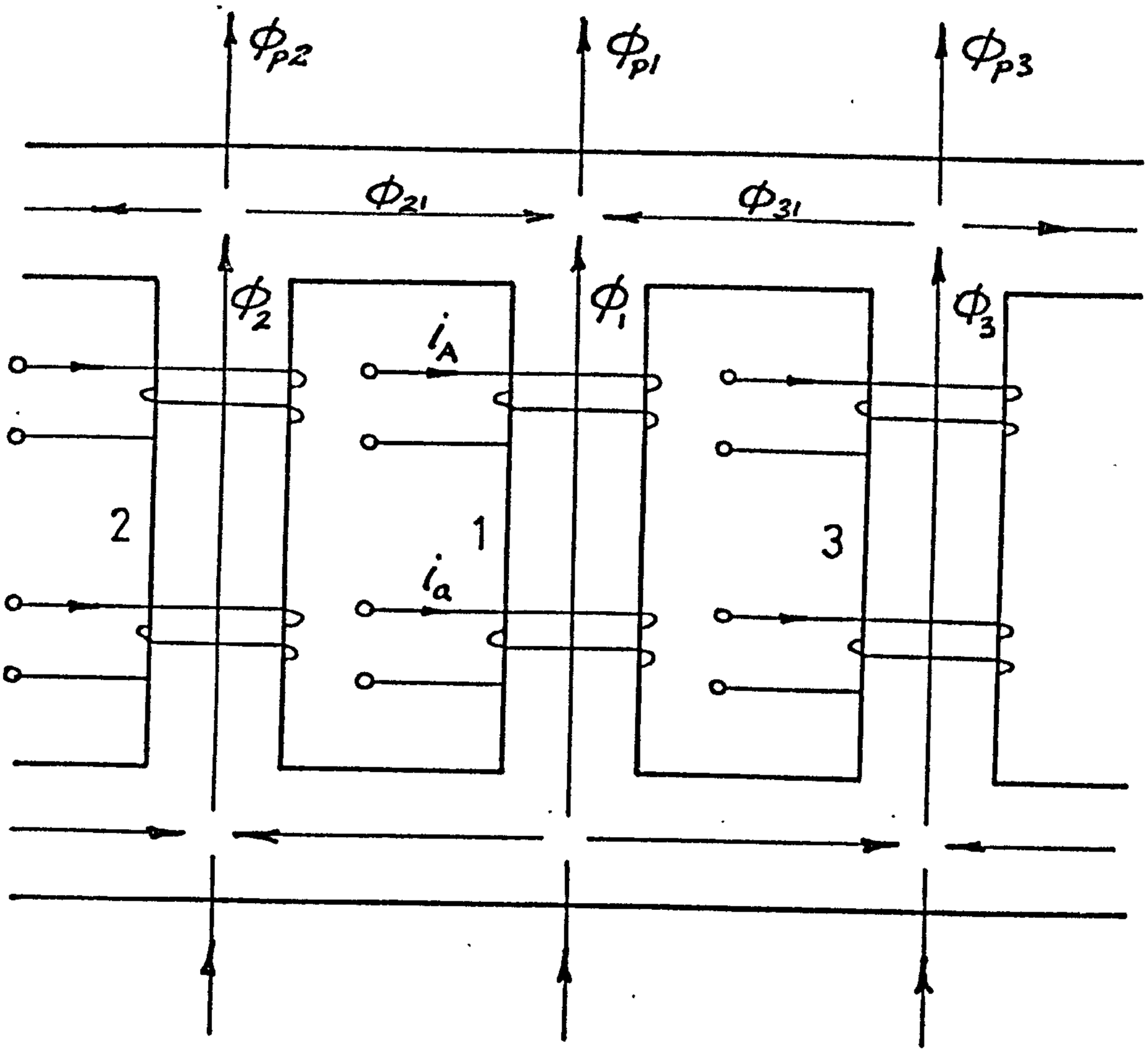

Fig. 2.2.2 Assumed flux paths in general system.

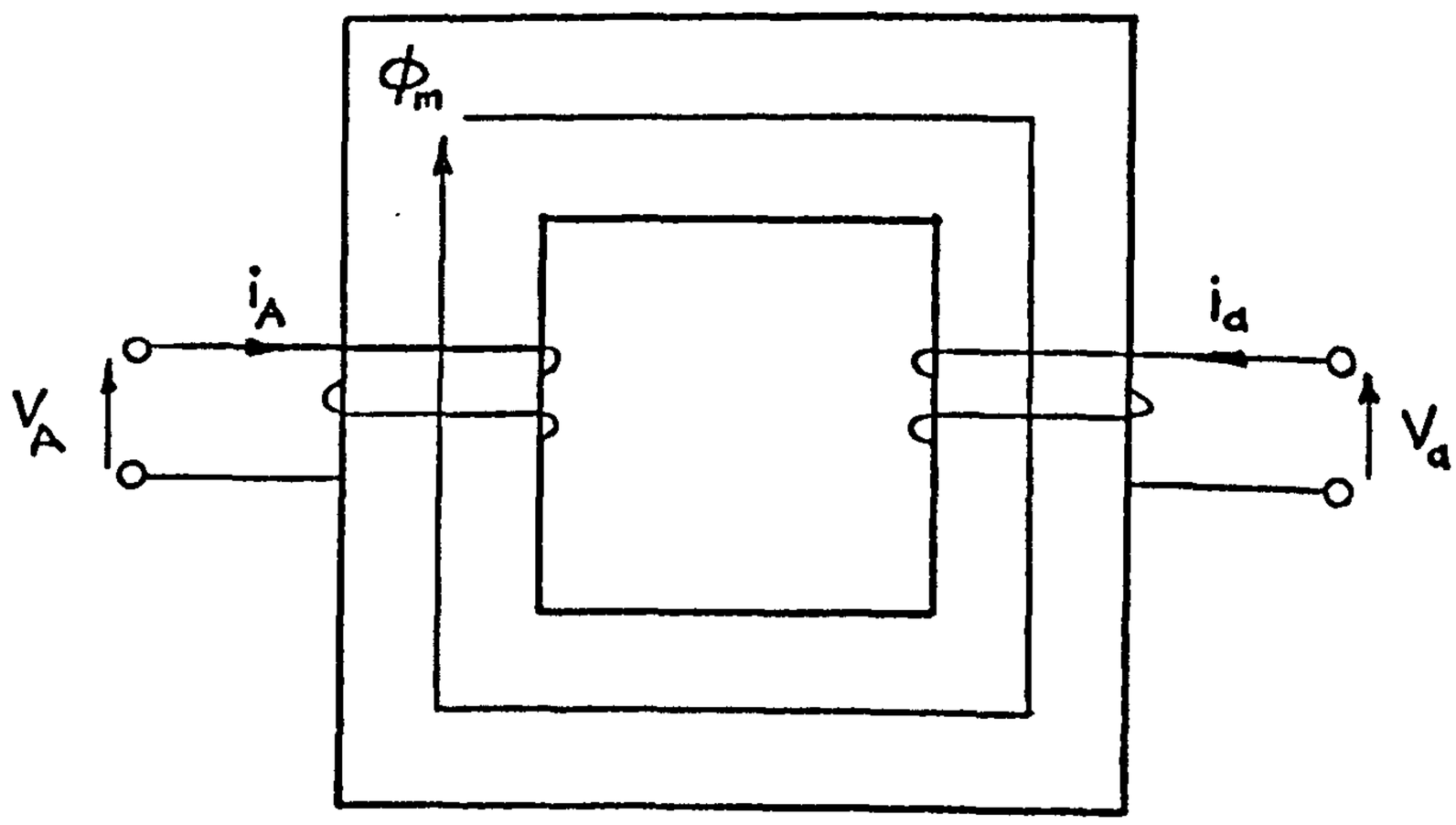

Fig. 2.3.1 Single-phase, two winding transformer.

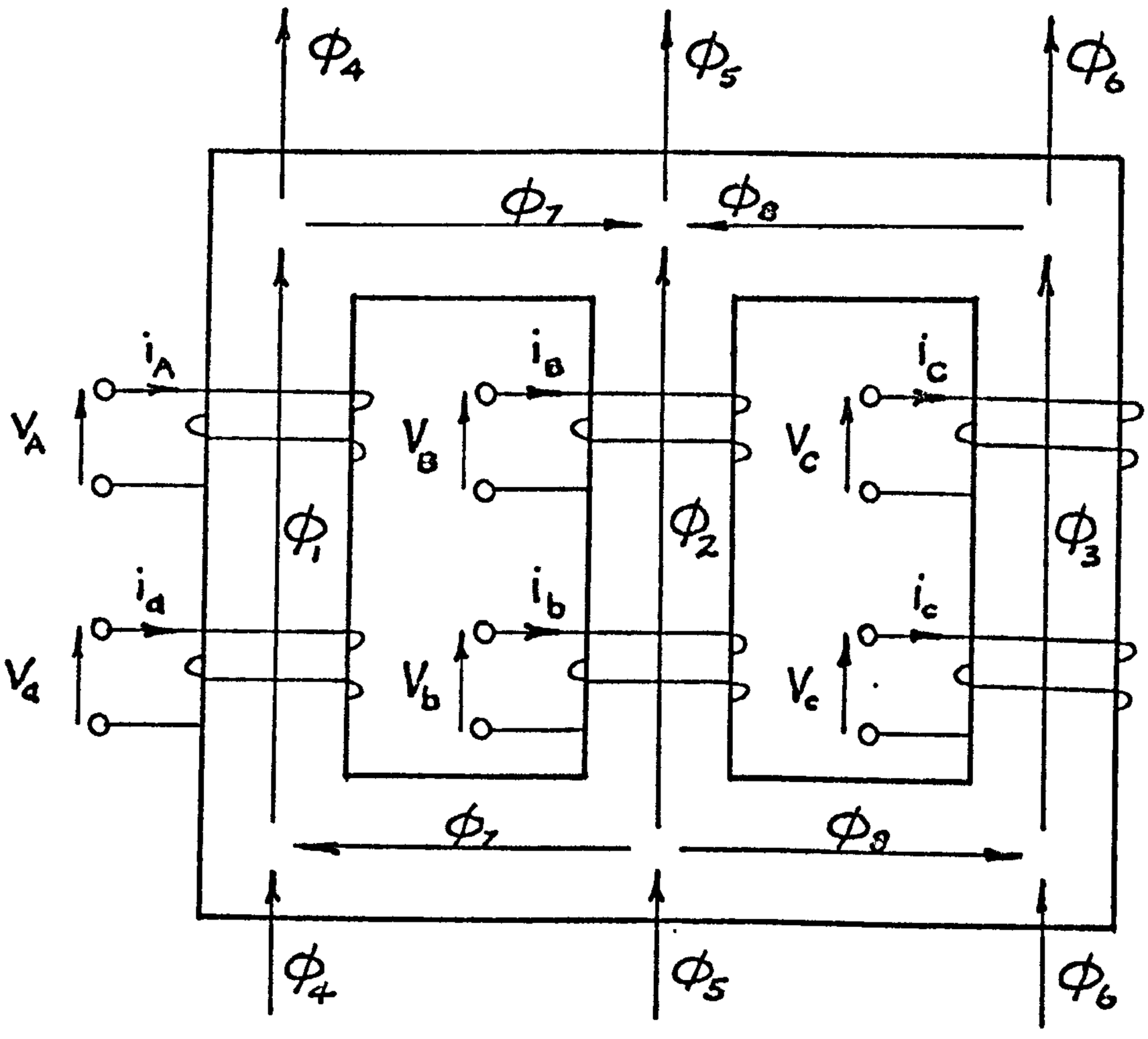

Fig. 2.4.1 Three-phase, three limb transformer.

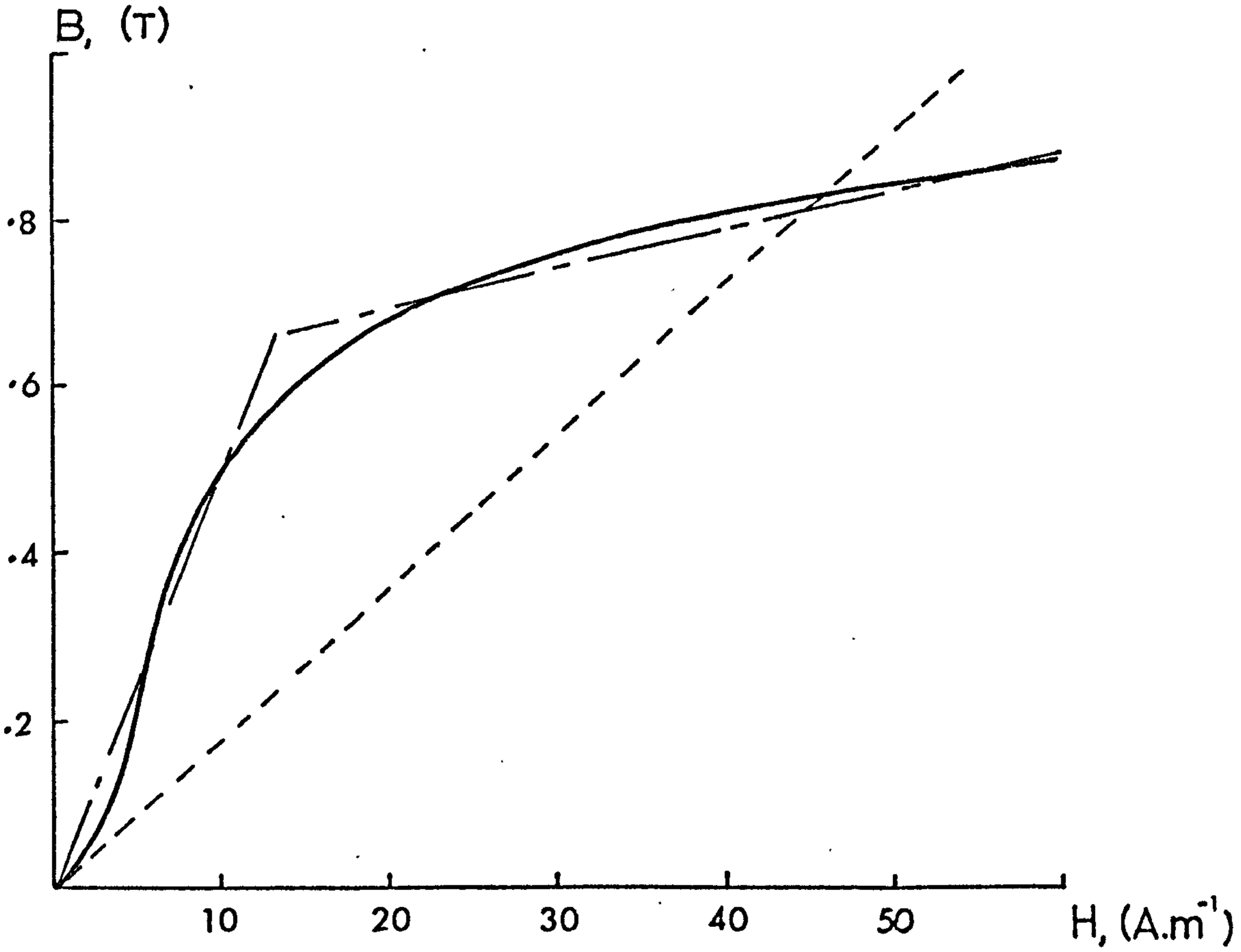

——— typical magnetisation curve.

- - - - - - linear approximation.

——— - ——— two-line representation

Fig. 2.5.1 Magnetisation curve – linear approximation.

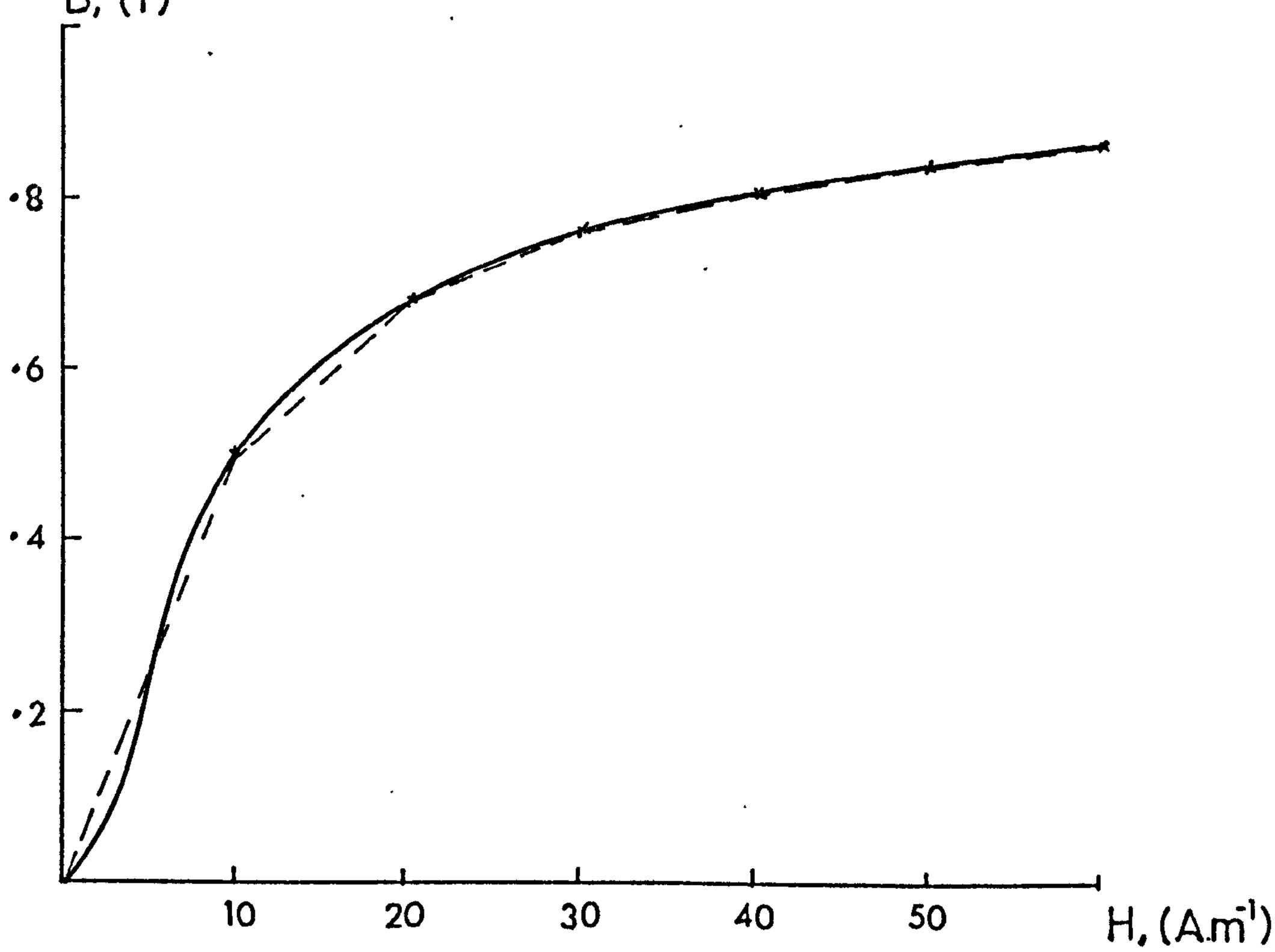

——— typical B/H curve.

— — — — piecewise-linear approximation.

Fig. 2.5.2 Piecewise-linear approximation of B/H curve.

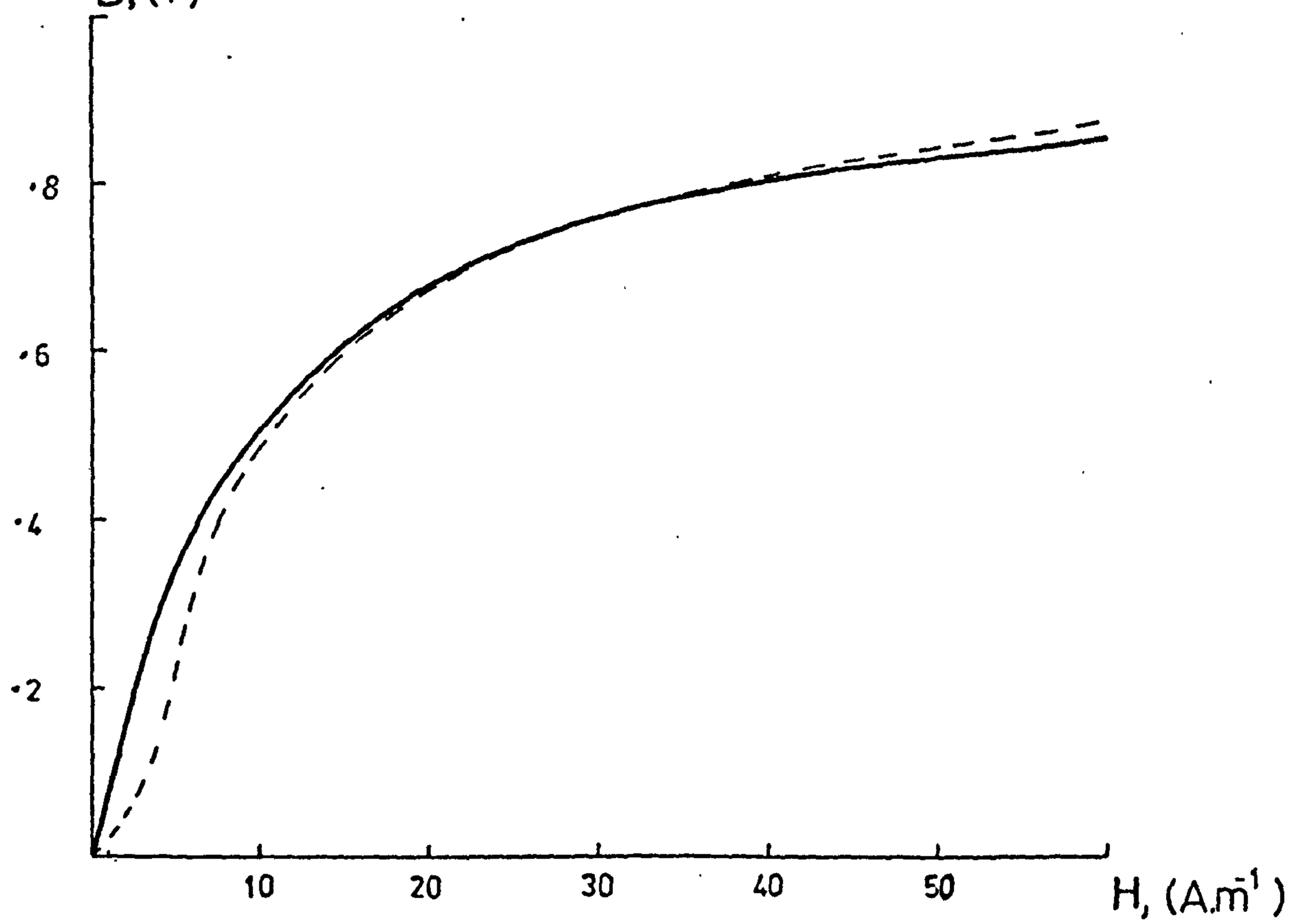

——— exponential series.

- - - - - - - B/H curve.

Fig. 2.5.3 General shape of exponential series curve.

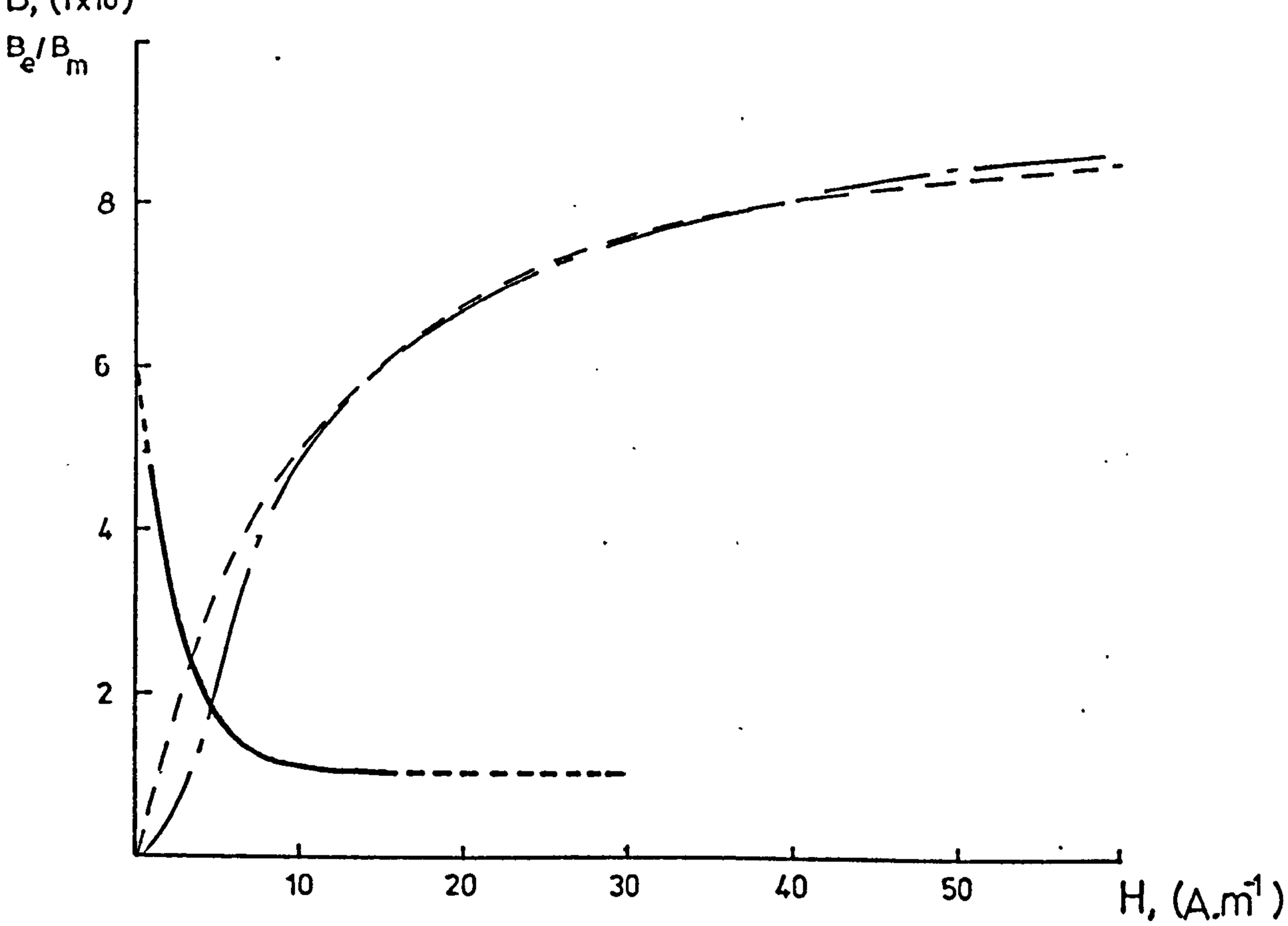

Fig. 2.5.4 Representation of region near origin — Division curve method.

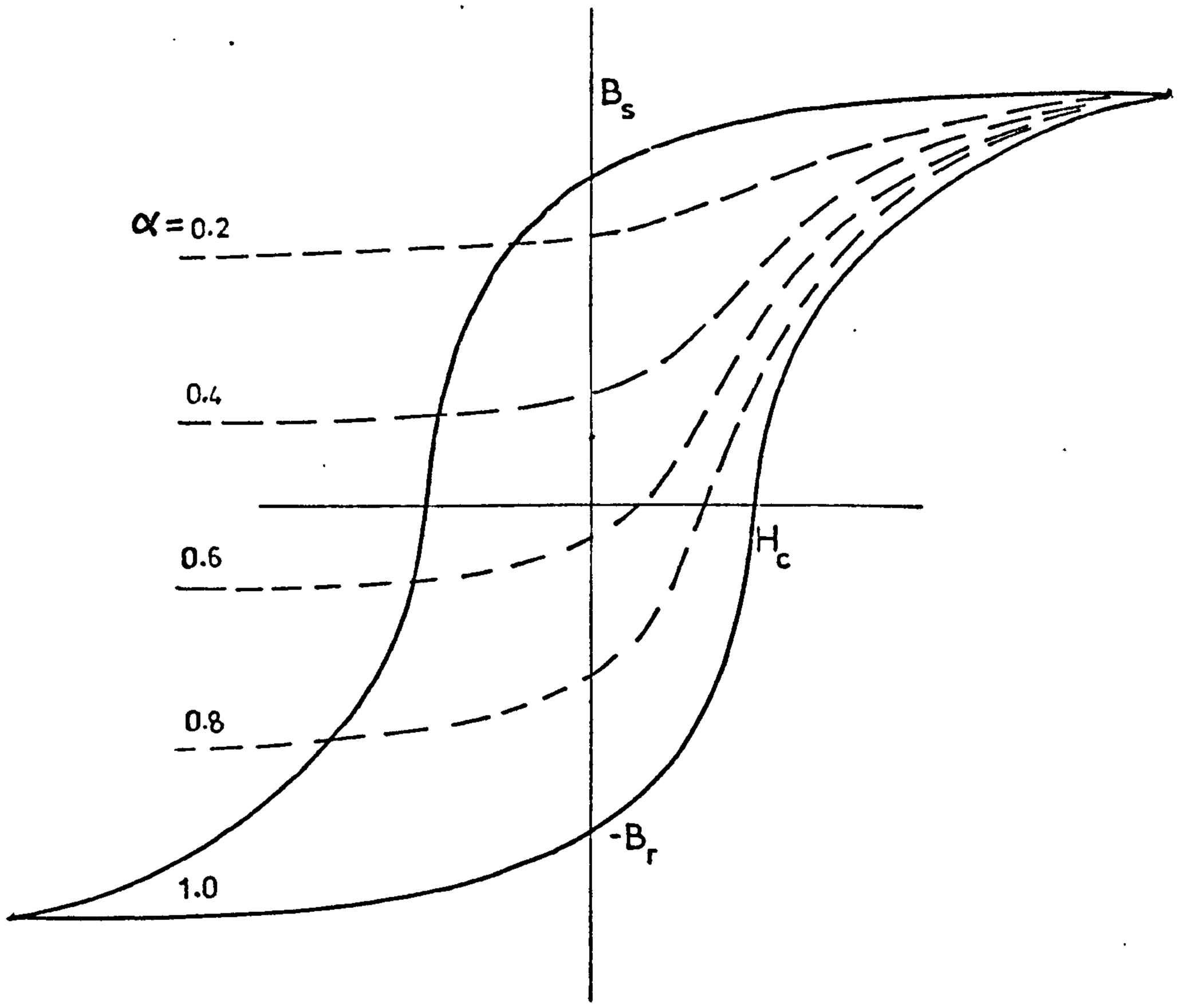

Fig.2.6.1 Variation of magnetisation curve with α.

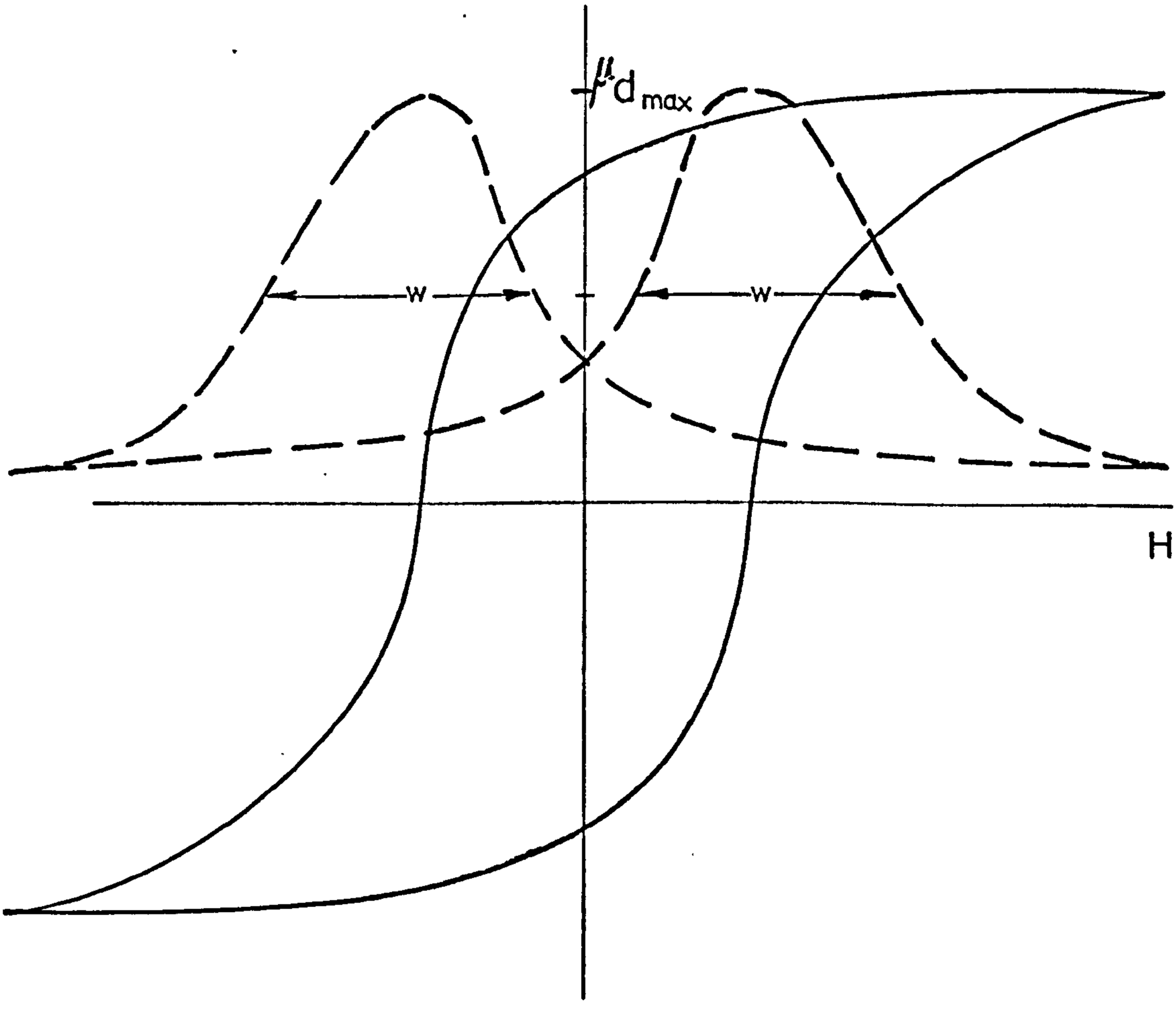

— — — — differential permeability curve.

Fig. 2.6.2 Half-height width of differentiated loop.

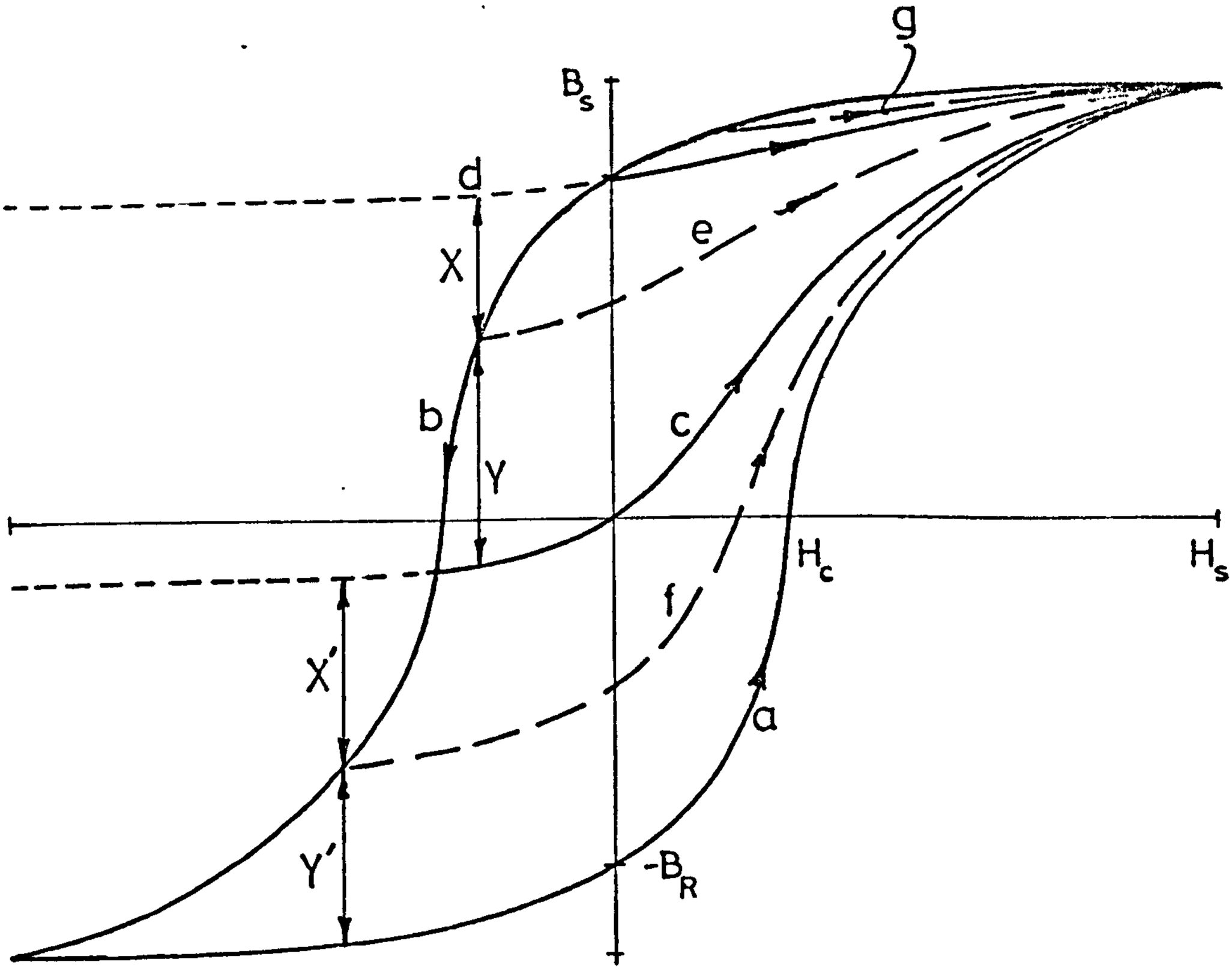

Fig. 2.6.3 Typical B/H loop showing salient points and curves.

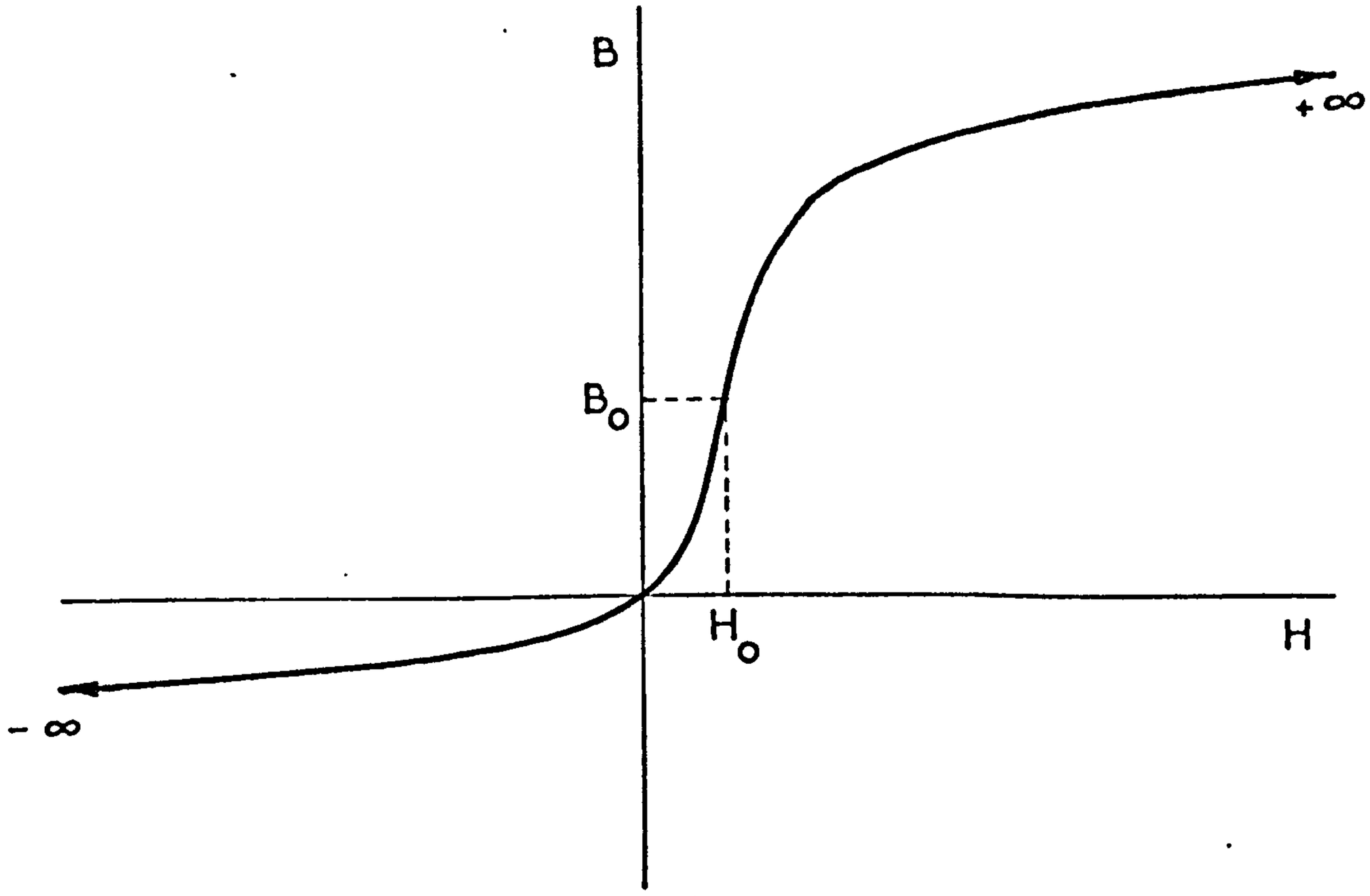

Fig. 2.6.4 General shape of complete B/H curve.

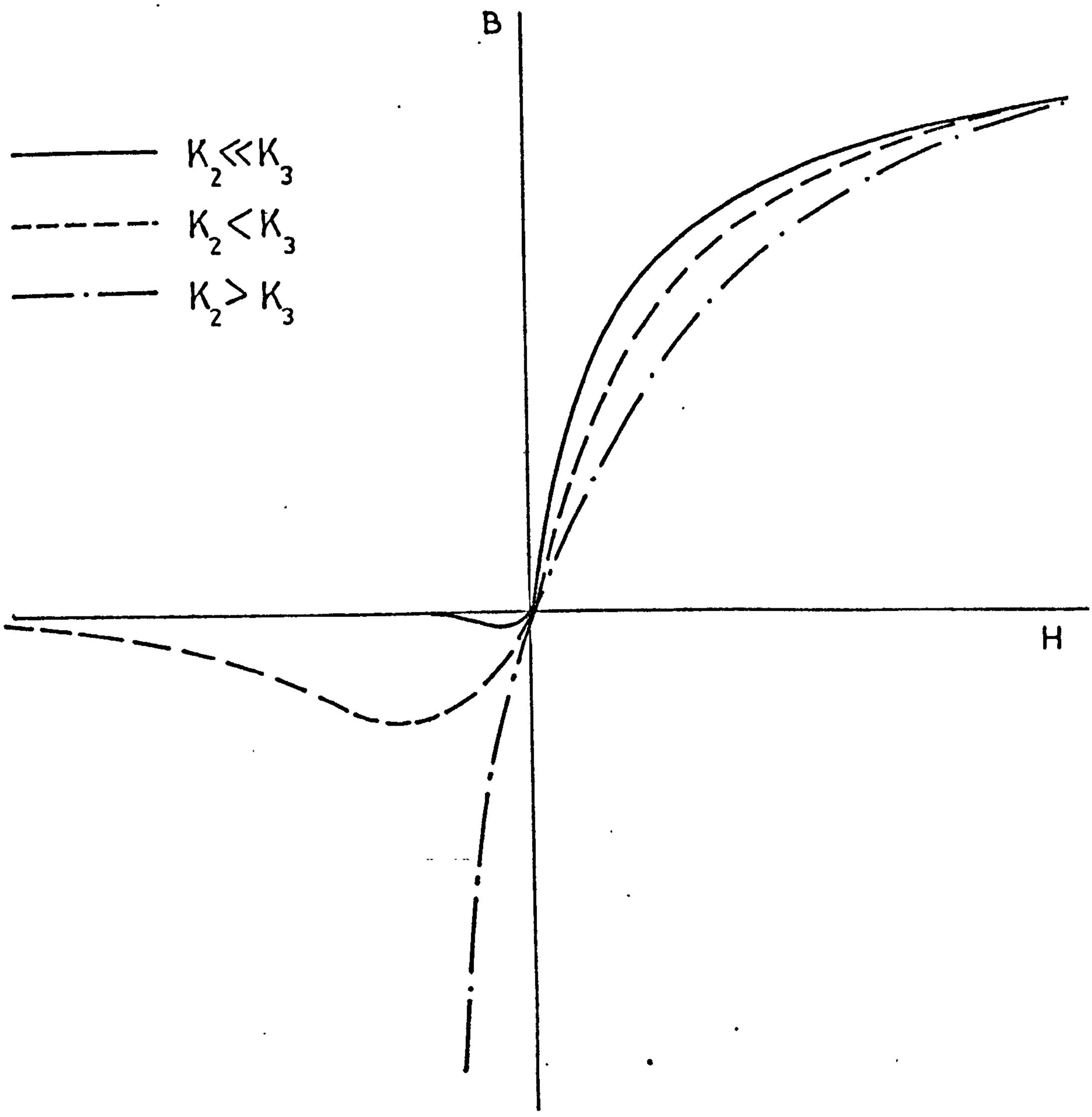

Fig. 2.6.5 Effect of varying K_2 and K_3 in eqn. 2.6.3

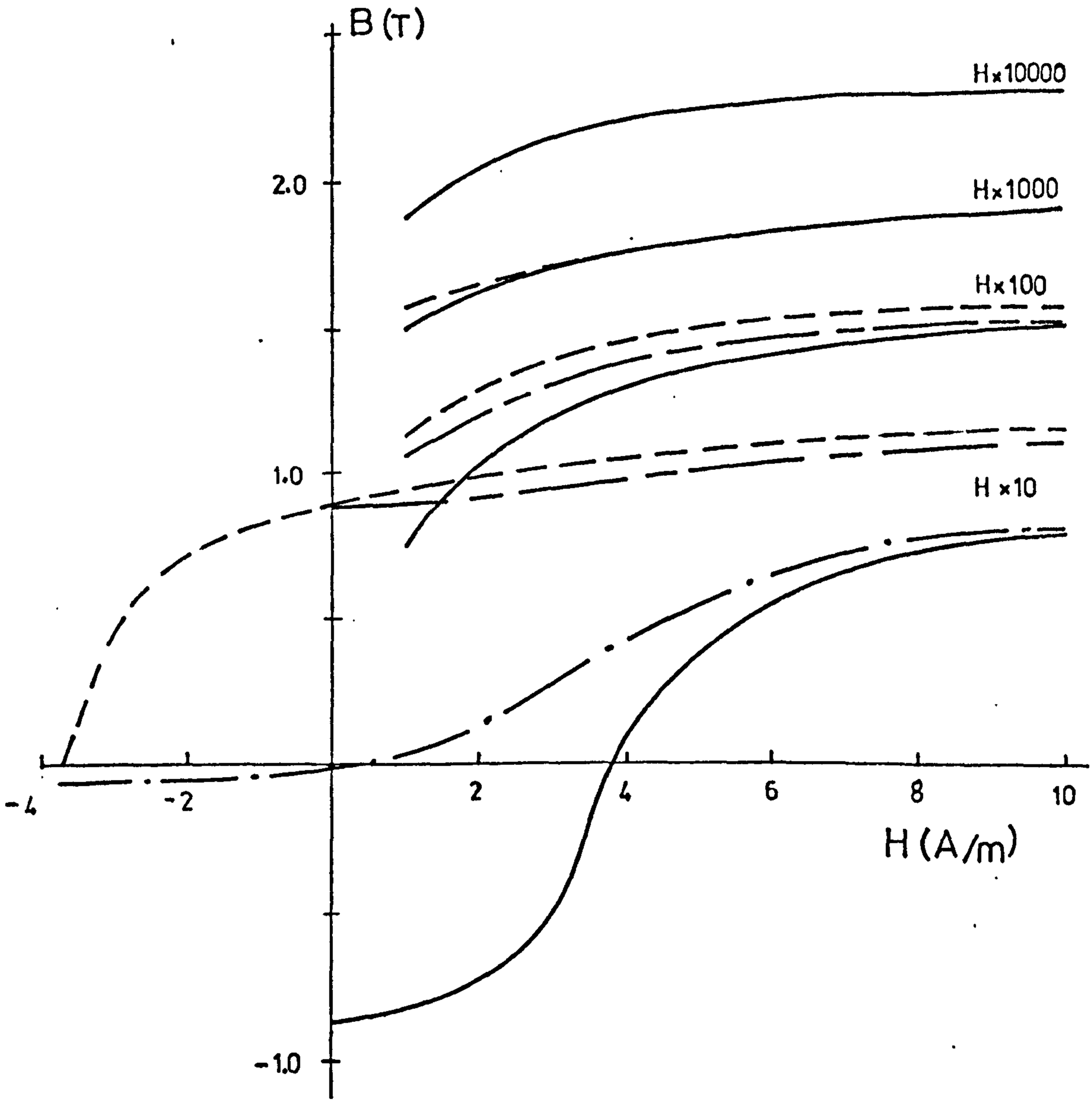

——————— Lower boundary curve.

— — — — Upper boundary curve.

——— · ——— Curve for $B_r = 0$

——— — ——— Curve for $B_r = B_R$

Fig. 2.6.6(a) Recorded B/H characteristic of Single-phase transformer.

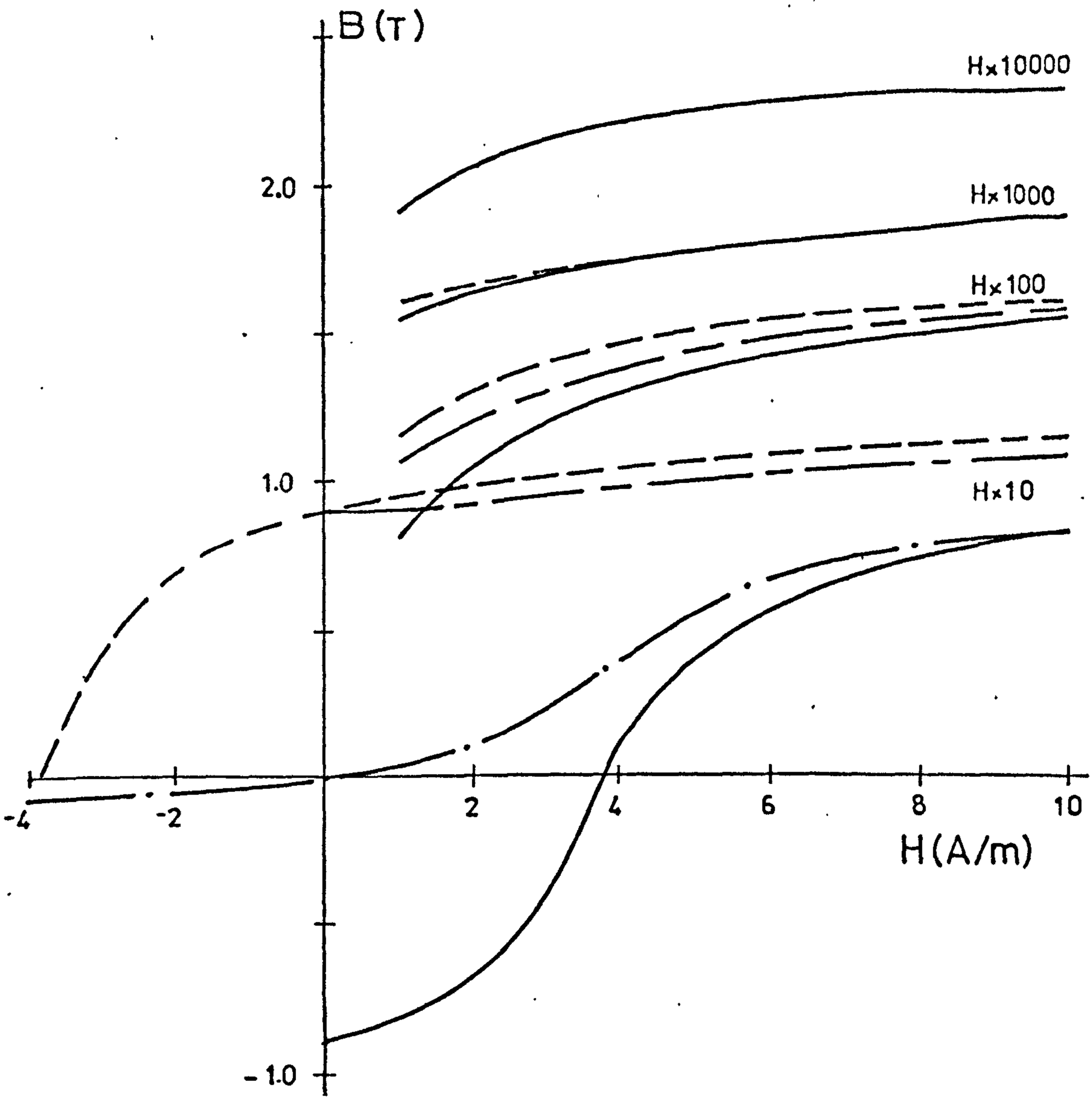

——— Lower boundary curve

— — — — Upper boundary curve

——·—— $B_r = 0$ curve

——–——– $B_r = B_R$ curve

Fig. 2.6.6(b) Representation of B/H characteristic of Single-phase transformer.

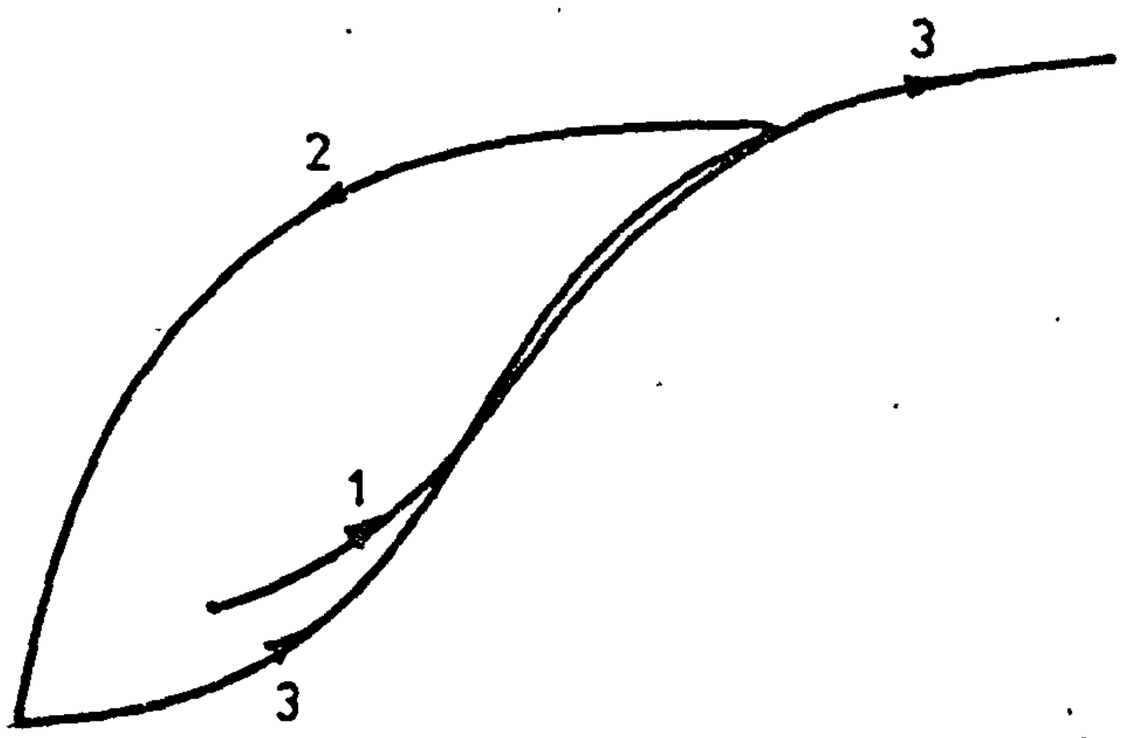

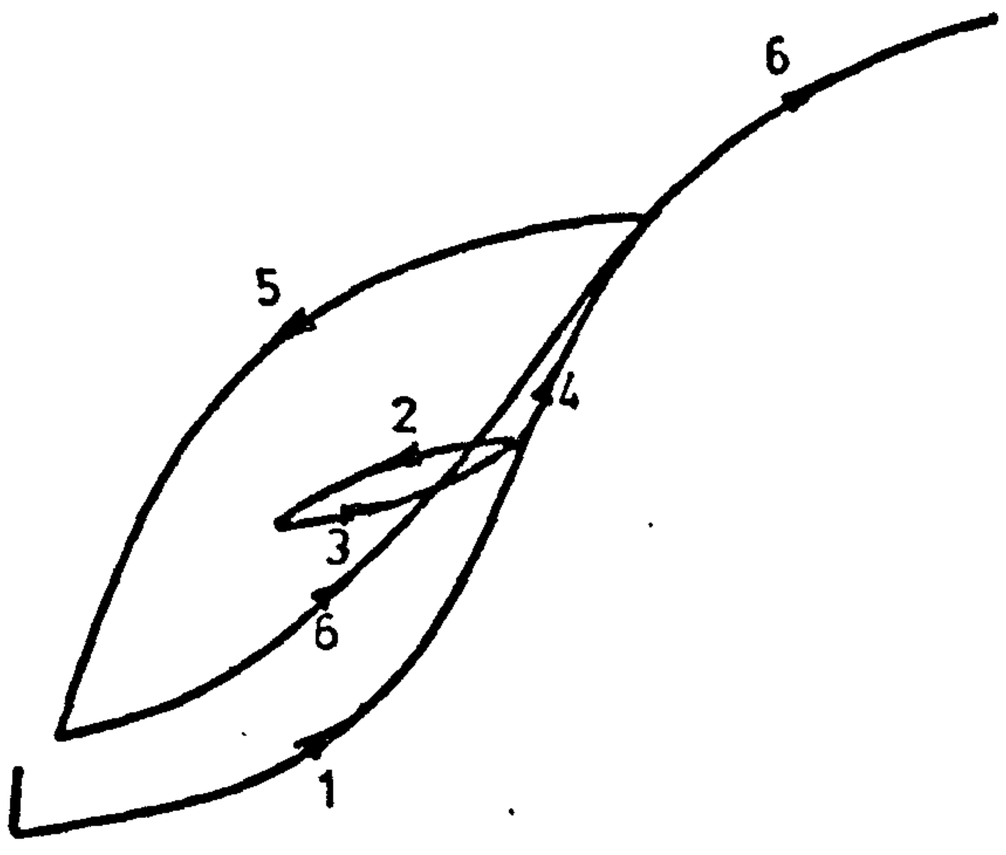

Fig. 2.6.7 Intersection of increasing trajectories.

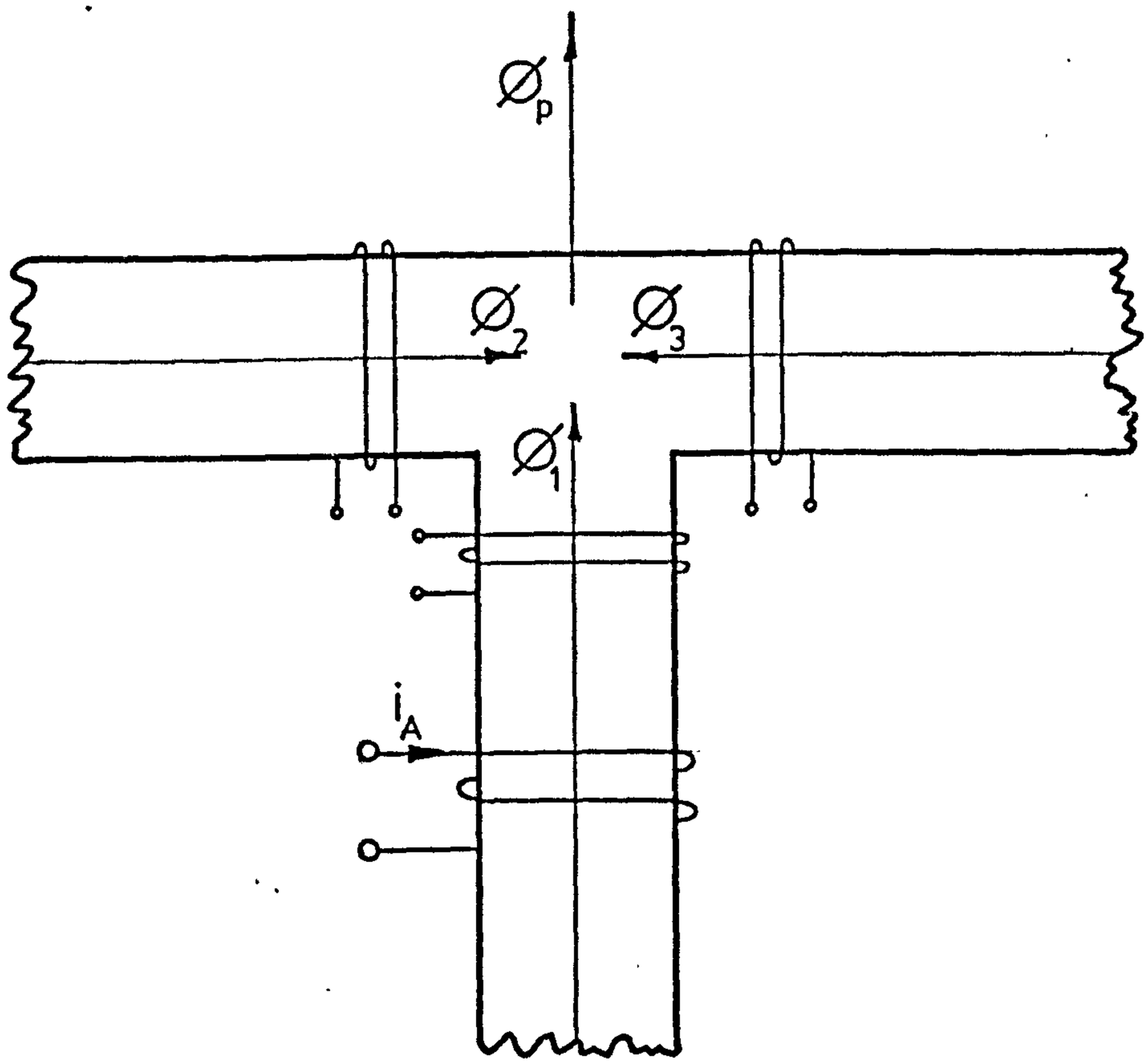

Fig. 3.1.1 Location of search coils.

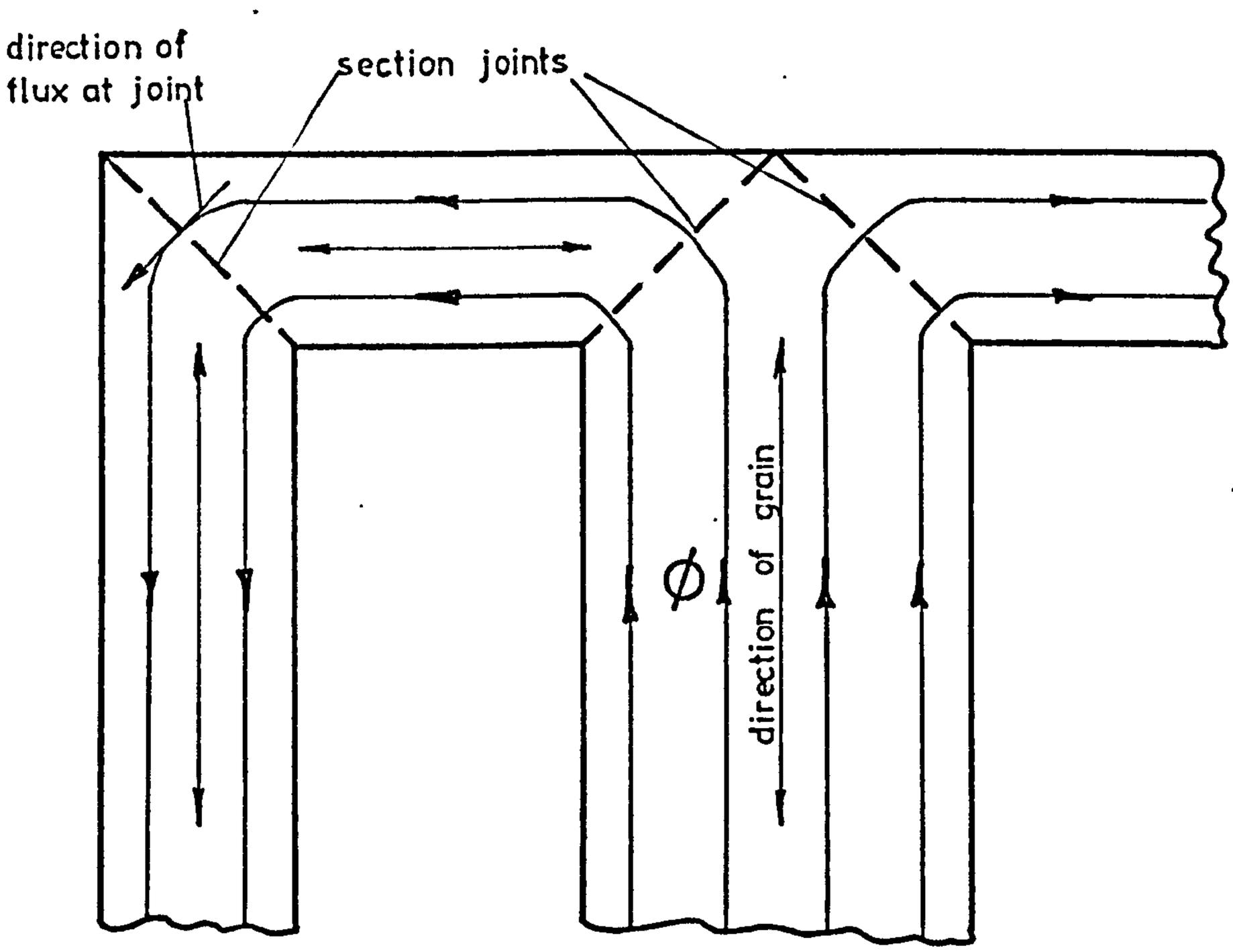

Fig. 3.2.1 Cross-grain flux at core joints.

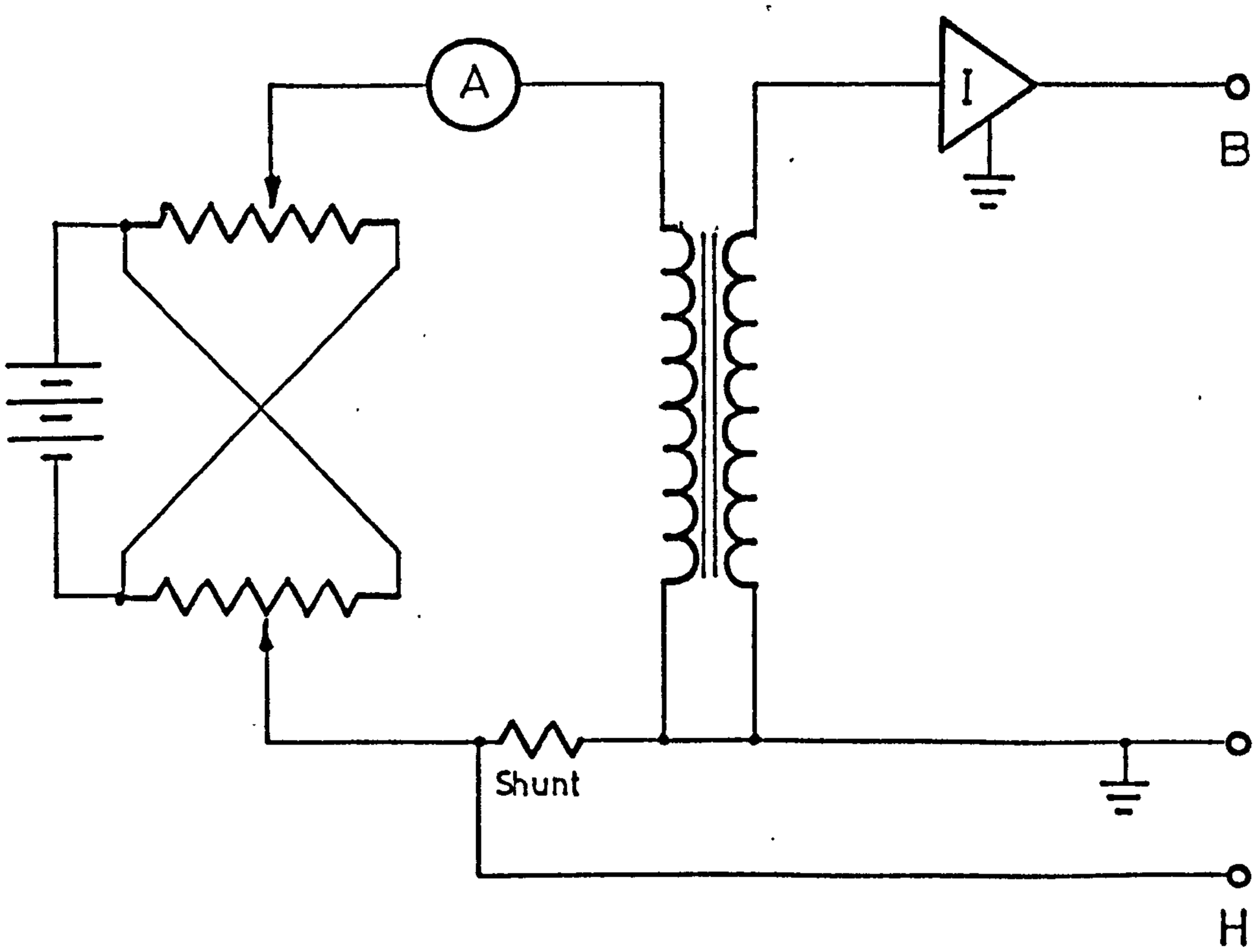

Fig. 3.2.2 Circuit used to obtain B/H characteristic.

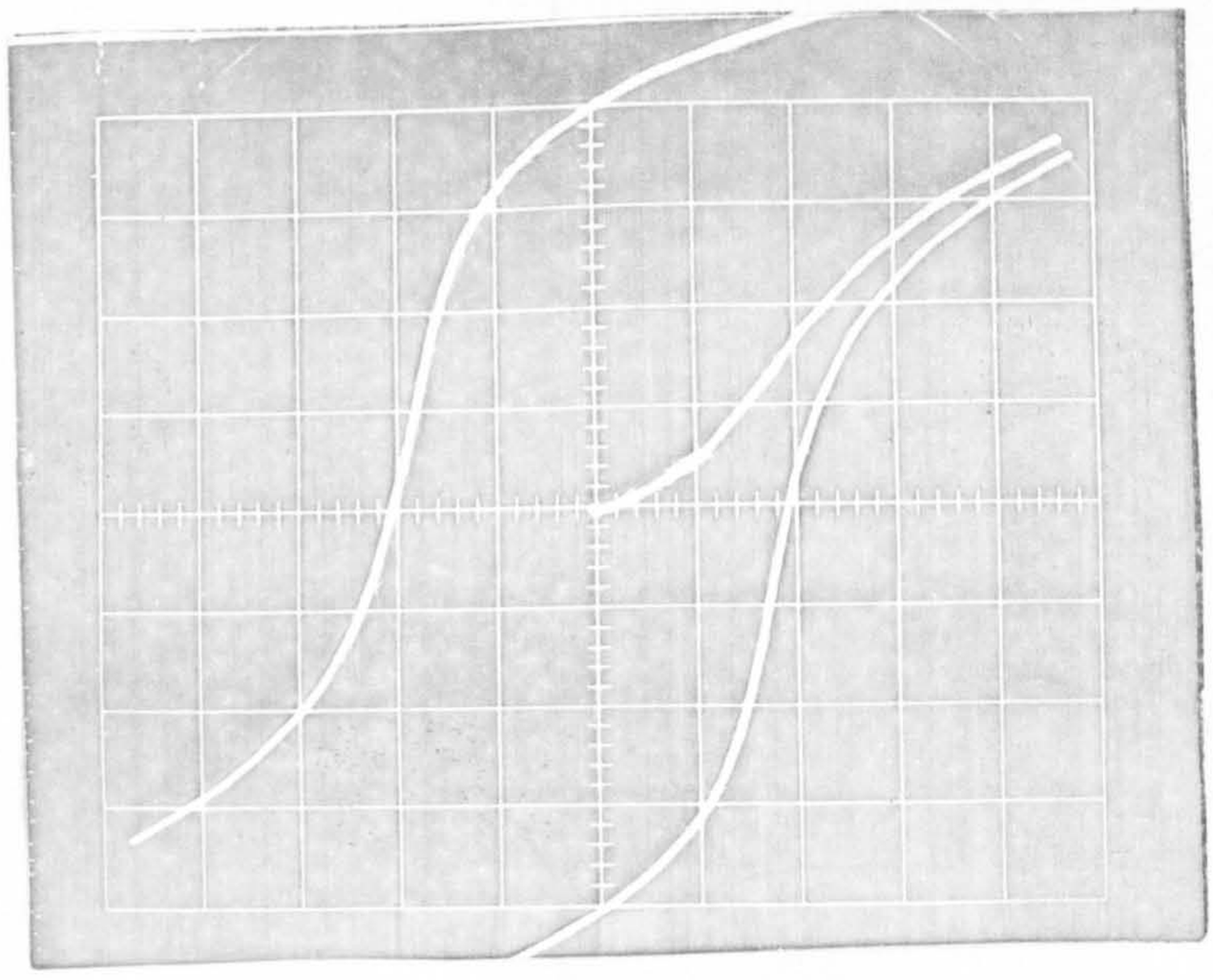

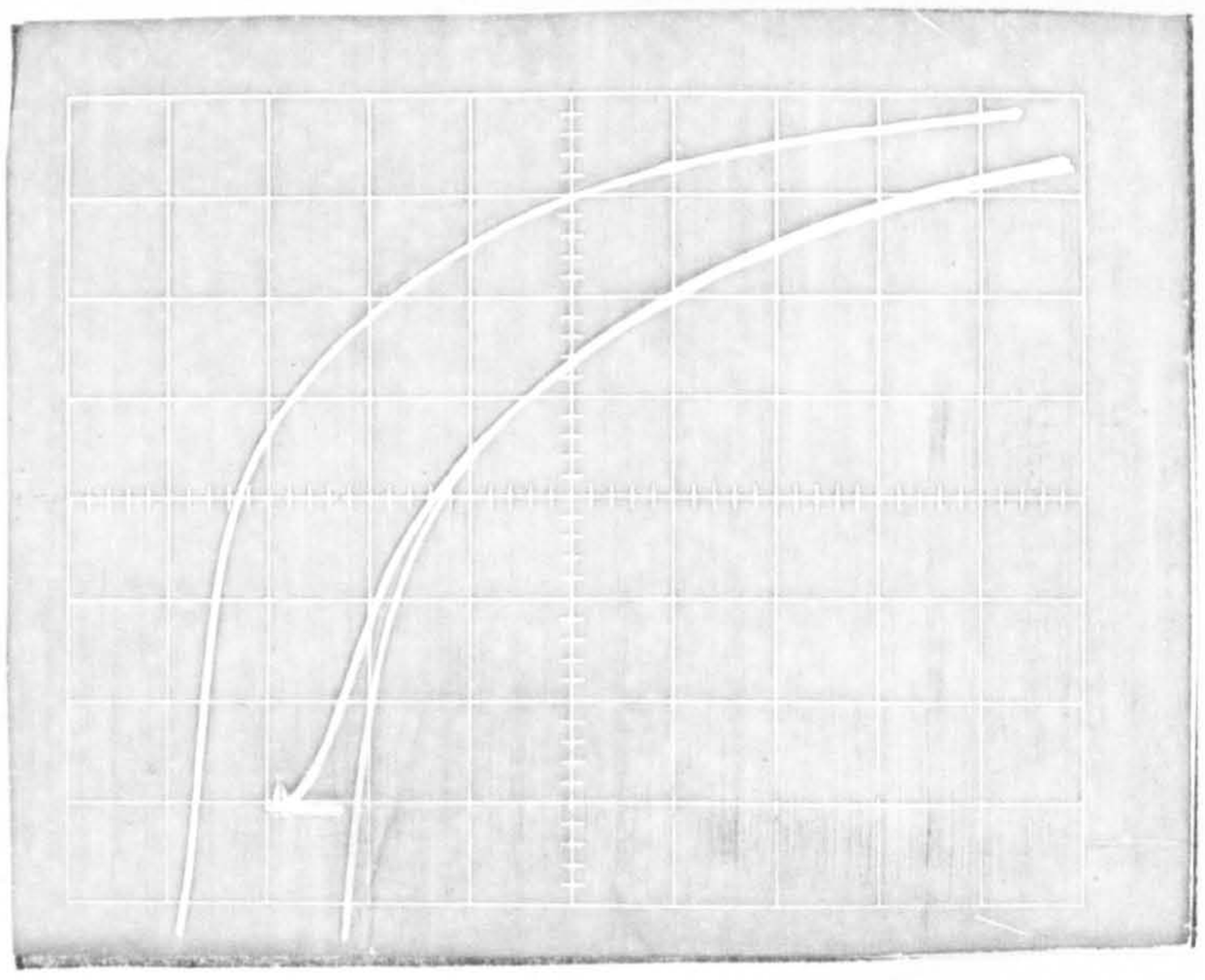

Fig. 3.2.3 Oscillograms of B/H characteristic of 8-kVA three-phase transformer.

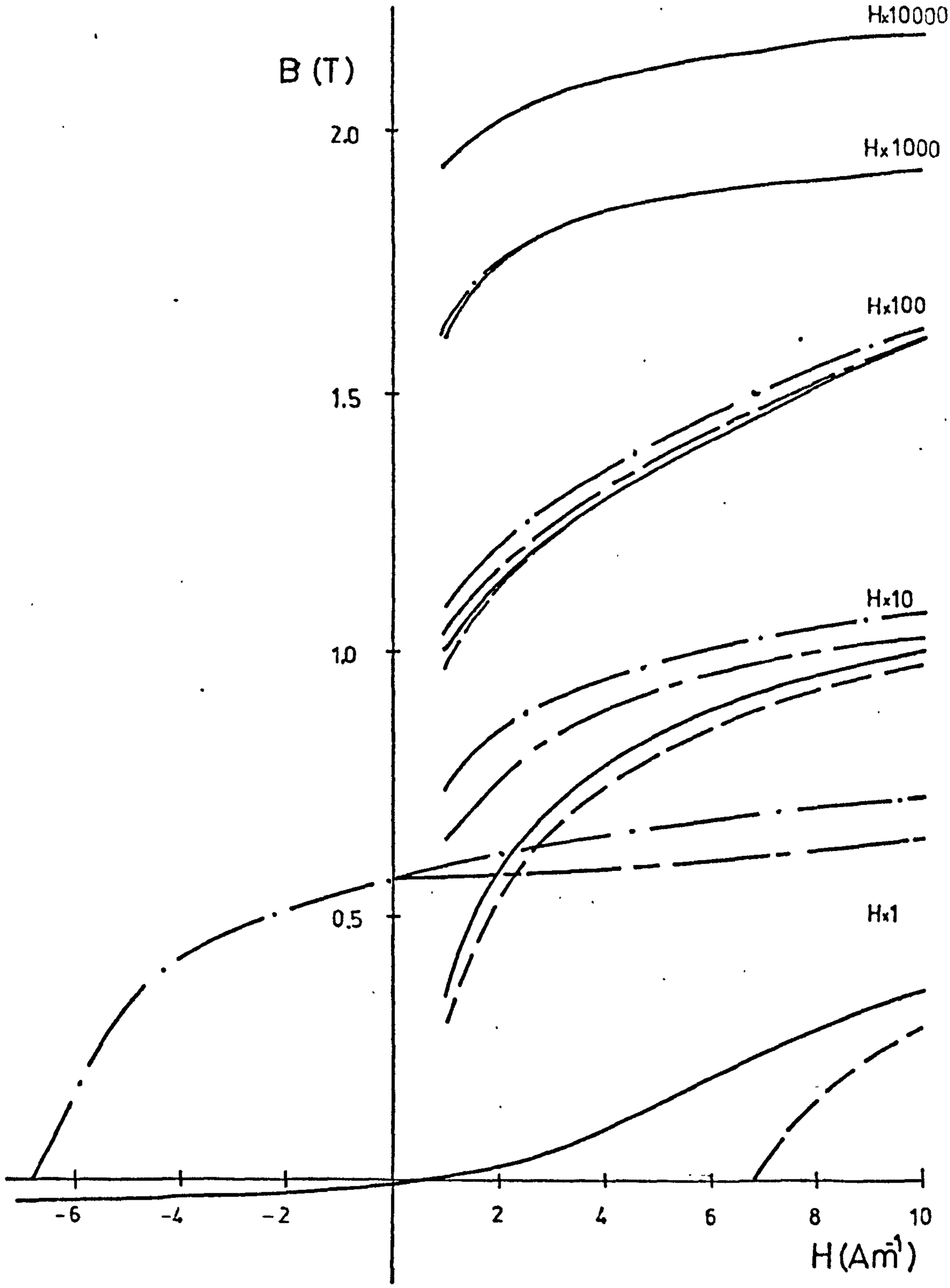

Fig. 3.2.4(a) Recorded B/H characteristic – 8 kVA, three-phase transformer.

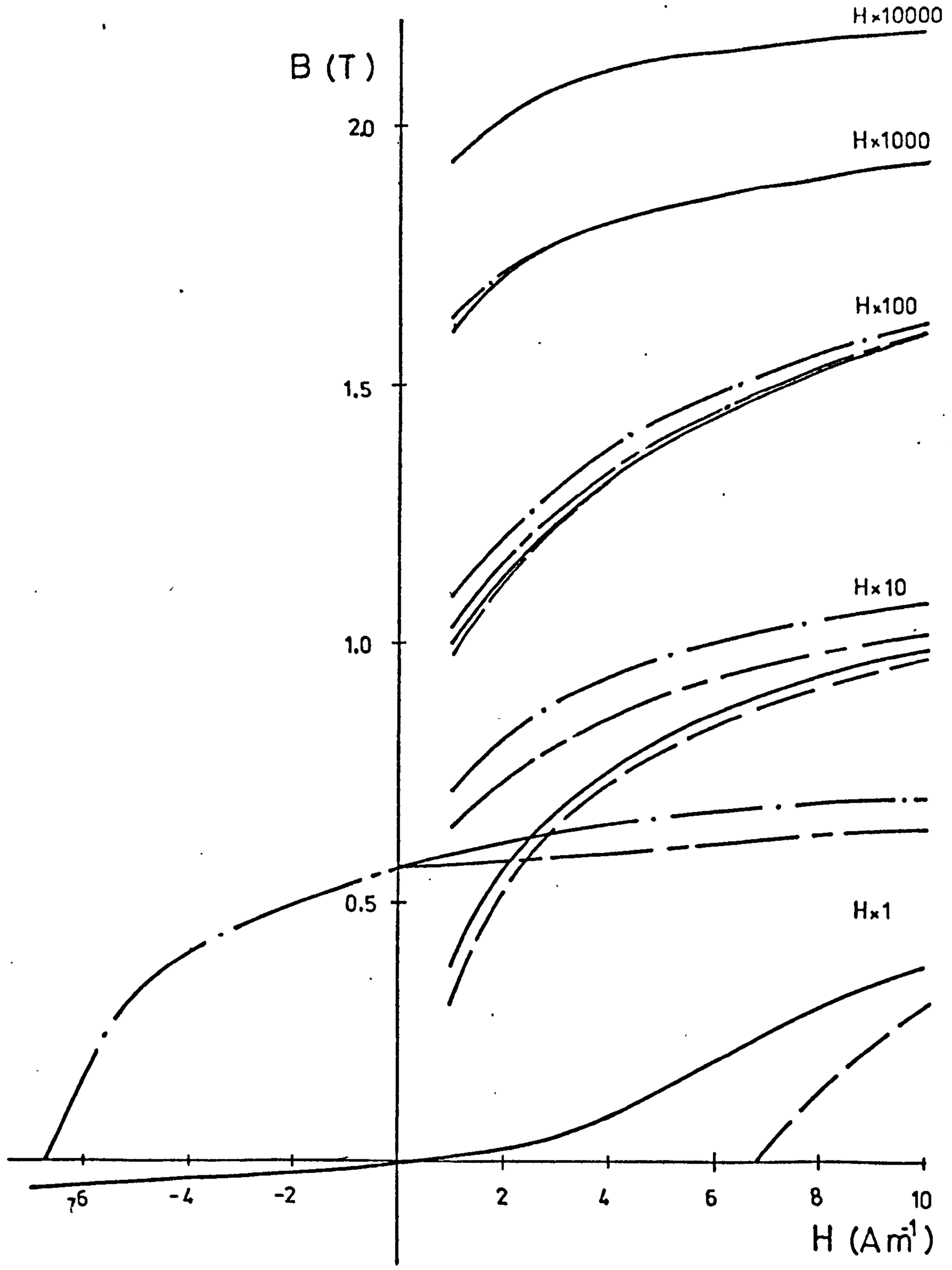

Fig. 3.24(b) Representation of B/H characteristic — 8 kVA, three-phase transformer.

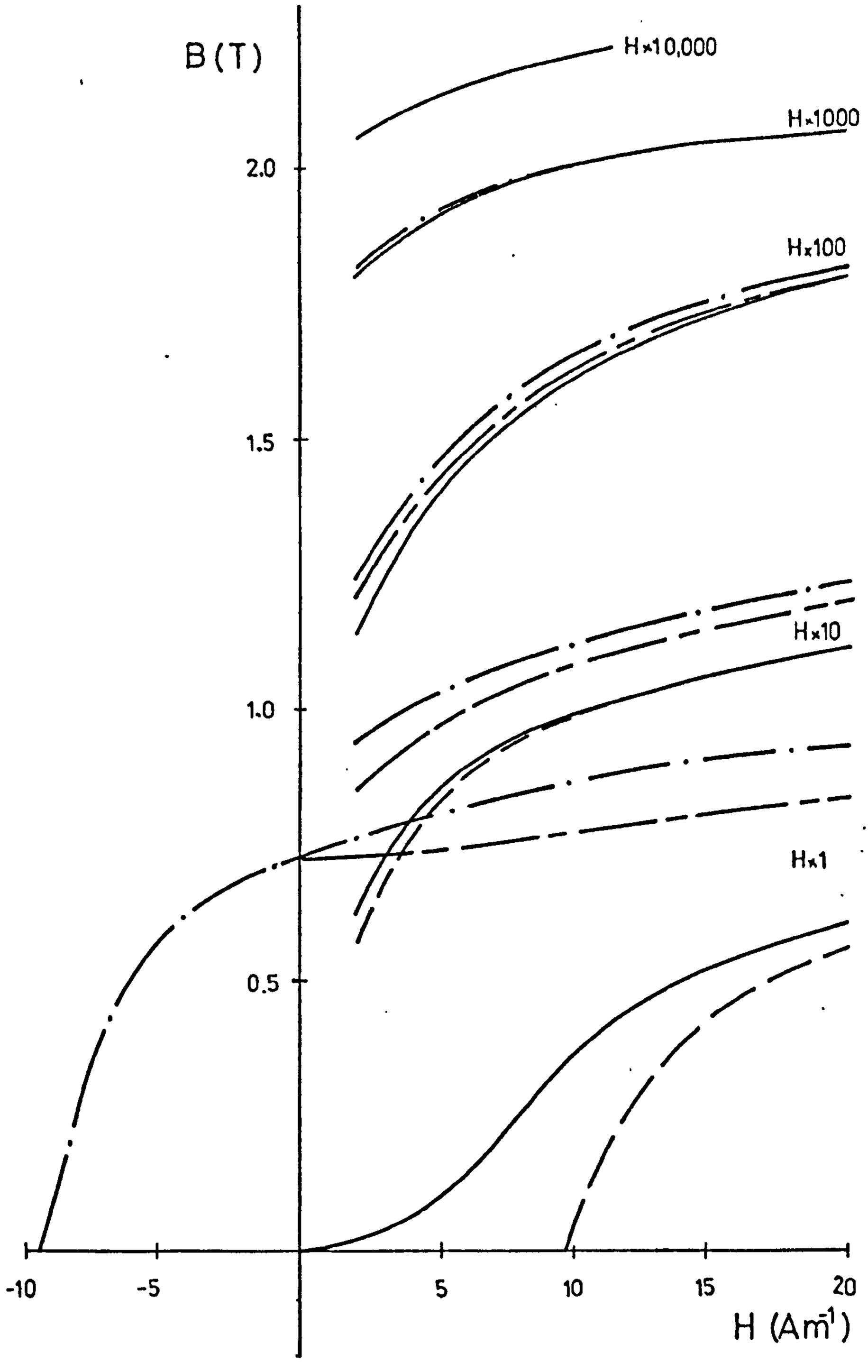

Fig. 3.2.5(a) Recorded B/H characteristic — 50 kVA, three-phase transformer.

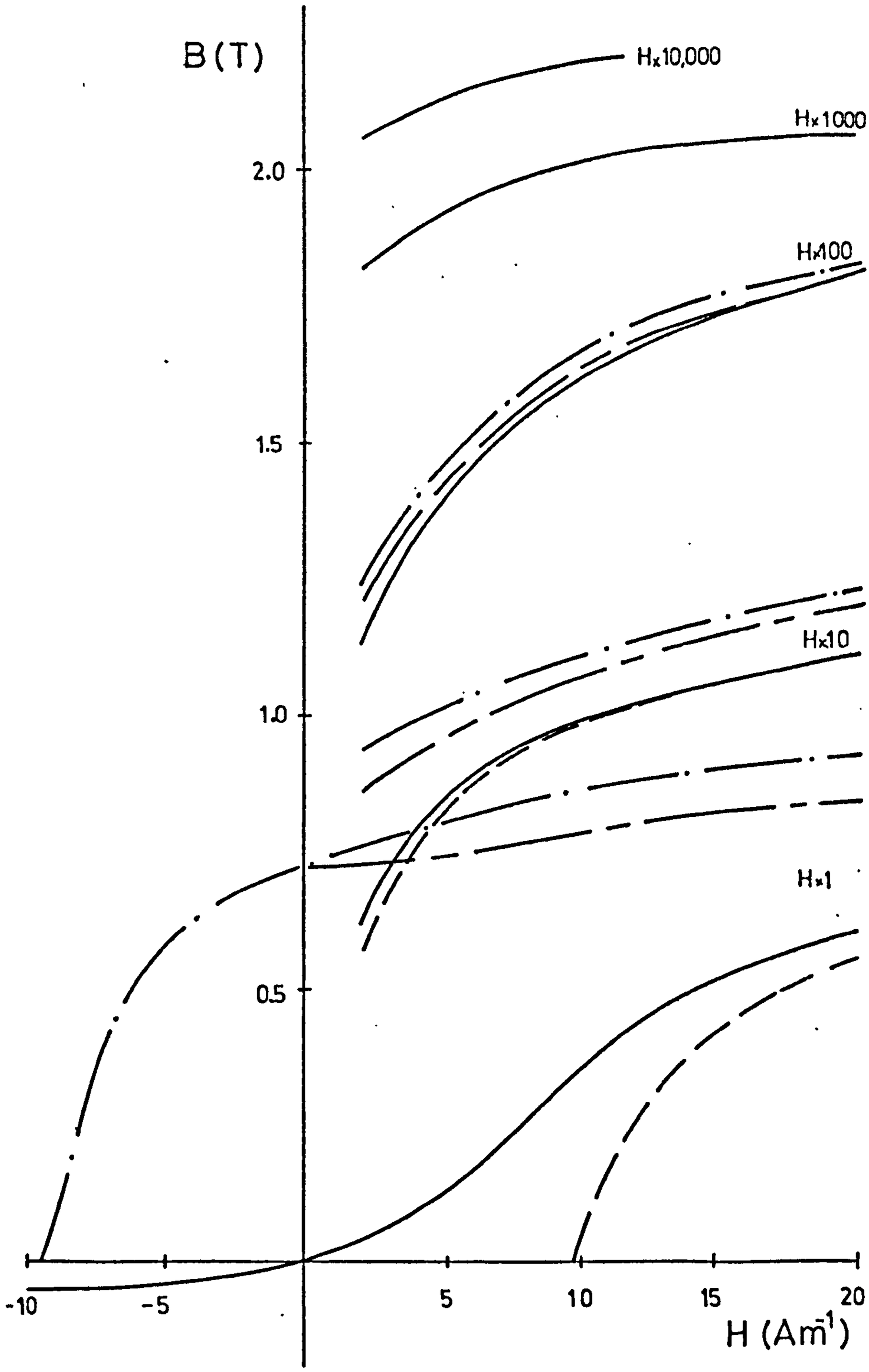

Fig. 3.2.5(b) Representation of B/H characteristic – 50 kVA three-phase transformer.

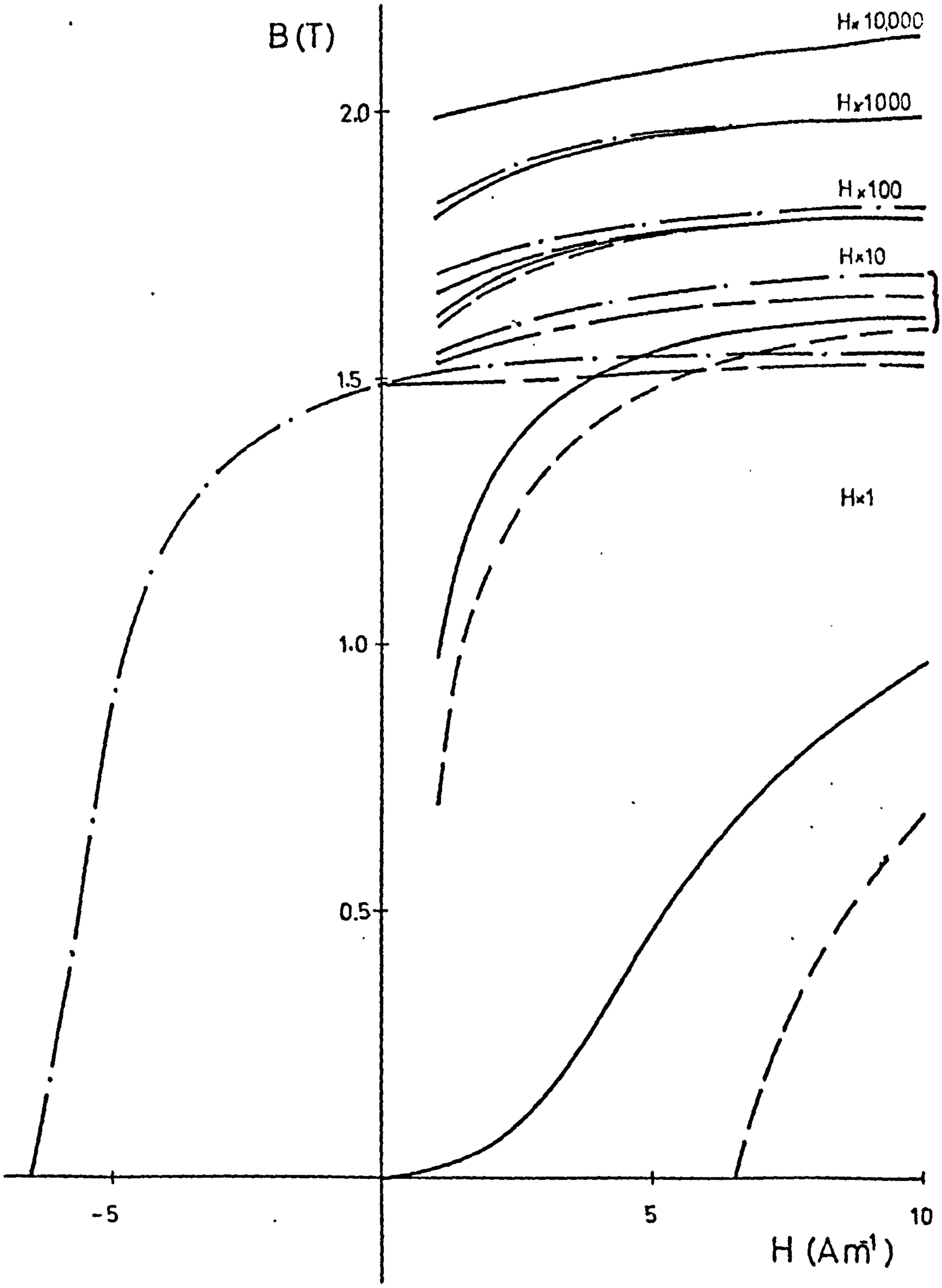

Fig. 3.2.6 Manufacturer's curves – 0° to grain 50 kVA, three-phase transformer.

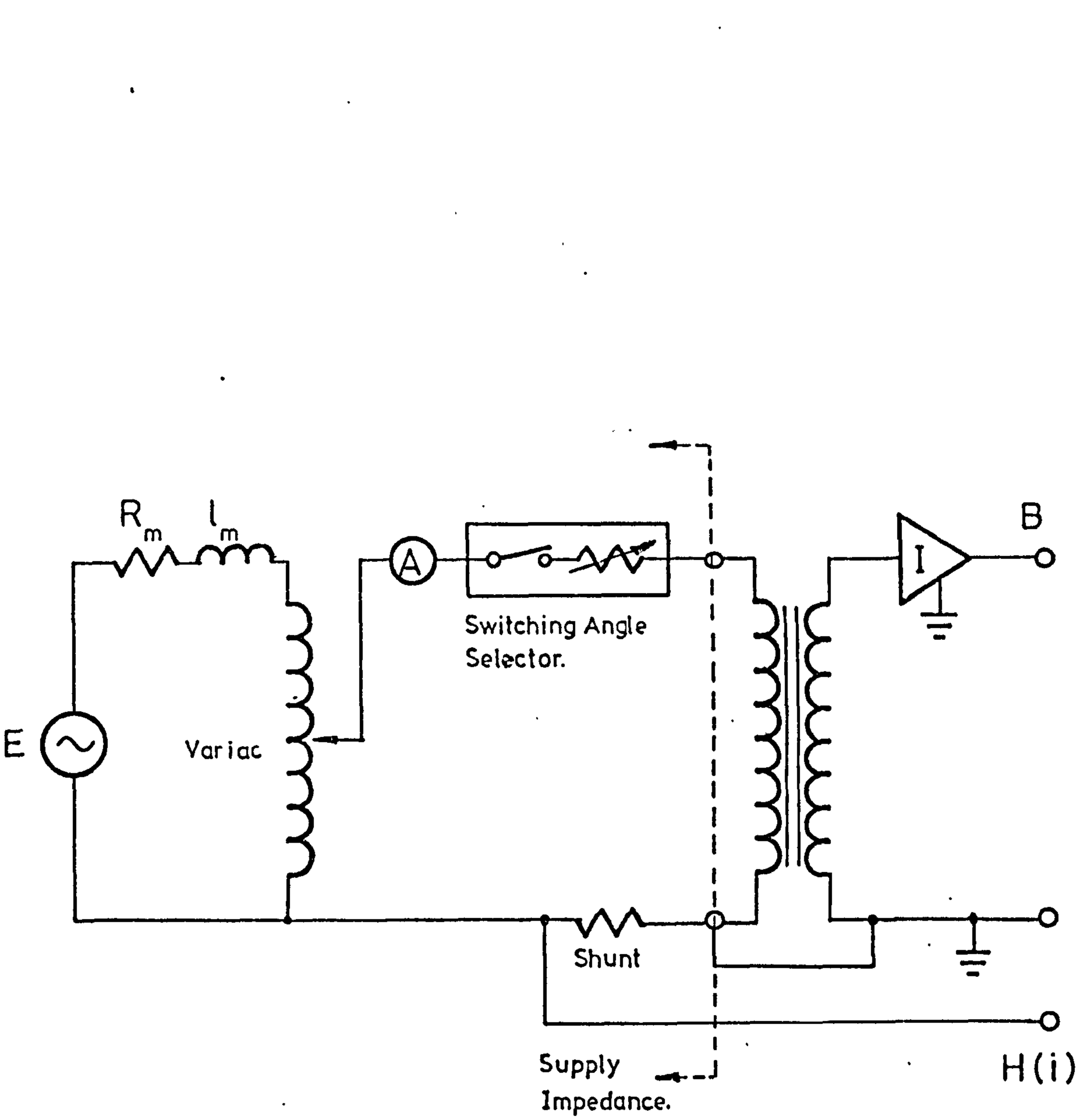

Fig. 3.3.1 Circuit used to control and record transformer conditions.

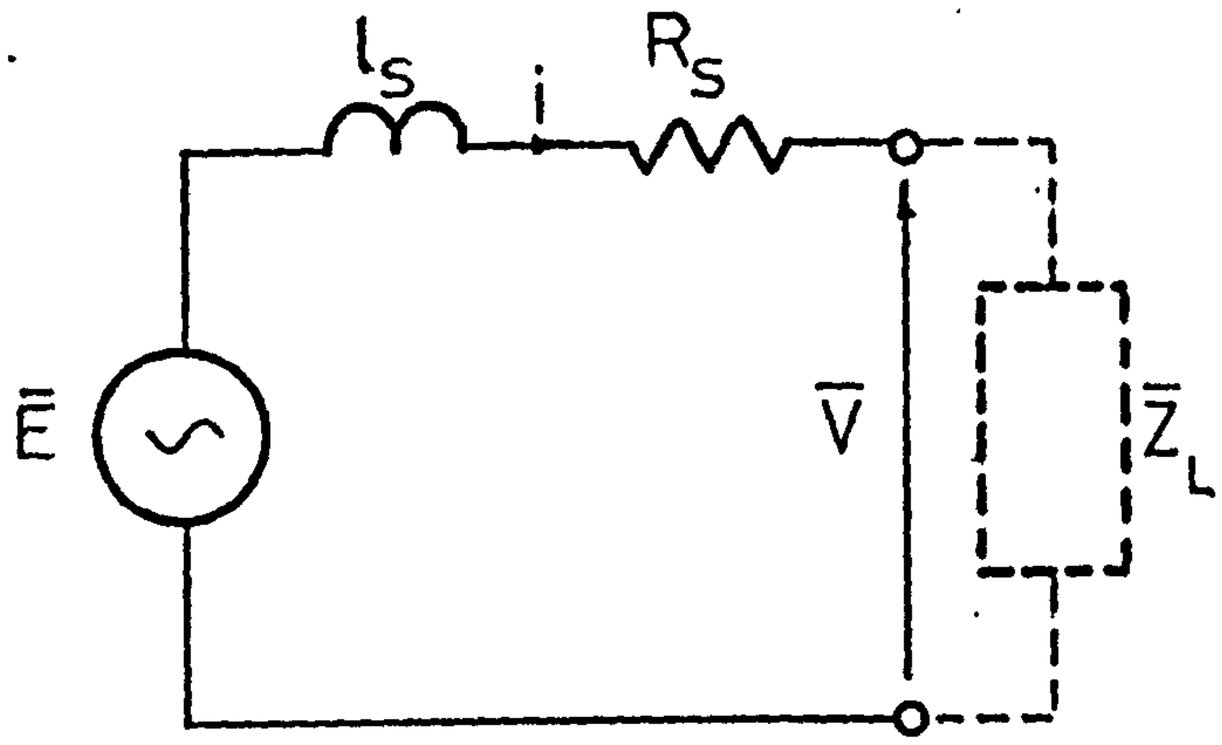

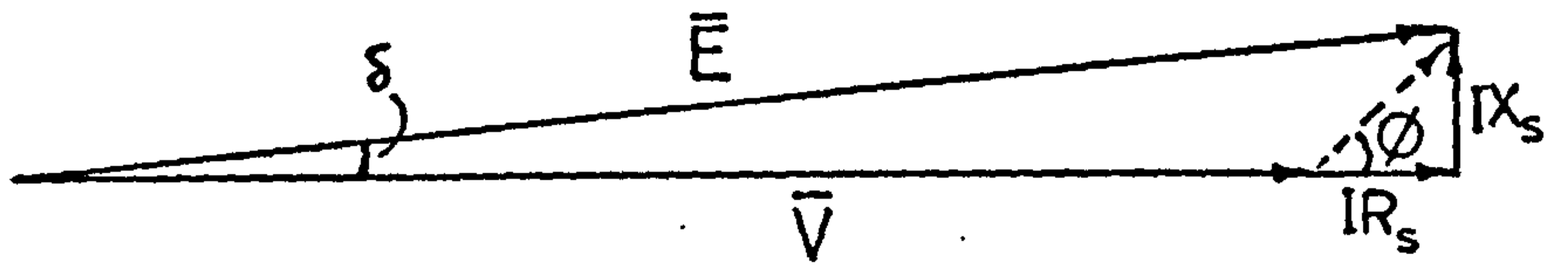

Fig. 3.3.2 Supply equivalent circuit and phasor diagram.

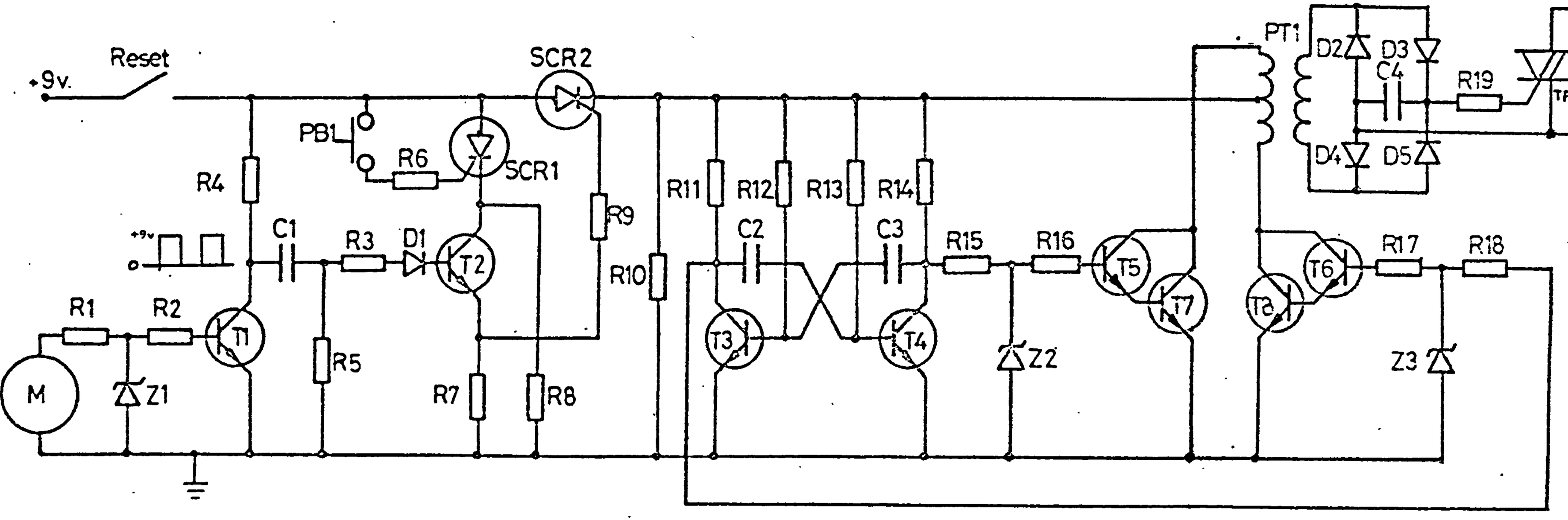

Fig. 3.4.1(a) Circuit diagram of switching angle selector.

Resistance (kΩ)		Capacitance (μF)	
R1	2.2	C1	0.047
R2	1.0	C2	0.01
R3	4.7	C3	0.01
R4	1.0	C4*	0.33
R5	10.0		
R6	0.47		
R7	2.2	D1-5	1N4001
R8	0.47		
R9	0.47	T1-6	BC107
R10	0.47	T7-8	2N3053
R11	0.22		
R12	4.7	SCR1-2	BTX-30
R13	4.7		
R14	0.22	Z1-3	3v zener diodes
R15	2.2		
R16	4.7		
R17	4.7		
R18	2.2		
R19*	0.15		

All resistors $\frac{1}{4}$watt except R8 and R10 which are $\frac{1}{2}$watt

* values of R19 and C4 depend on gate characteristics of triac used.

Fig. 3.4.1(b) Component values of Switching Angle Selector.

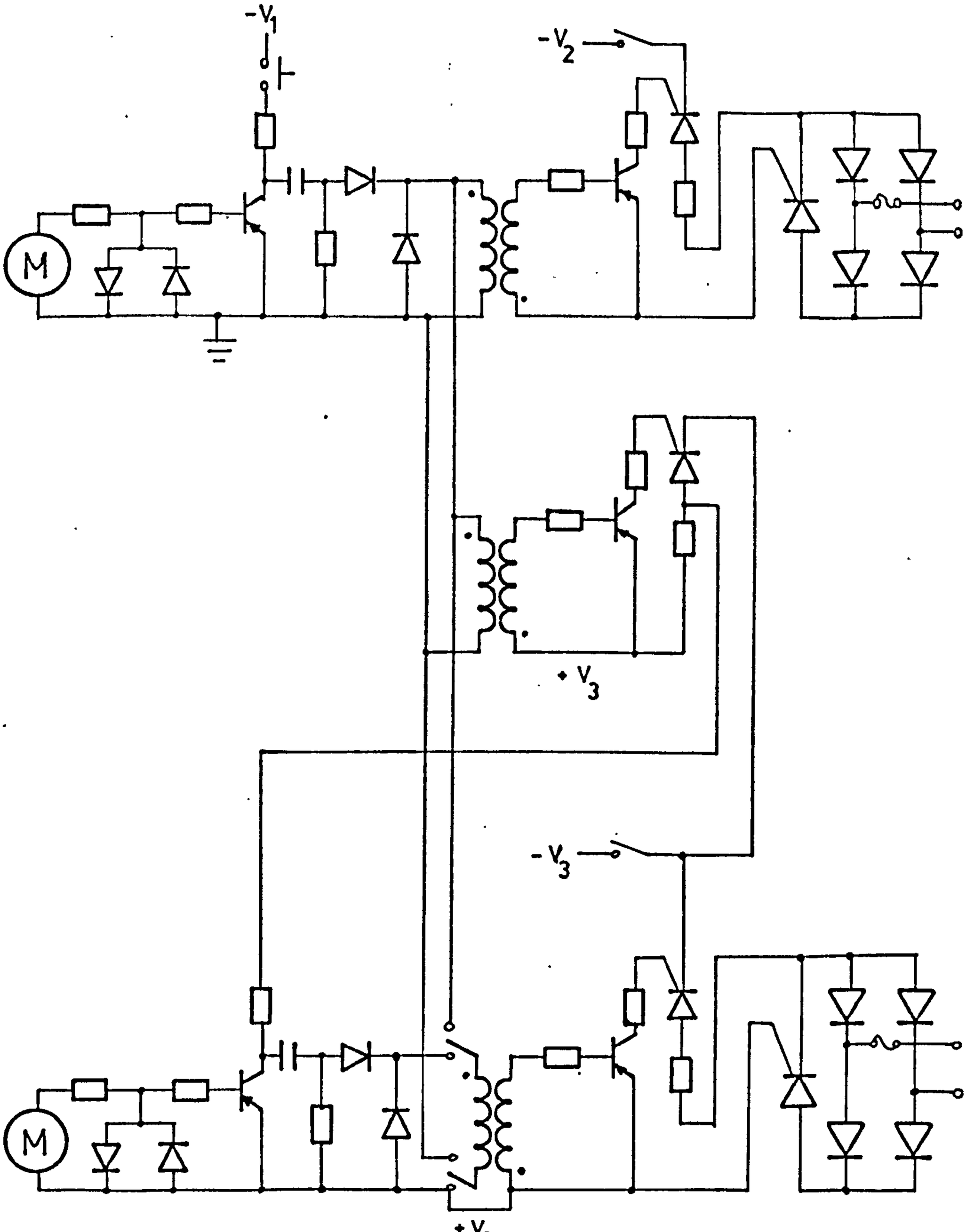

Fig. 3.4.2 Switching angle selector – original design.

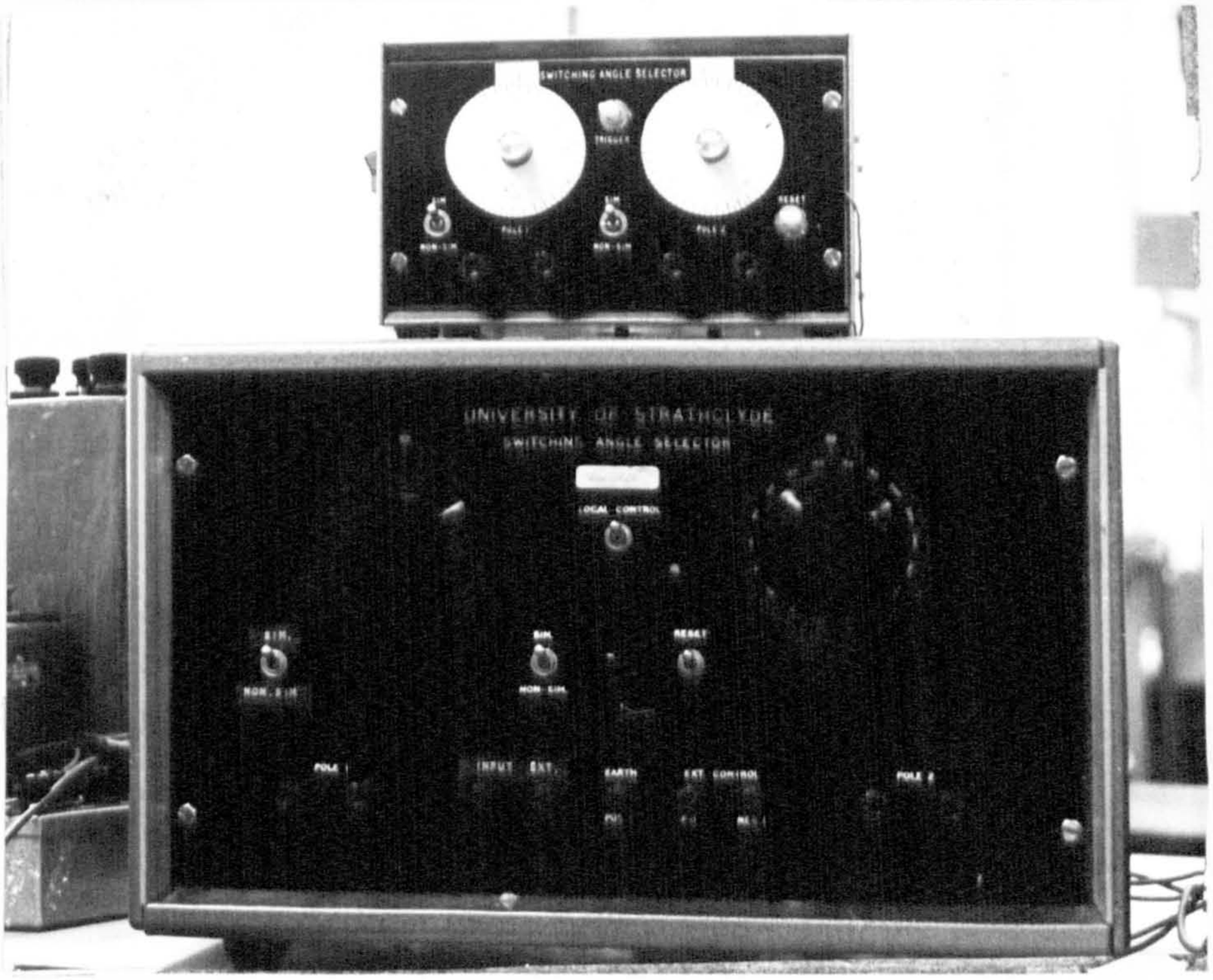

Fig. 3.4.3 Switching angle selectors - front panels.

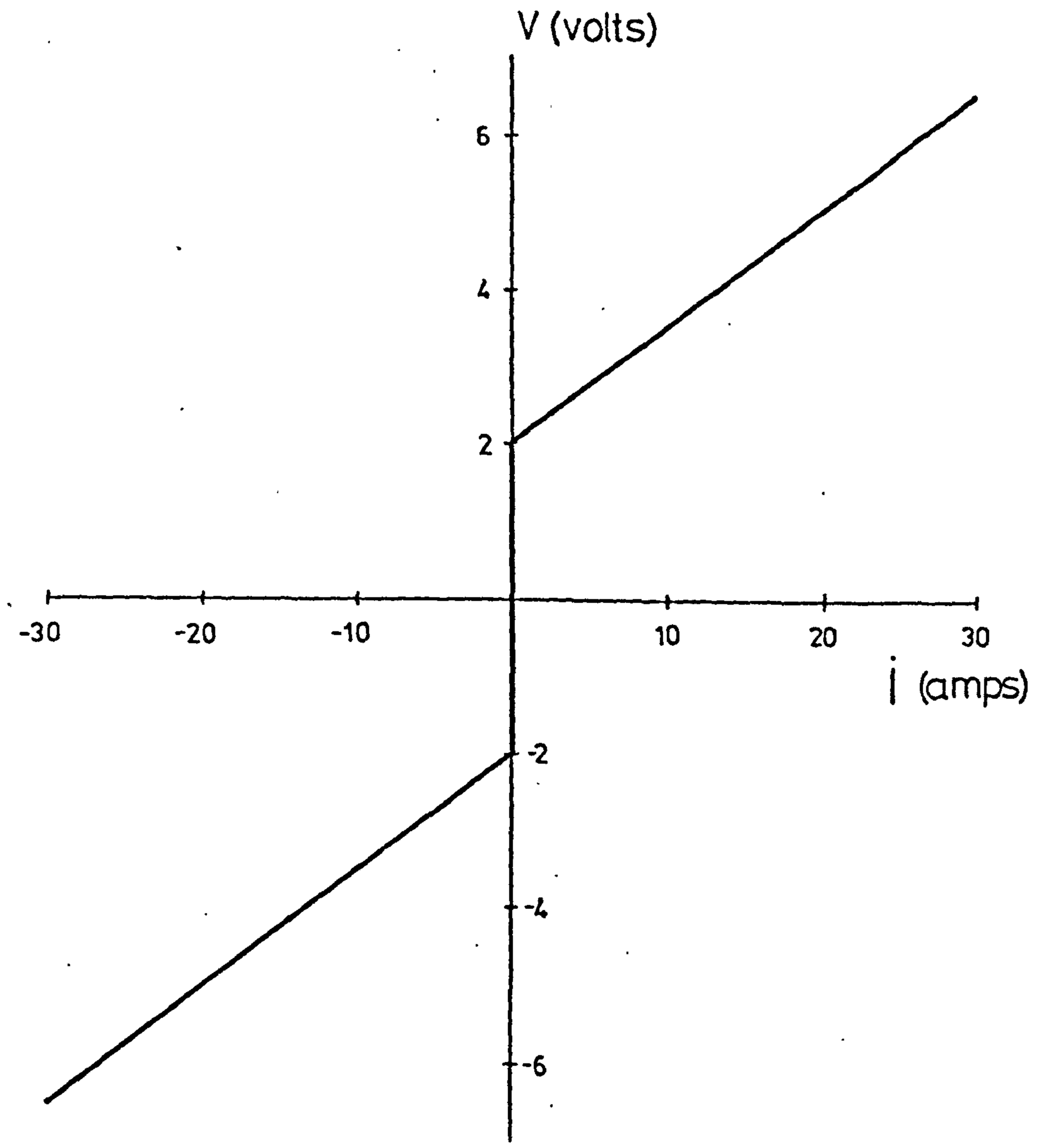

Fig. 3.4.4 Voltage/current characteristic of S.A.S.

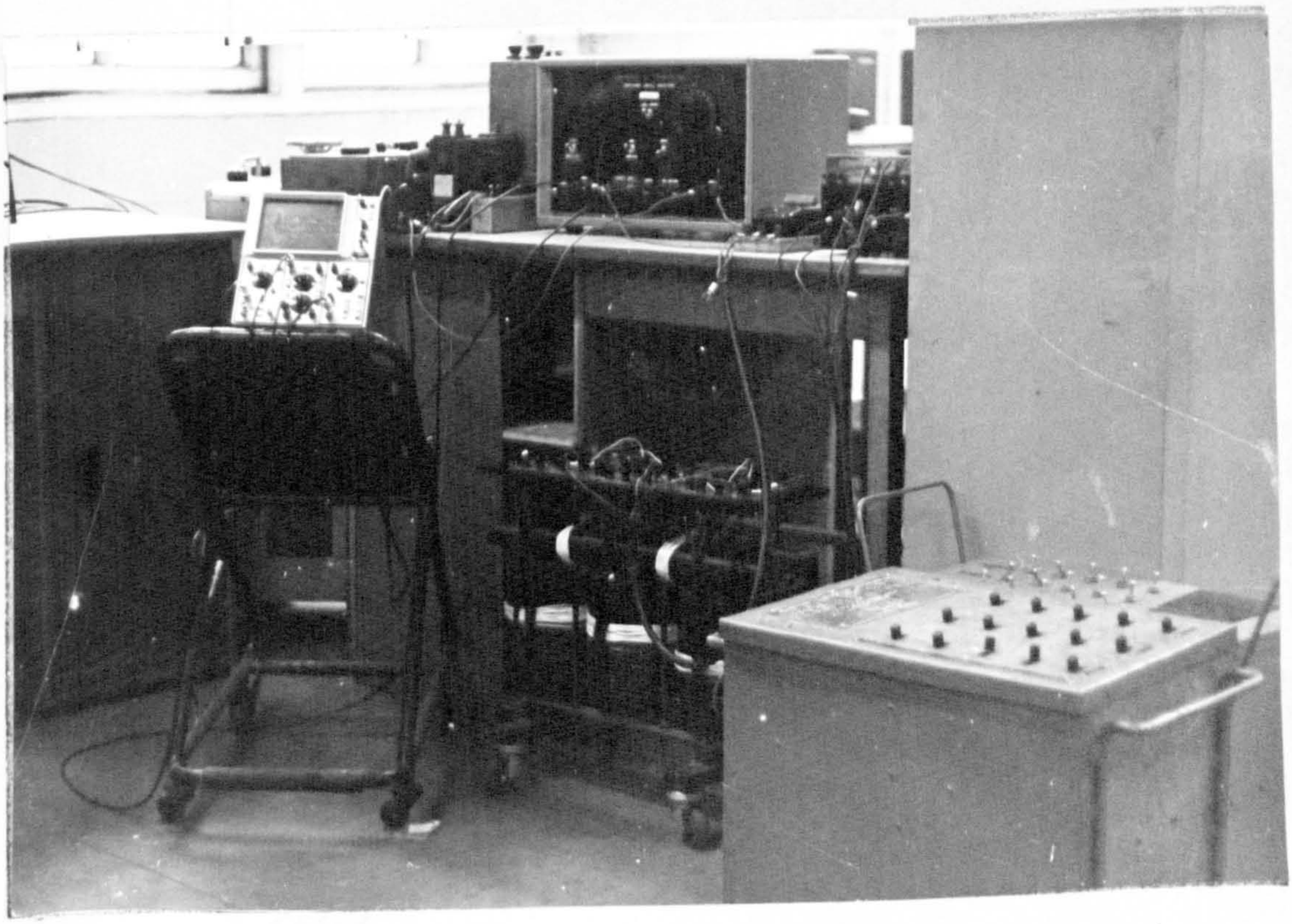

Fig. 3.5.1 Experimental equipment.

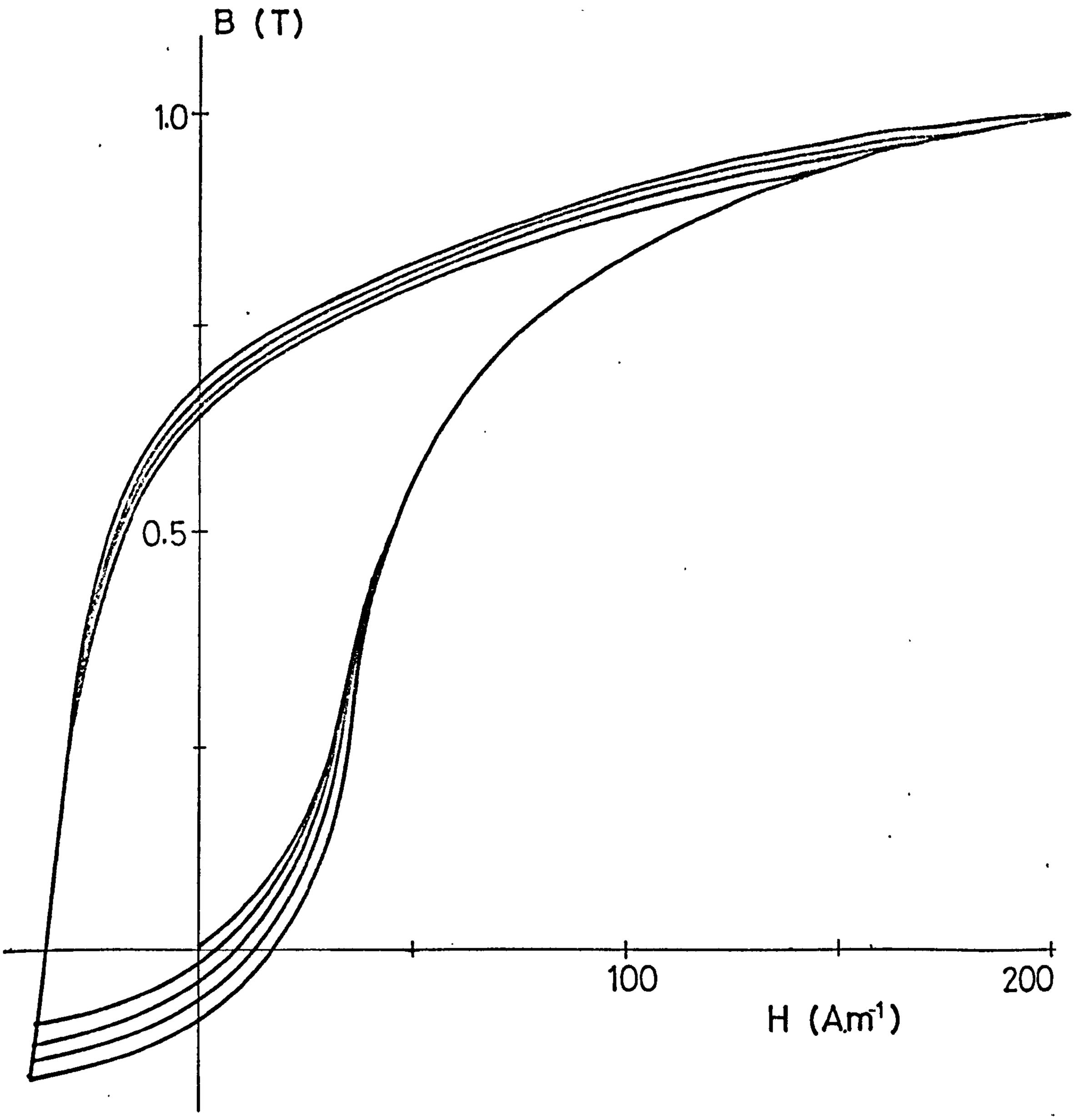

Fig. 4.1.1(a) Computed transient B/H characteristic for 1-kVA single-phase transformer.
$\alpha = 30°$, $V = 65v$.

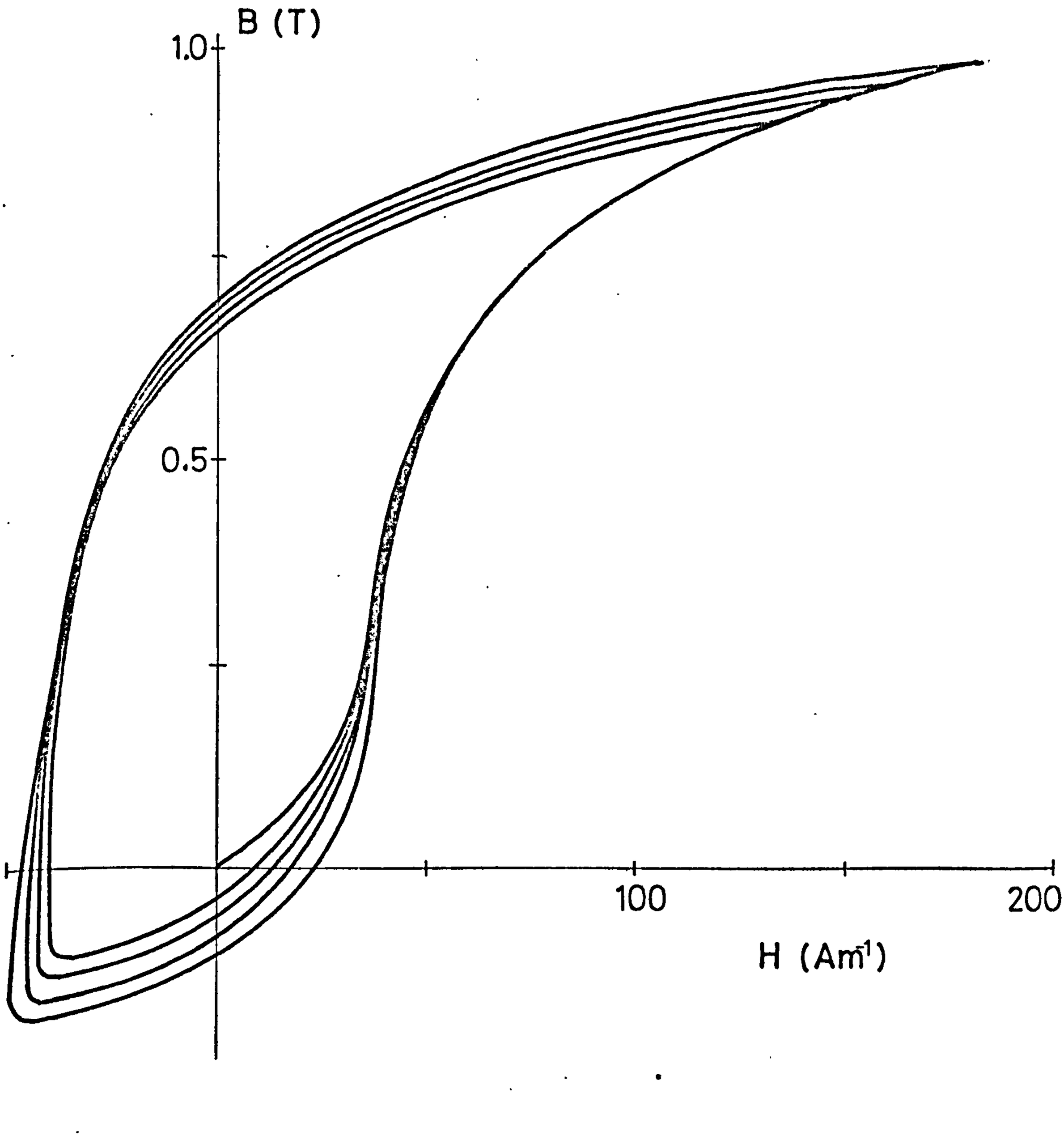

Fig. 4.1.1(b) Recorded transient B/H characteristic.
$\alpha = 30°$, $V = 65v$.

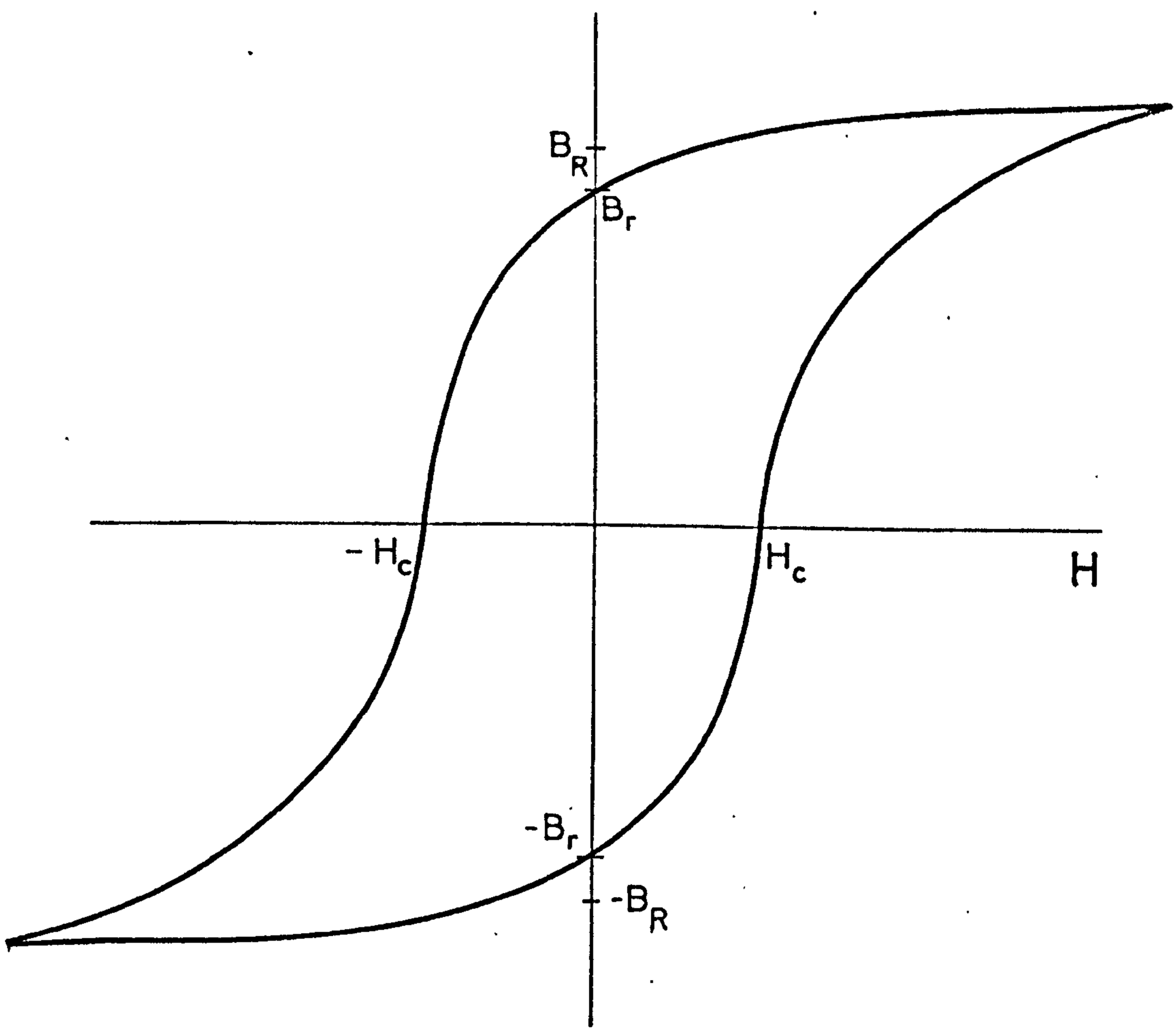

Fig. 4.2.1 Typical steady-state B/H loop.
(rated voltage)

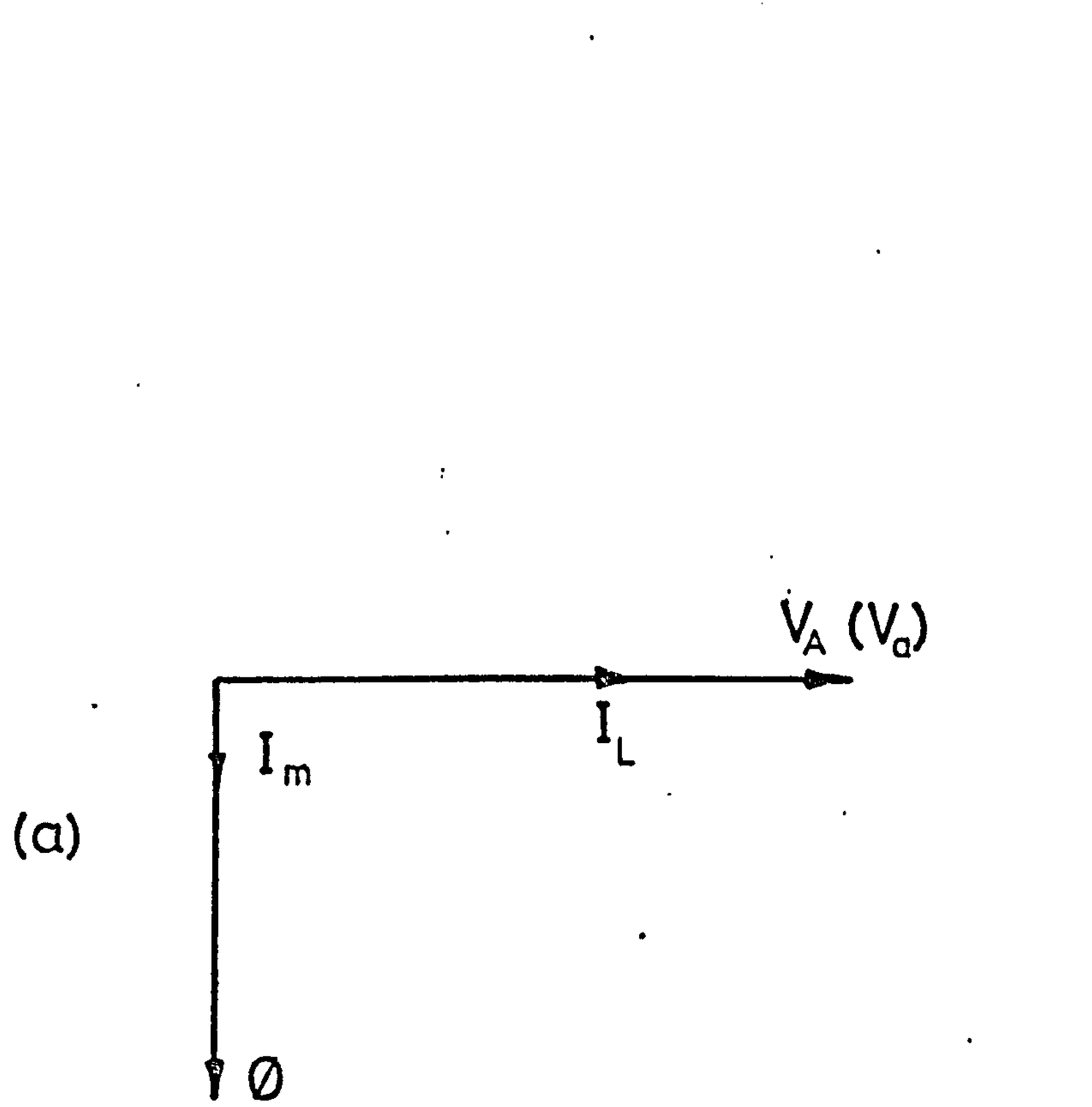

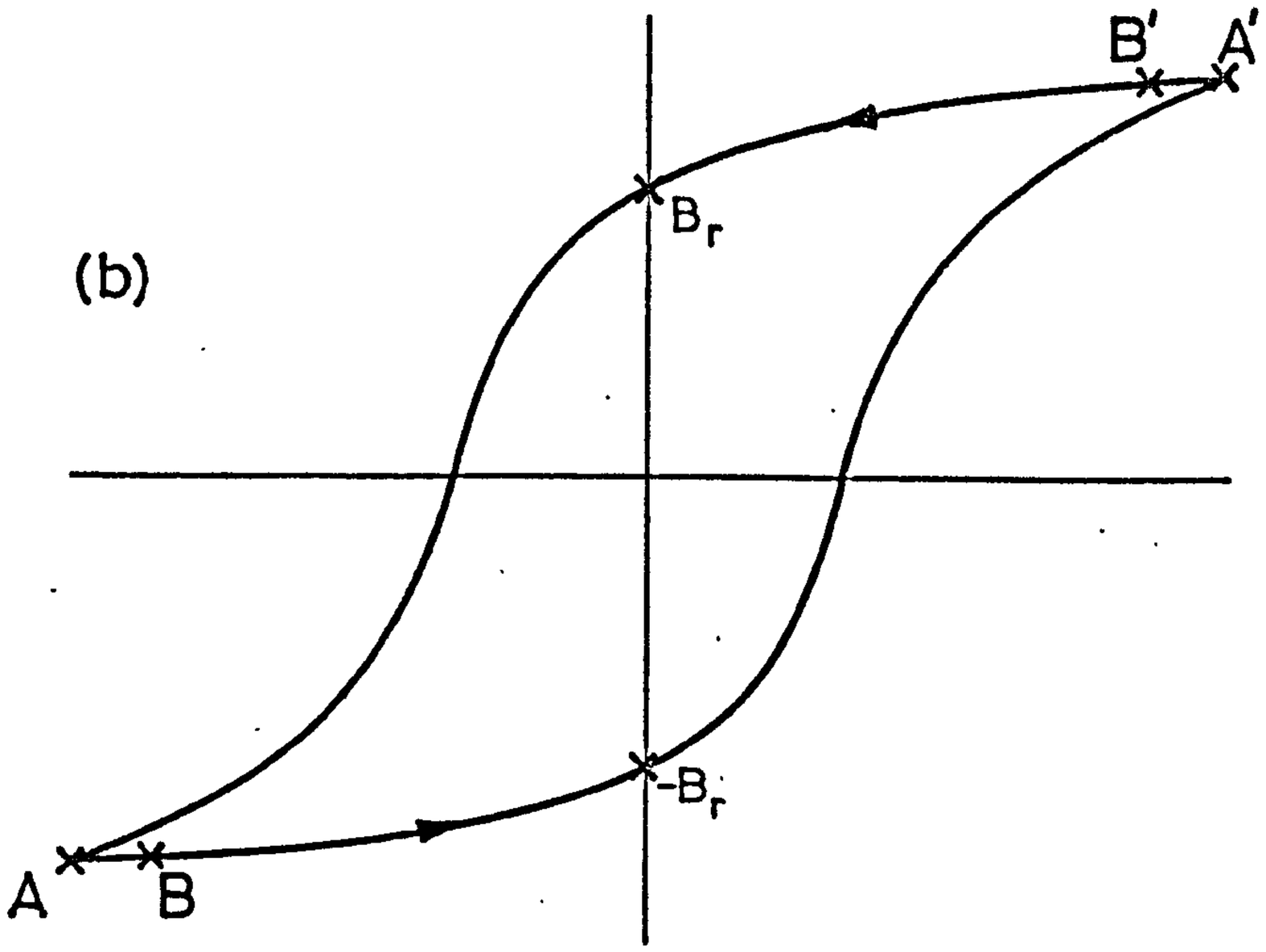

Fig. 4.2.2 Interruption of current - resistive load.

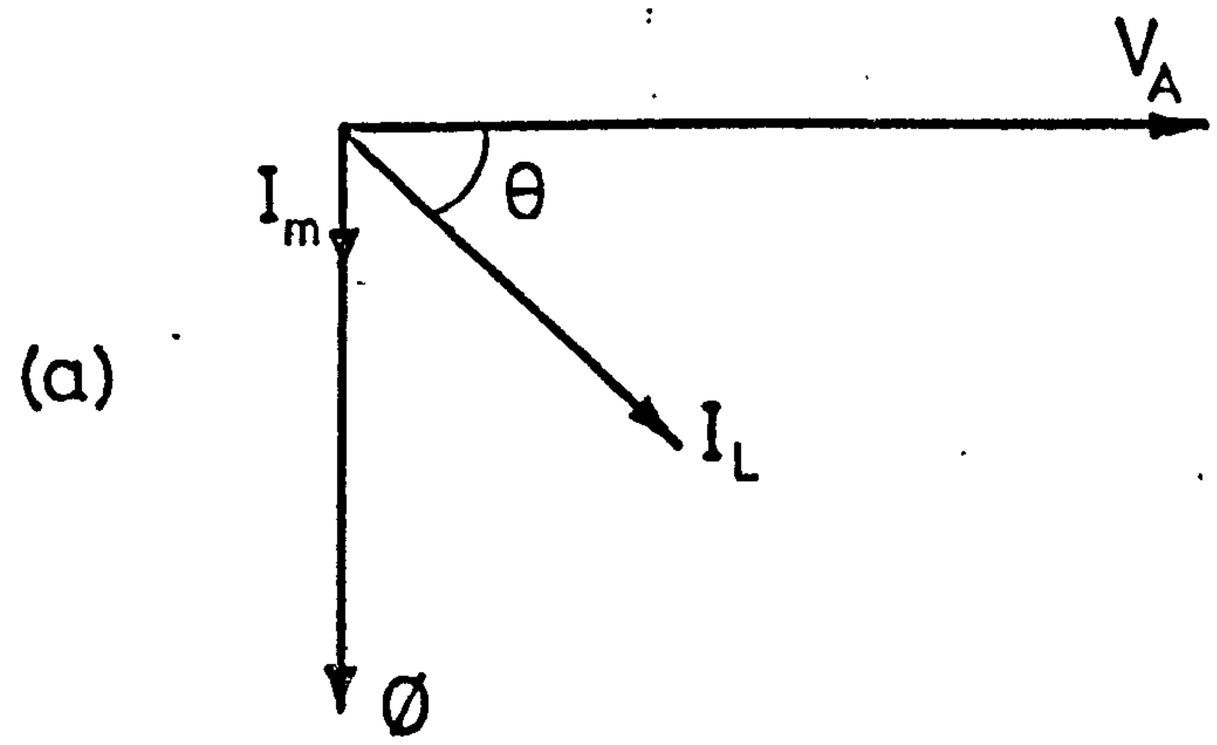

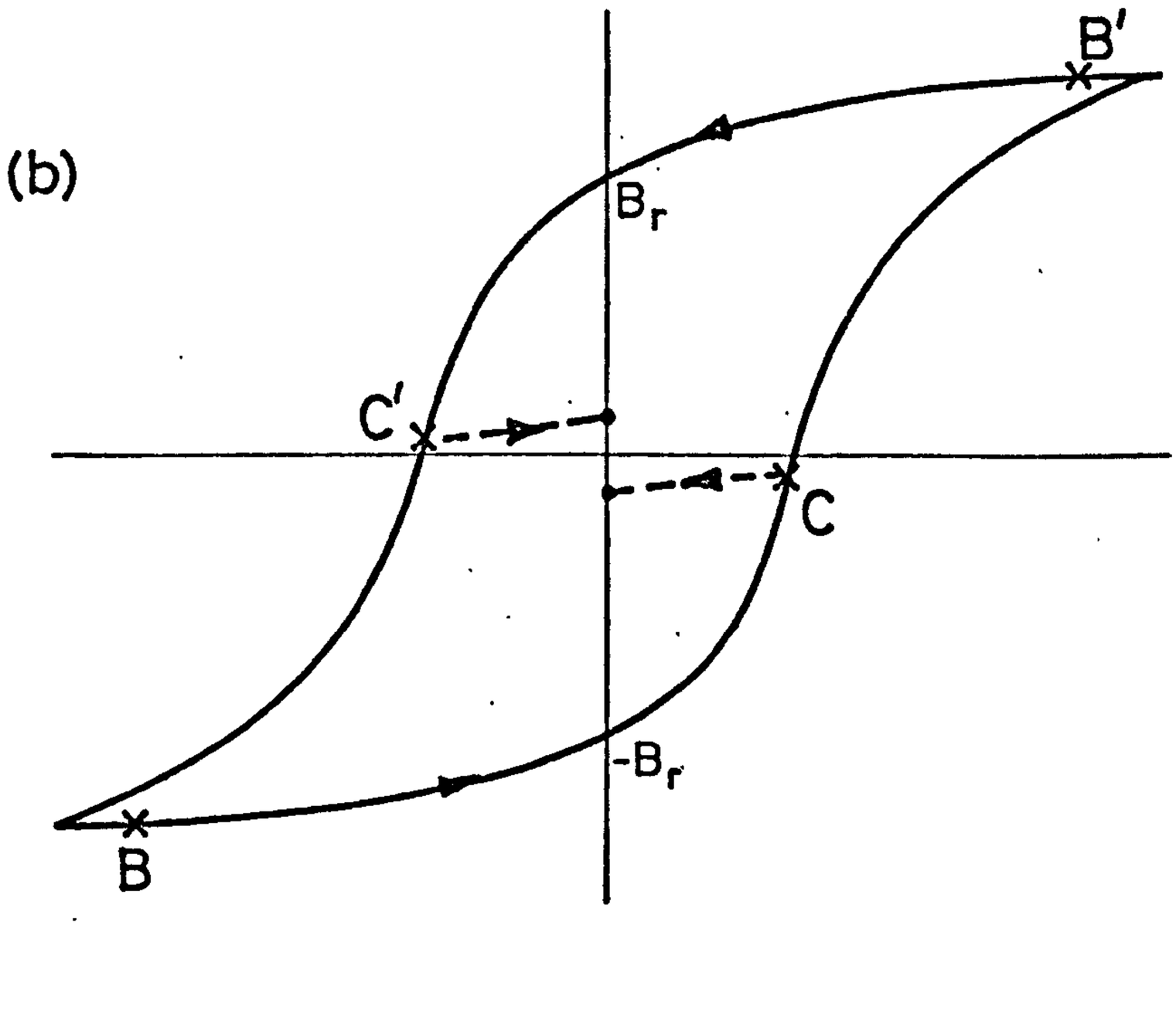

Fig. 4.2.3 Supply interruption – lagging p.f. load.

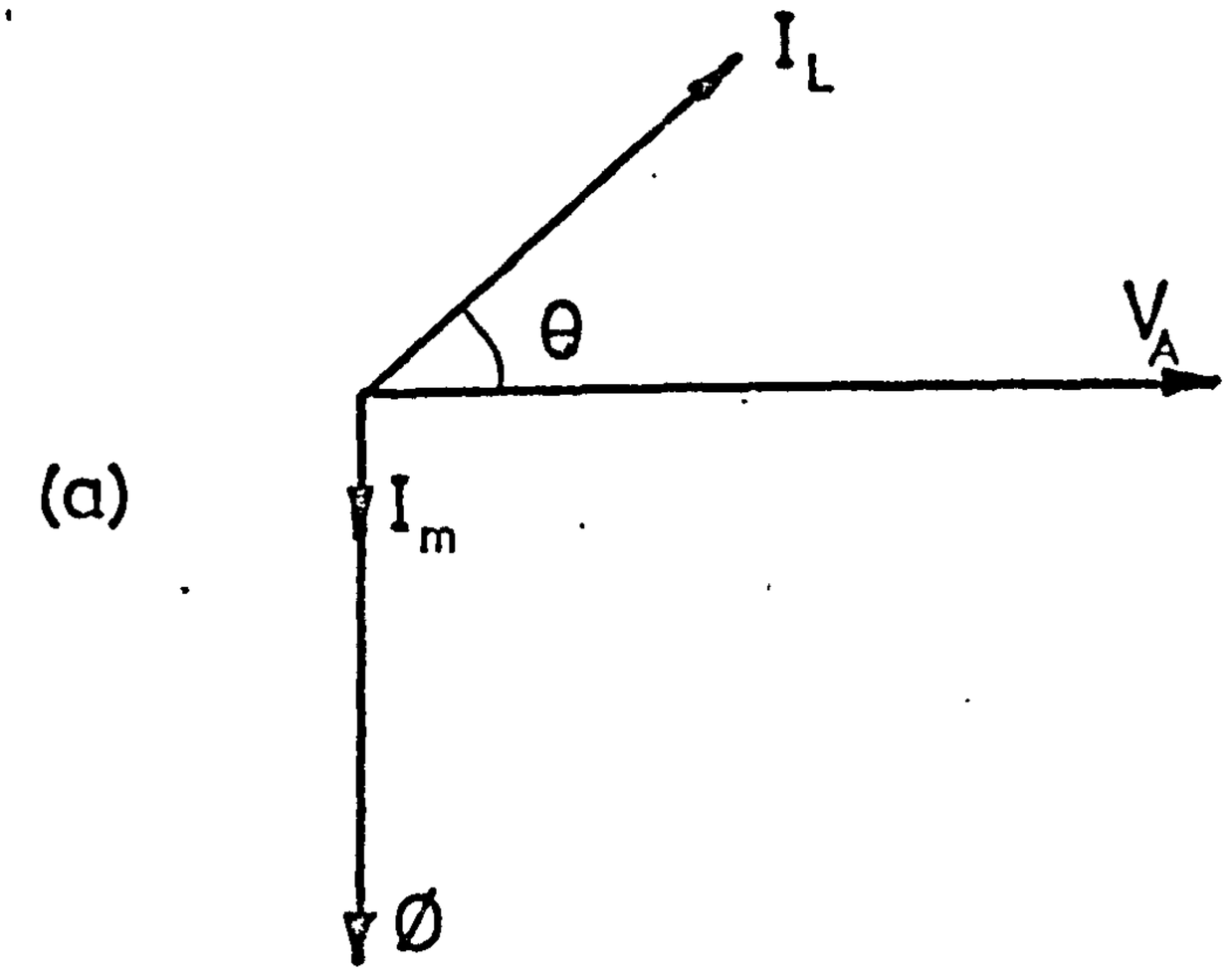

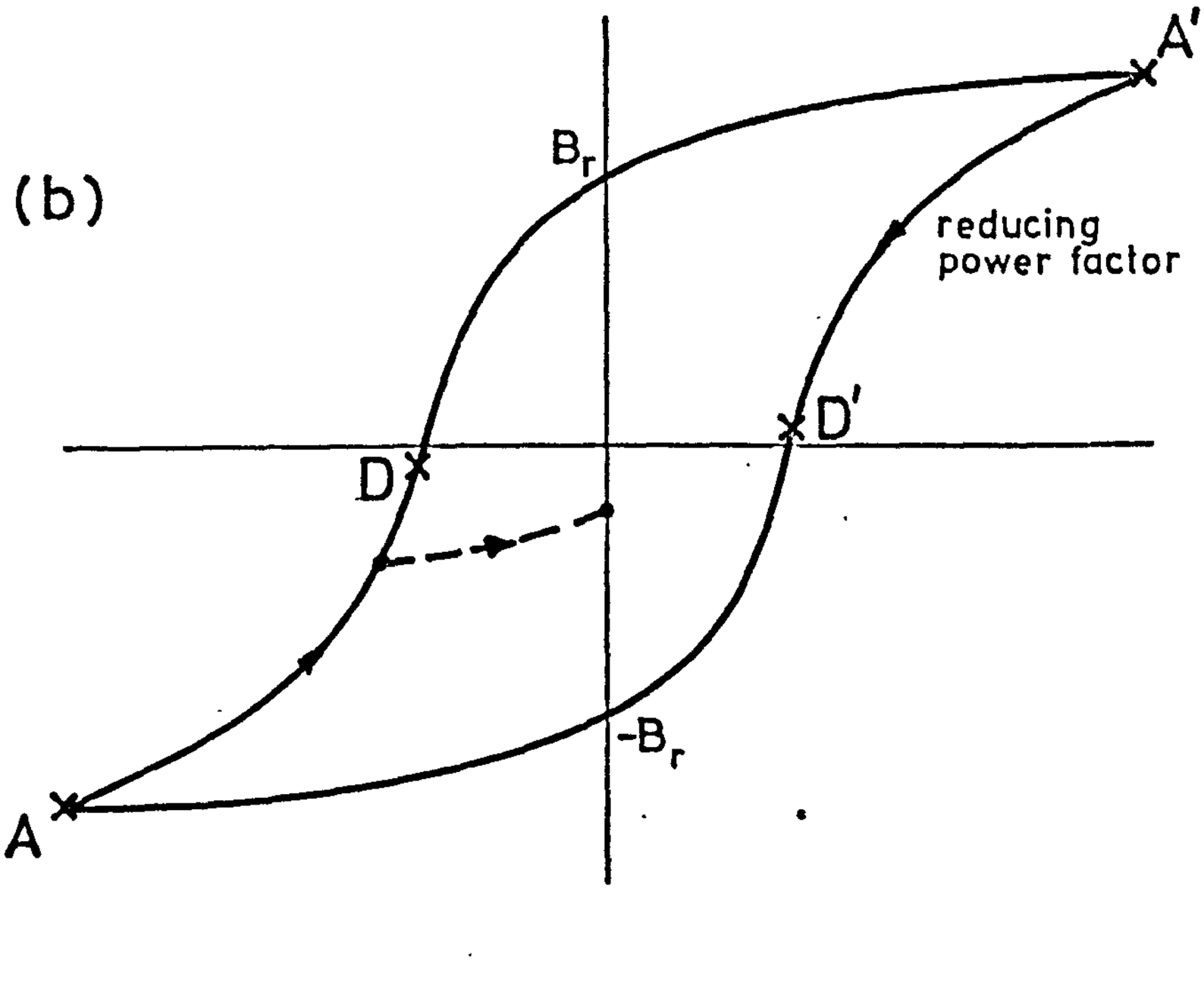

Fig. 4.2.4 Supply interruption — leading p.f. load.

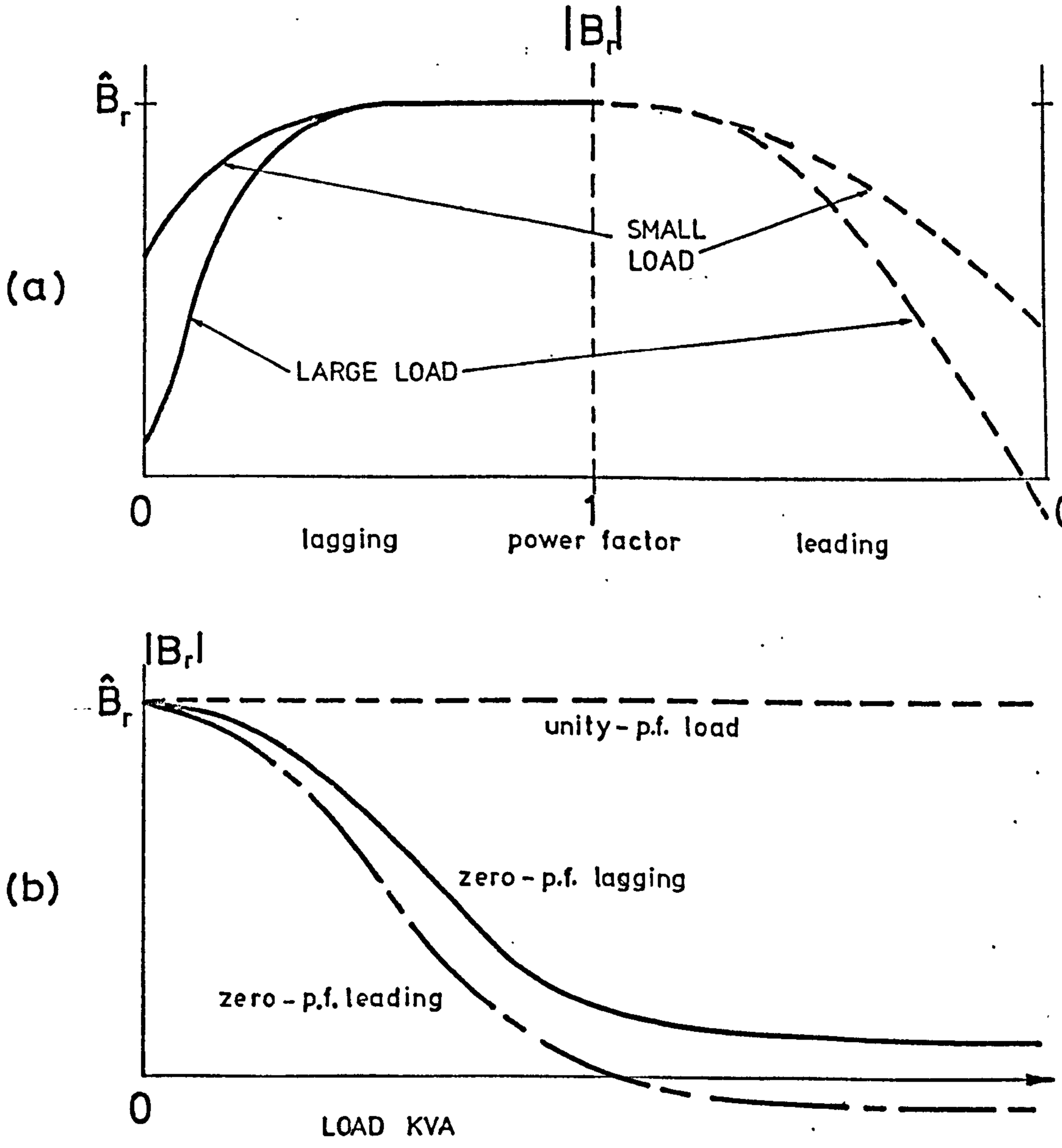

Fig. 4.2.5 Variation of residual flux density with:
(a) power factor (constant load kVA)
(b) load kVA

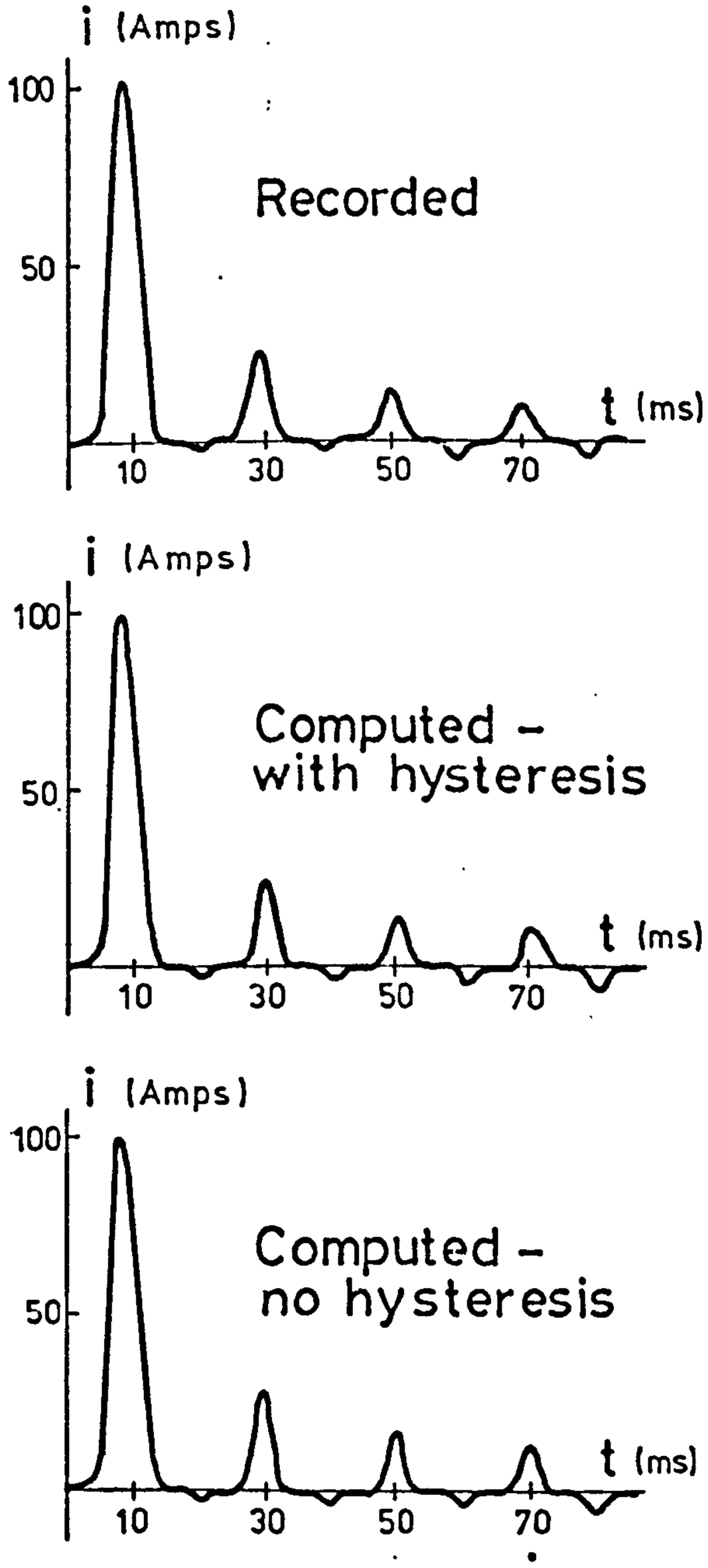

Fig. 4.2.6 Transient current in 1-kVA single-phase transformer: $\alpha = 0°$, $V = 250v$.

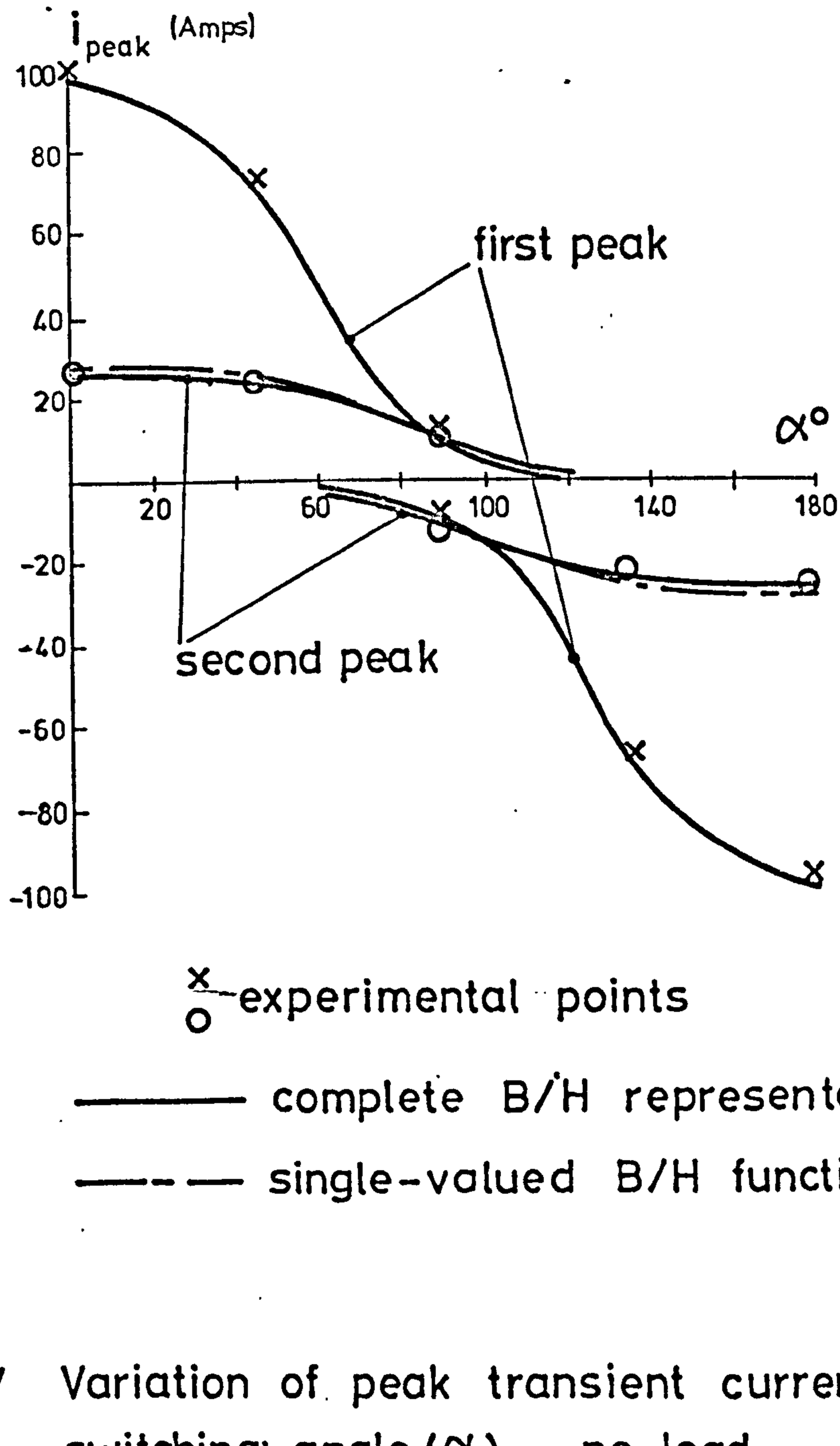

Fig. 4.2.7 Variation of peak transient current with switching angle (α) — no load.
$B_r = 0$, V=250v.

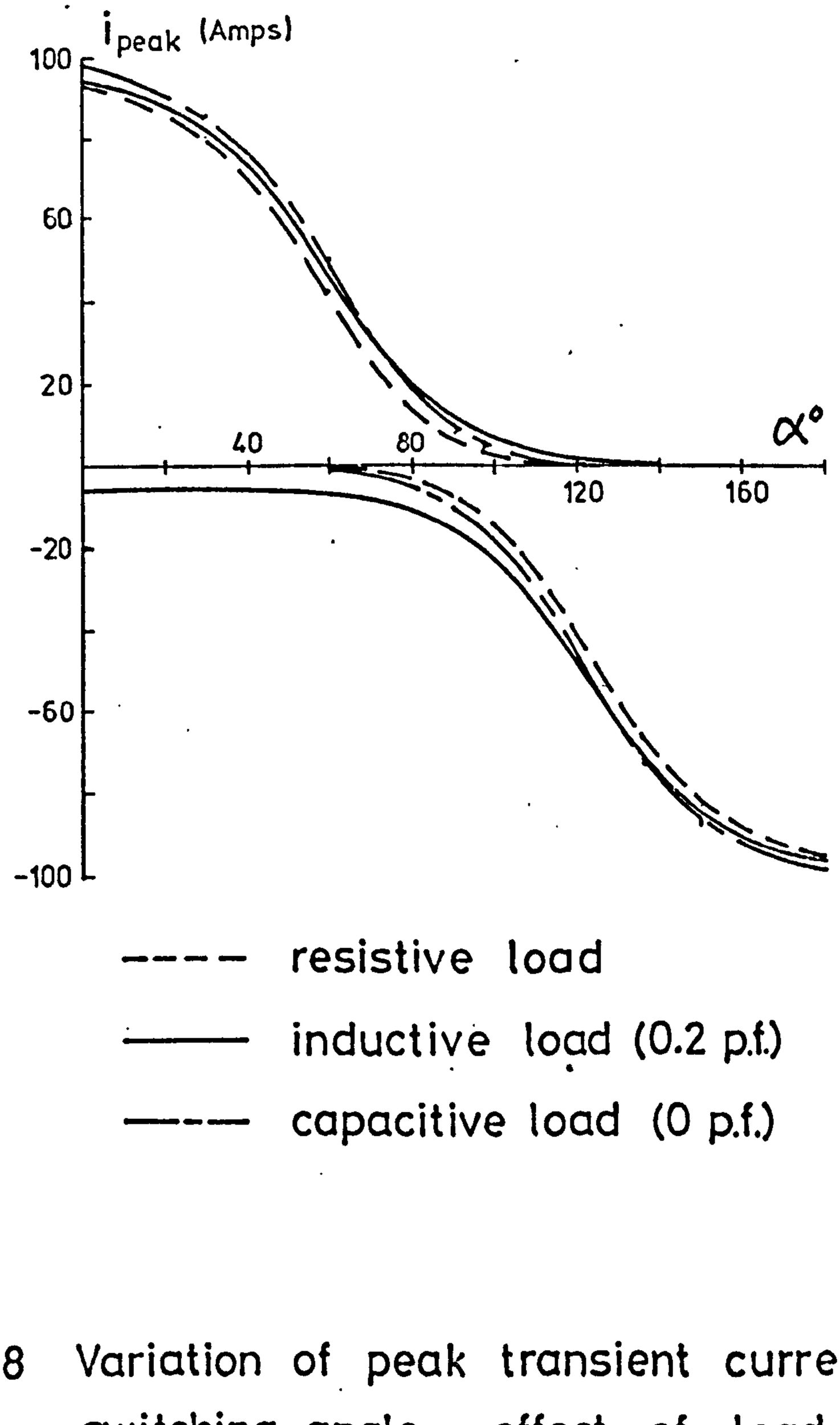

Fig. 4.2.8 Variation of peak transient current with switching angle — effect of load.

$B_r = 0$ $V = 250$ v.

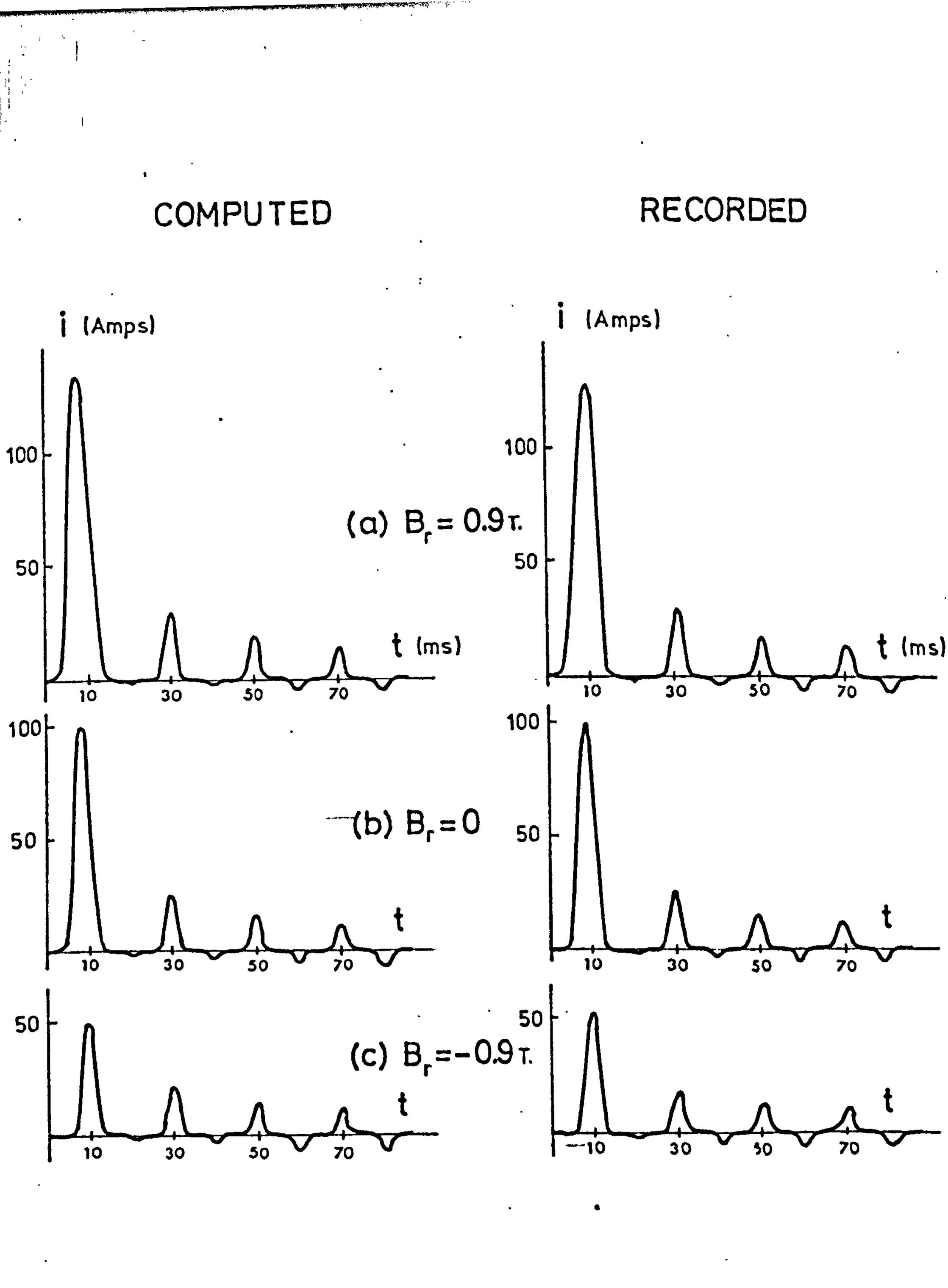

Fig. 4.2.9 Effect of residual flux density on single-phase transient current.
$\alpha = 0°$, V=250v.

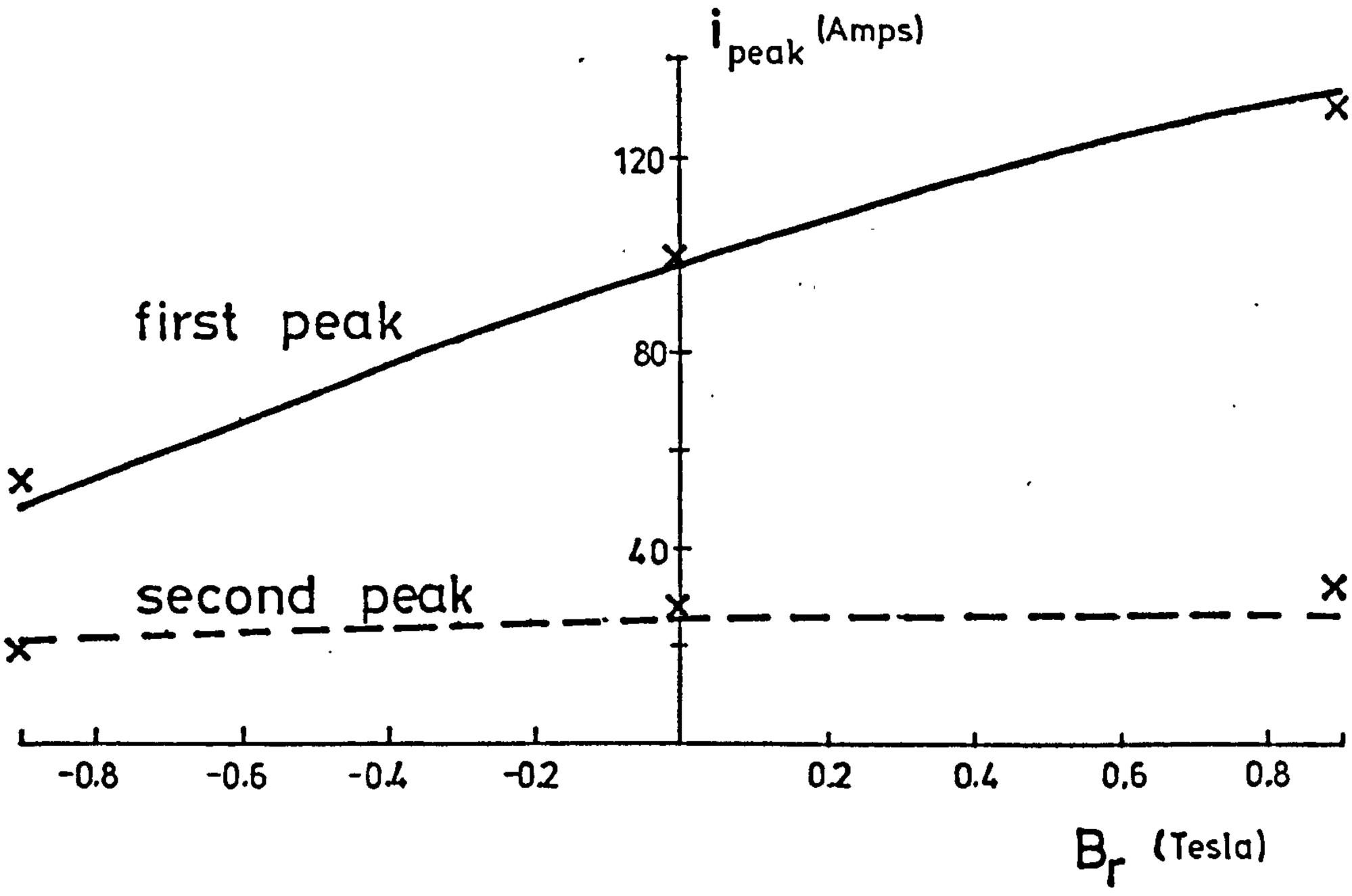

x – experimental points

Fig. 4.2.10 Variation of peak transient current with residual flux density level, (computed).
$\alpha = 0°$ $V = 250v.$

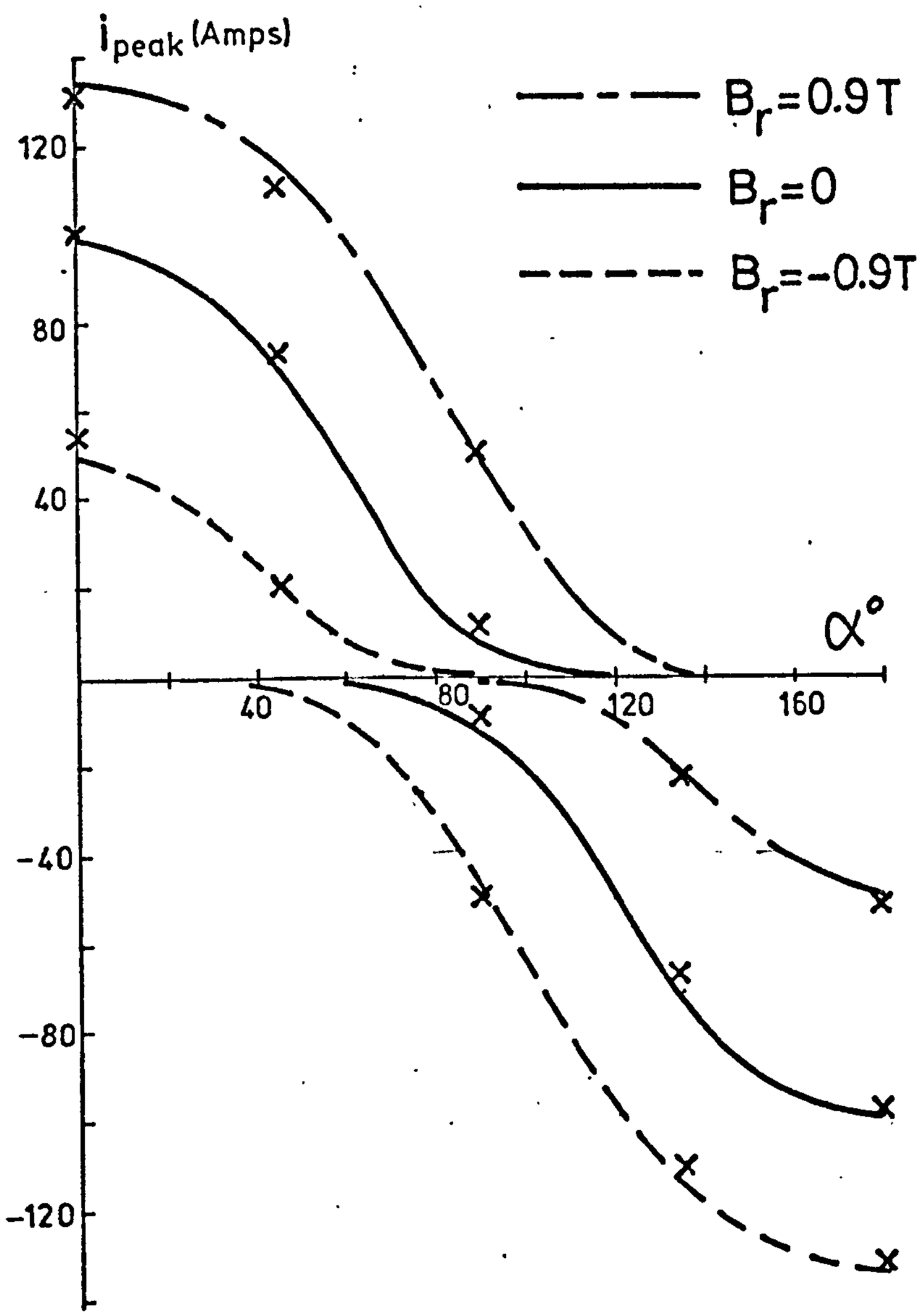

x - experimental points.

Fig. 4.2.11 Effect of residual flux on peak transient current variation with switching angle.— no load. V=250v.

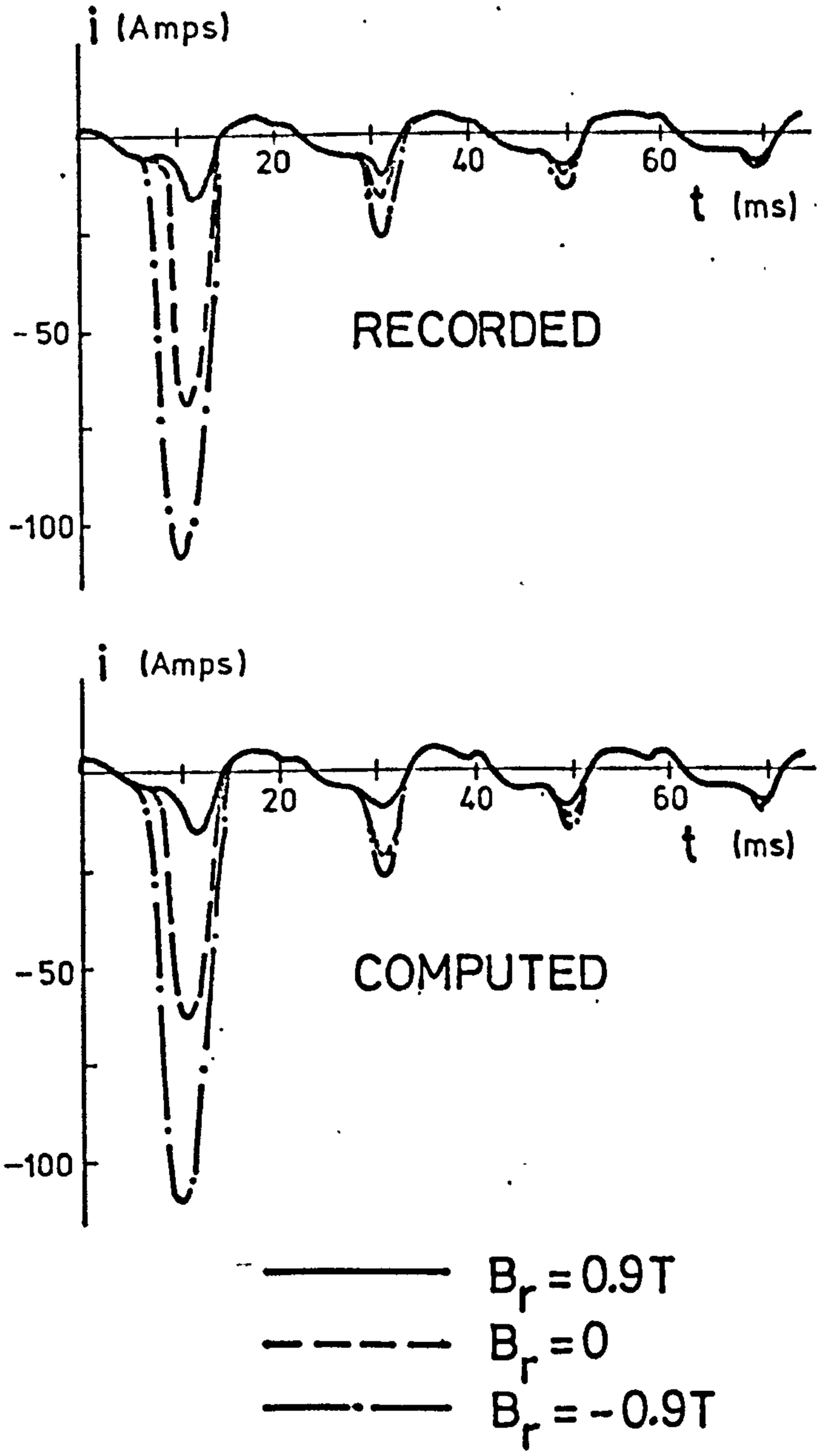

Fig. 4.2.12(a) Transient current - unity p.f. load.
$\alpha = 135°$ V = 250 v.

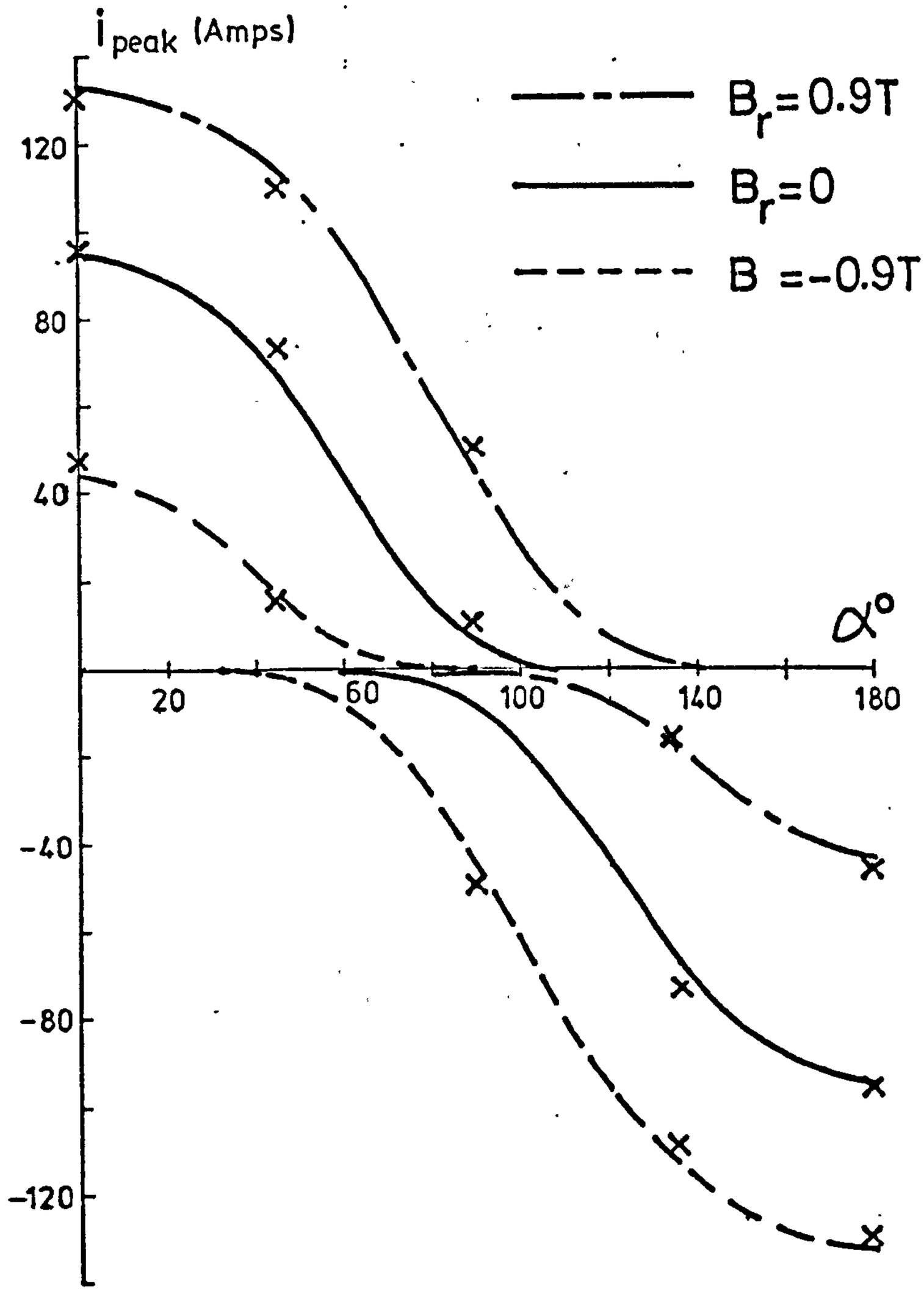

× – experimental points

Fig. 4.2.12(b) Effect of residual flux on peak transient current variation with switching angle— unity p.f. load. V=250v.

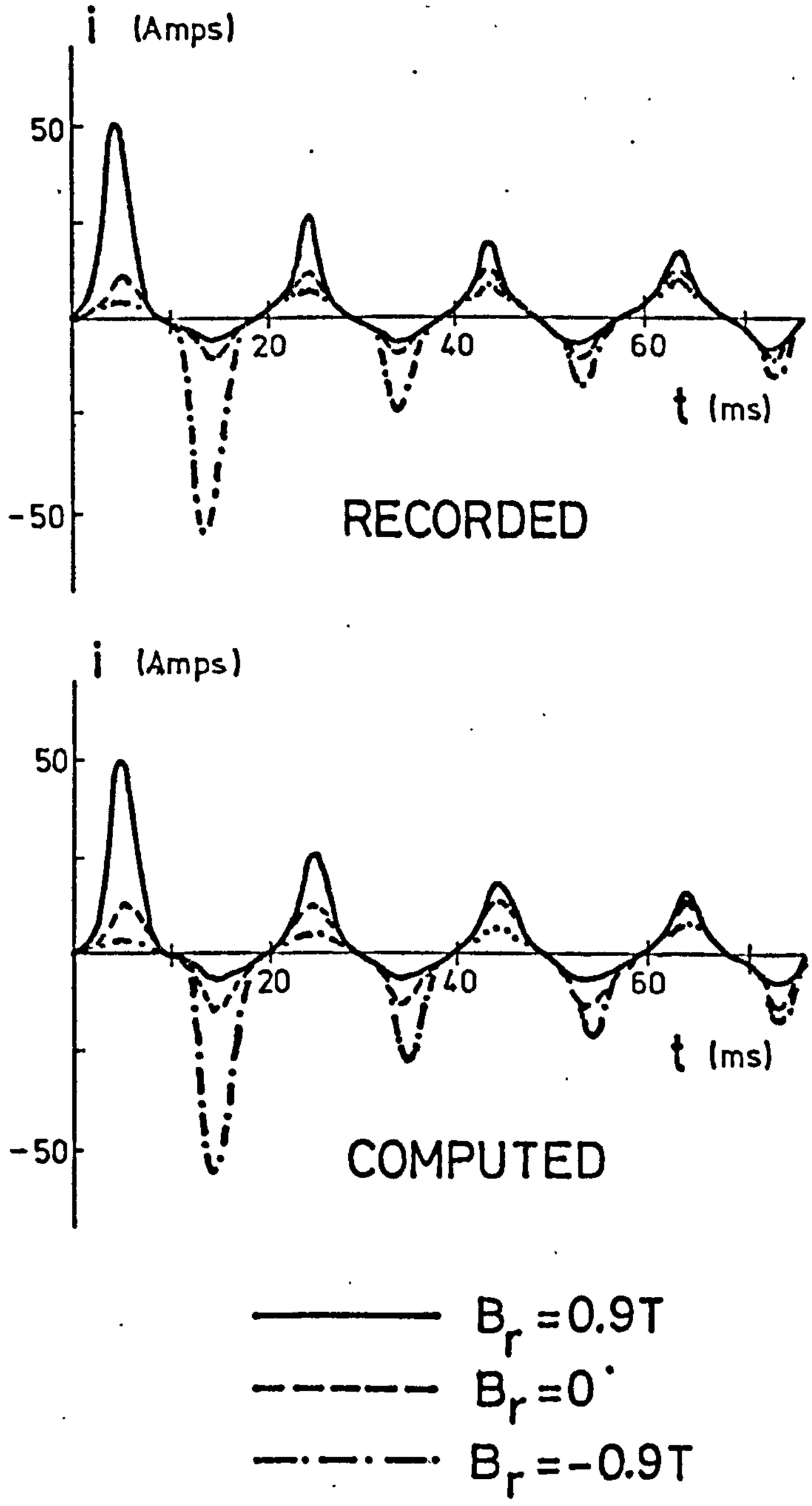

Fig. 4.2.13(a) Transient current - 0.2 p.f. lagging load.
$\alpha = 90°$ V=250v.

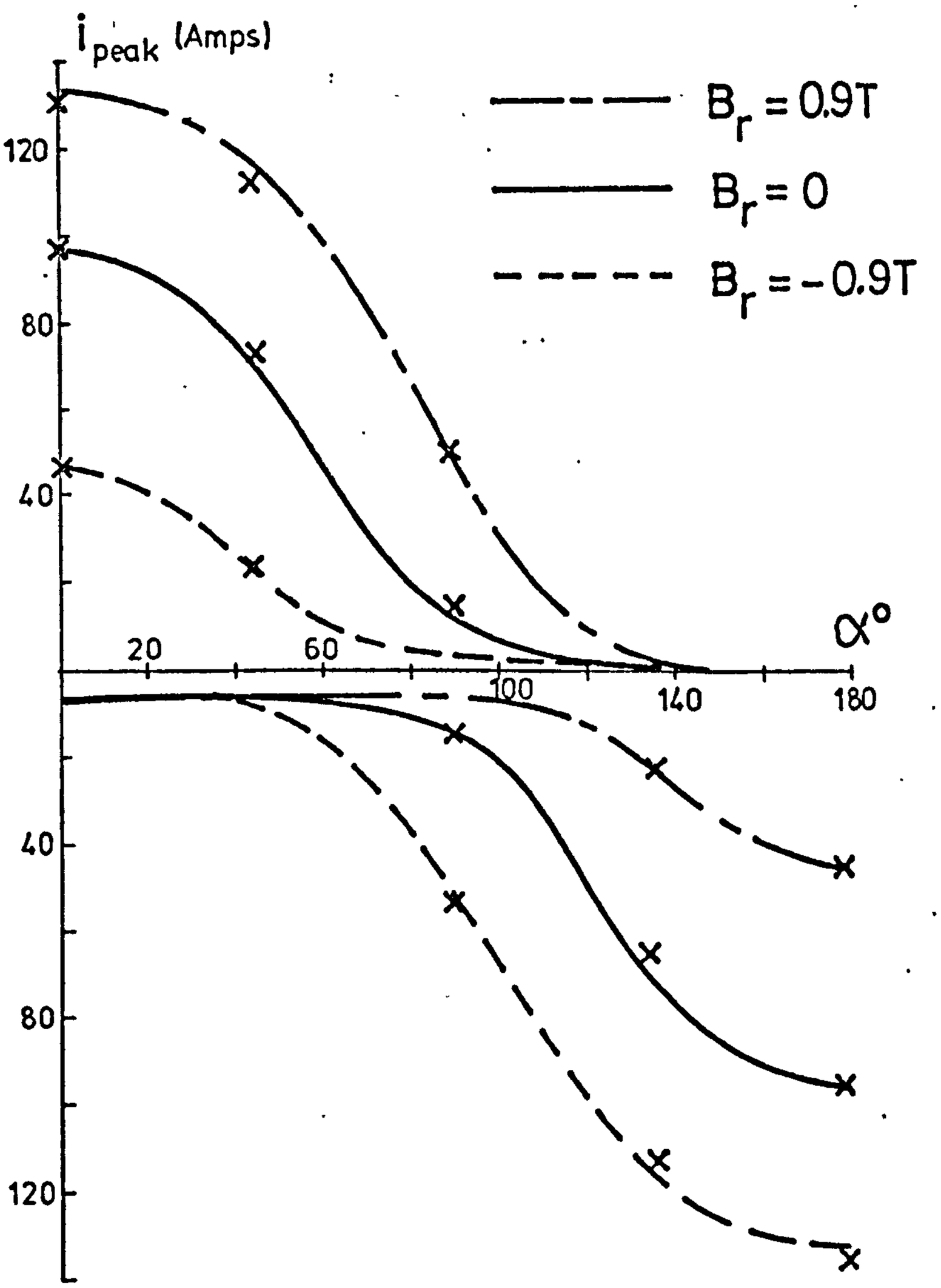

Fig. 4.2.13(b) Effect of residual flux on peak transient current variation with switching angle — 0.2 p.f. lagging load. V=250v.

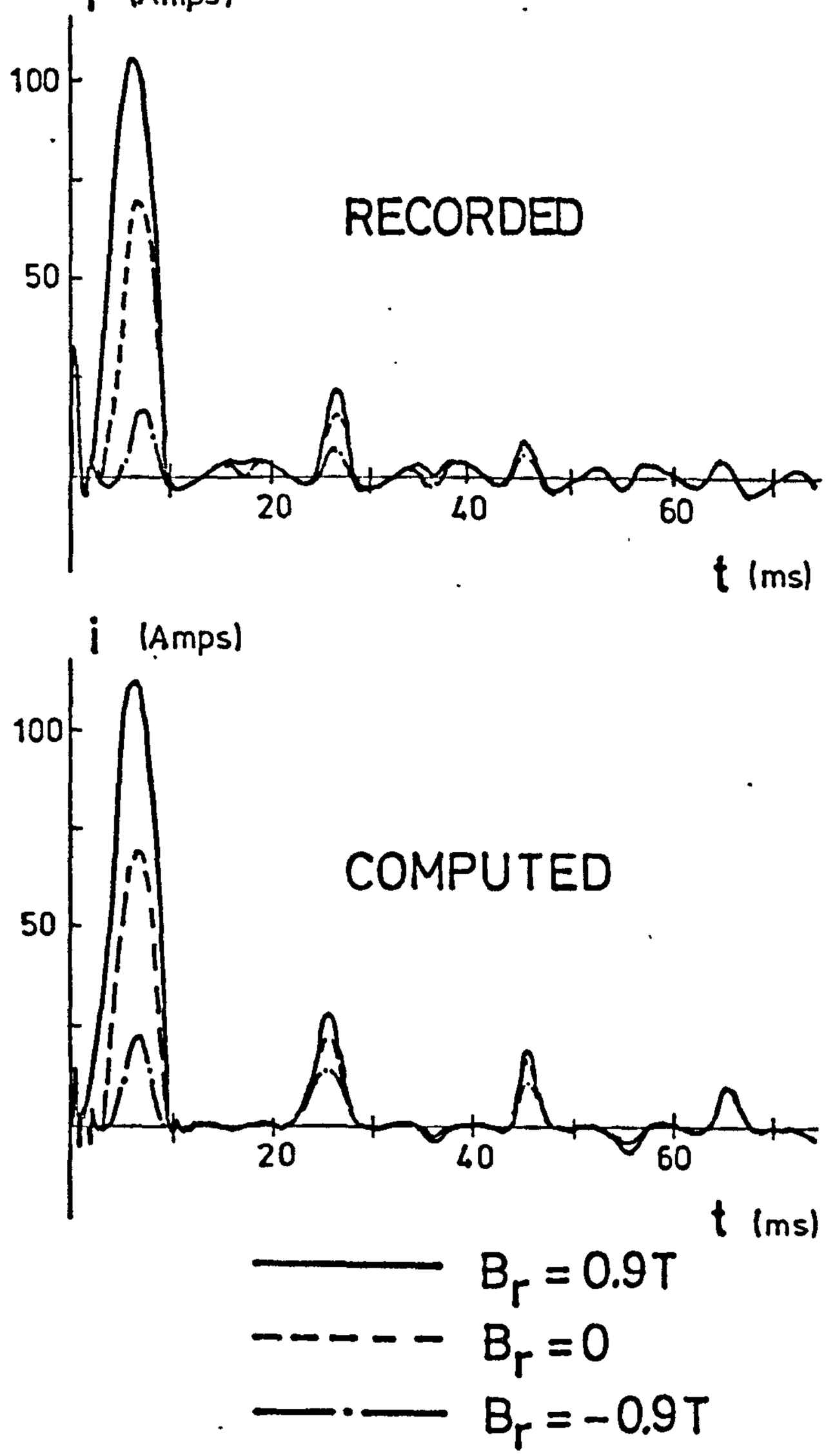

Fig. 4.2.14(a) Transient current - 0 p.f. leading load.
$\alpha = 45°$ V=250v.

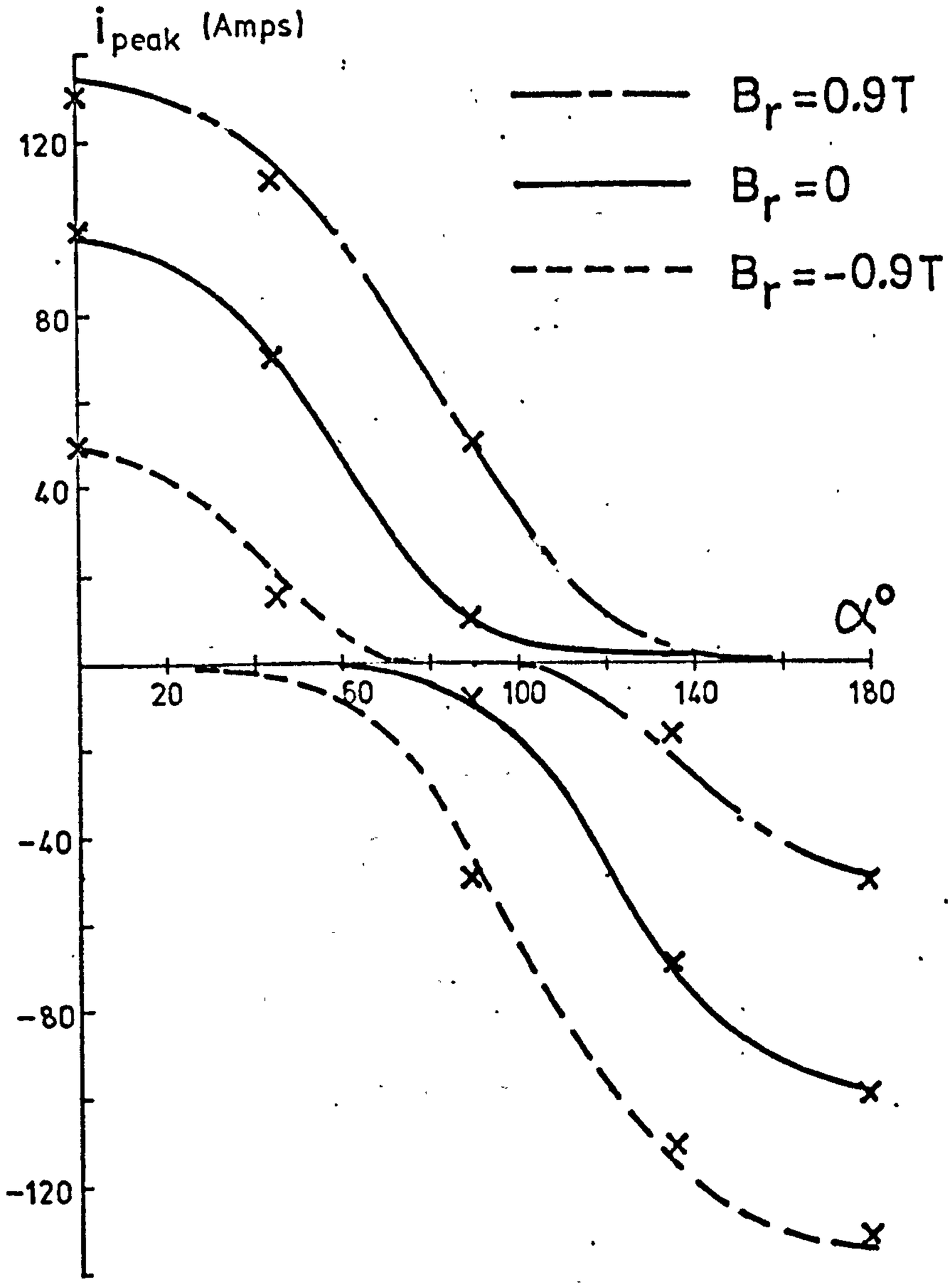

Fig. 4.2.14(b) Effect of residual flux on peak transient current variation with switching angle— 0 p f leading load. V=250v.

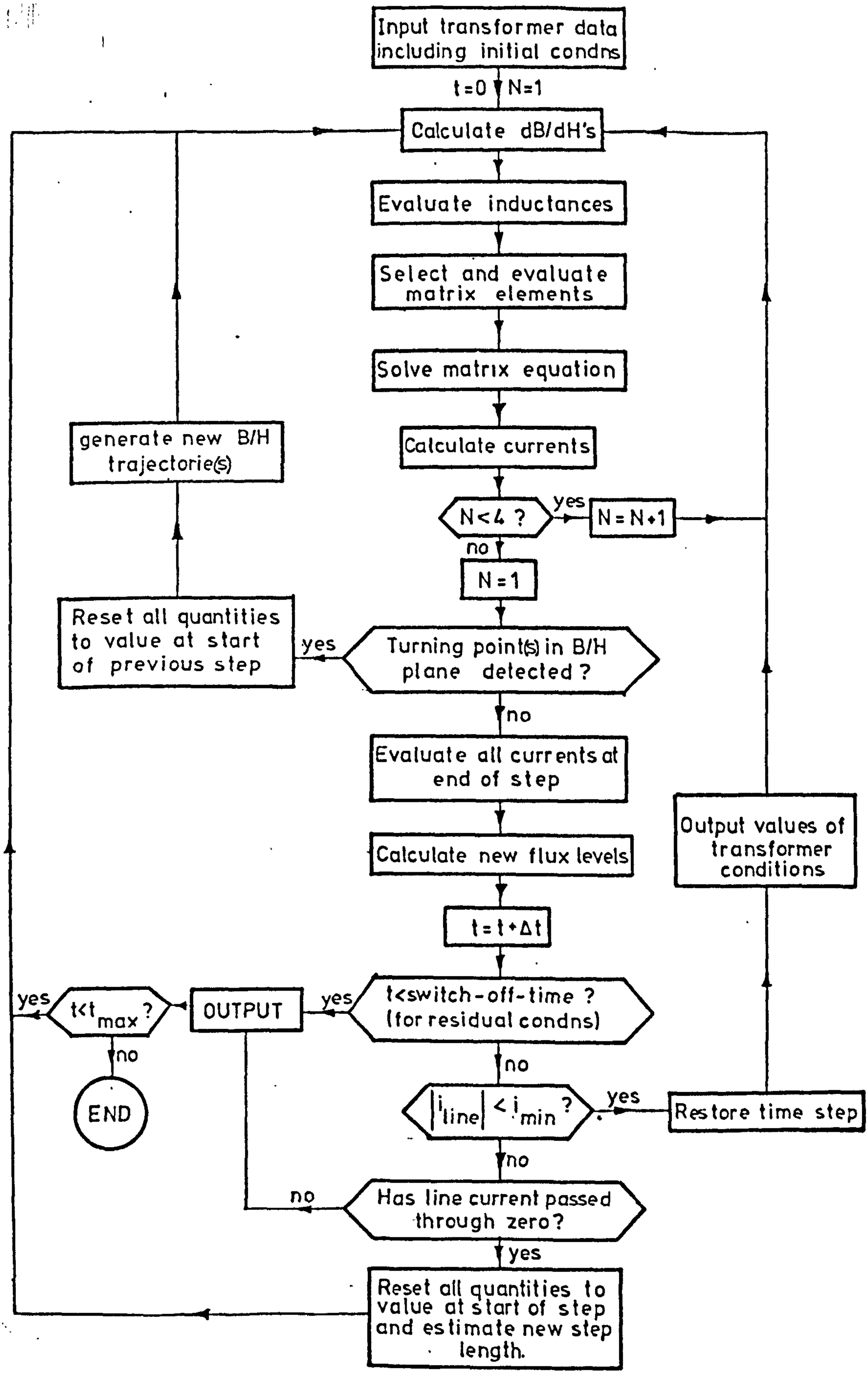

Fig. 4.3.1 Flow diagram of three-phase transient computer program.

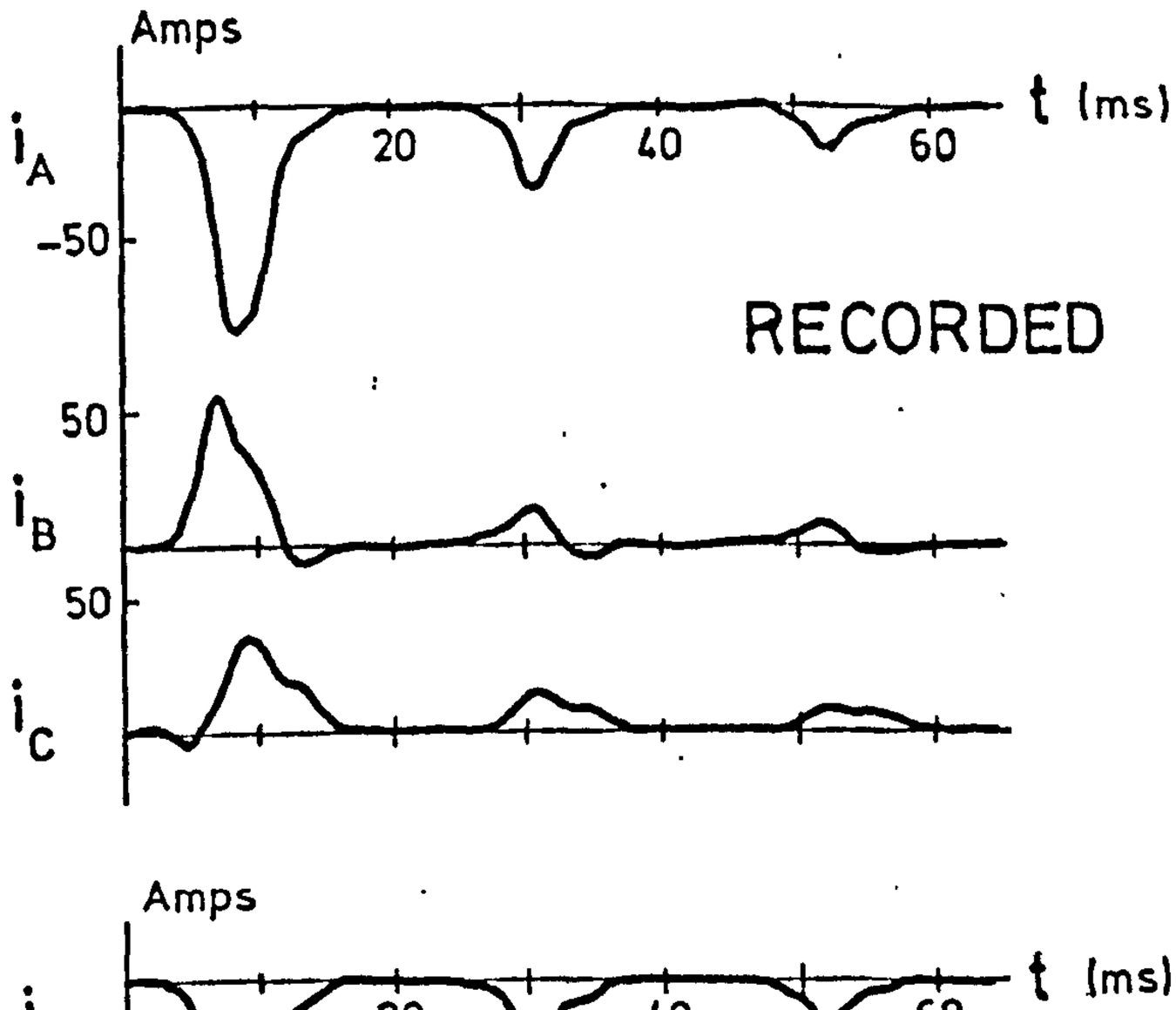

Fig. 4.4.1 Effect of hysteresis on the transient current in an unloaded 8-kVA, three-phase transformer - simultaneous switching.

$\alpha = 90°$

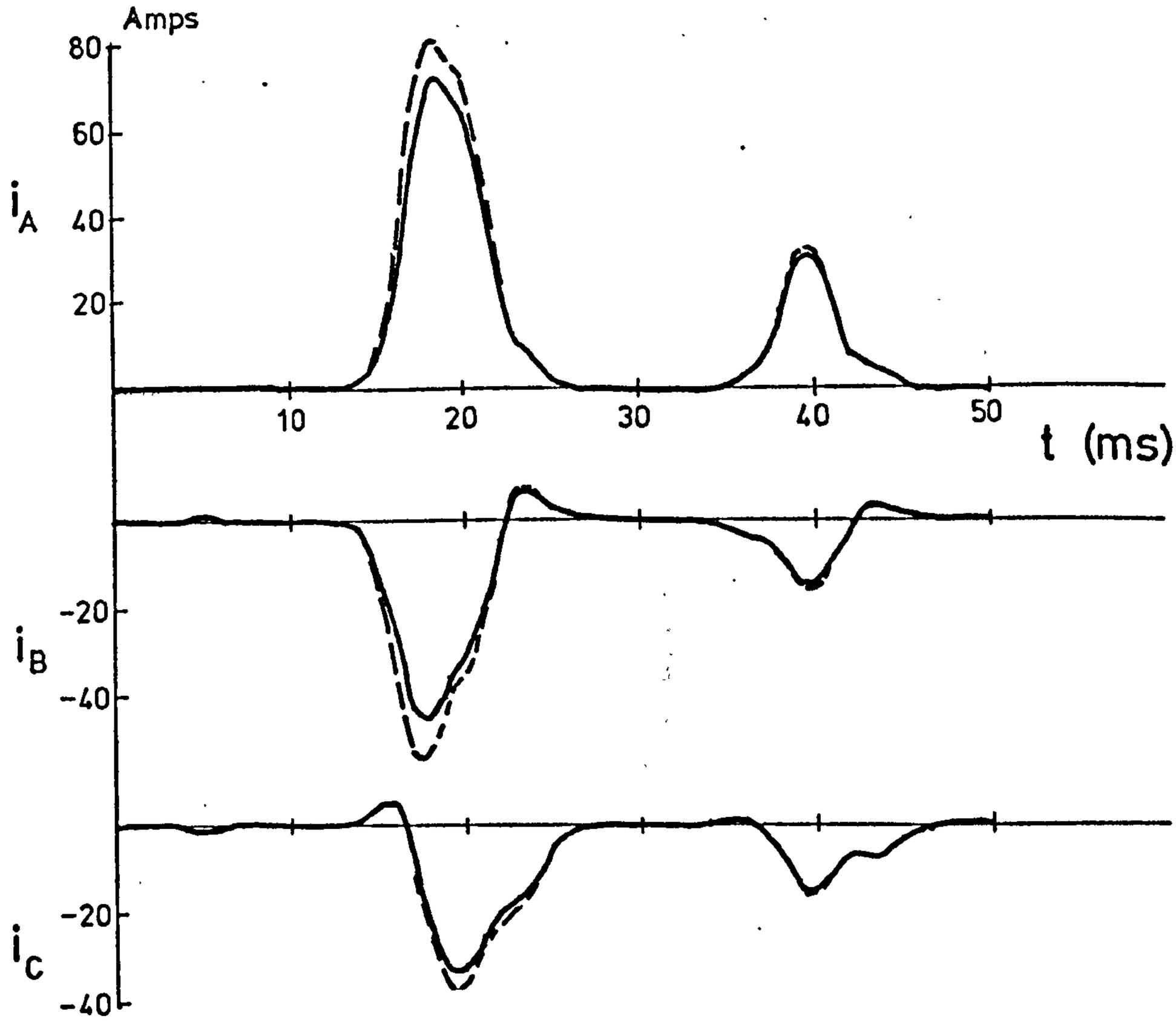

——— complete B/H representation

– – – – – single-valued function

Fig. 4.4.2 Effect of hysteresis on transient current — non-simultaneous switching, no load, 3-wire star connection. $\alpha = 90°$, $\beta = 180°$

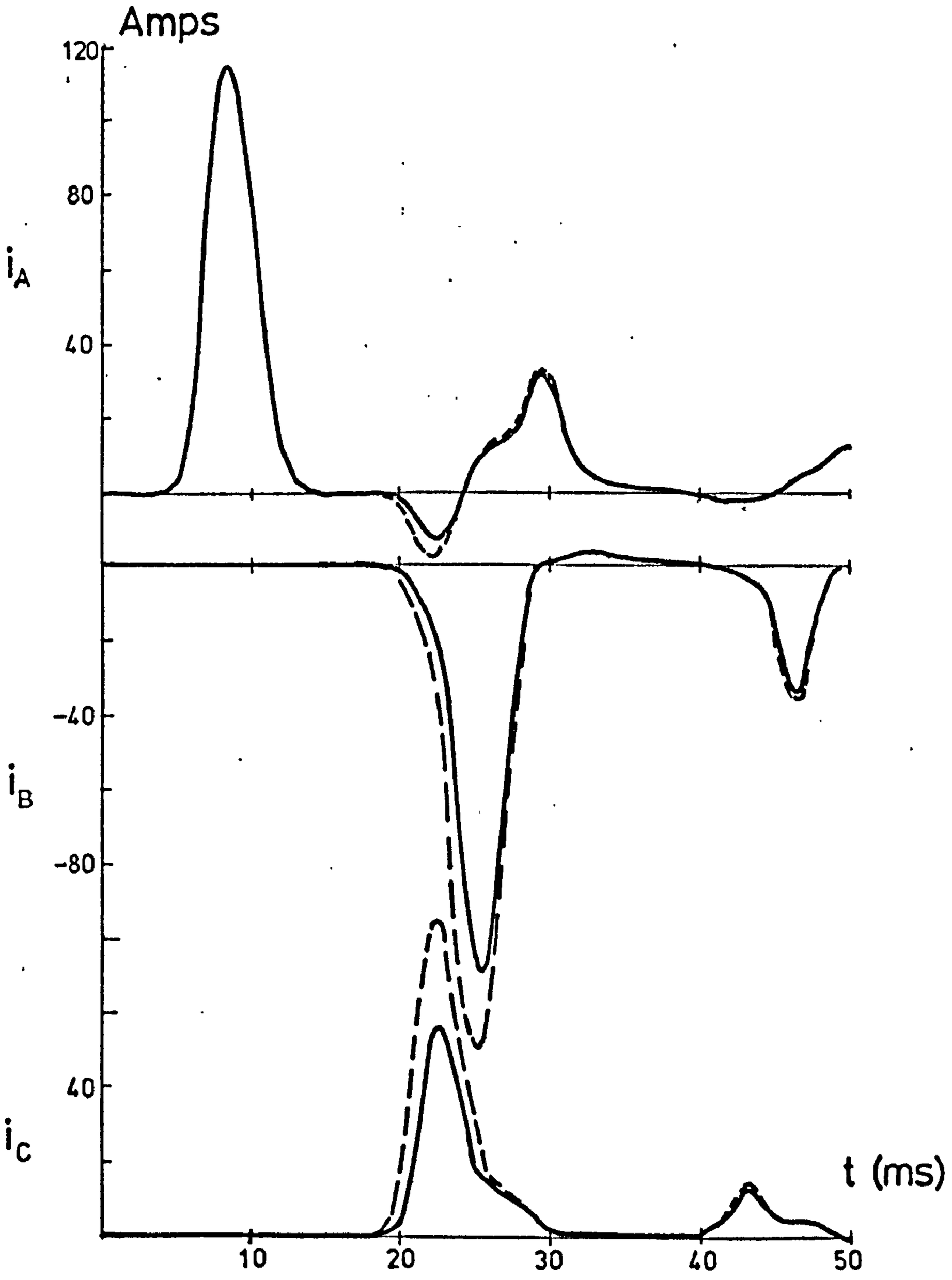

——— with hysteresis

----- no hysteresis

Fig. 4.4.3 Effect of hysteresis on transient current— non-simultaneous switching, no load, 4-wire supply. $\alpha=0°$, $\beta=270°$, $\gamma=0°$

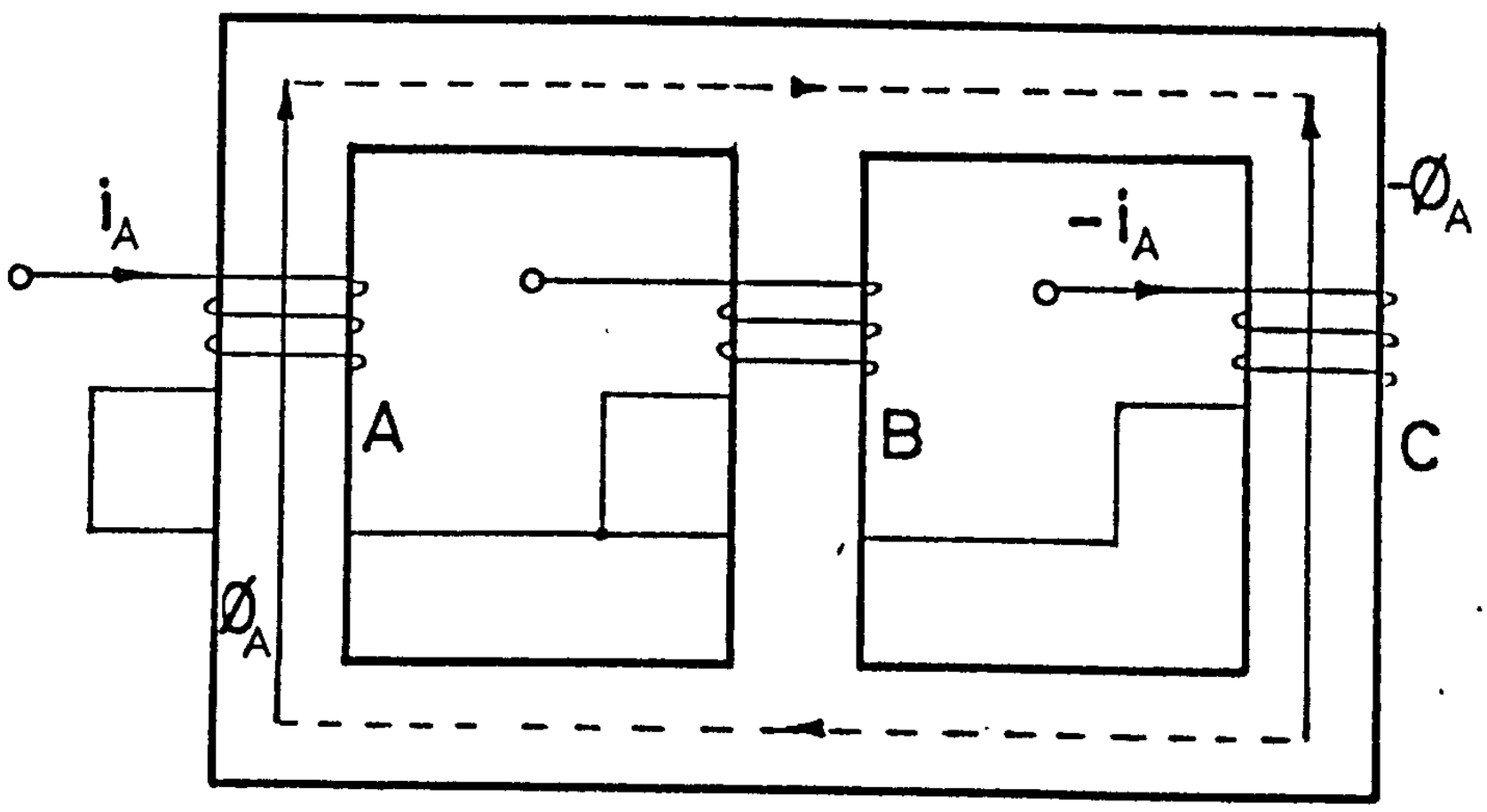

Fig. 4.4.4 Three wire star connected primary; phases A and C energised.

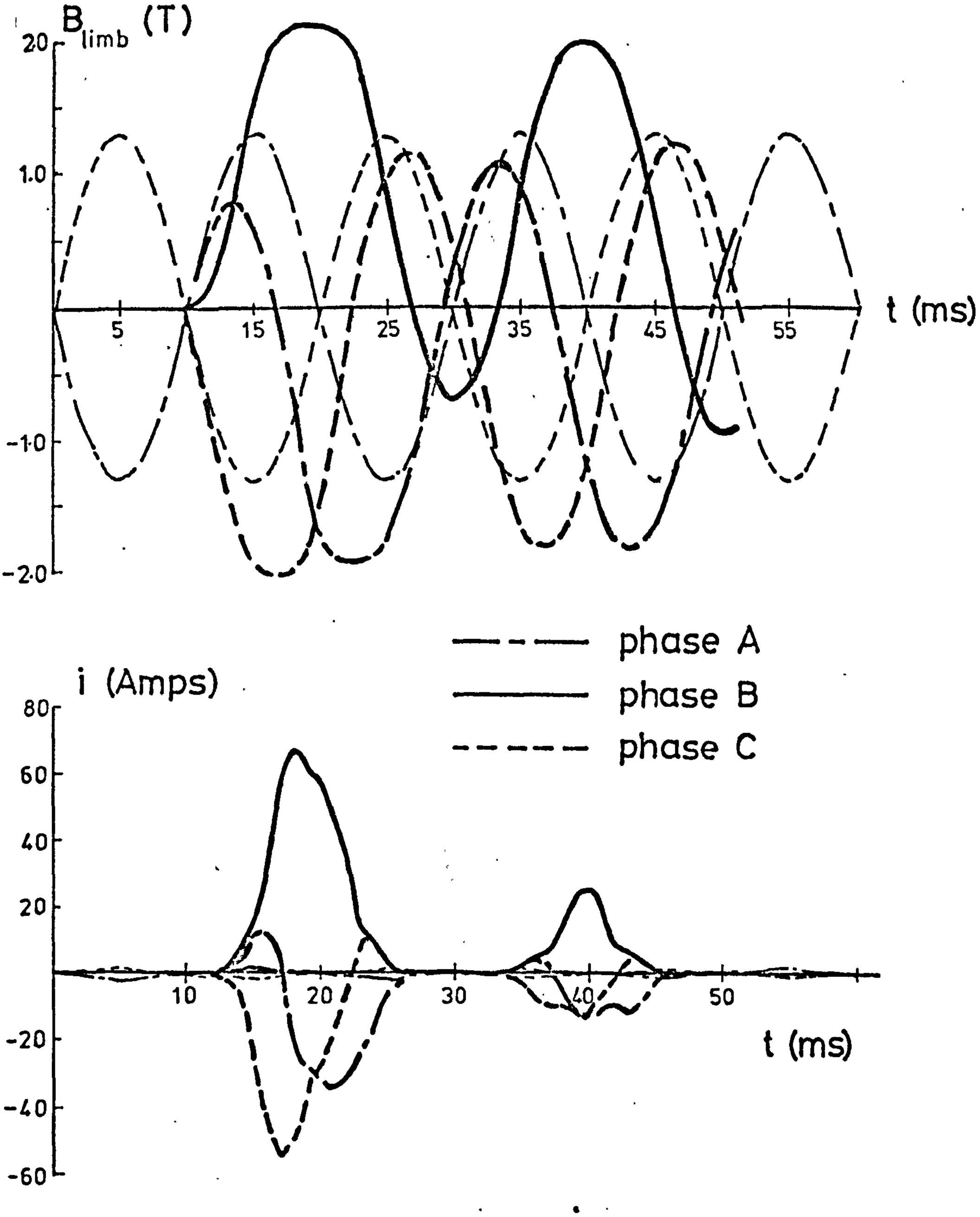

Heavy lines illustrate effect of connecting line B at t=10 ms.

Fig. 4.4.5 Transient flux density and current patterns for symmetrical energisation: 3-wire star connected primary - no load. Phases A and C connected first (α=90°)

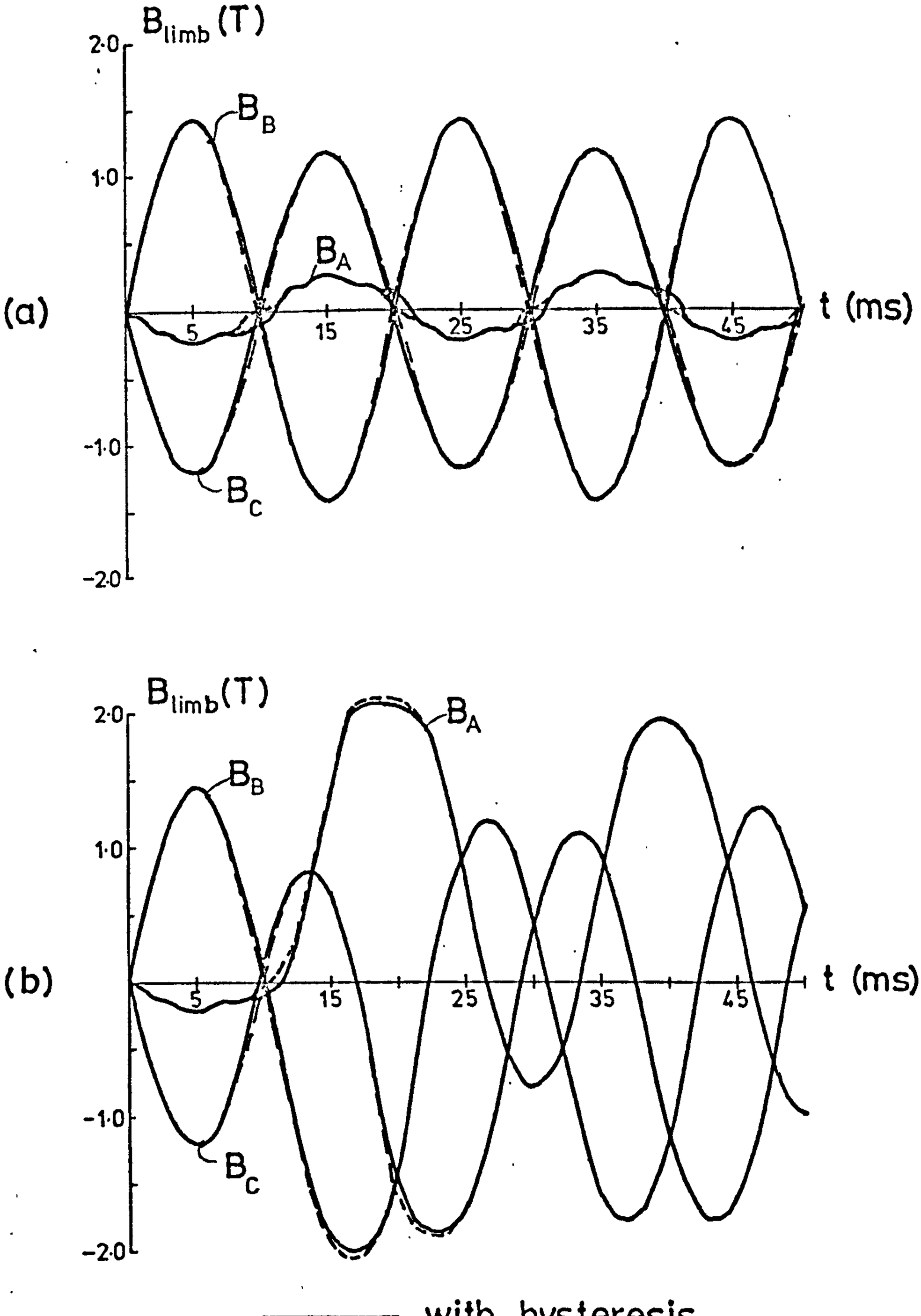

Fig. 4.4.6 Transient flux density - asymmetrical energisation, 3-wire star primary, no load.
(a) Phases B and C energised. (α=90°).
(b) Line A connected 10 ms after B and C.

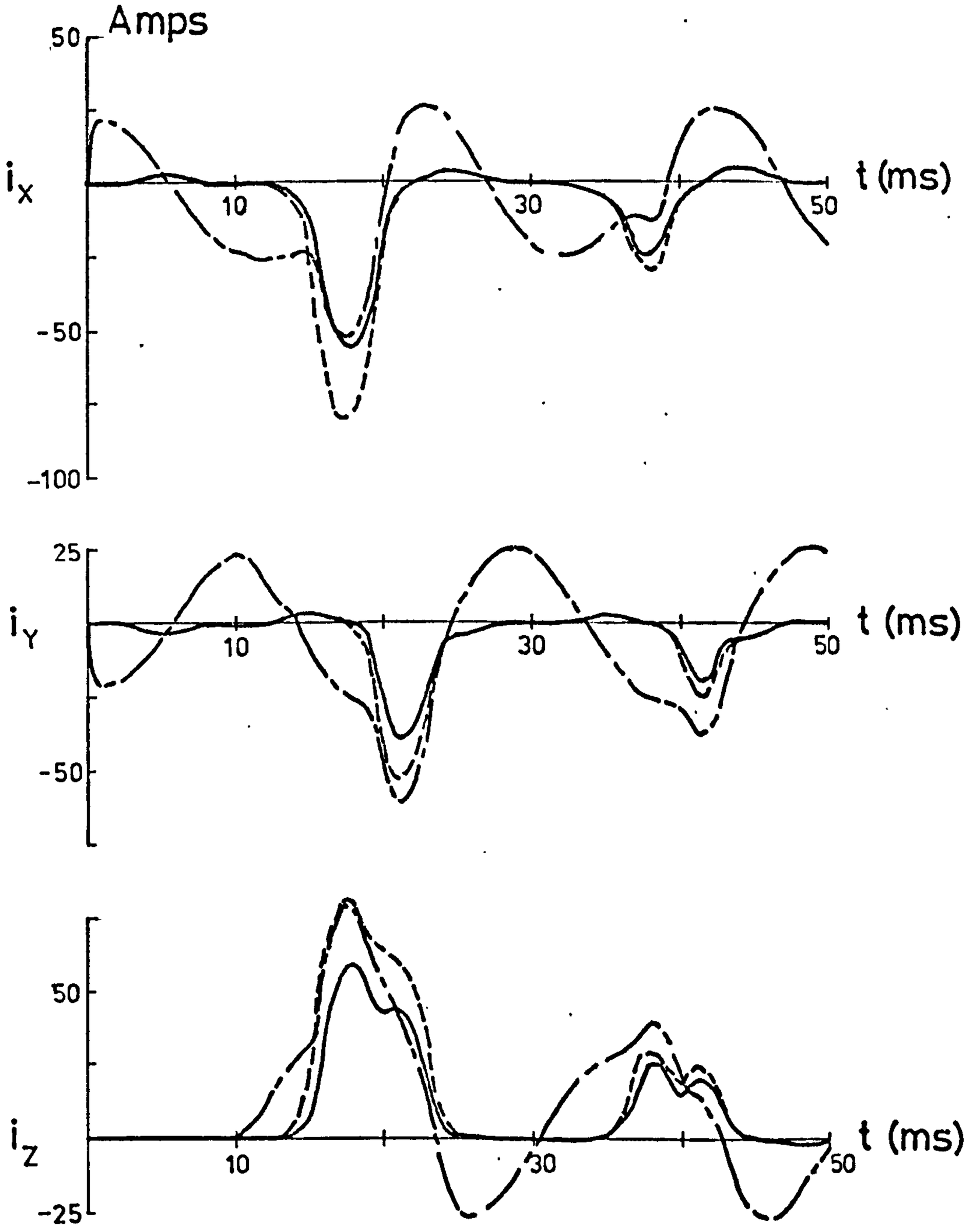

——— balanced unity p.f. load

——— no load - with hysteresis

----- no load - no hysteresis

Fig. 4.4.7 Transient current for delta connected primary, secondary, (and load). — asymmetrical energisation. $\alpha = 90°$, $\beta = 180°$

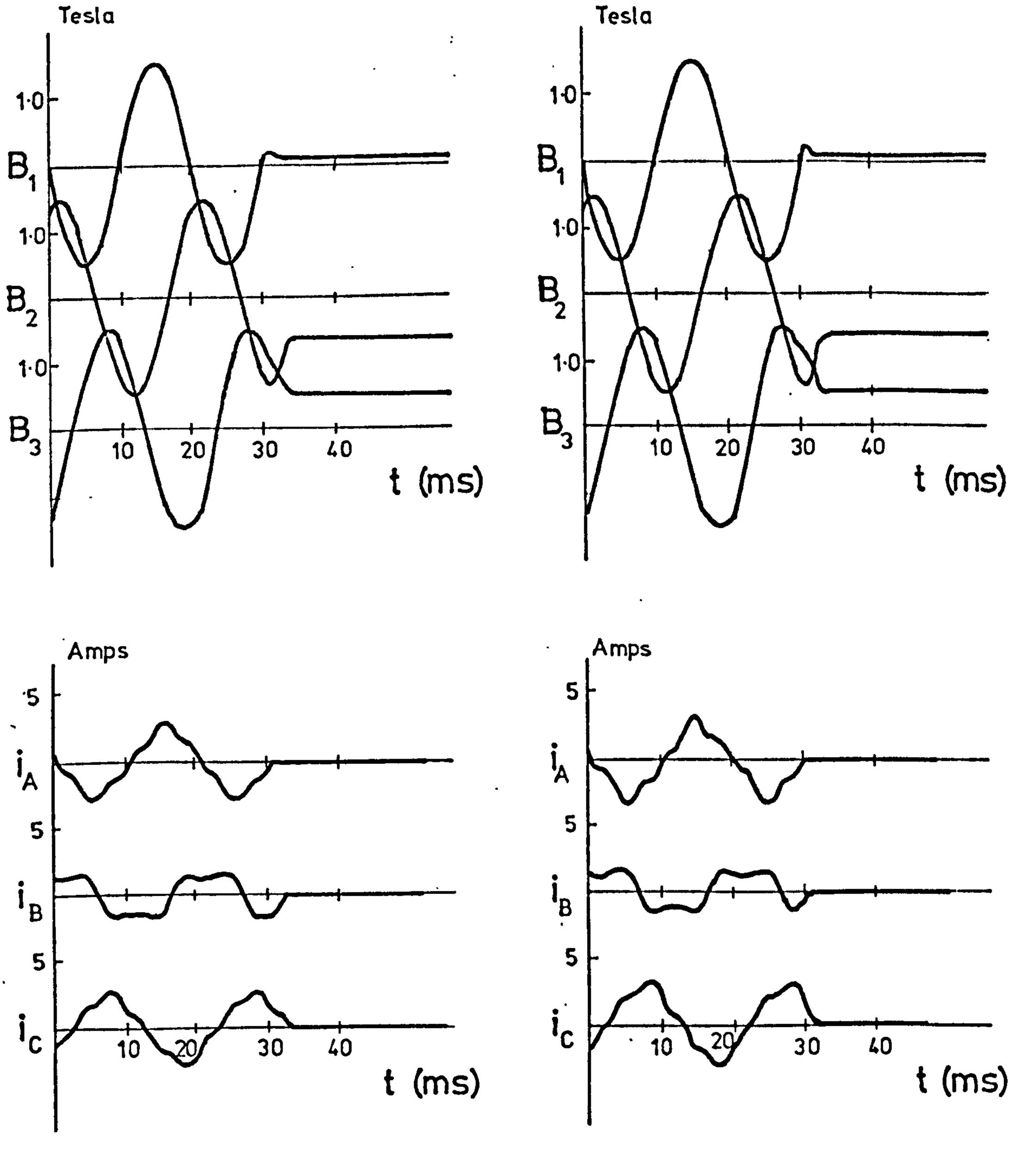

Fig. 4.5.1 Limb fluxes and line currents during disconnection of supply to unloaded transformer - 3-wire star primary.

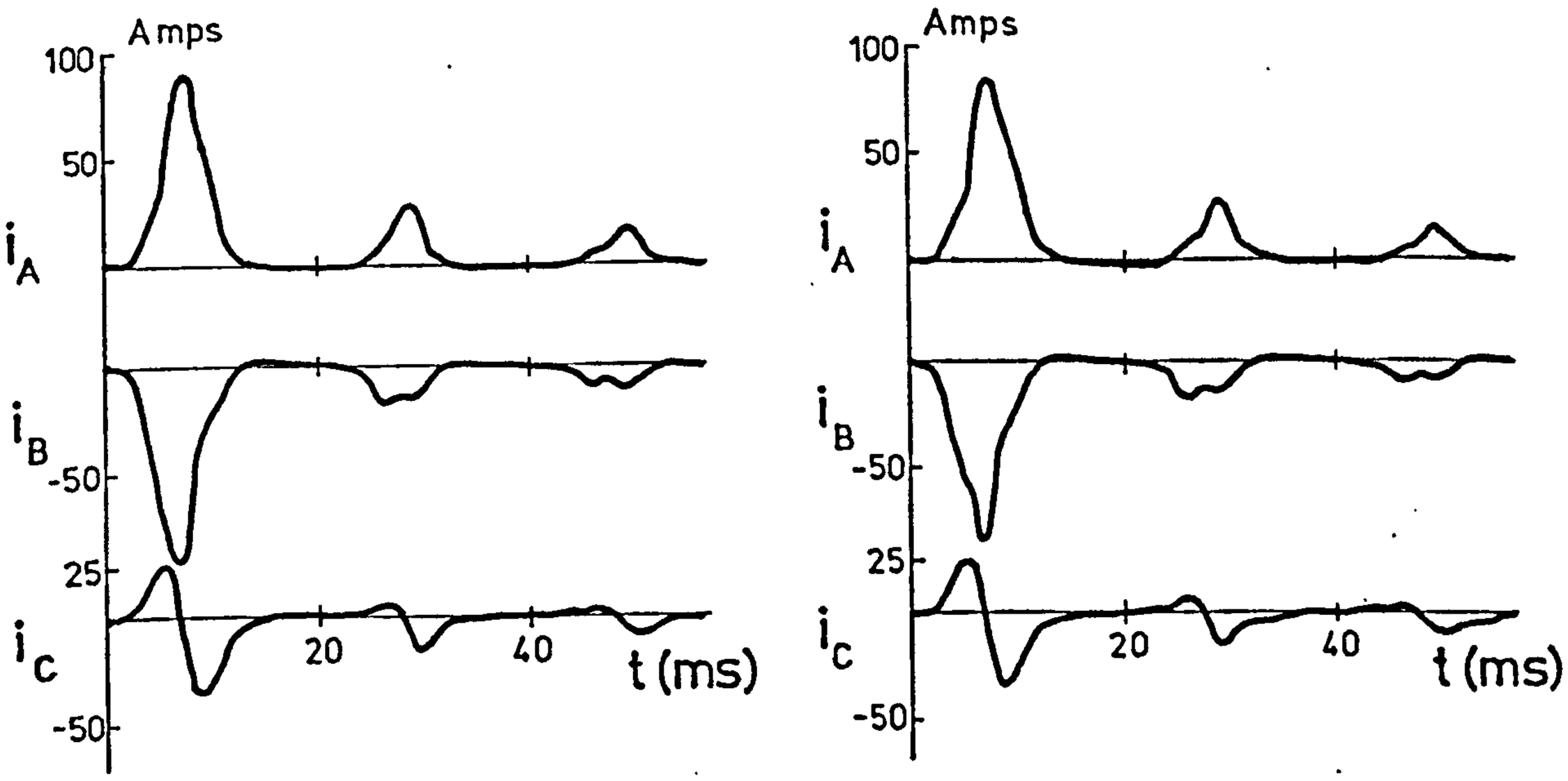

Fig. 4.5.2 Reconnection transient currents for residual conditions as in Fig. 4.5.1. Simultaneous switching, $\alpha = 270°$.

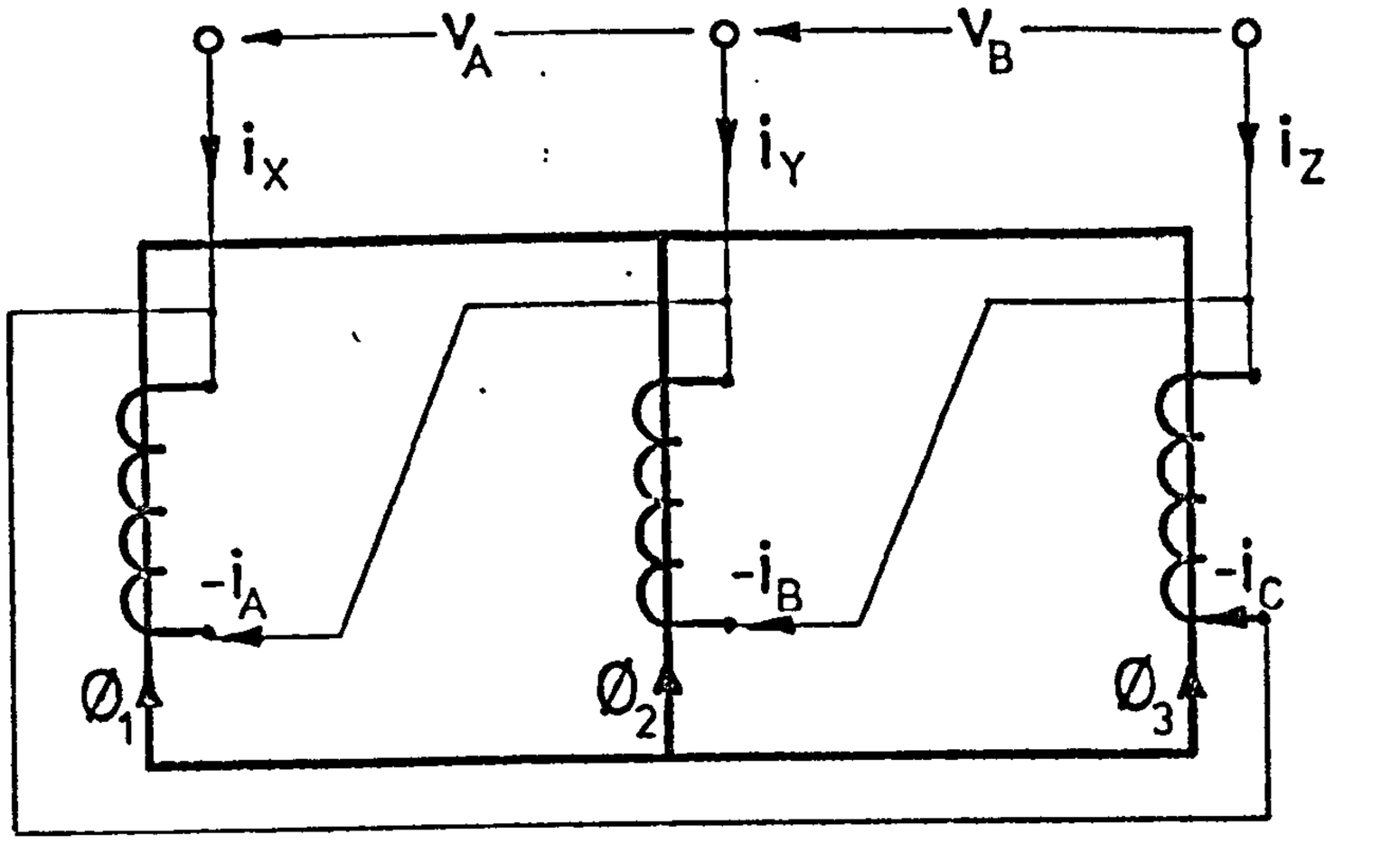

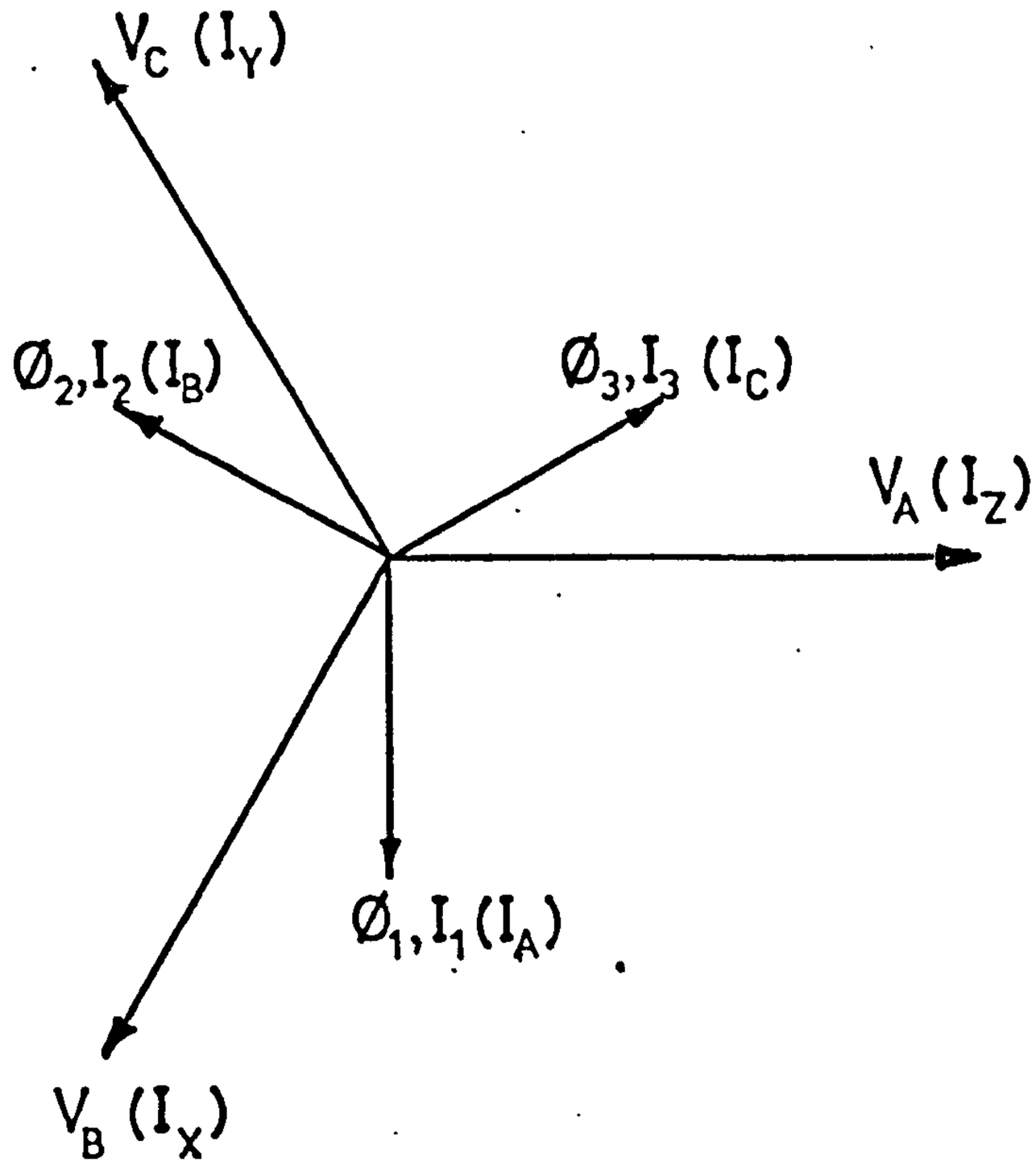

Fig. 4.5.3 Approximate steady-state phase relationships for delta connected primary winding — no load.

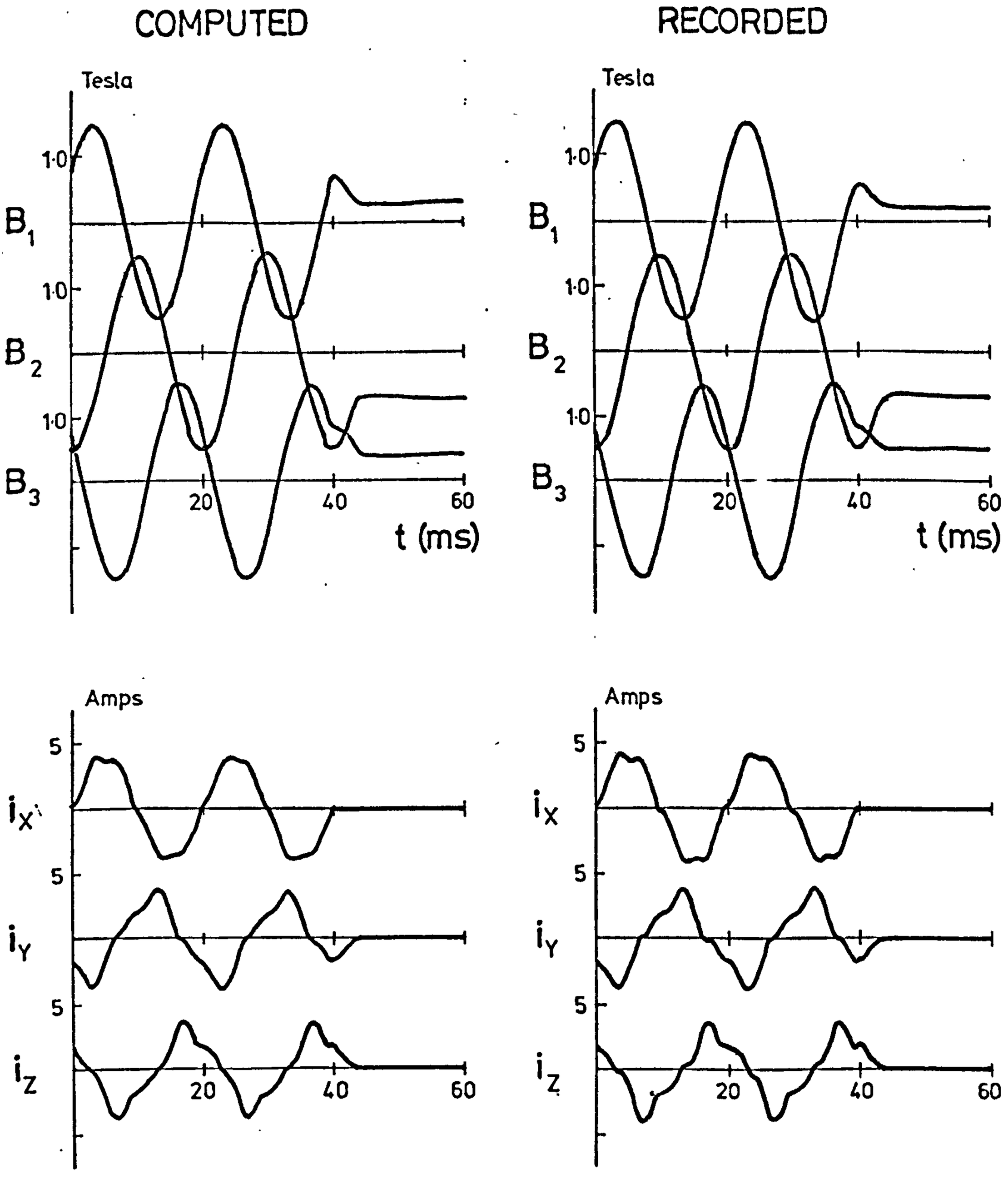

Fig. 4.5.4 Limb fluxes and line currents during disconnection of supply to unloaded transformer – delta connected primary.

Not to scale

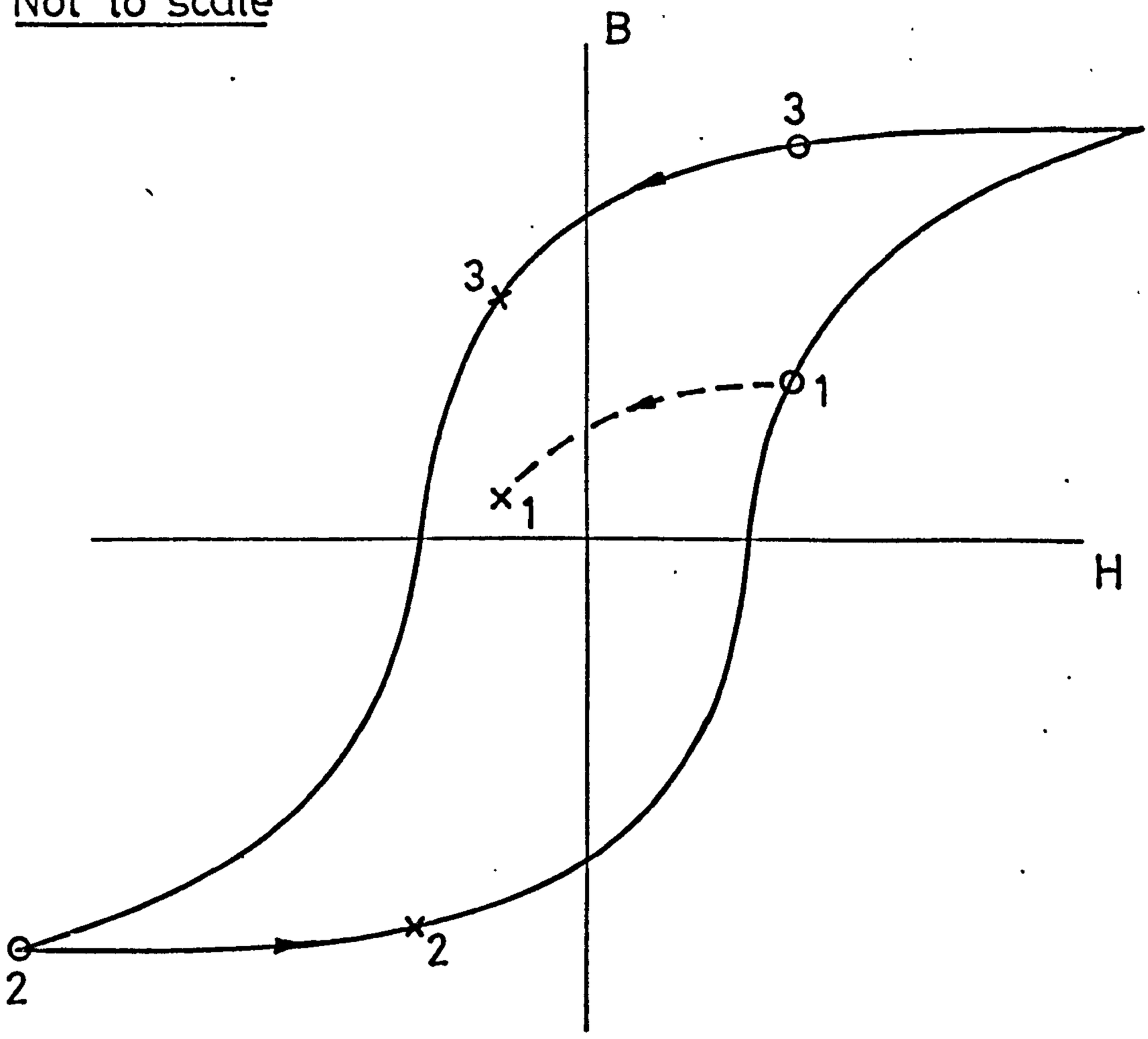

o - conditions when $i_x = 0$

x - conditions when all coil currents zero.

Fig. 4.5.5 Magnetic condition of core during disconnection of supply to unloaded transformer – delta connected primary.

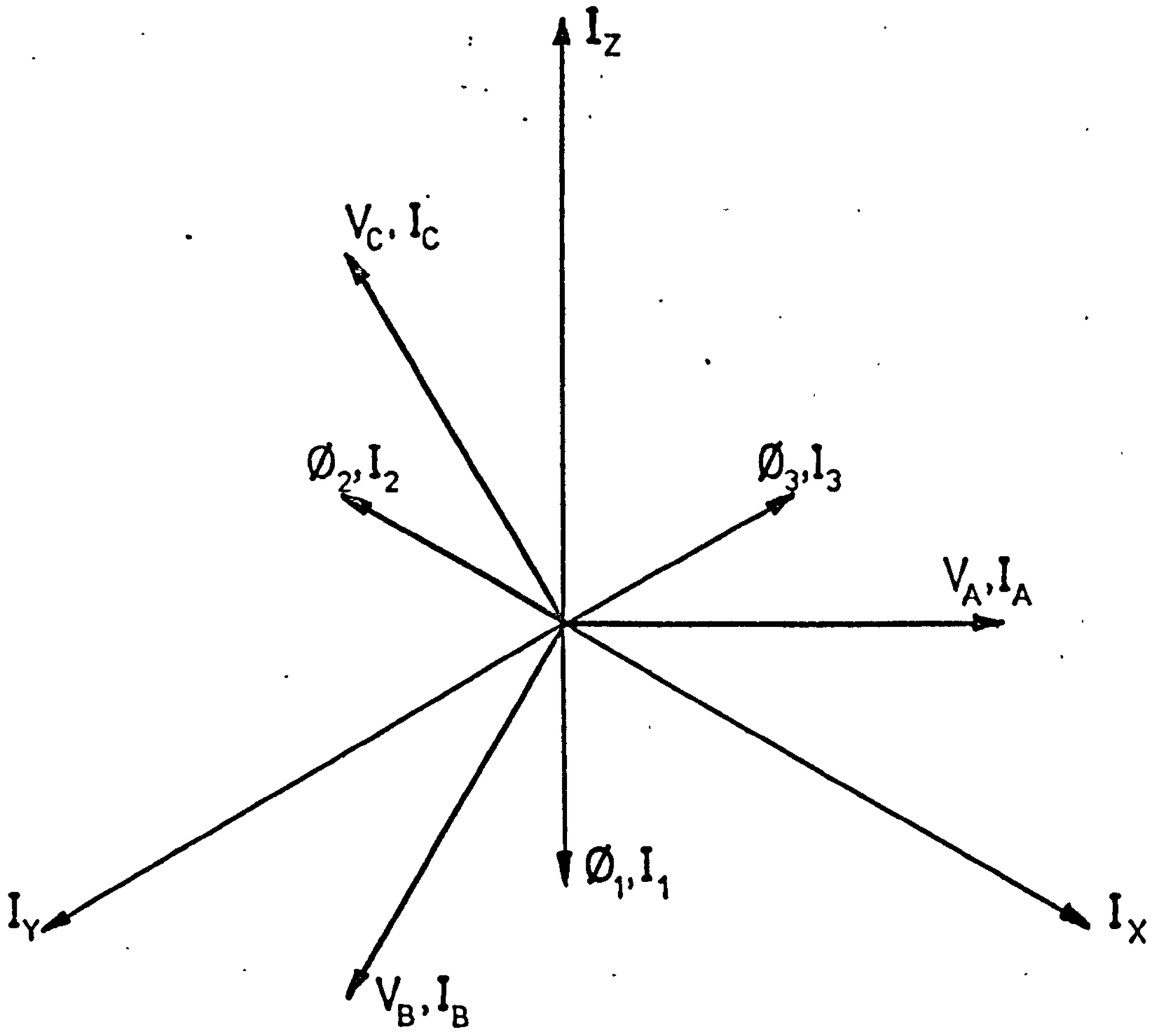

Fig. 4.5.6 Approximate steady-state phase relationships for delta connected primary winding — unity p.f. load.

Not to scale

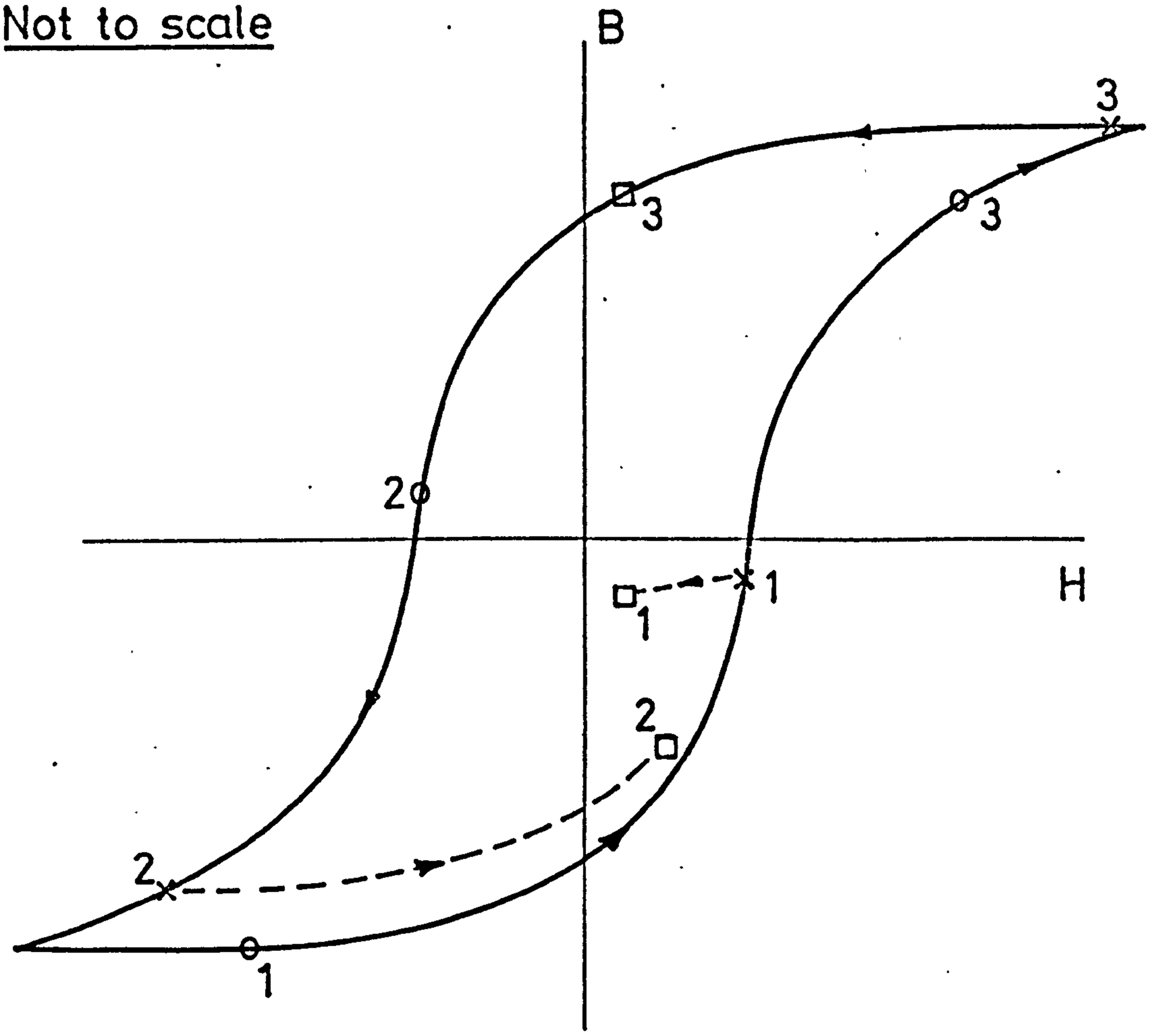

o - conditions when $i_x = 0$

x - conditions when all line currents zero

□ - final residual conditions

Fig. 4.5.7 Magnetic condition of core during supply disconnection — delta connected primary; unity p.f. load.

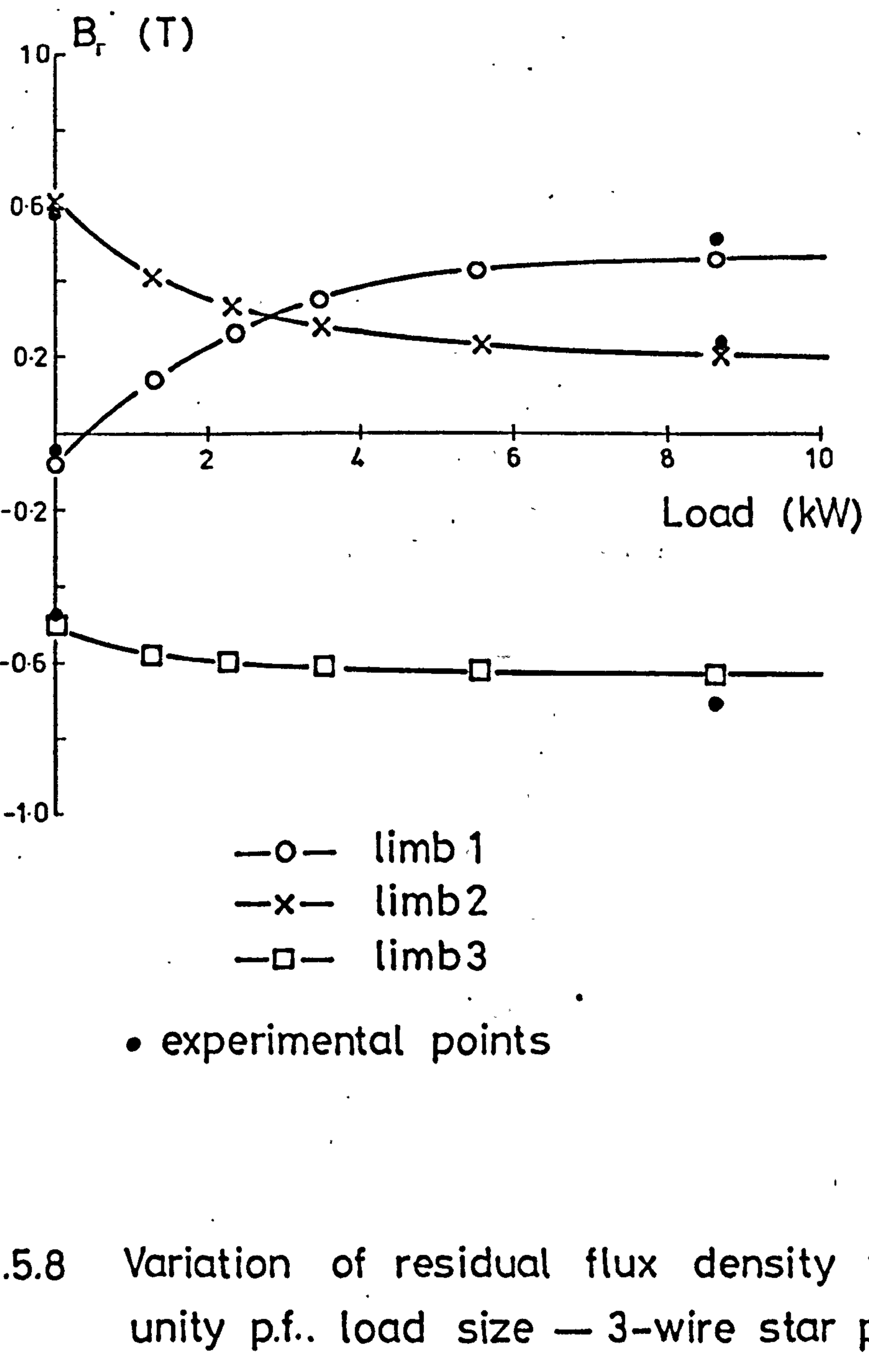

Fig. 4.5.8 Variation of residual flux density with unity p.f.. load size — 3-wire star primary. Line A disconnected first.

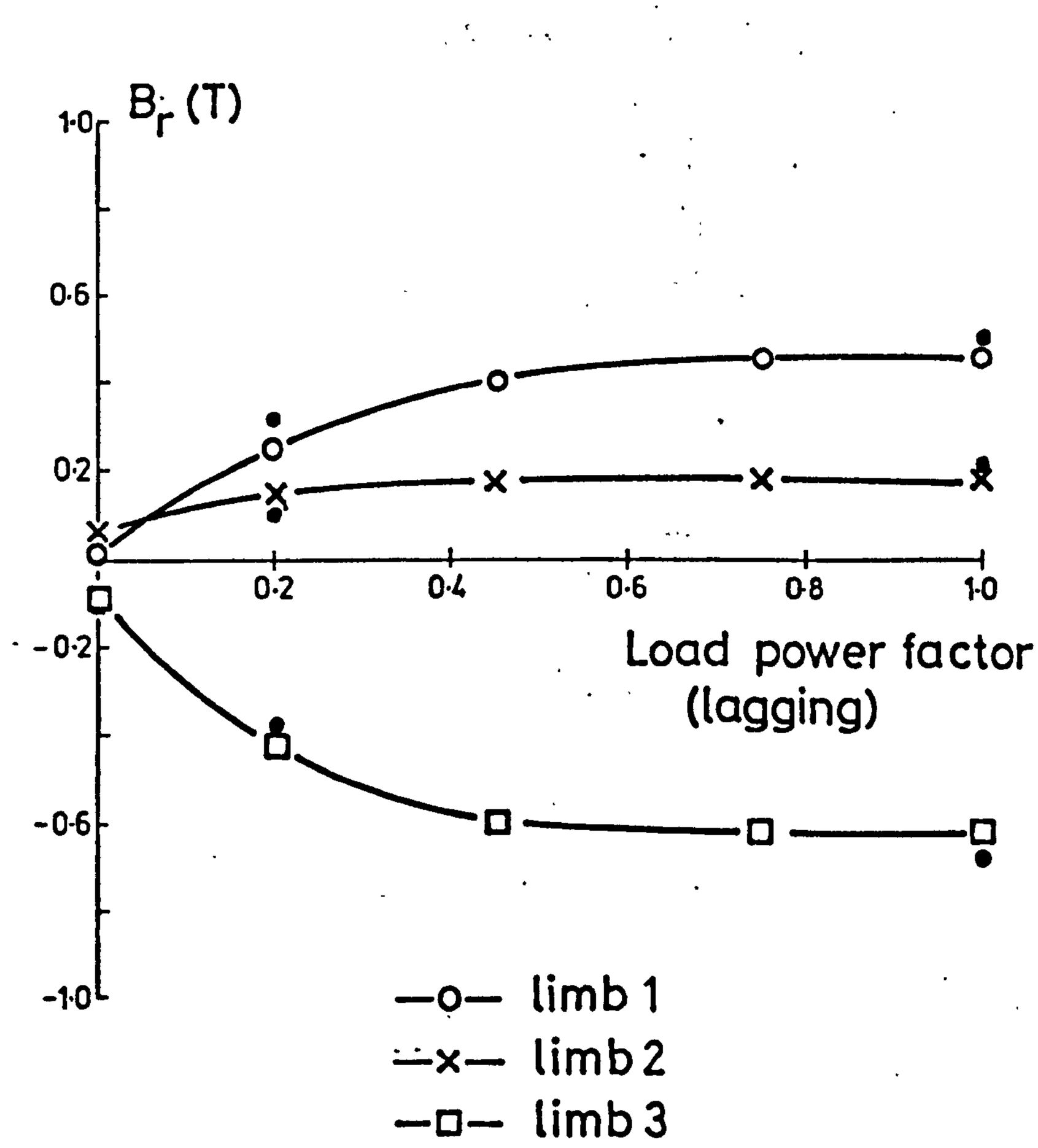

Fig. 4.5.9(a) Variation of residual flux density with load power factor (constant kVA) — 3-wire star primary; line A first to be disconnected.

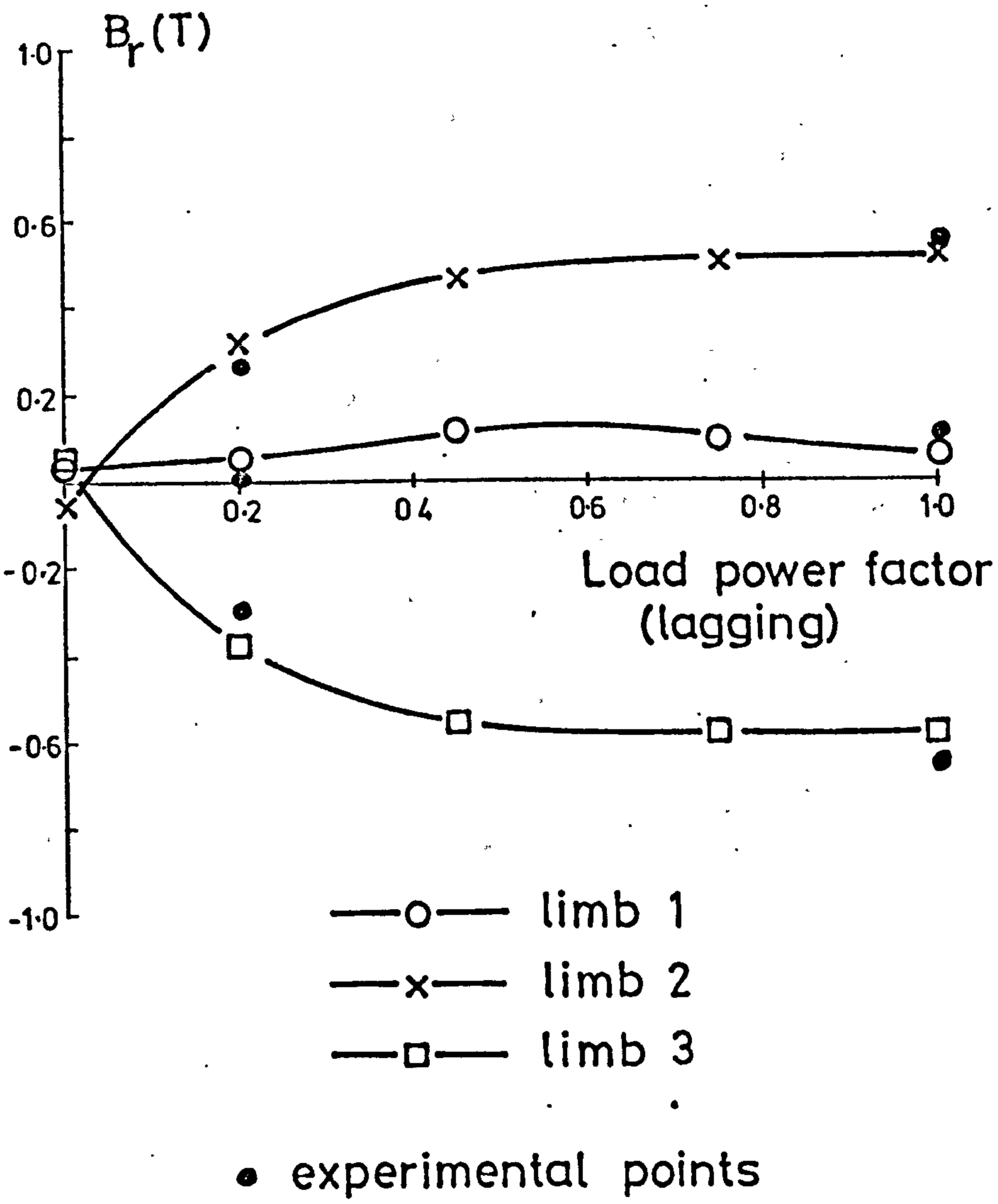

Fig. 4.5.9(b) Variation of residual flux density with load power factor (constant kVA) — 4-wire star and delta connected primary. Line A(X) disconnected first.

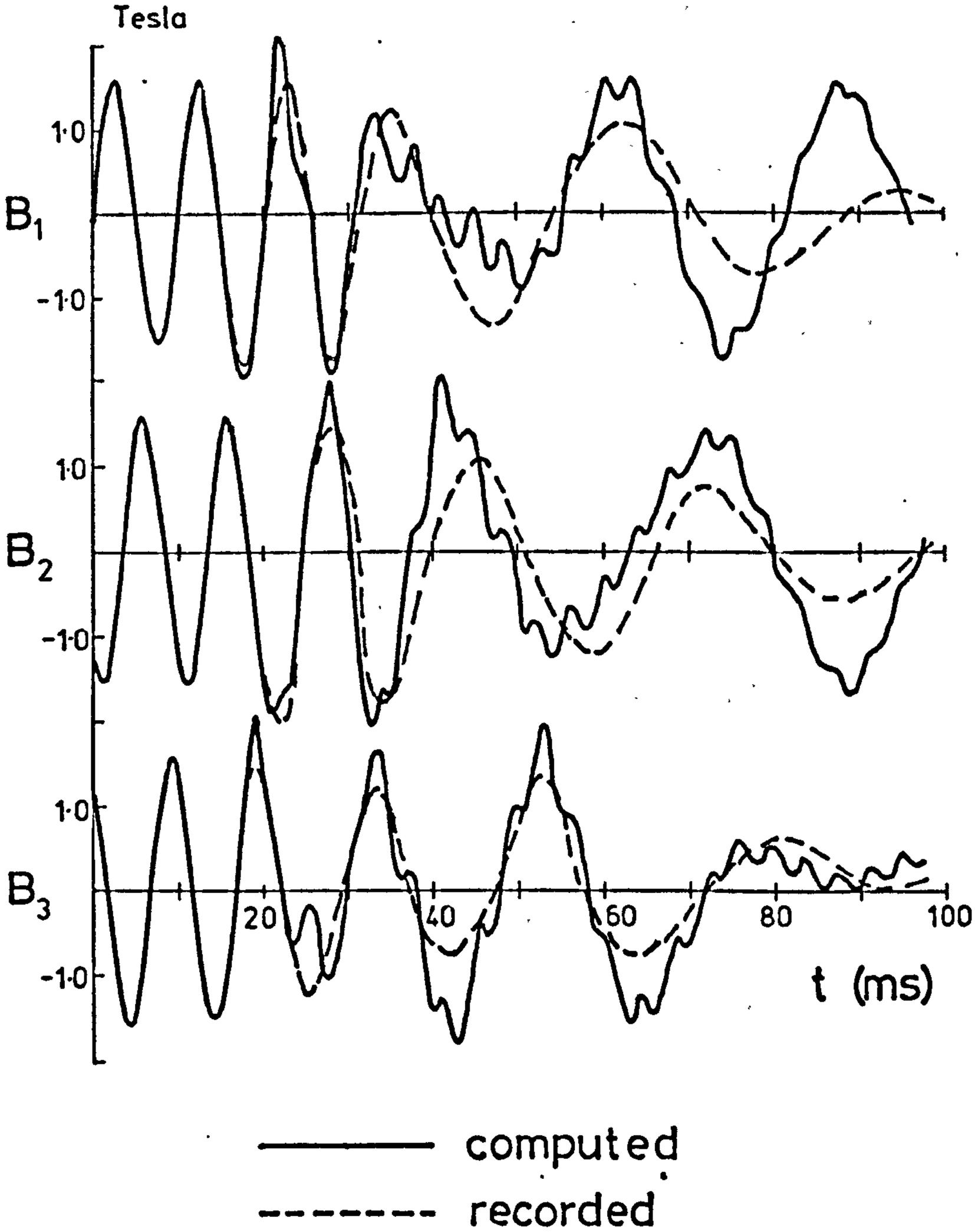

Fig. 4.5.10 Limb flux densities during supply disconnection. — 4-wire star primary, leading power factor (0) load.

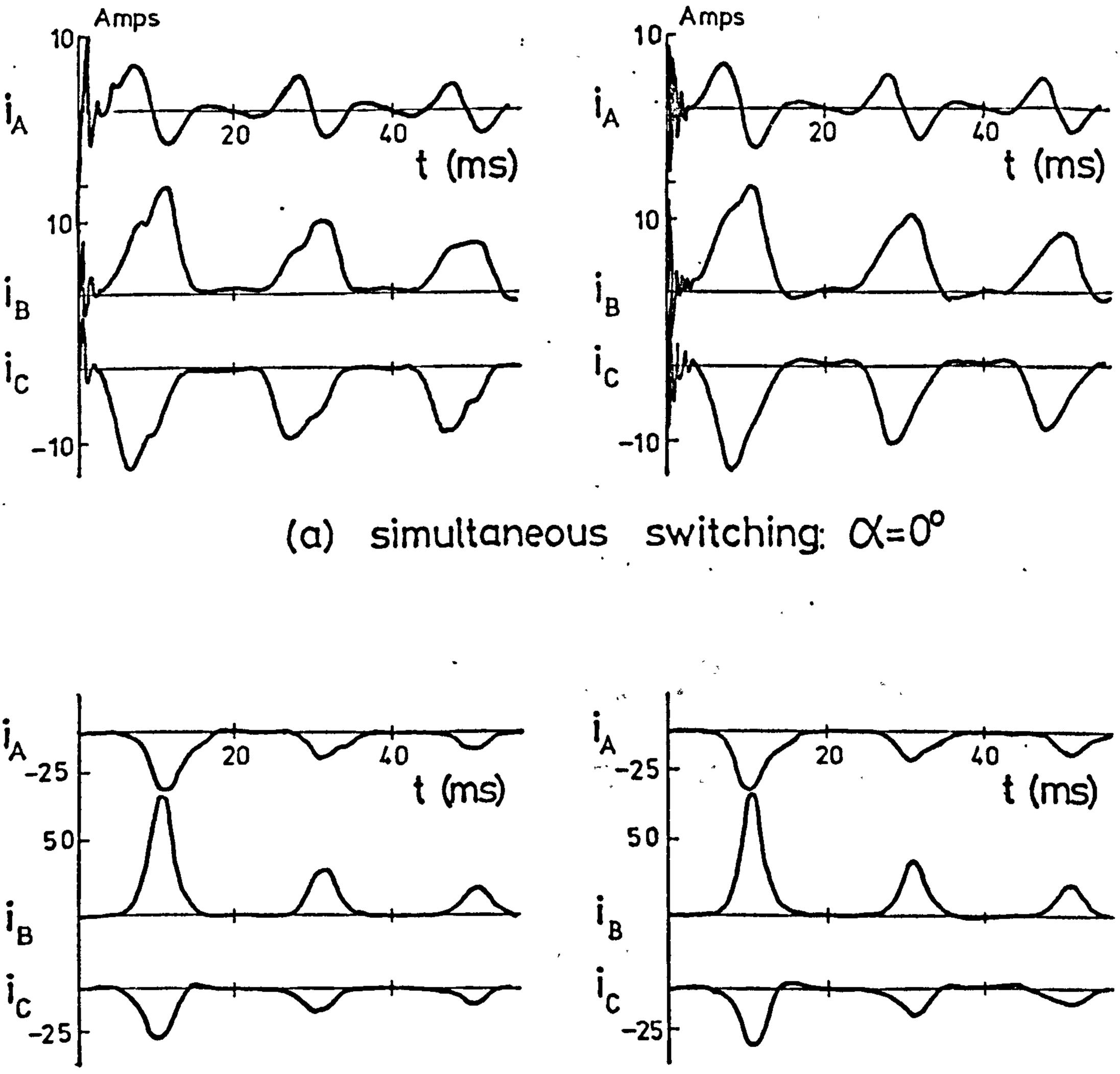

(a) simultaneous switching: $\alpha=0°$

(b) non-sim. switching: $\alpha=0°$, $\beta=90°$

Fig. 4.5.11 Transient current patterns for 50-kVA, 433v/11 kV transformer — 3-wire star primary, no load, zero residual conditions. $V_L=340v$.

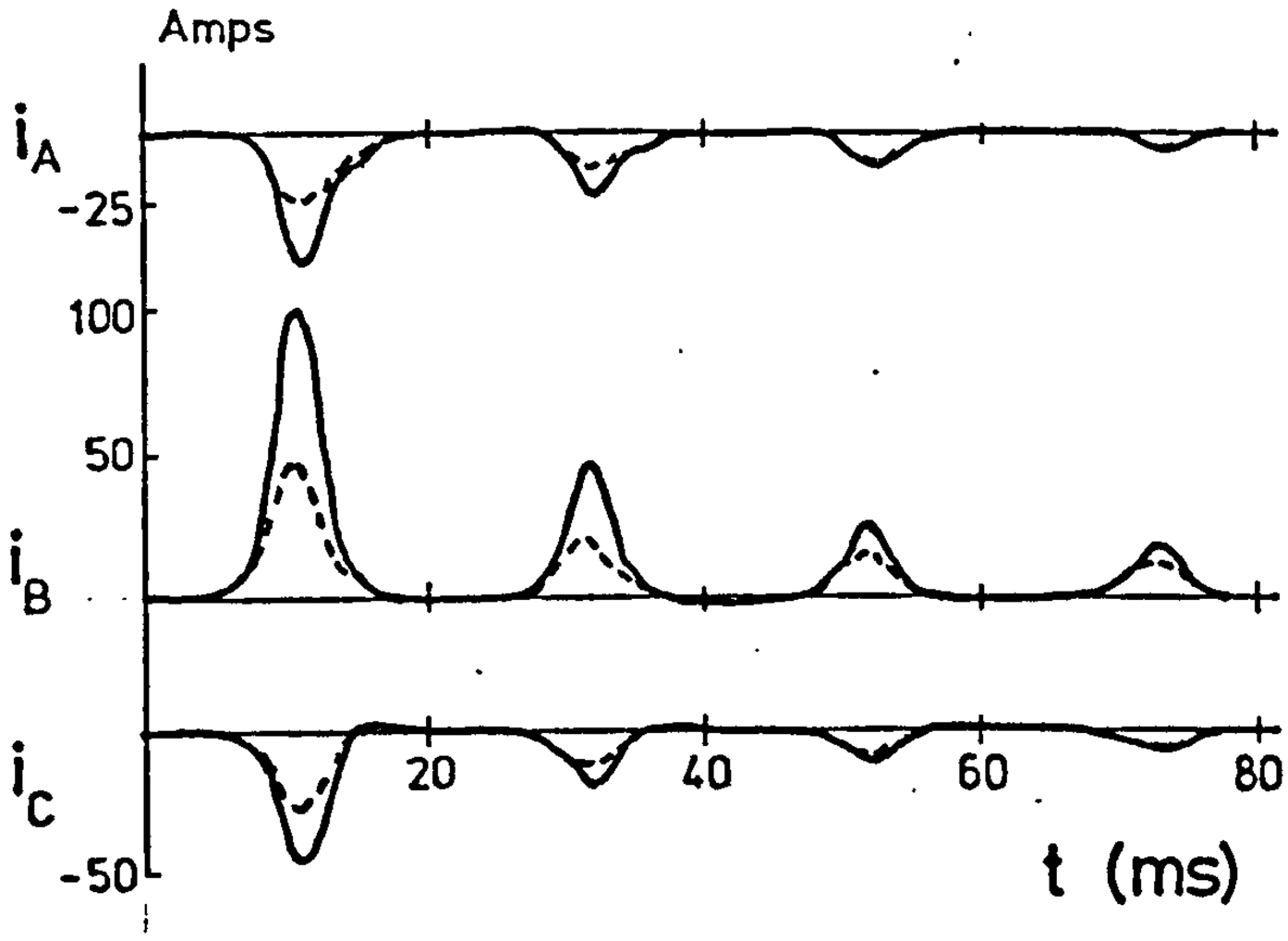

Fig. 4.5.12 Reconnection transient currents for 50-kVA transformer – 3-wire star primary, no load, V =340v; α=0°; β =90°

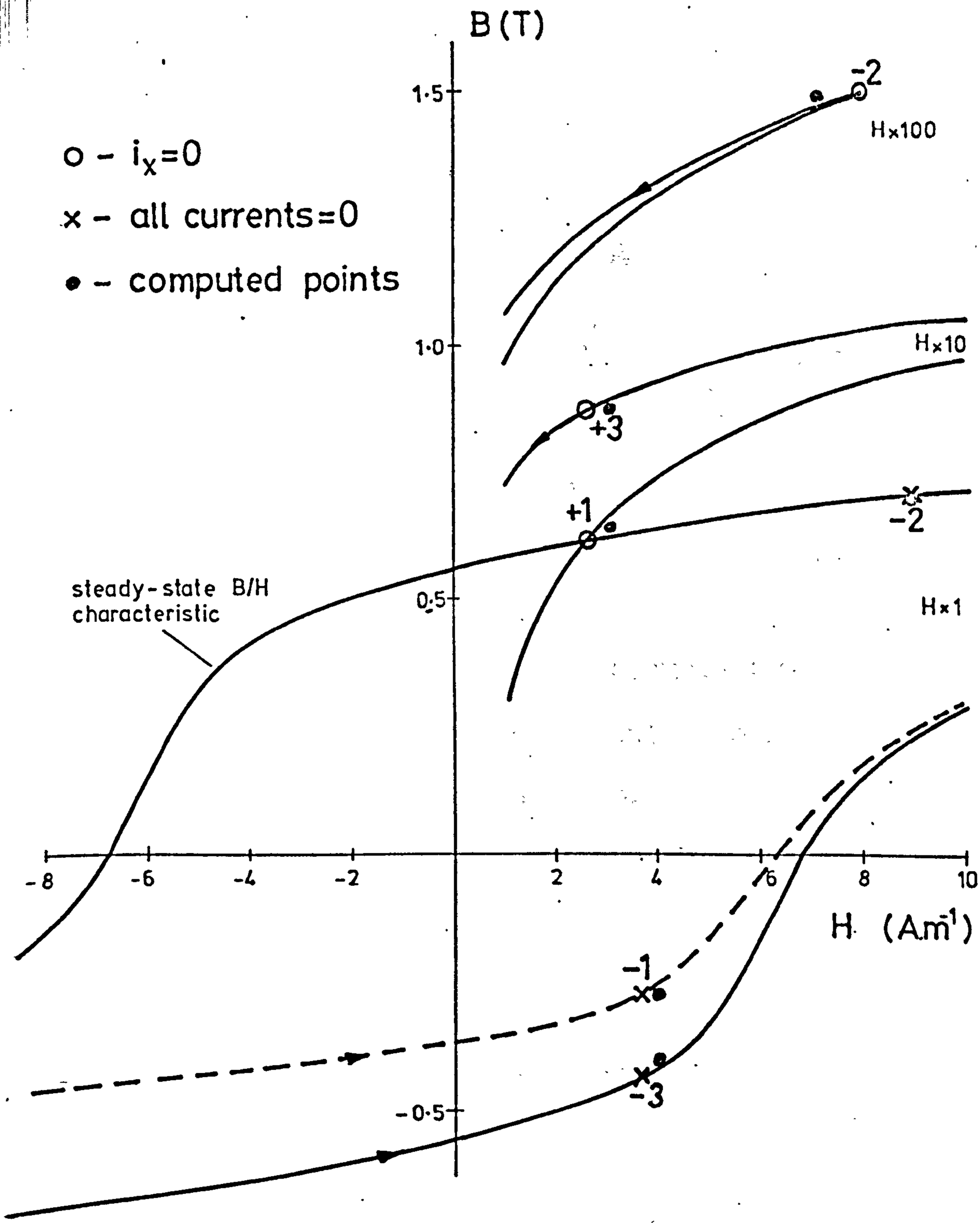

Fig. 4.5.13 Graphical estimation of residual conditions — delta connected primary, no load. Line X disconnected first.

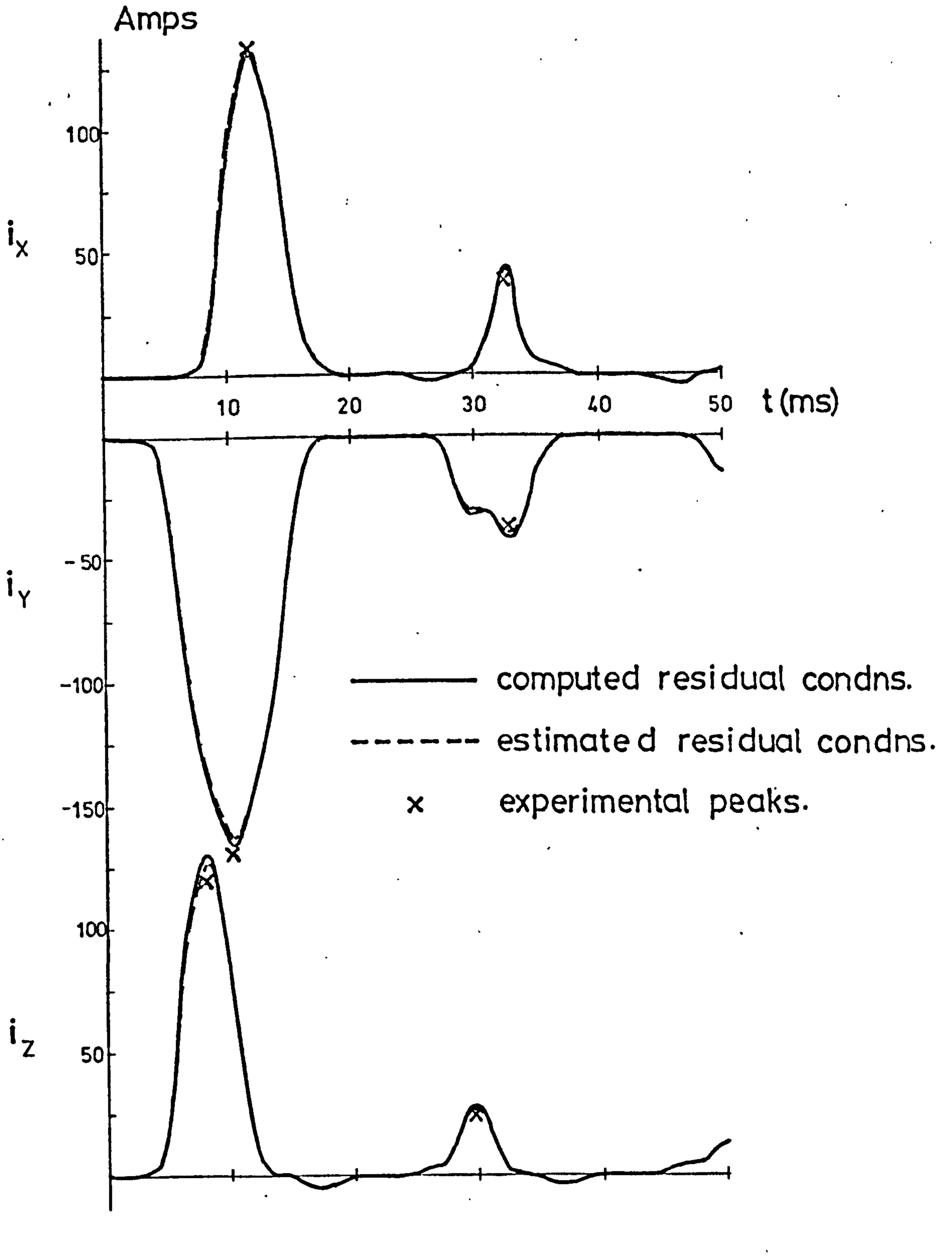

Fig. 4.5.14 Reconnection transient currents for the estimated and computed residual conditions given in Fig. 4.5.13. $\alpha=180°$, $\beta=90°$

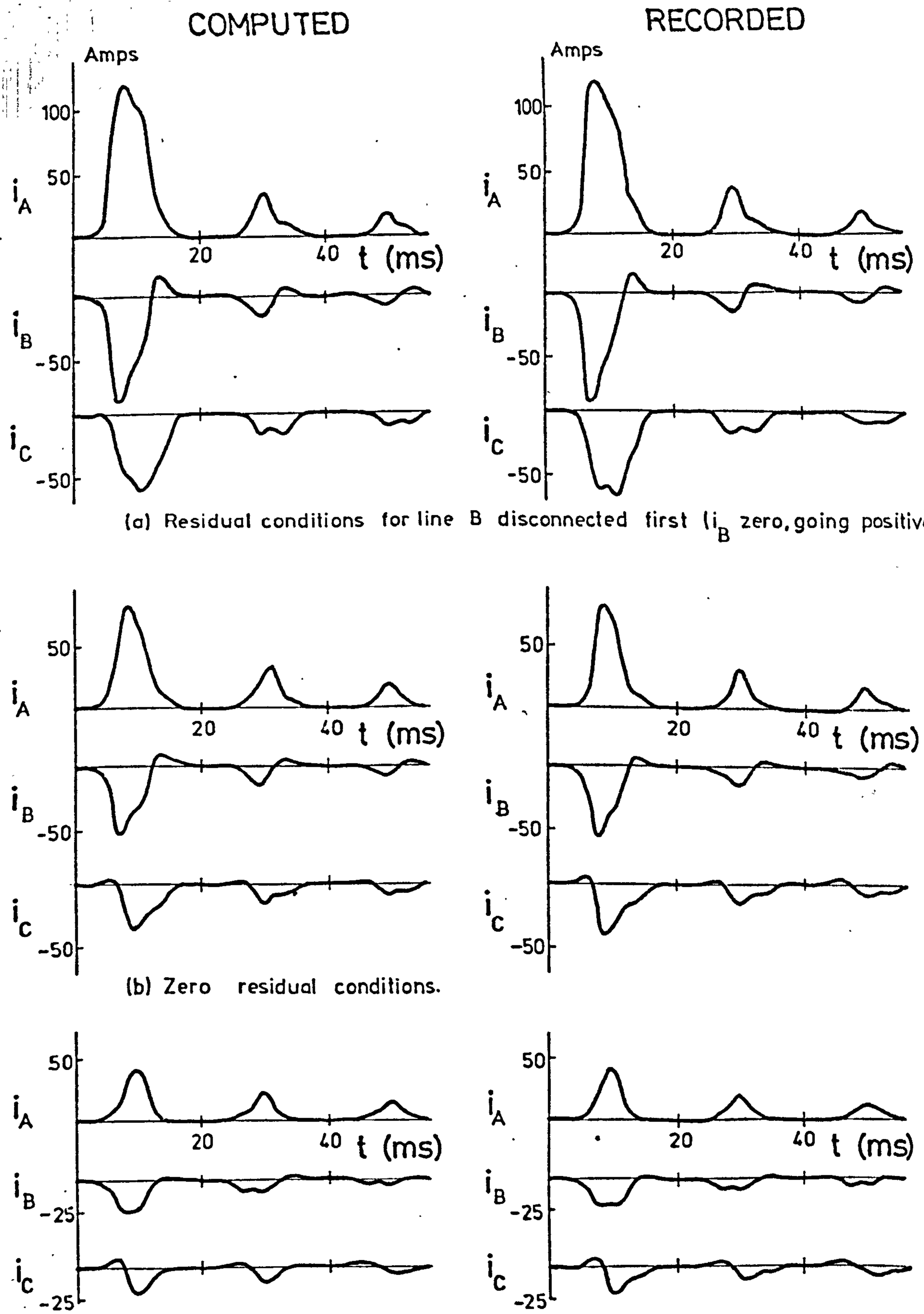

(a) Residual conditions for line B disconnected first (i_B zero, going positive).

(b) Zero residual conditions.

(c) Residual conditions opposite in polarity to (a).

Fig. 4.6.1 Effect of polarity of residual conditions.
3-wire star primary, no load. $\alpha = -90°$: $\beta = 0°$

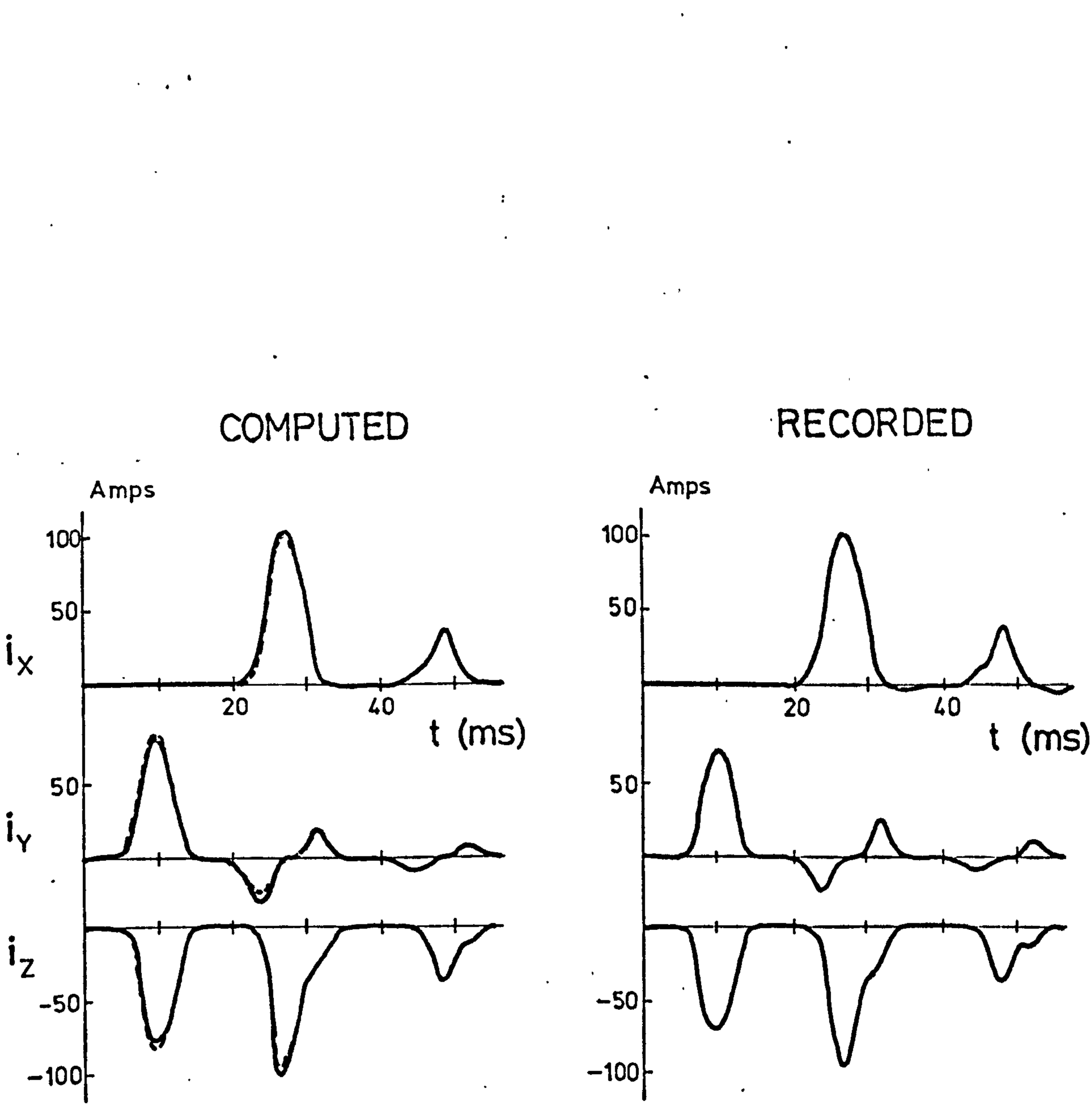

Fig. 4.6.2 Effect of suppressing residual phase-leakage flux on reclosure transients. Delta connected primary, no load. $\alpha=0°; \beta=270°$

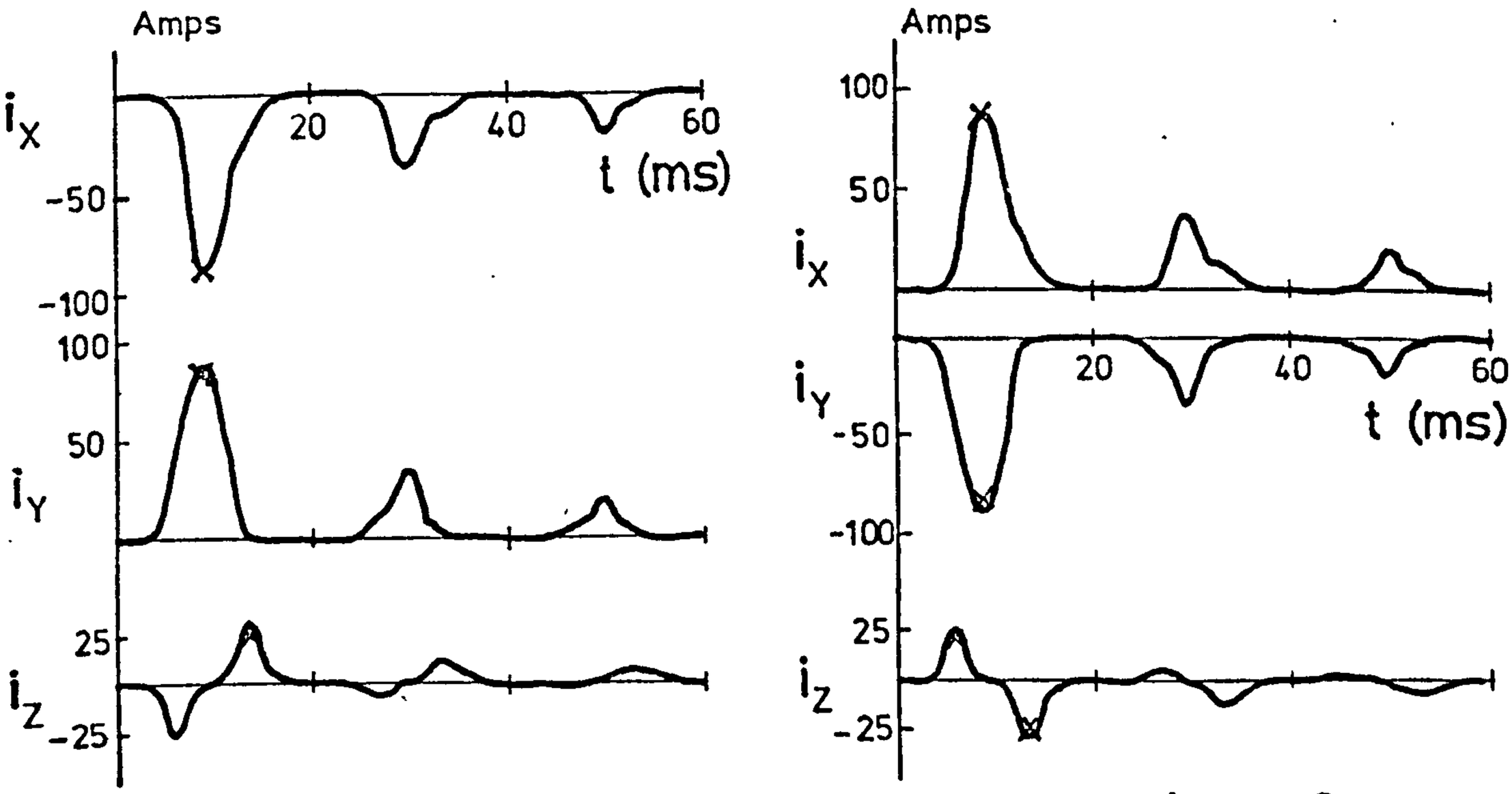

x experimental peaks

Fig. 4.6.3 Transient current patterns for 180° change in initial switching angle (α) — no residual flux. Delta connected primary, no load.

$\beta = 0°$

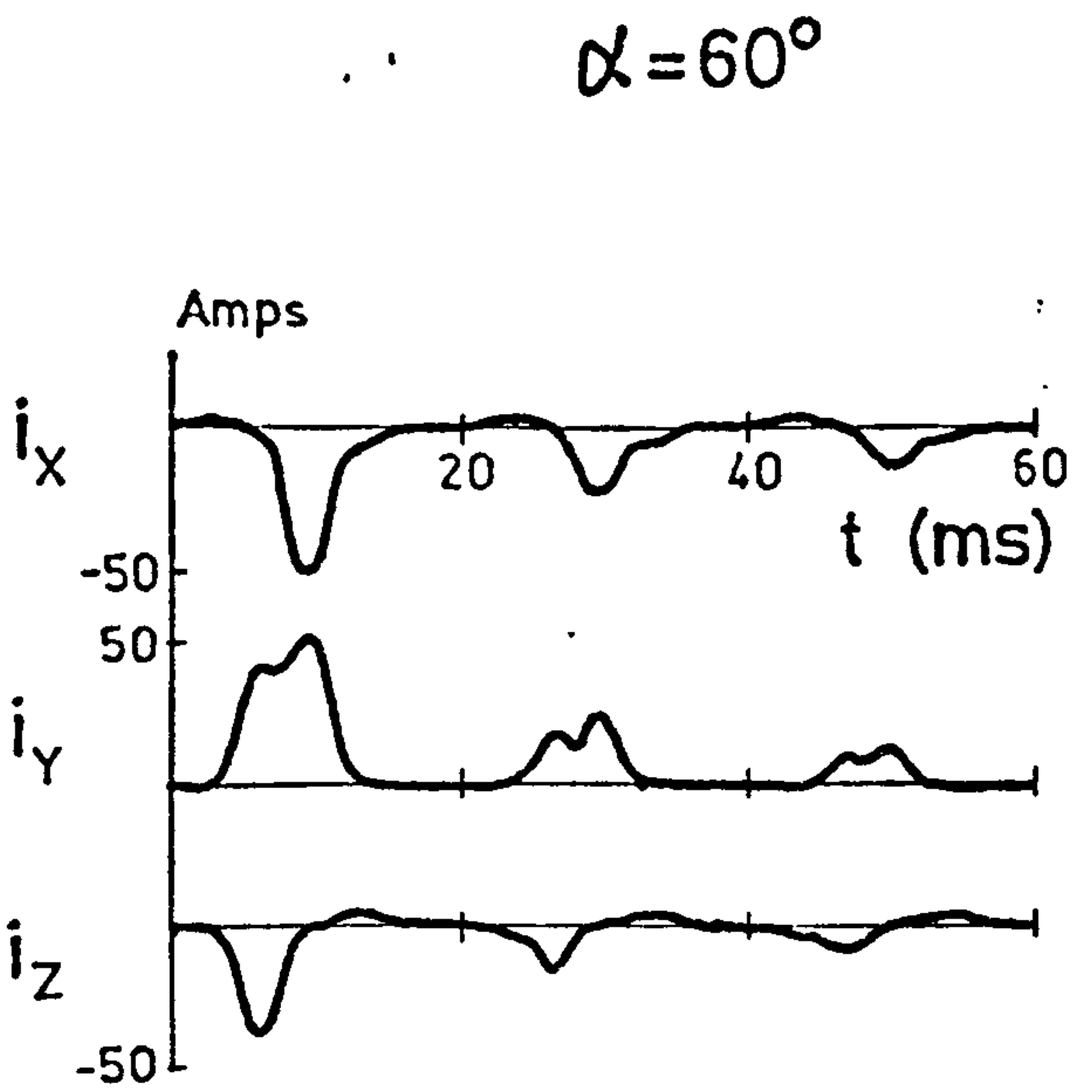

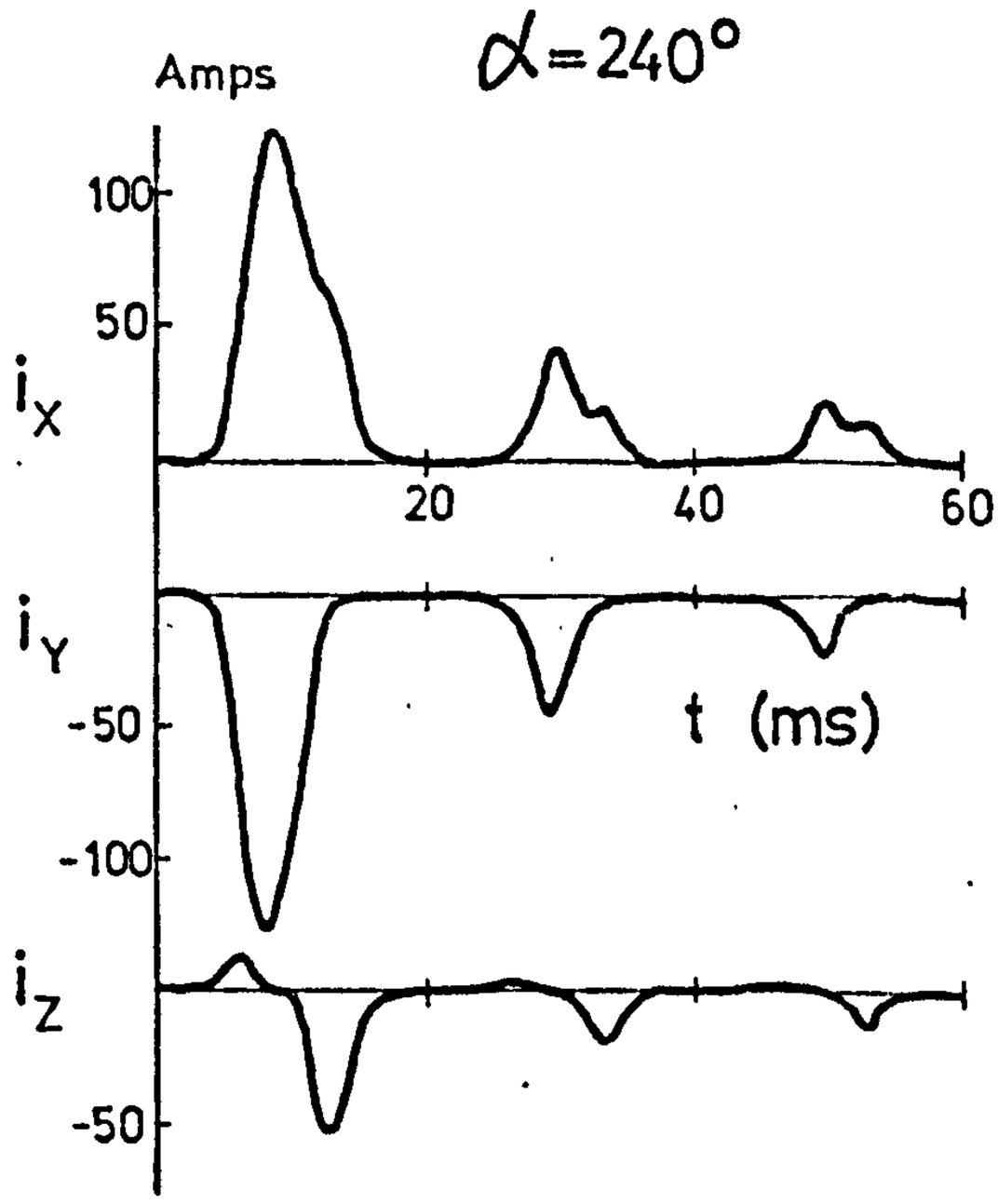

(a) Residual conditions for line Y disconnected first - i_Y zero, going positive.

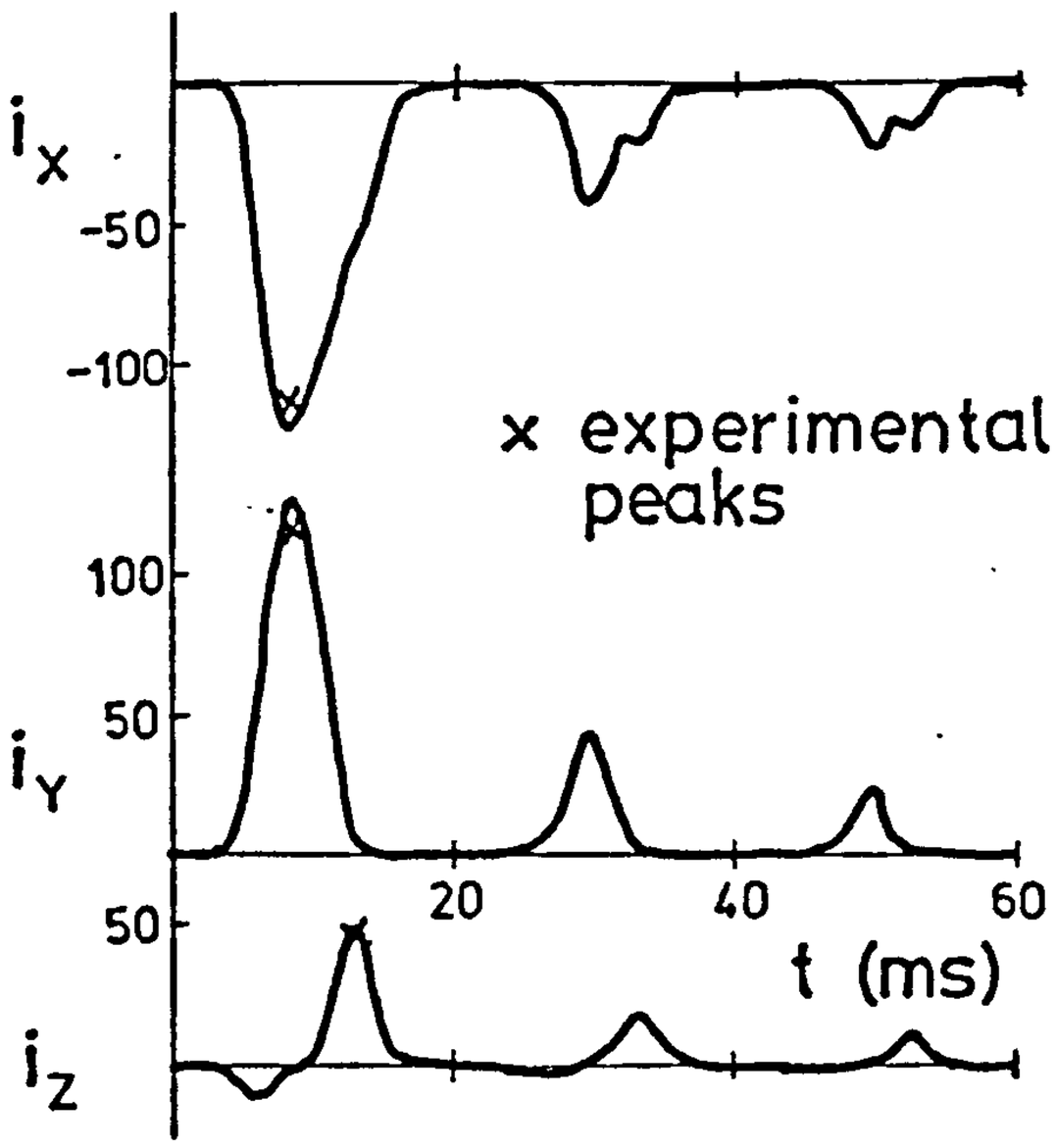

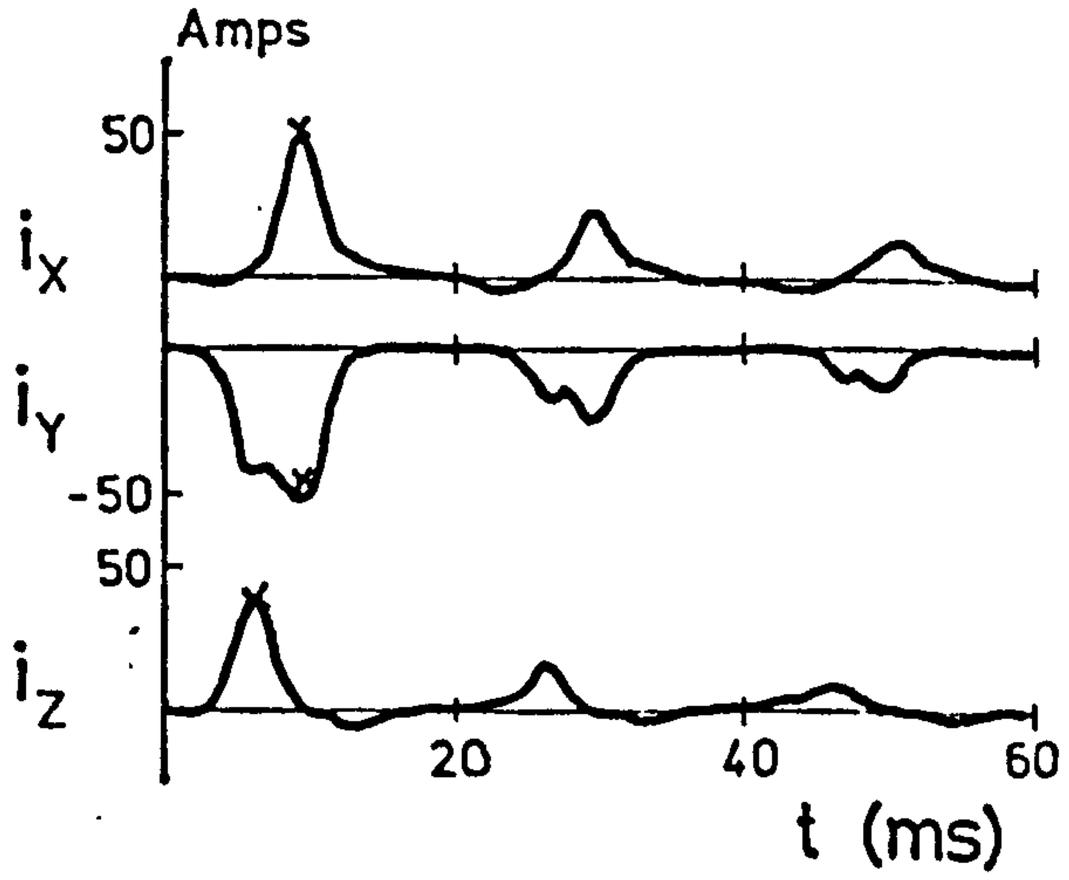

(b) As for (a) except, i_Y zero, going negative

Fig. 4.6.4 Transient current patterns for 180° change in α — residual flux present. β=0° Delta connected primary, no load.

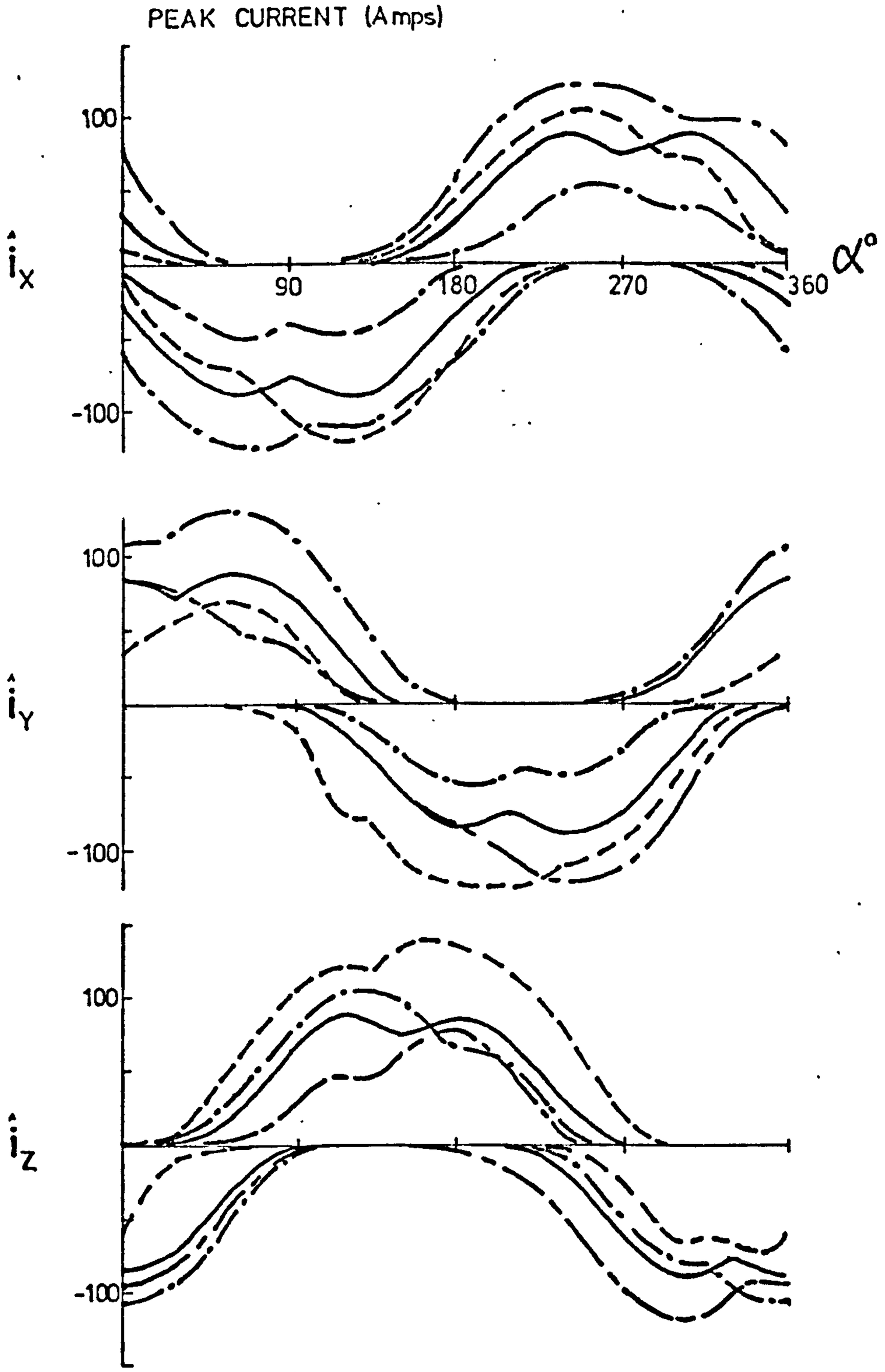

Fig. 4.6.5 Variation of peak transient current with α — effect of residual flux. Delta connected primary, no load. Simultaneous switching.

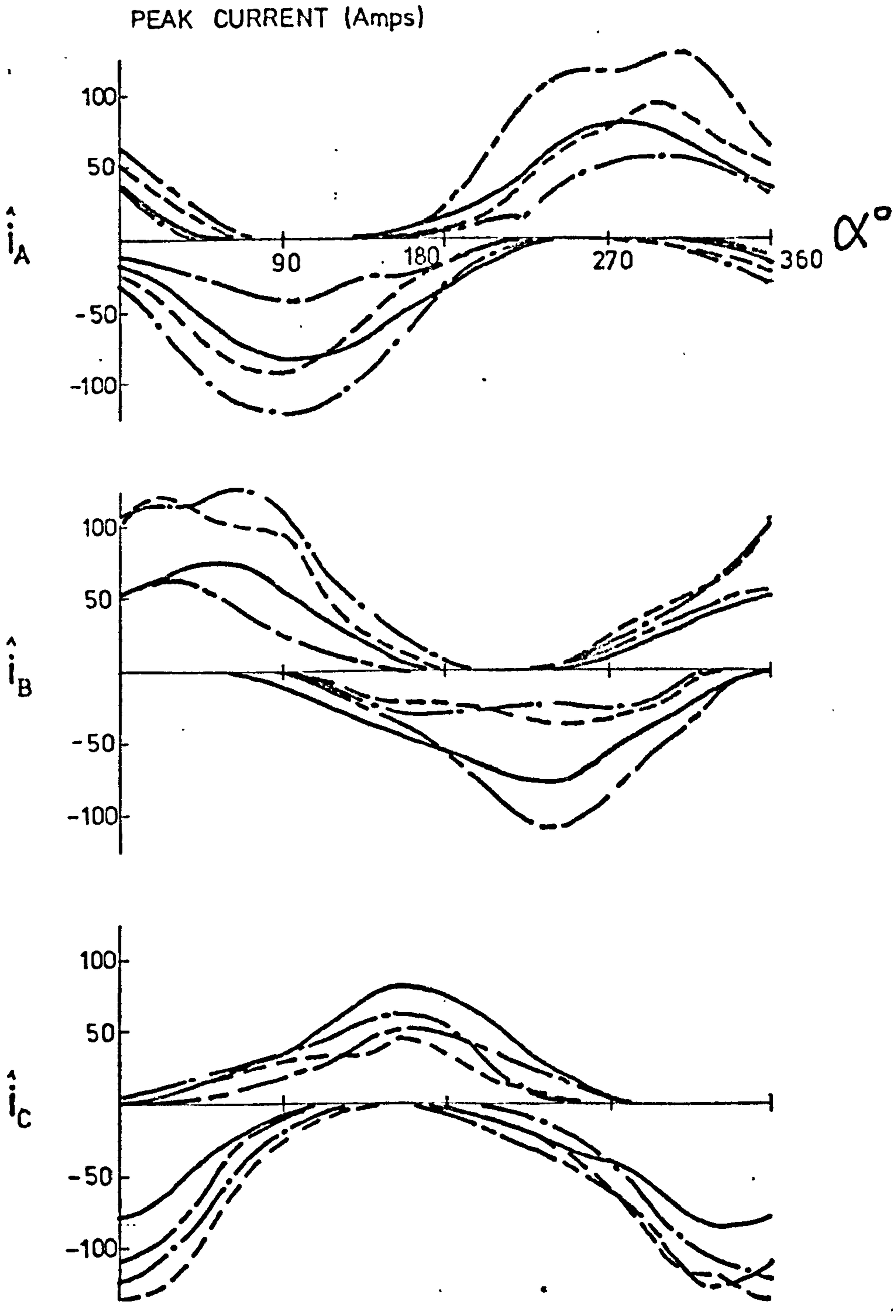

Fig. 4.6.6 Variation of peak transient current with simultaneous switching angle — effect of residual flux. 3-wire star connected primary, no load.

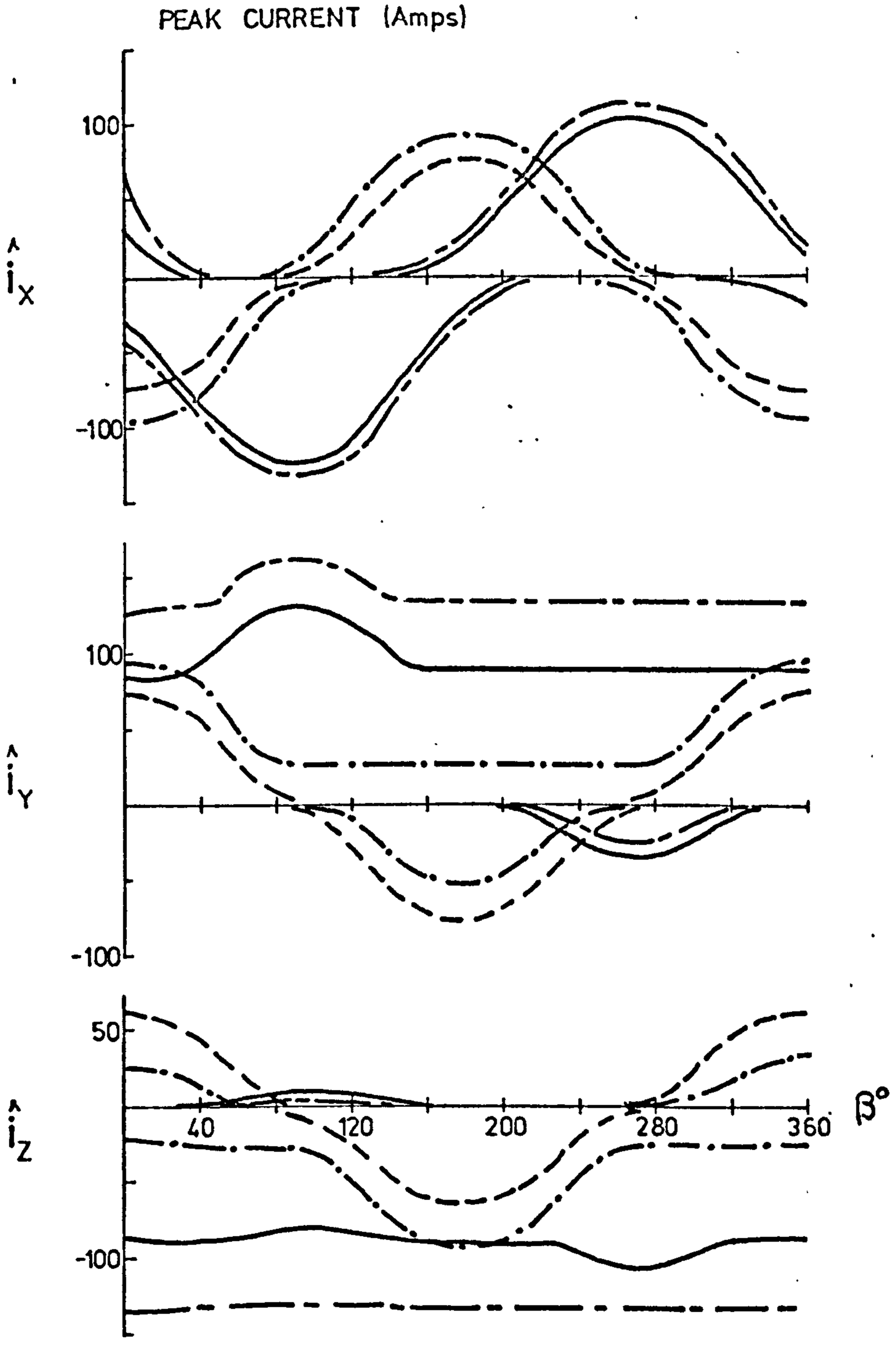

Fig. 4.6.7 Variation of peak transient current with β — effect of residual flux. Delta connected primary winding, no load.

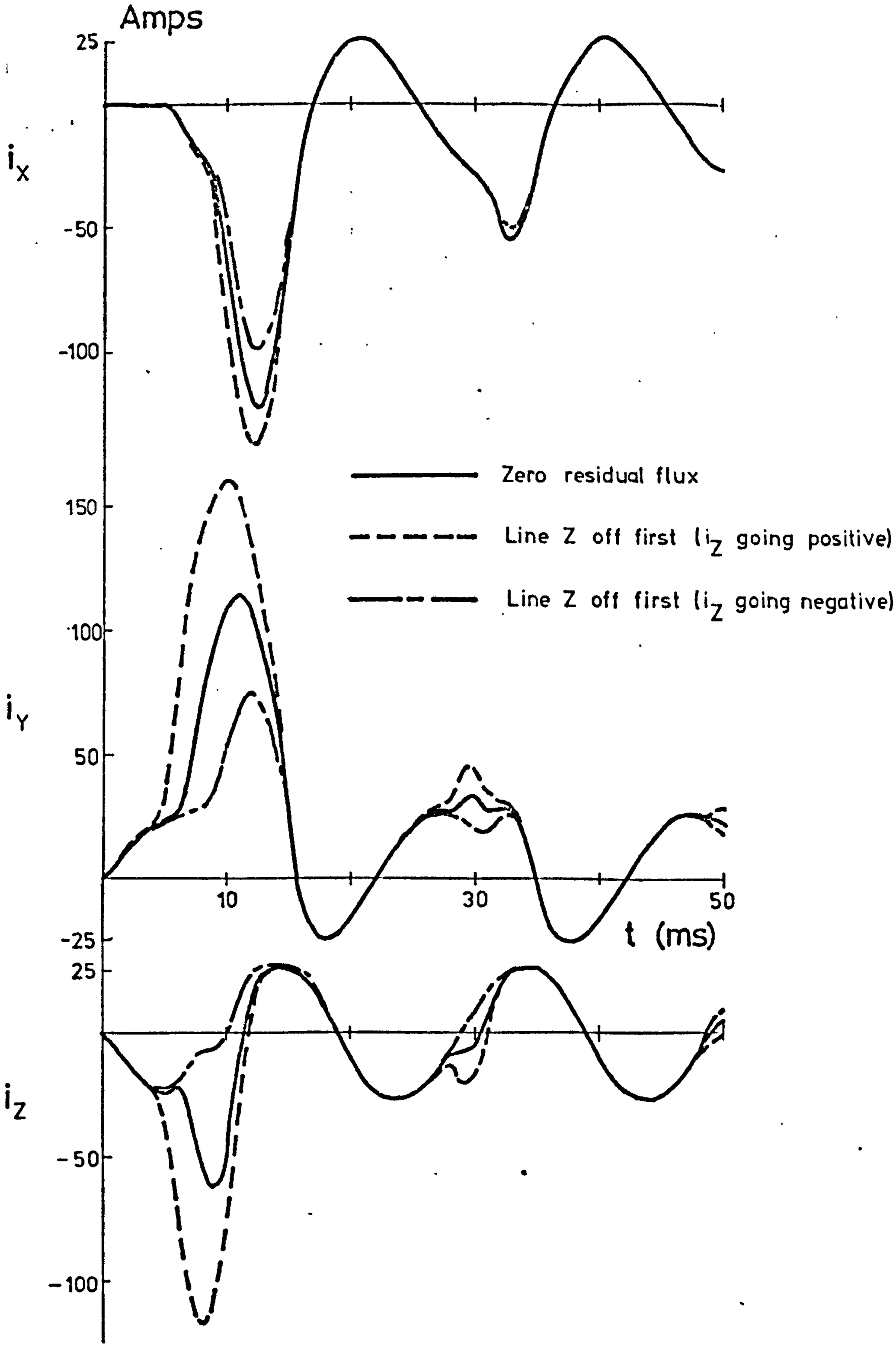

Fig. 4.6.8 Effect of residual conditions on transient currents — unity power factor load.
Delta connected primary; $\alpha = 0°$: $\beta = 90°$

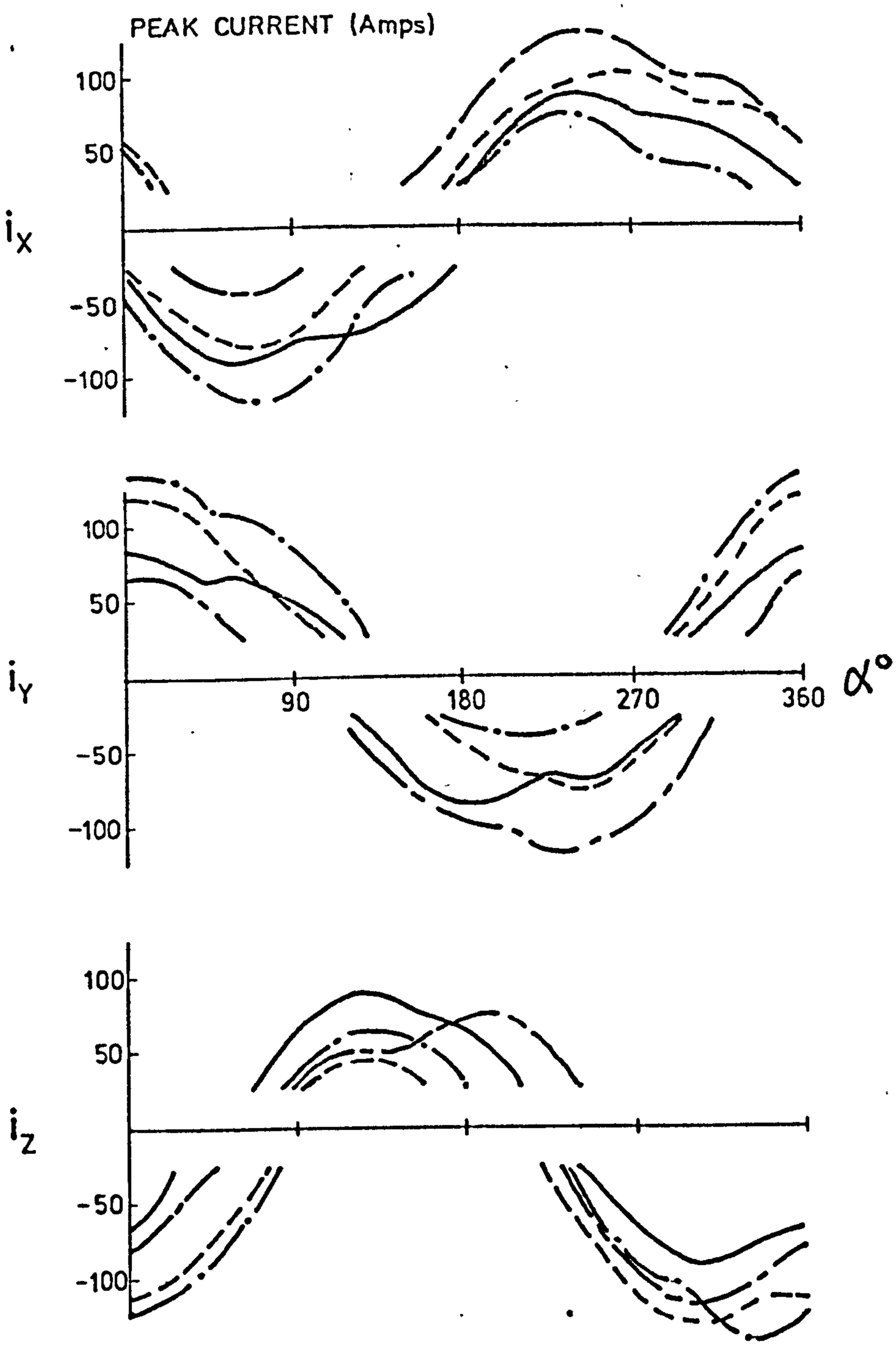

Fig. 4.6.9 Variation of peak transient current with α. Unity power factor load; delta connected primary; simultaneous switching.

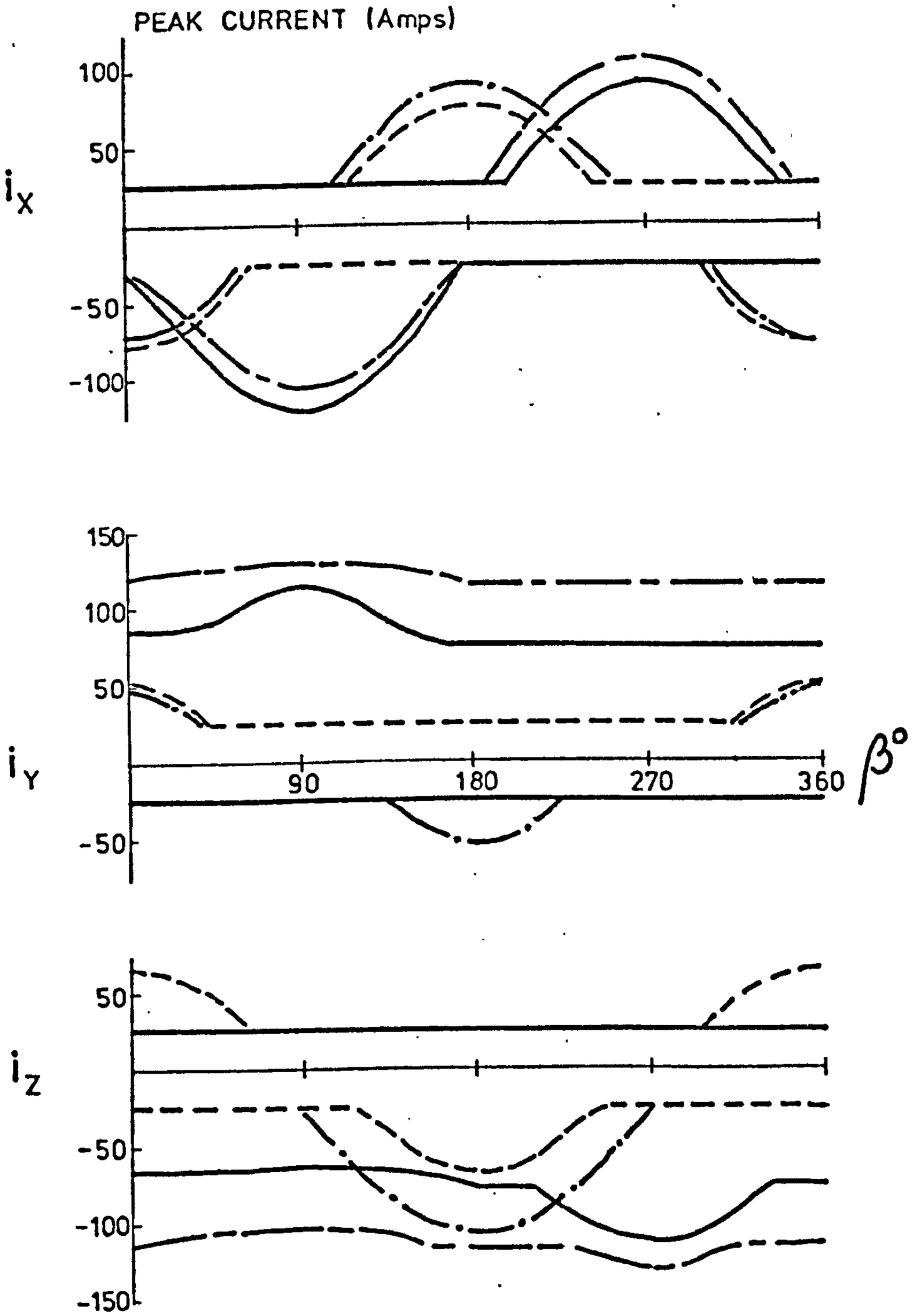

Fig. 4.6.10 Variation of peak transient current with β. Unity power factor load; delta connected primary winding.

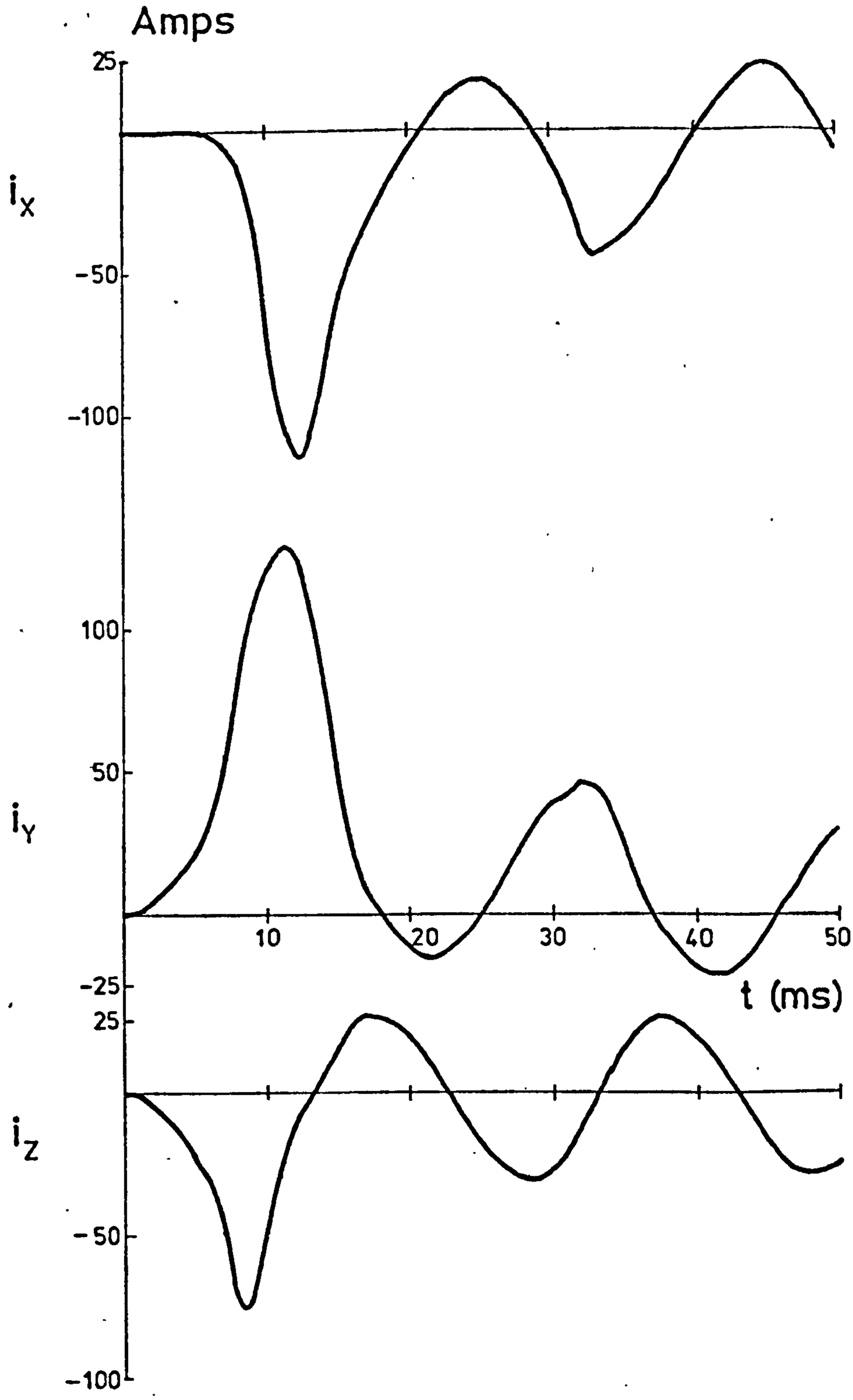

Fig. 4.6.11 Transient current patterns for zero power factor inductive load on transformer with delta connected primary. $\alpha=0°$, $\beta=90°$.

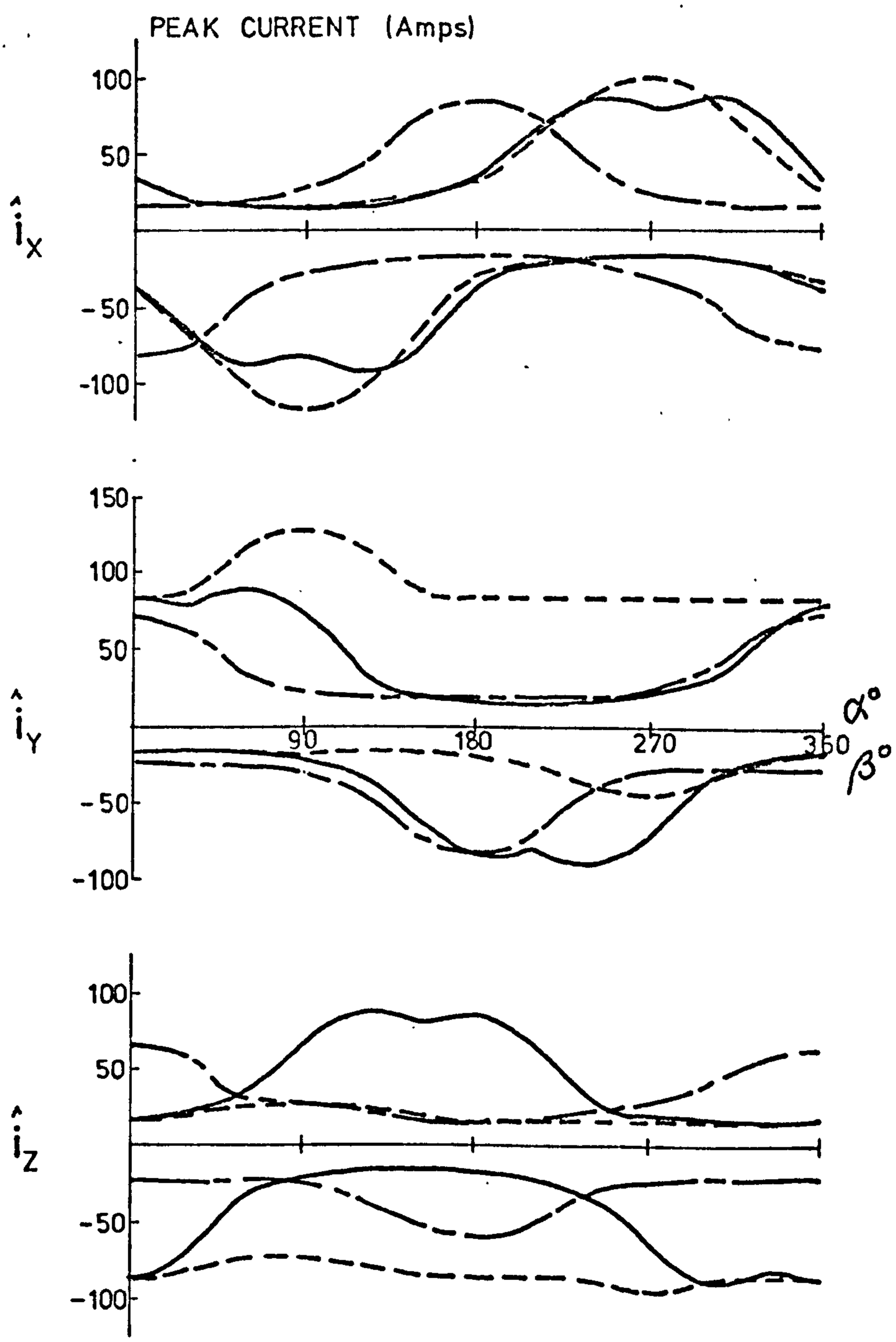

Fig. 4.6.12 Variation of peak transient current with α and β. Zero p.f. lagging load, delta connected primary - no residual flux.

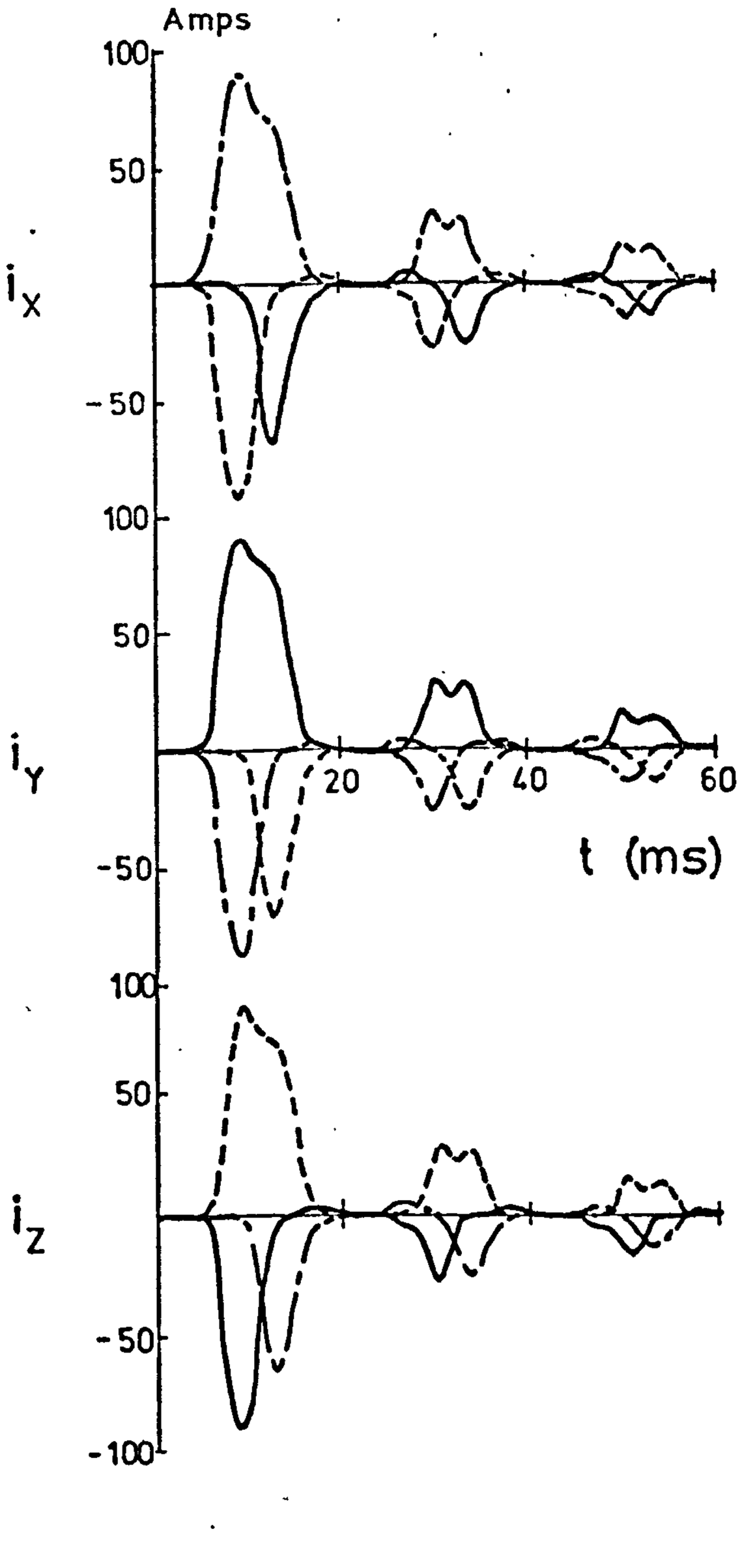

Fig. 4.6.13 Effect of varying the switching sequence for zero residual flux. Delta connected primary, no load.

$\alpha = 0°$ $\beta = 150°$

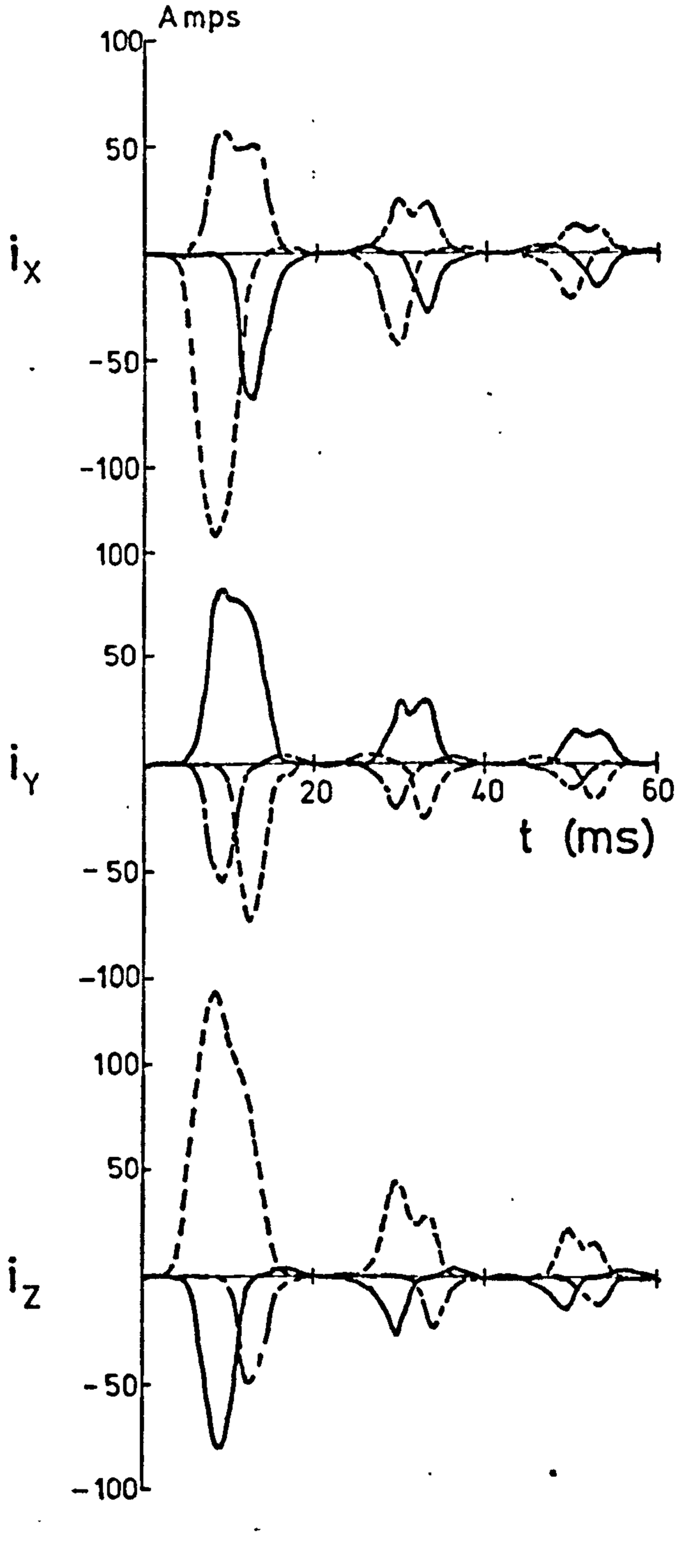

Fig. 4.6.14 Effect of varying the switching sequence for non-zero residual conditions. Delta connected primary, no load. $\alpha=0°$, $\beta=150°$

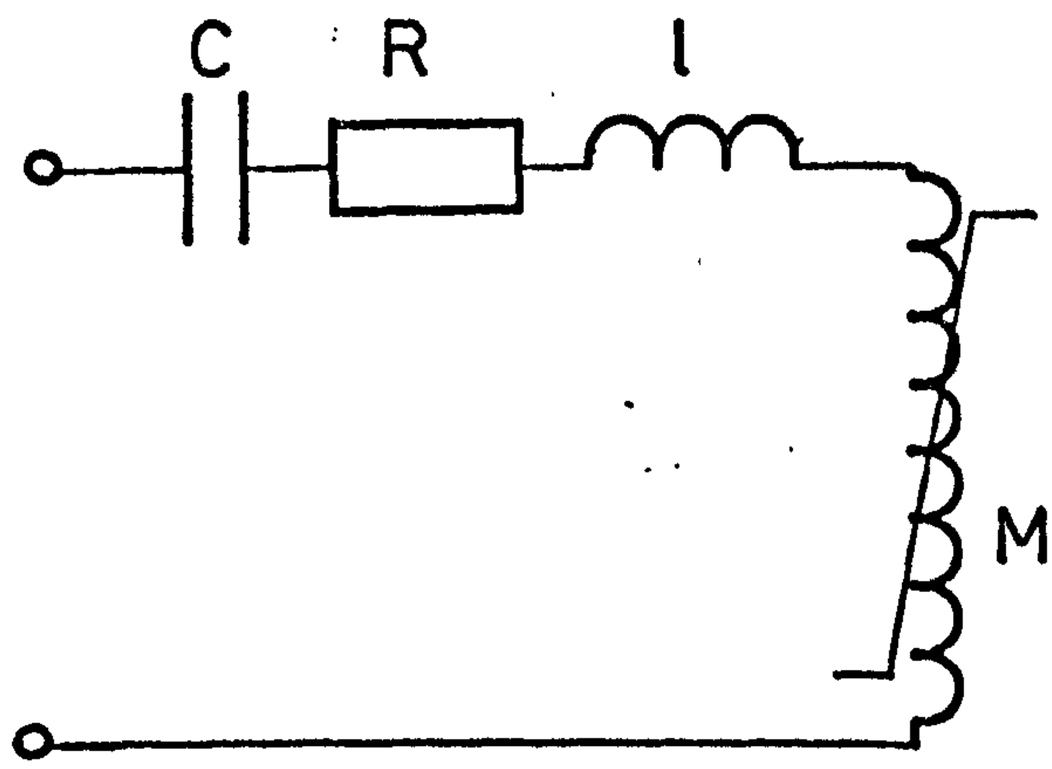

(a) Series-resonant circuit.

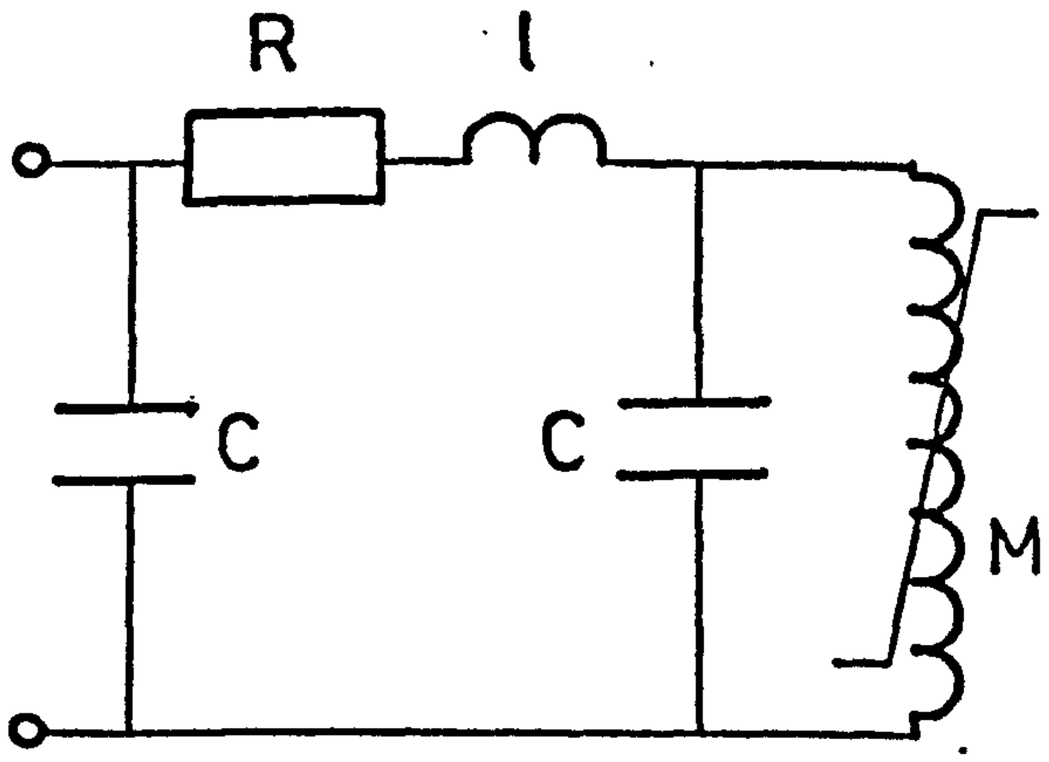

(b) Parallel-resonant circuit.

Fig. 5.1.1 Single-phase ferroresonant circuits.

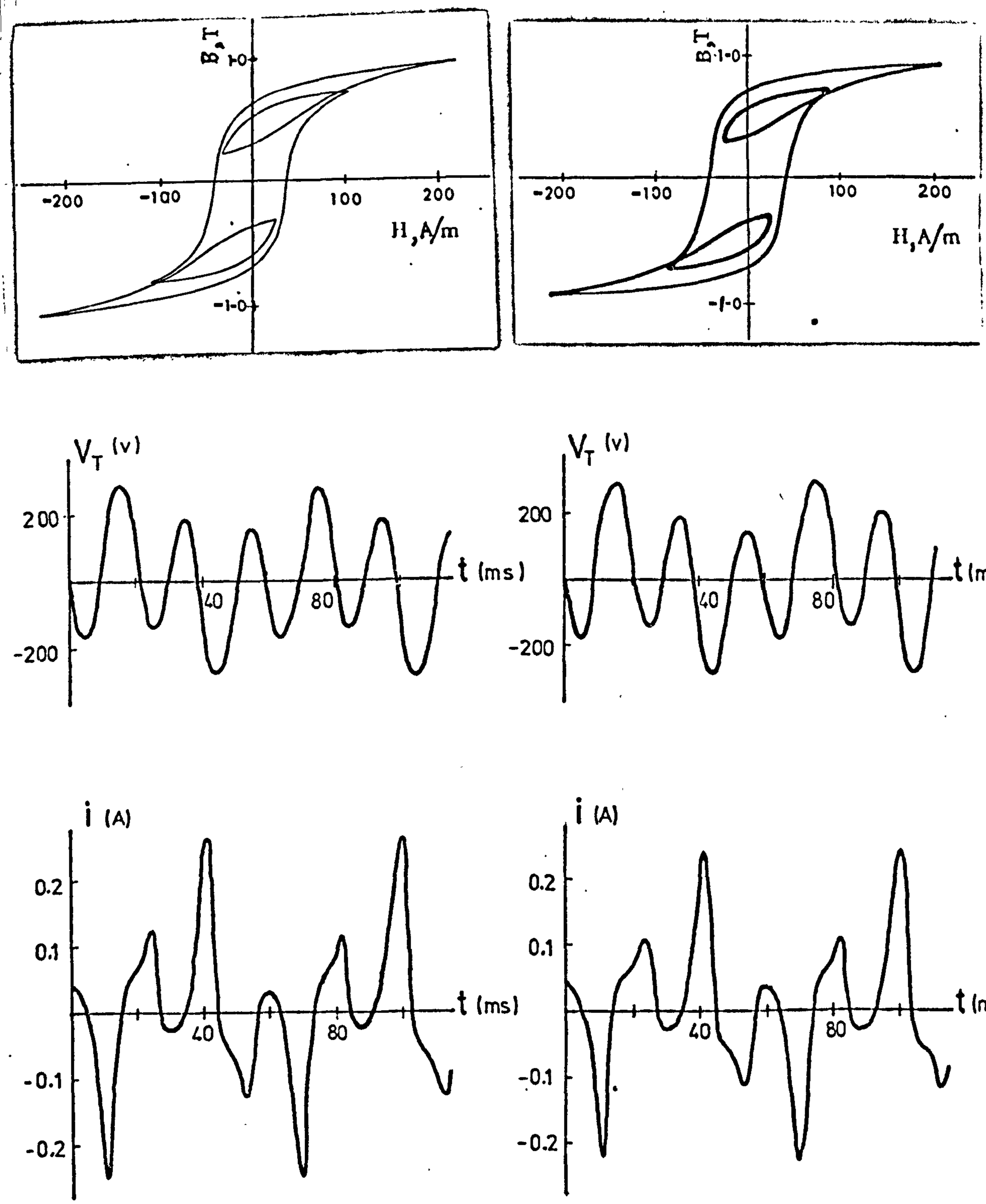

Fig. 5.1.2 Subharmonic ferroresonance (1-phase)

V=115v B_o=0 V_{C_o}=-50v C=6.8μF

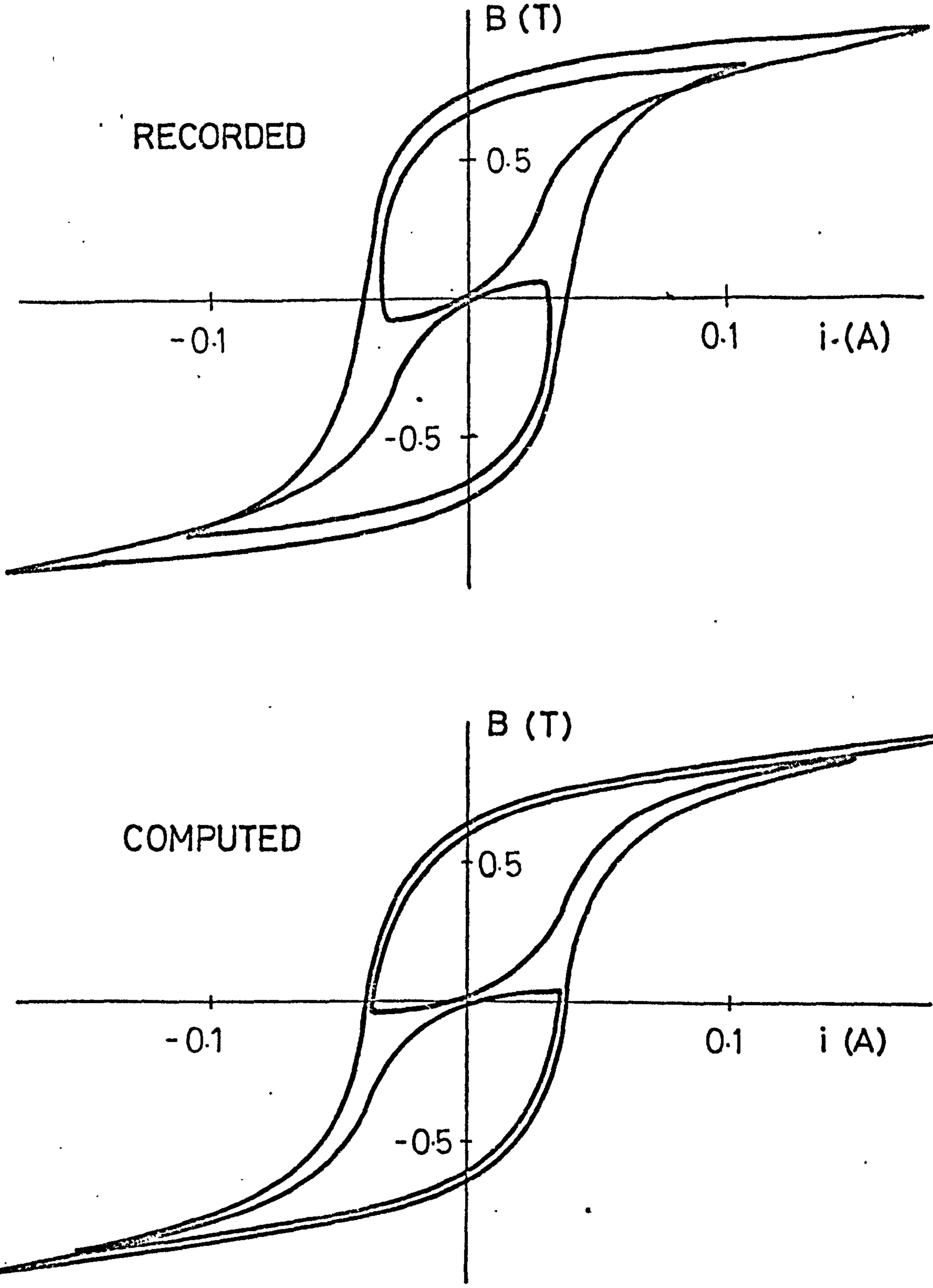

Fig. 5.1.3 Subharmonic ferroresonance (1-phase)

$V=140v \quad B_o=0 \quad V_{C_o}=-50v \quad C=6{\cdot}8\mu F$

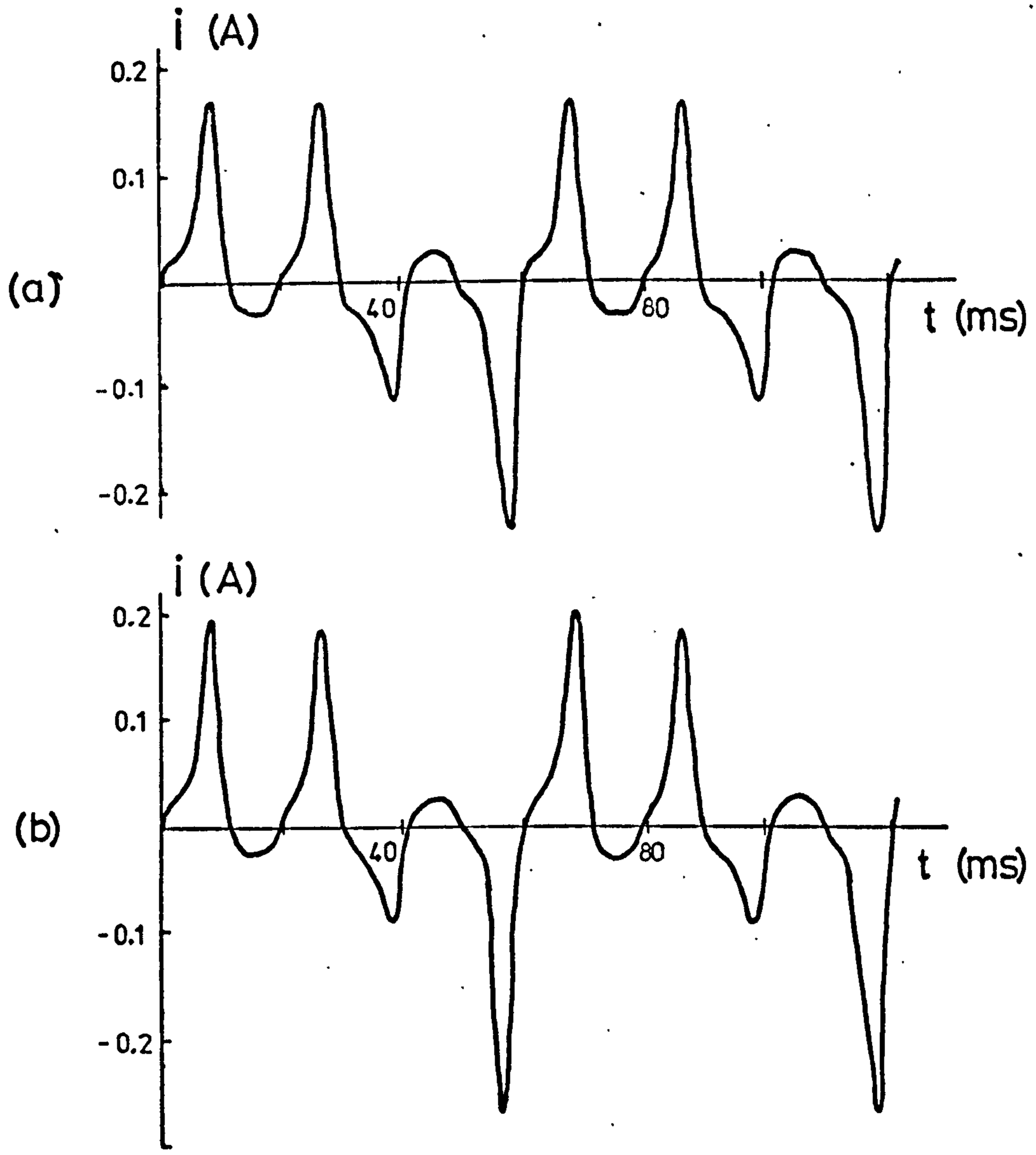

Fig. 5.1.4 Subharmonic ferroresonance (1-phase)
Current waveform for V=100v
(a) Recorded (b) Computed

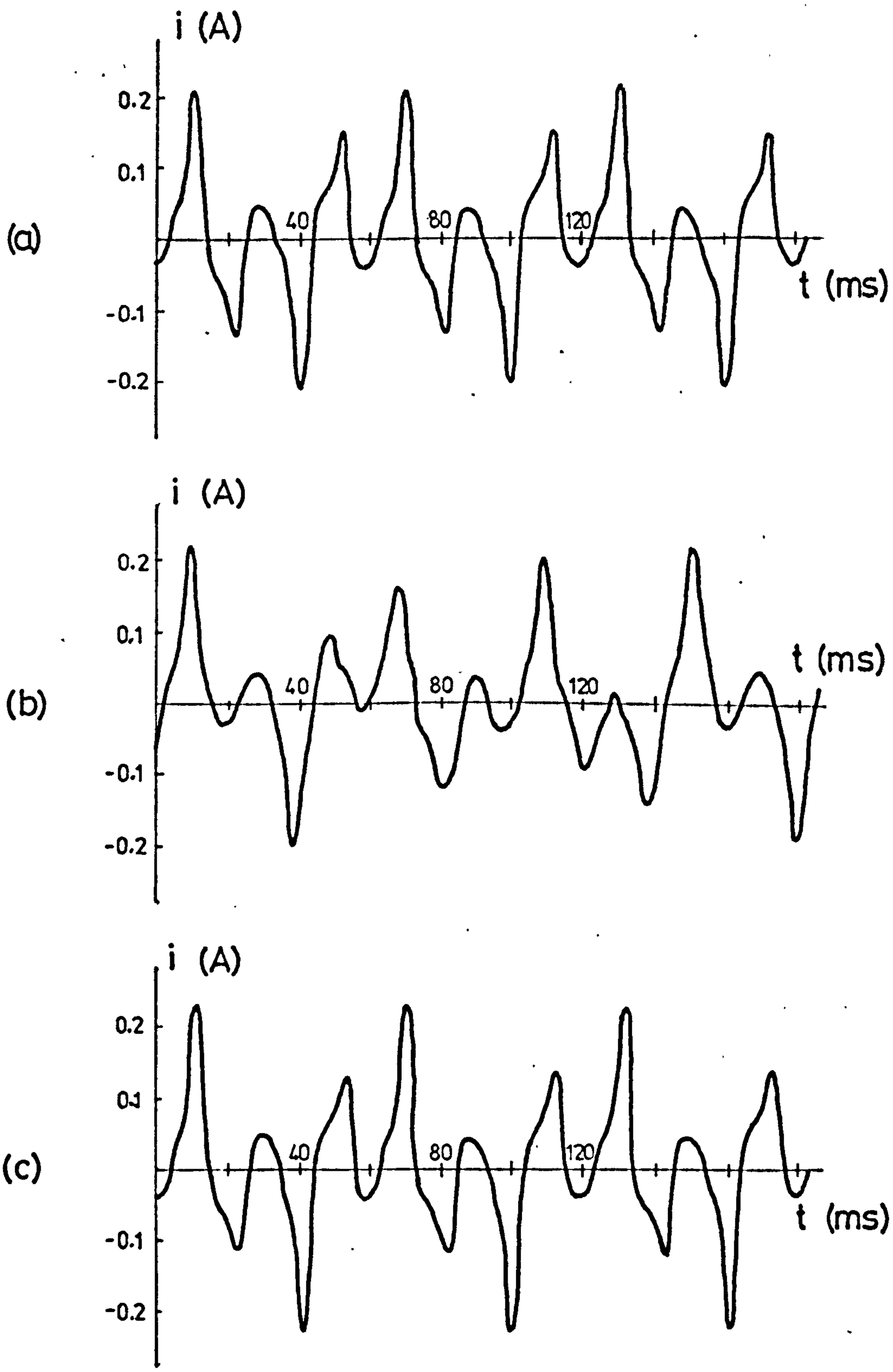

Fig. 5.1.5 Effect of hysteresis on subharmonic ferroresonance - current waveforms

(a) Recorded (b) Computed - no hysteresis

(c) Computed - with hysteresis

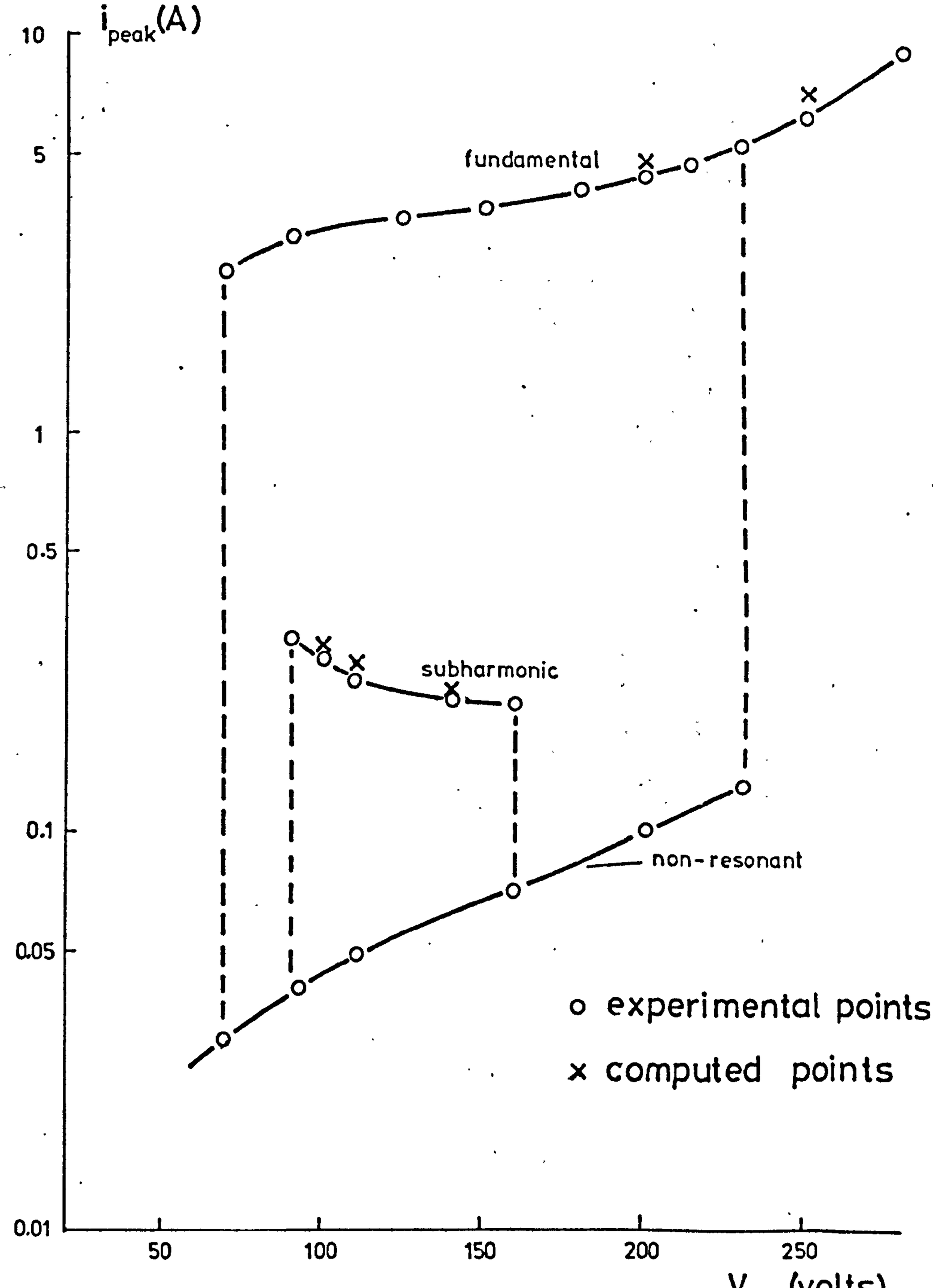

Fig. 5.1.6 Current – voltage characteristic of single-phase ferroresonant circuit (Fig. 5.1.1 a)

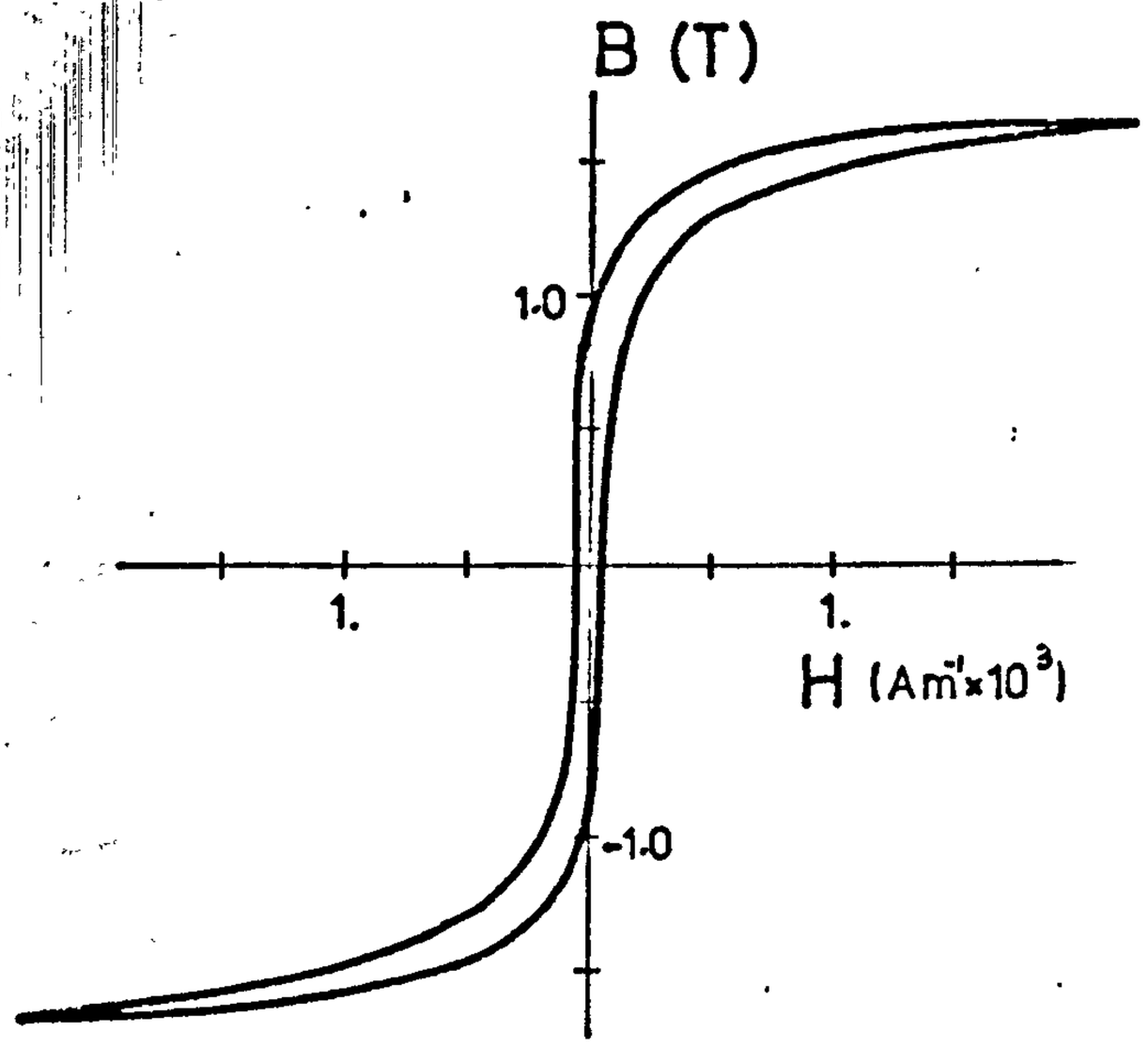

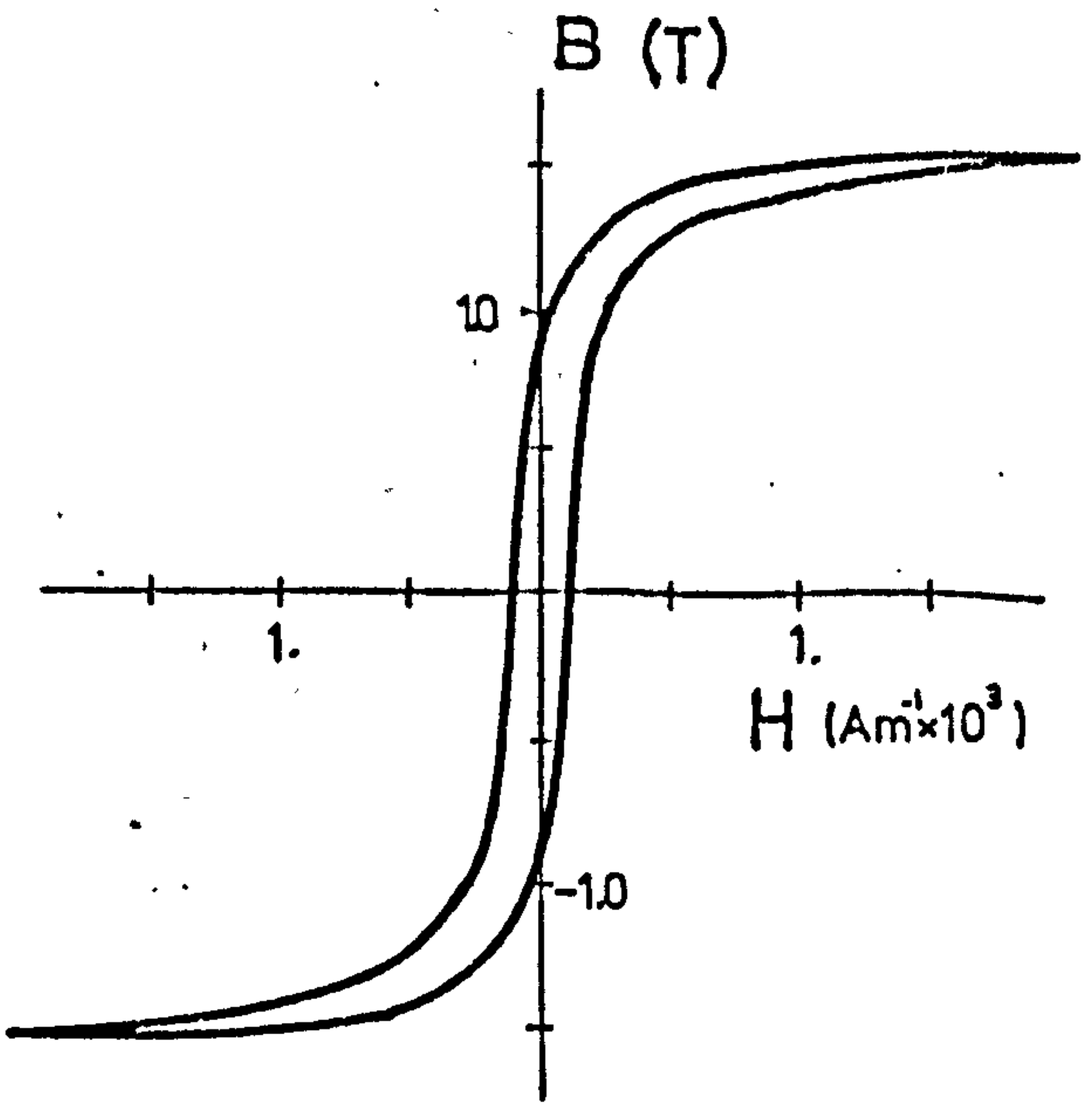

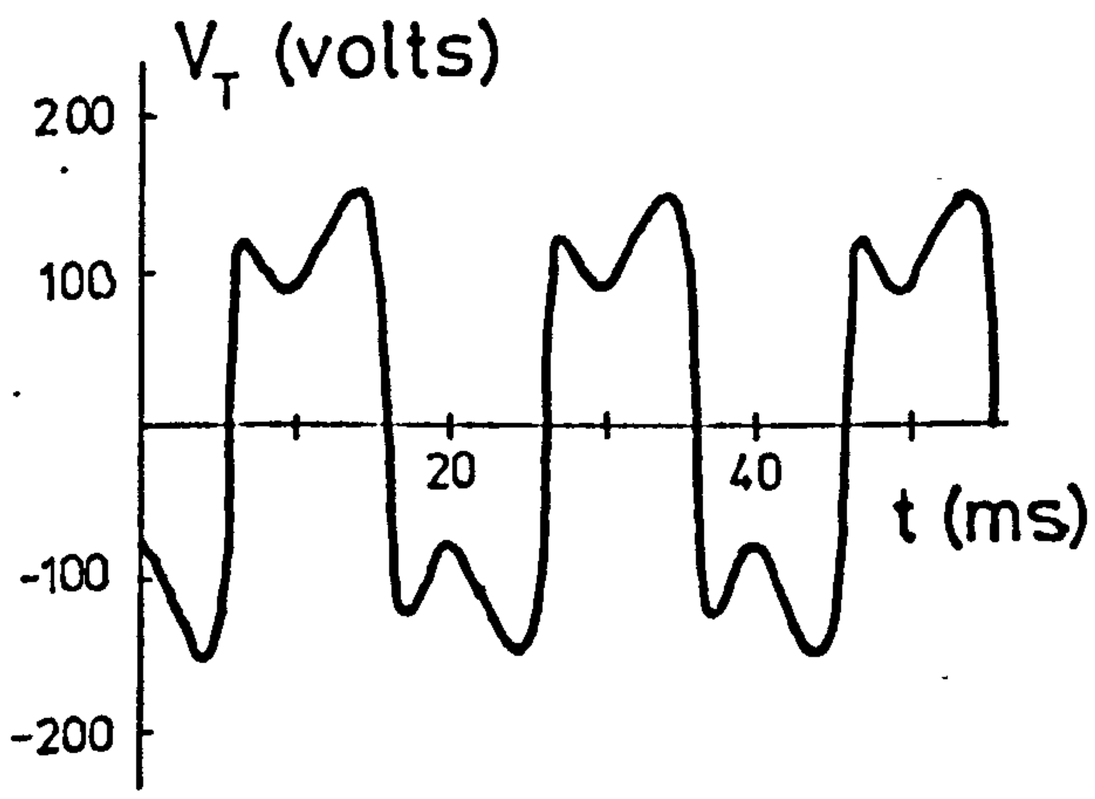

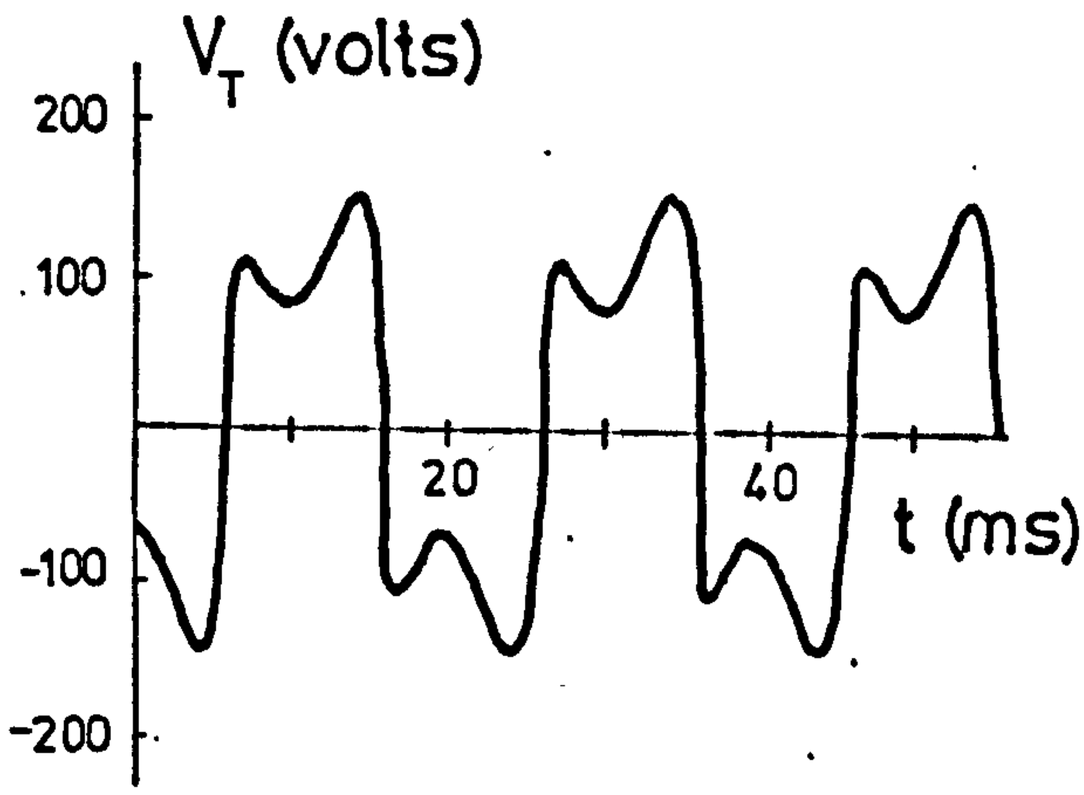

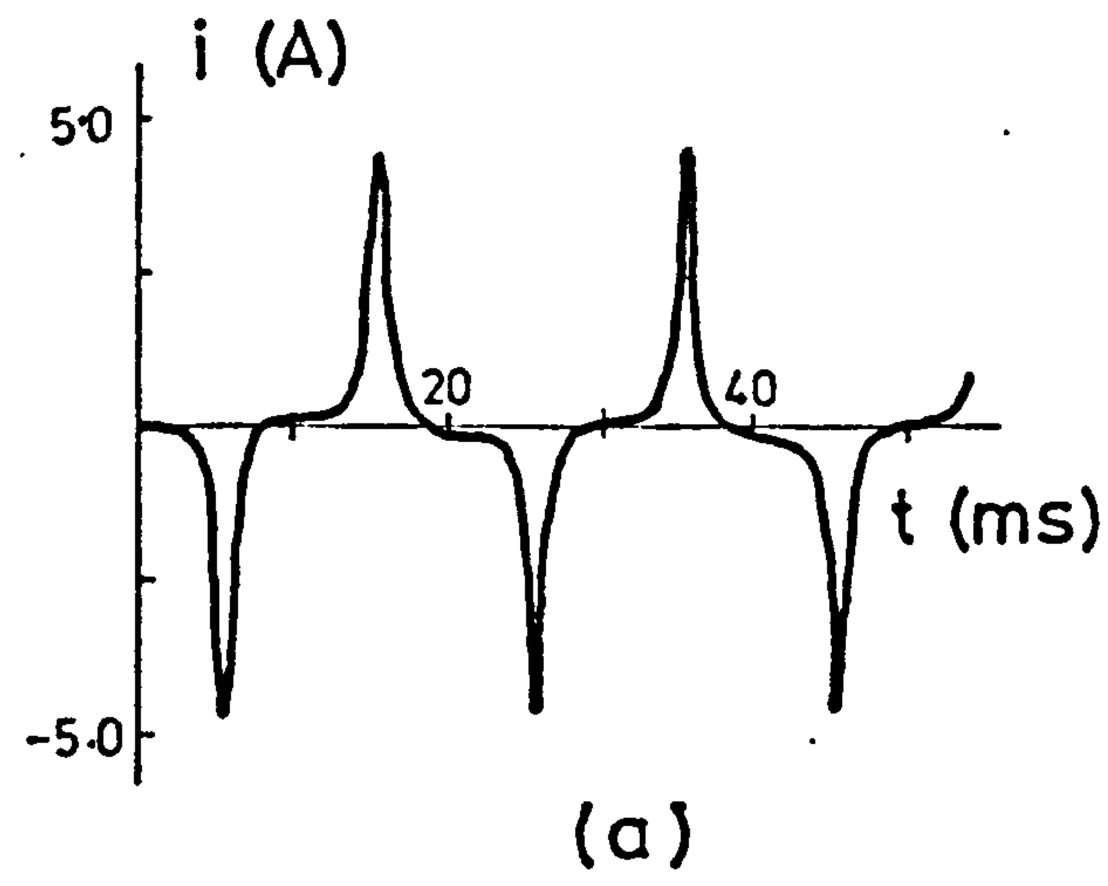

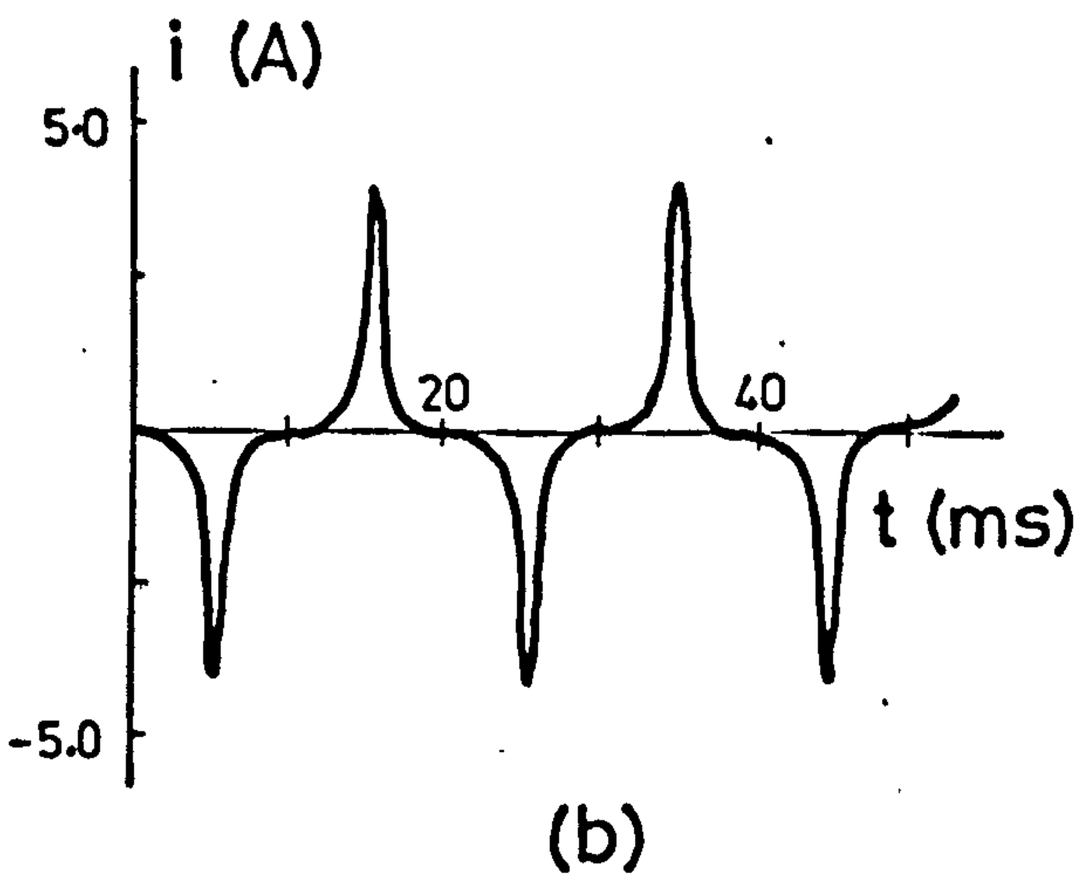

(a) (b)

Fig. 5.1.7 Single-phase; fundamental resonance.
(a) Computed and (b) Recorded results.

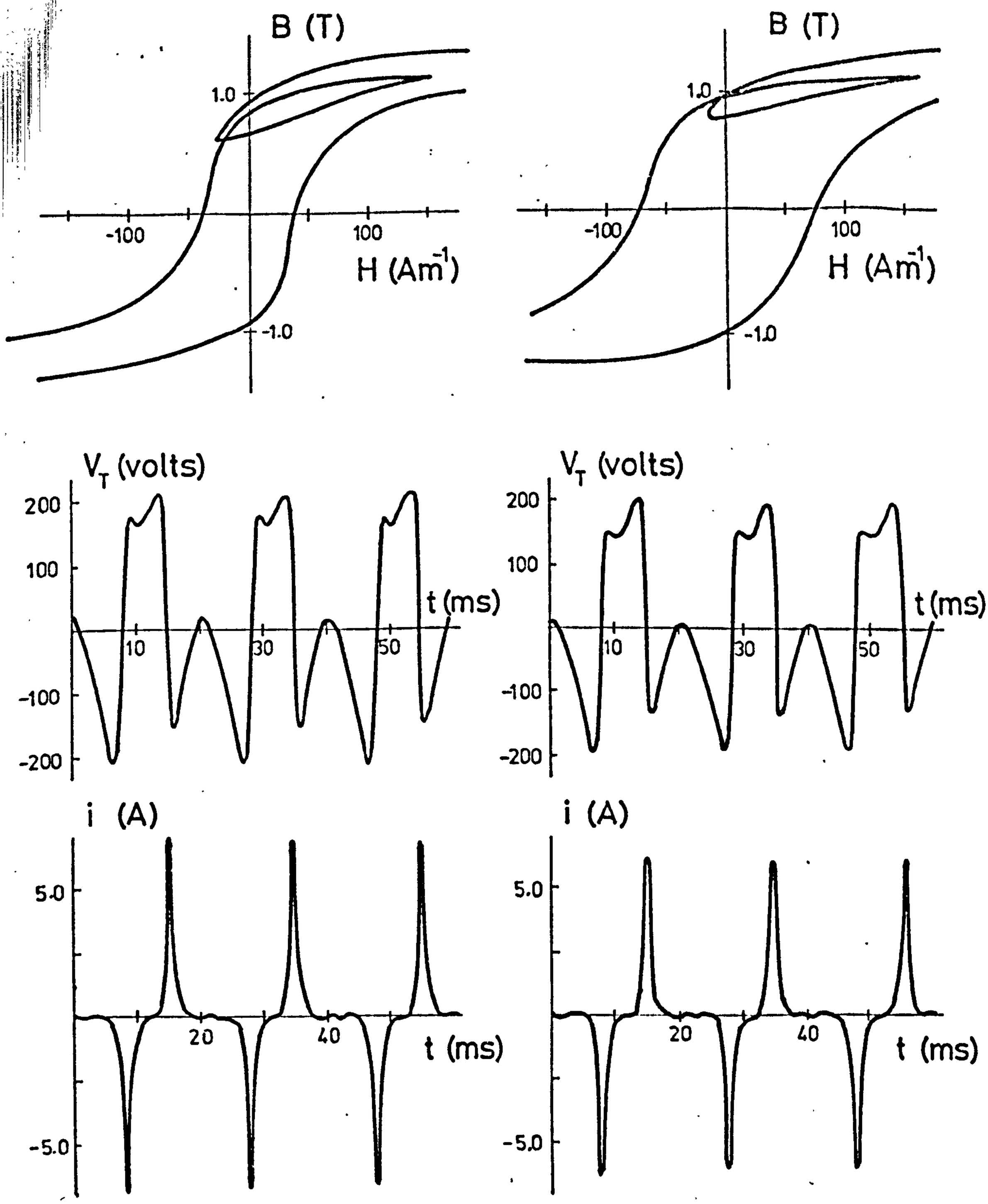

Fig. 5.1.8 Single-phase ferroresonance:-
Asymmetric mode. V=250v.

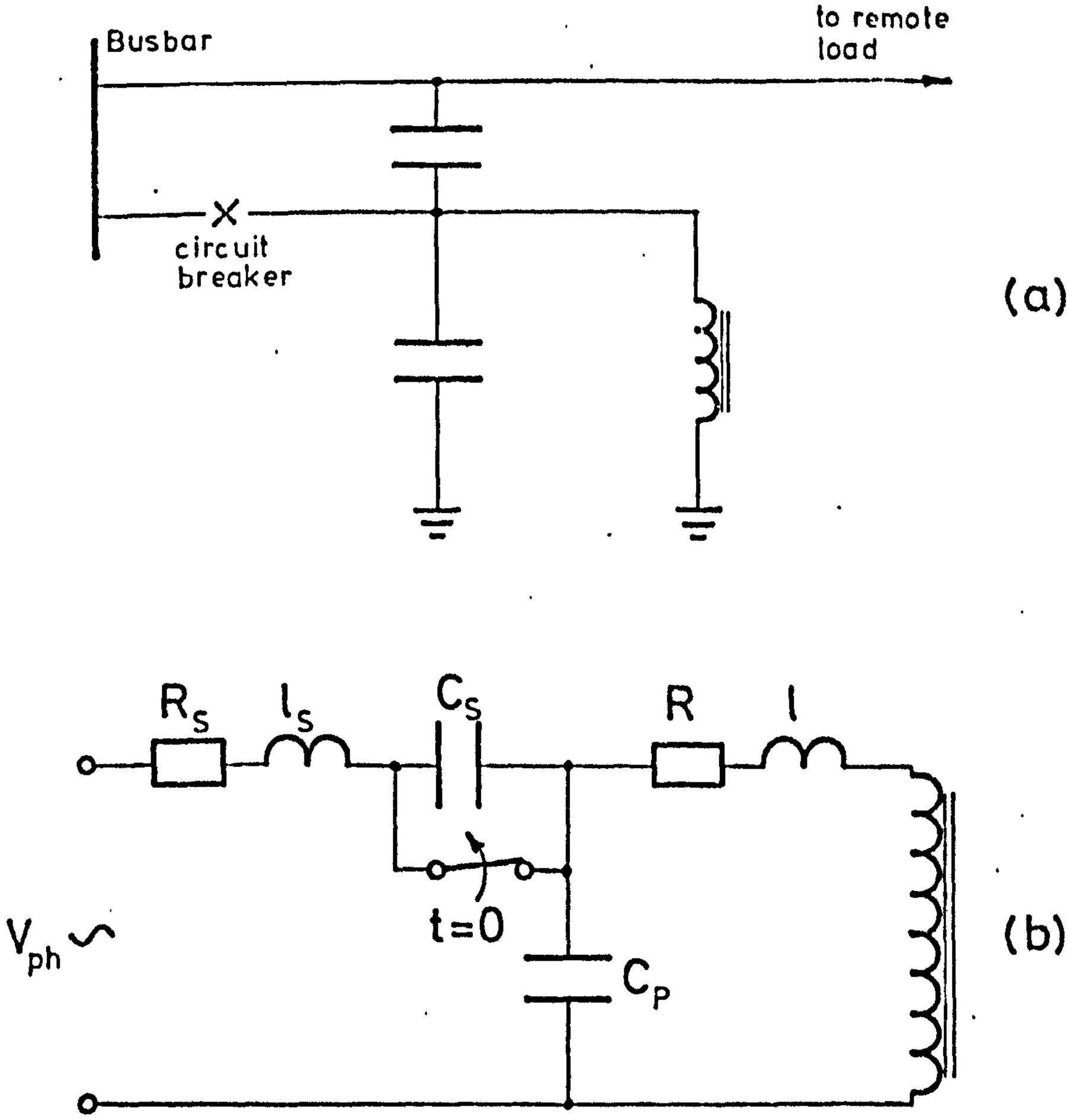

Fig. 5.2.1 Three-phase ferroresonance —
(a) Actual system
(b) Laboratory model

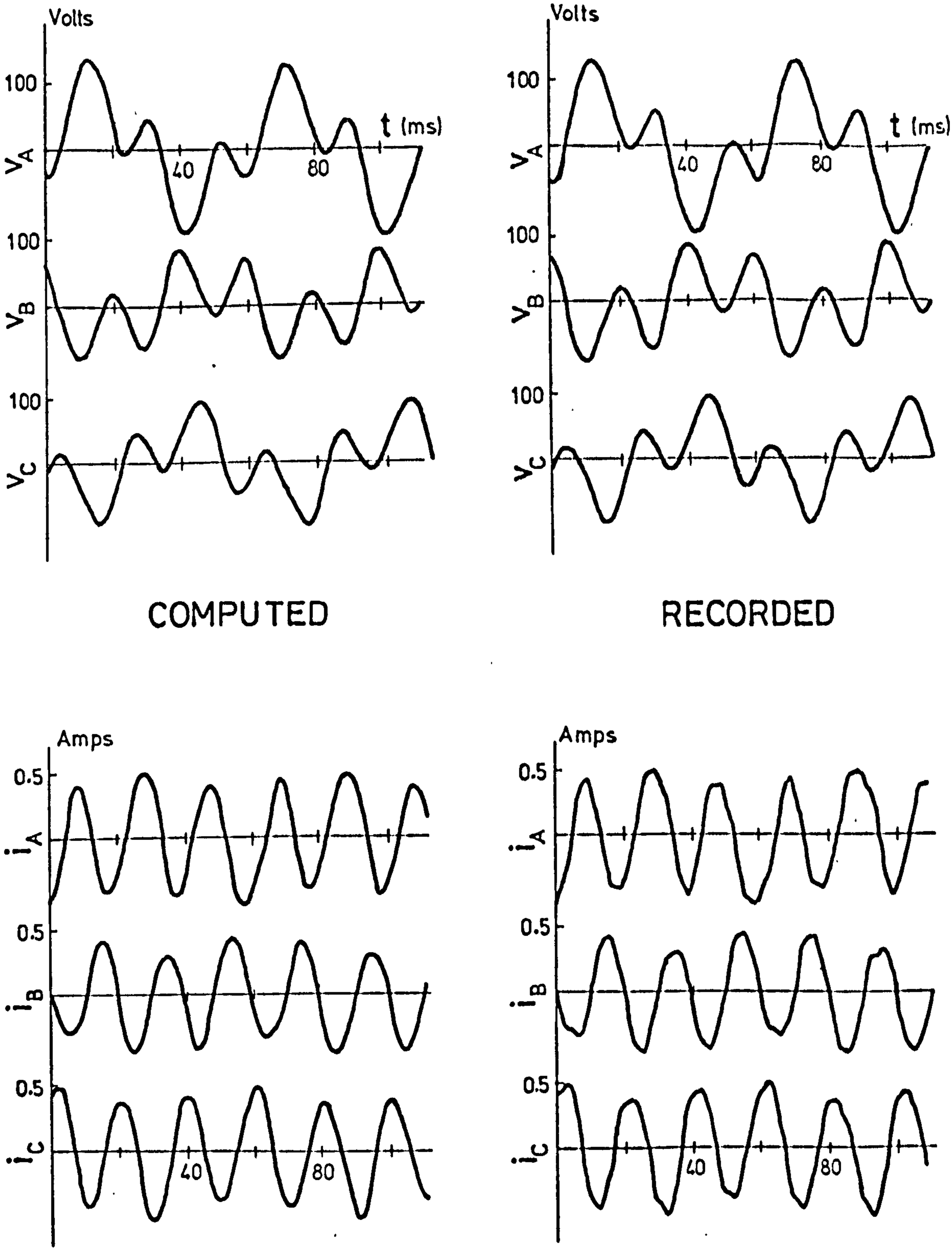

Fig. 5.2.2 Steady-state voltage and current waveforms for three-phase subharmonic ferroresonance:- $C_s = 12{\cdot}75\,\mu F$ $C_p = 25{\cdot}5\,\mu F$

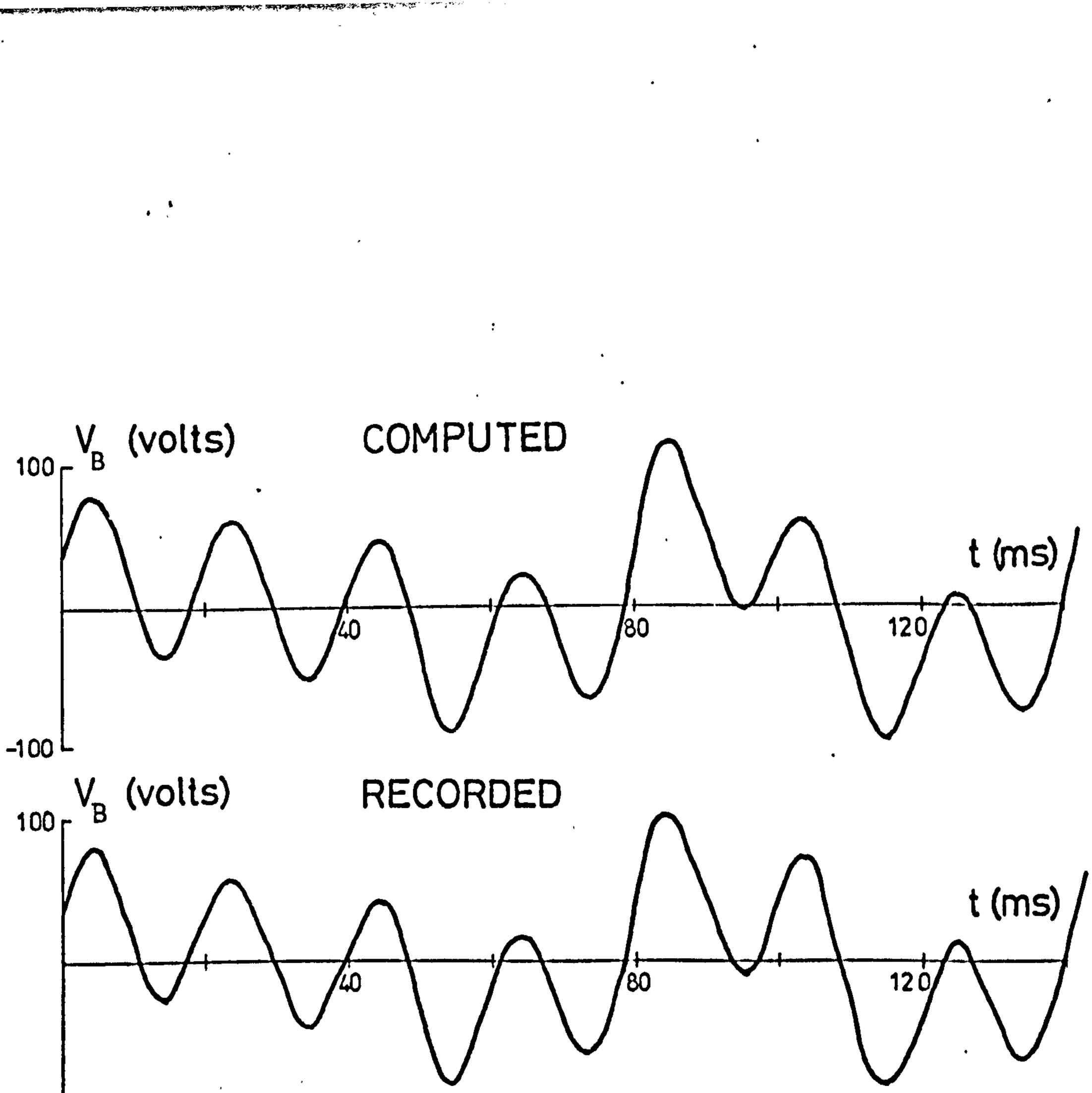

Fig. 5.2.3 Three-phase subharmonic resonance — transient voltage across phase B of transformer. Switches opened at t=0.

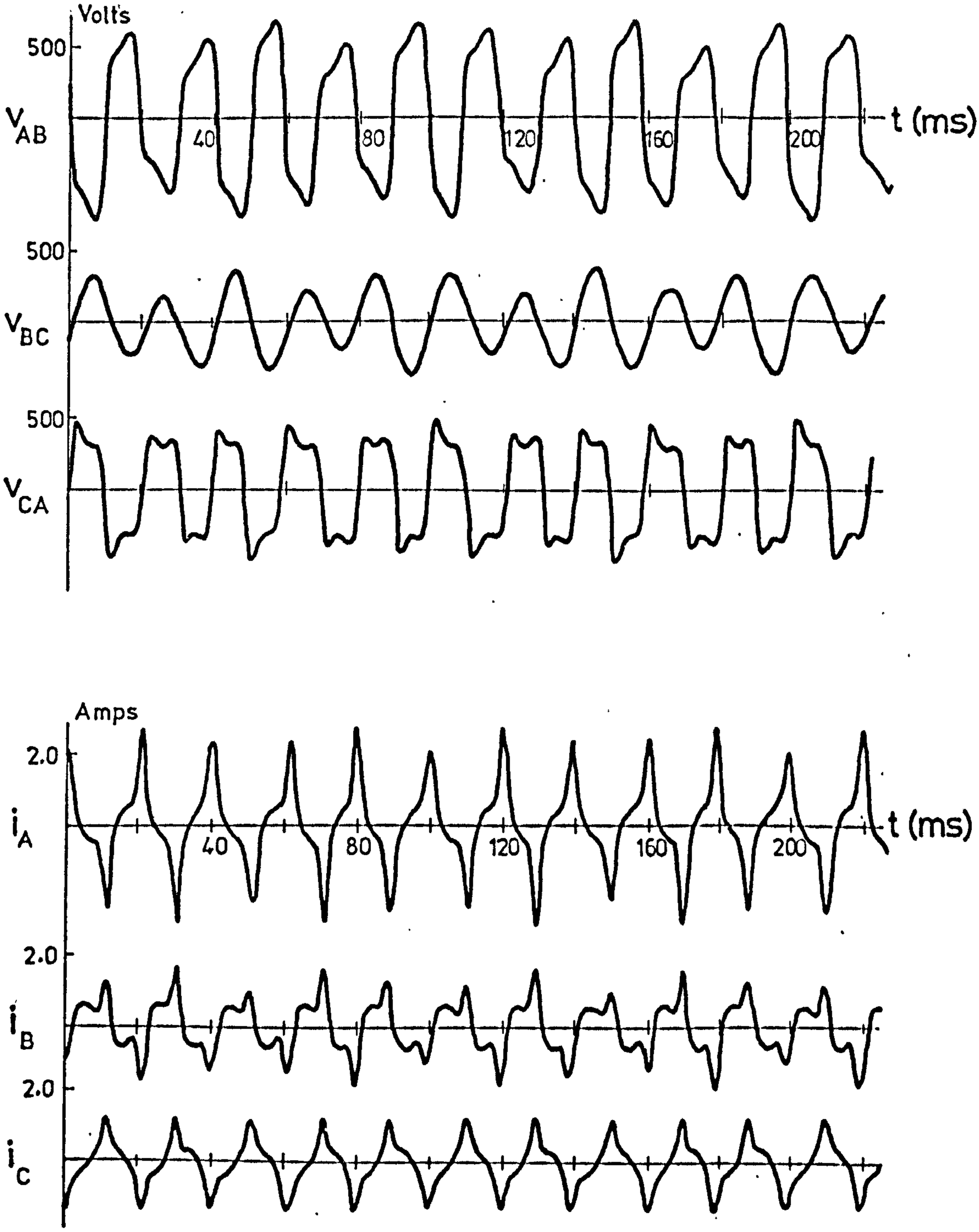

Fig. 5.2.4 Recorded steady-state waveforms for 1/5 subharmonic resonance.

$C_p = 12.75\,\mu F$ $C_s = 6.37\,\mu F$

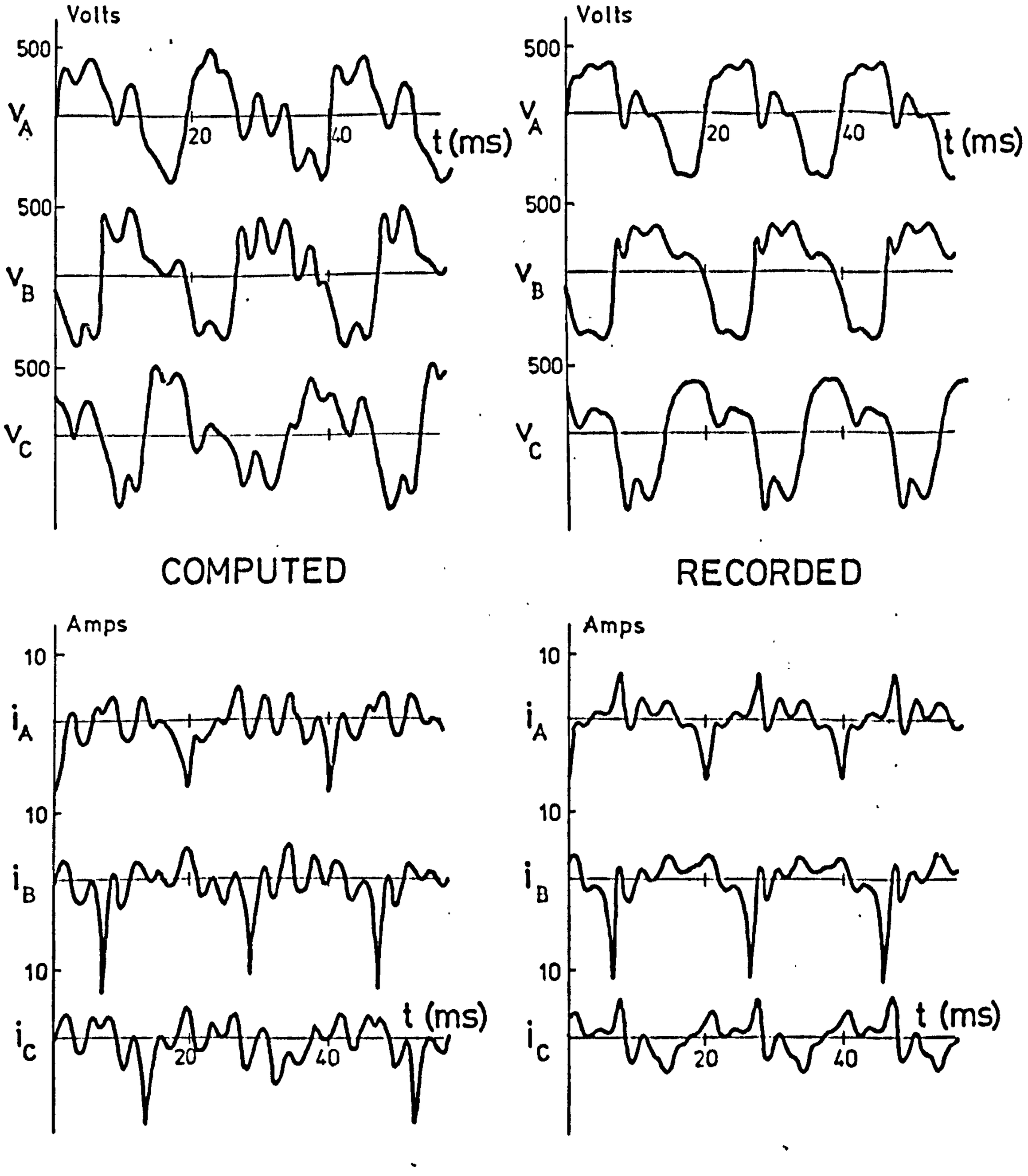

Fig. 5.2.5 Steady-state current and voltage waveforms — three-phase fundamental resonance.

$C_p = 25.5\,\mu F$ $C_s = 12.75\,\mu F$

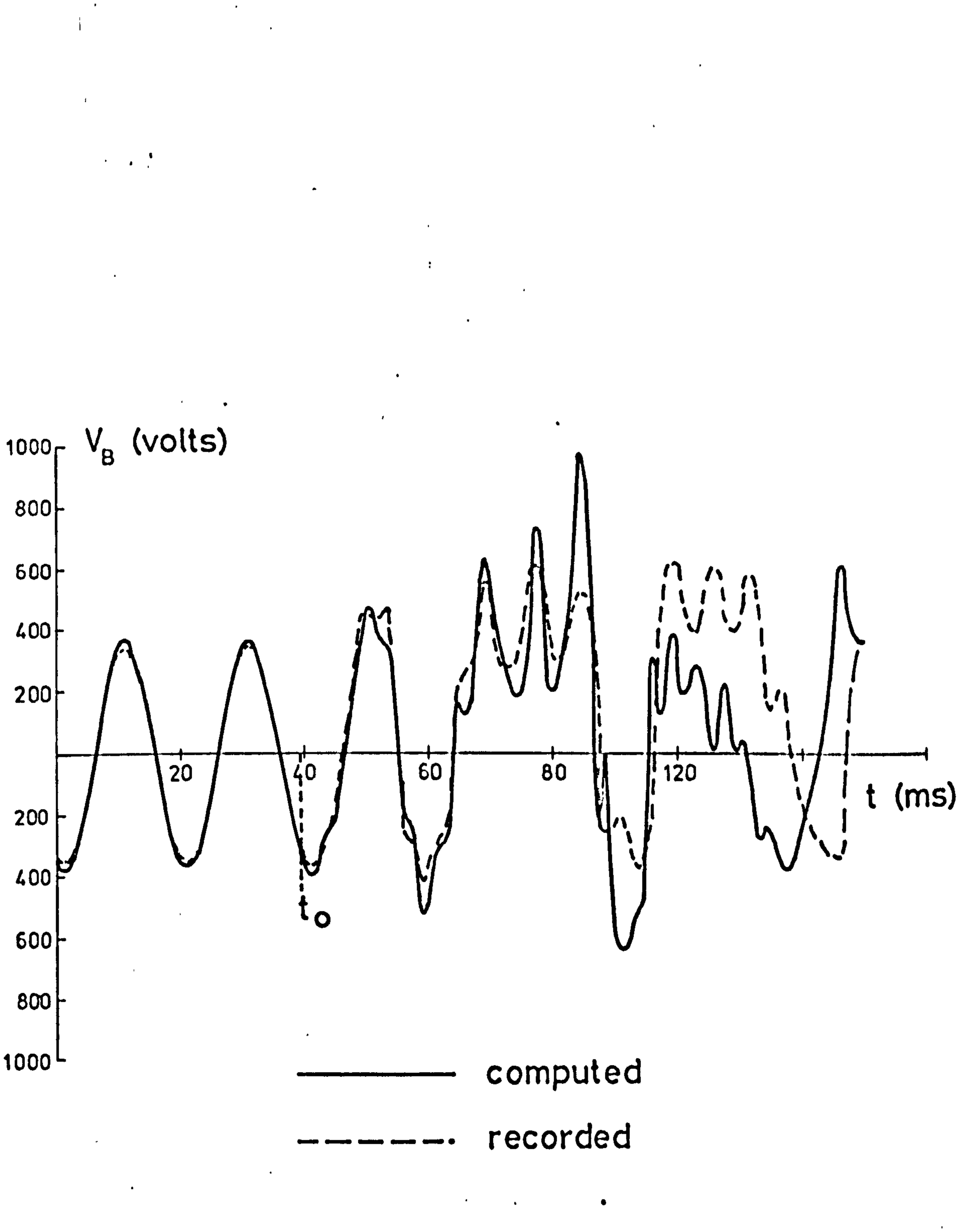

Fig. 5.2.6 Voltage across transformer phase B during opening of series capacitor switches.

(a)

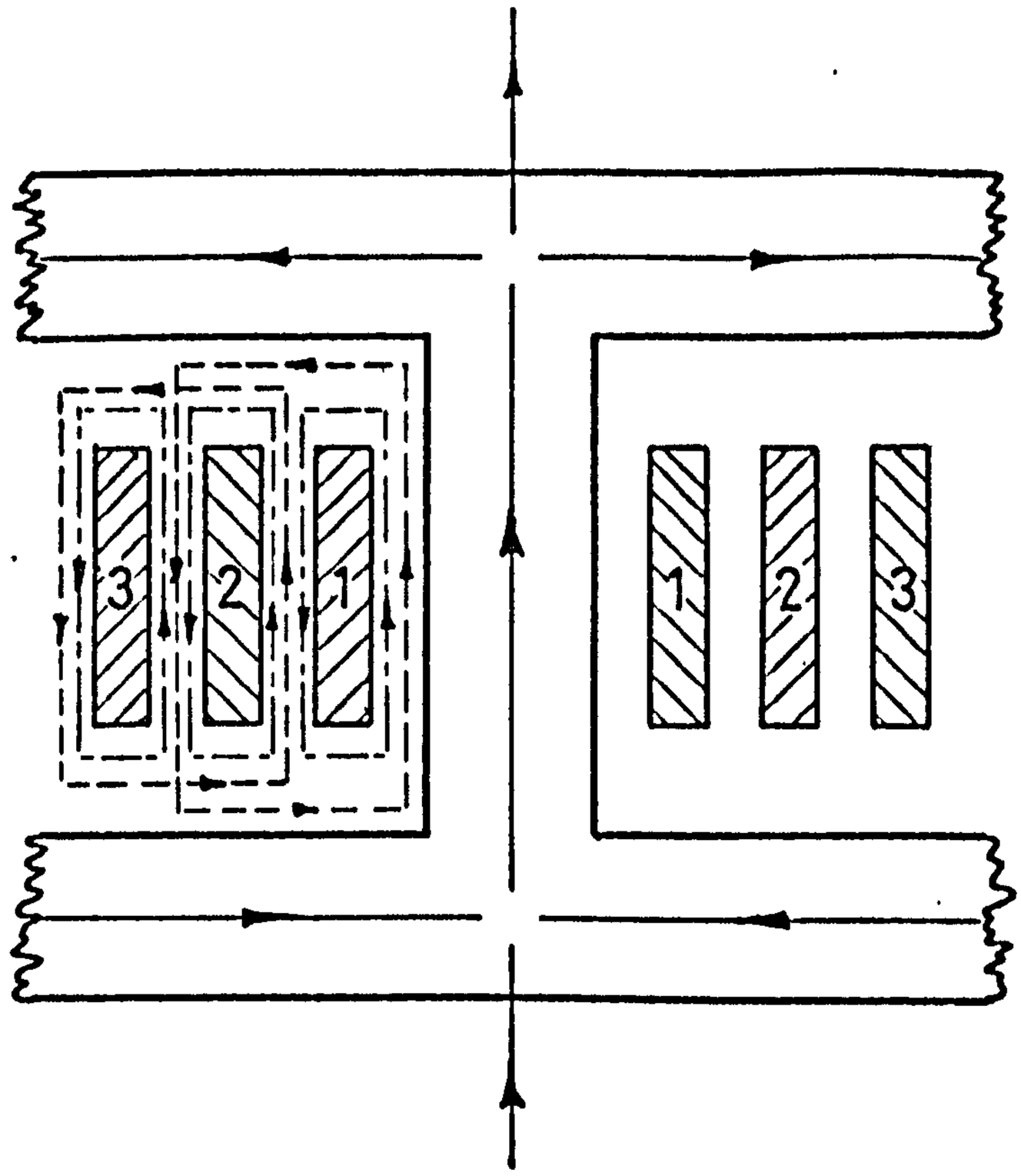

—— - —— coil self-leakage flux

– – – – – mutual leakage flux

——————— main and phase-leakage flux

(b)

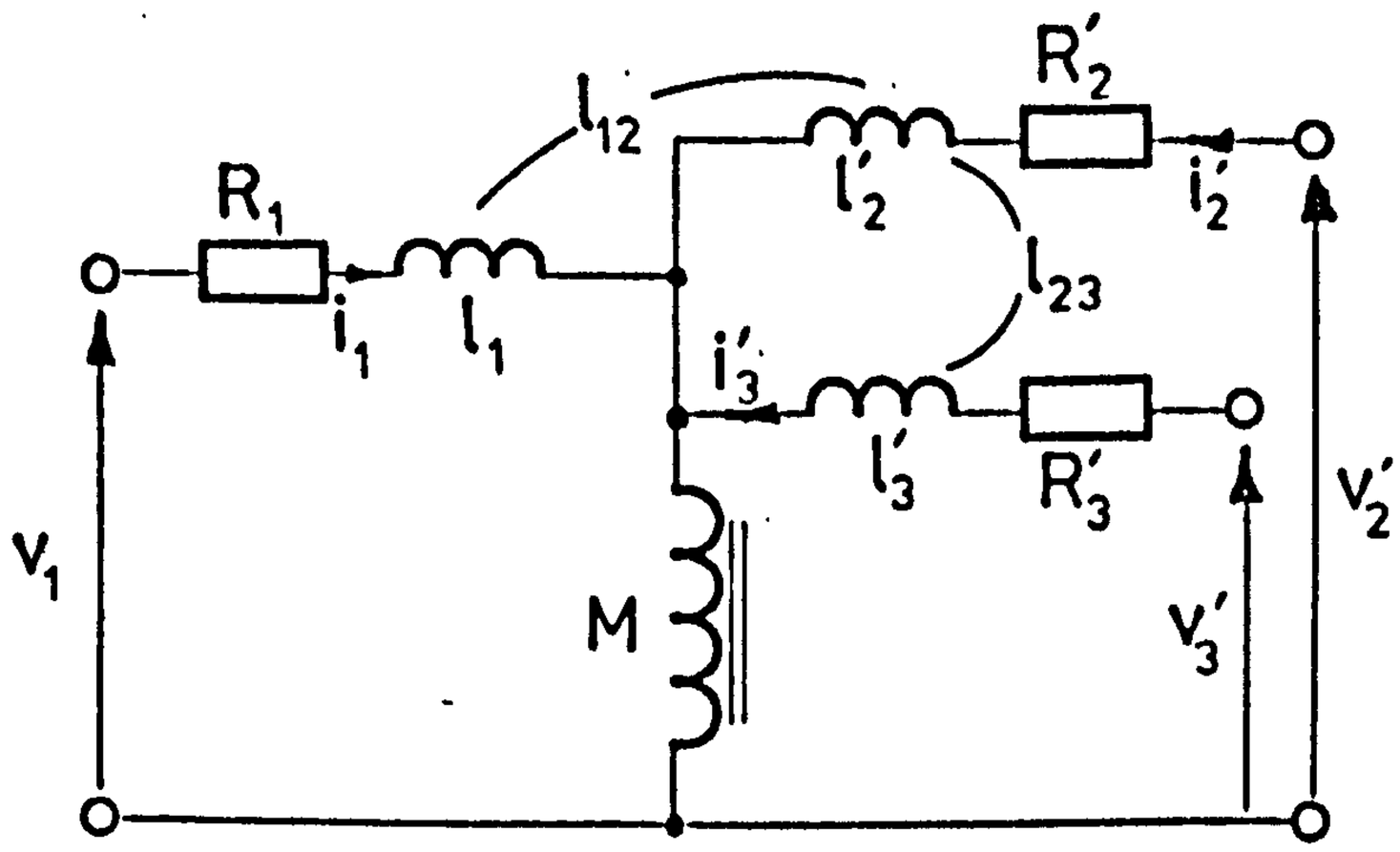

Fig. 6.1 Multi-winding transformer.

(a) simplified flux paths for three coils per phase.

(b) single-phase equivalent circuit.

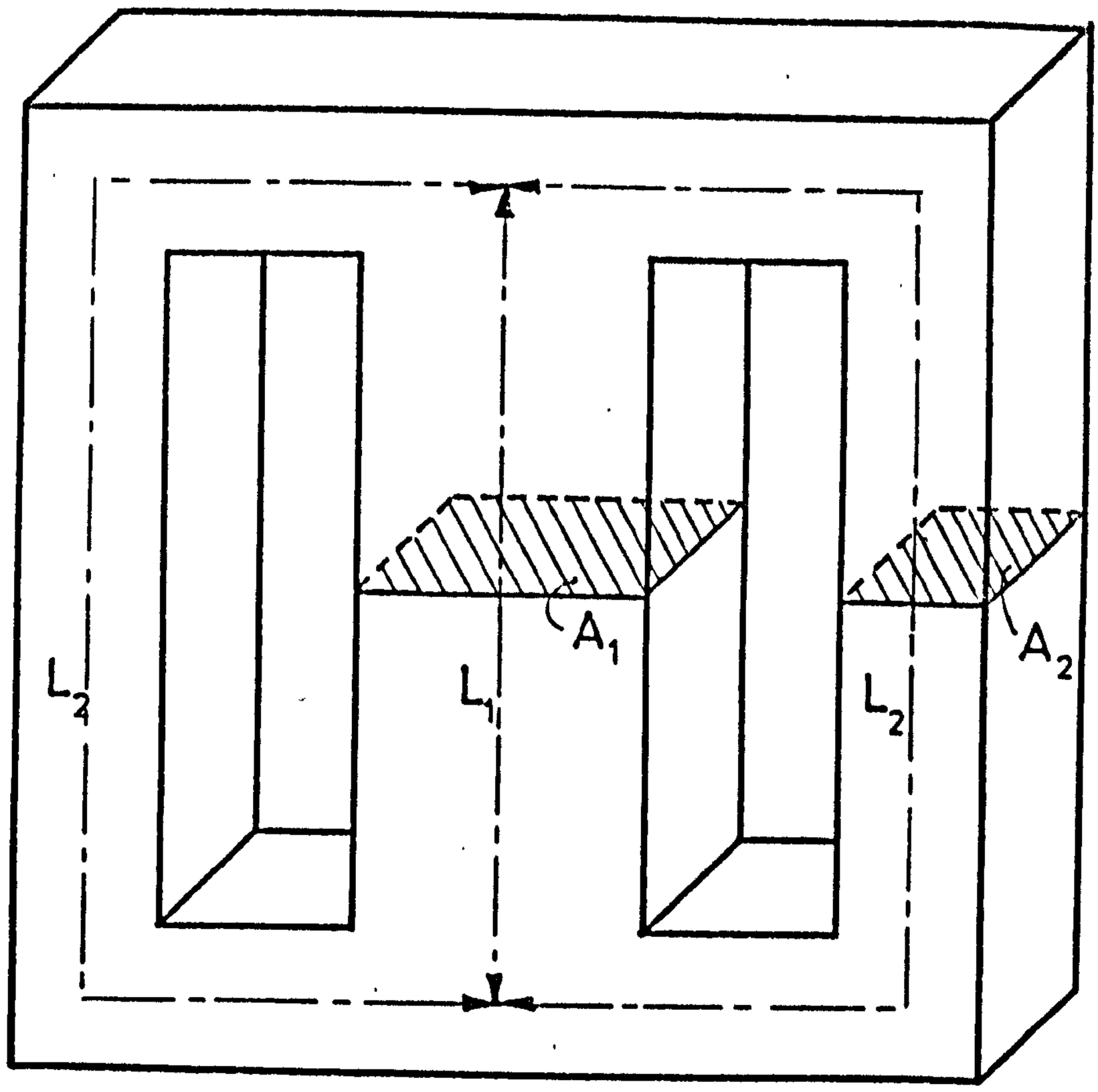

Fig. A1.1 Single-phase transformer construction.

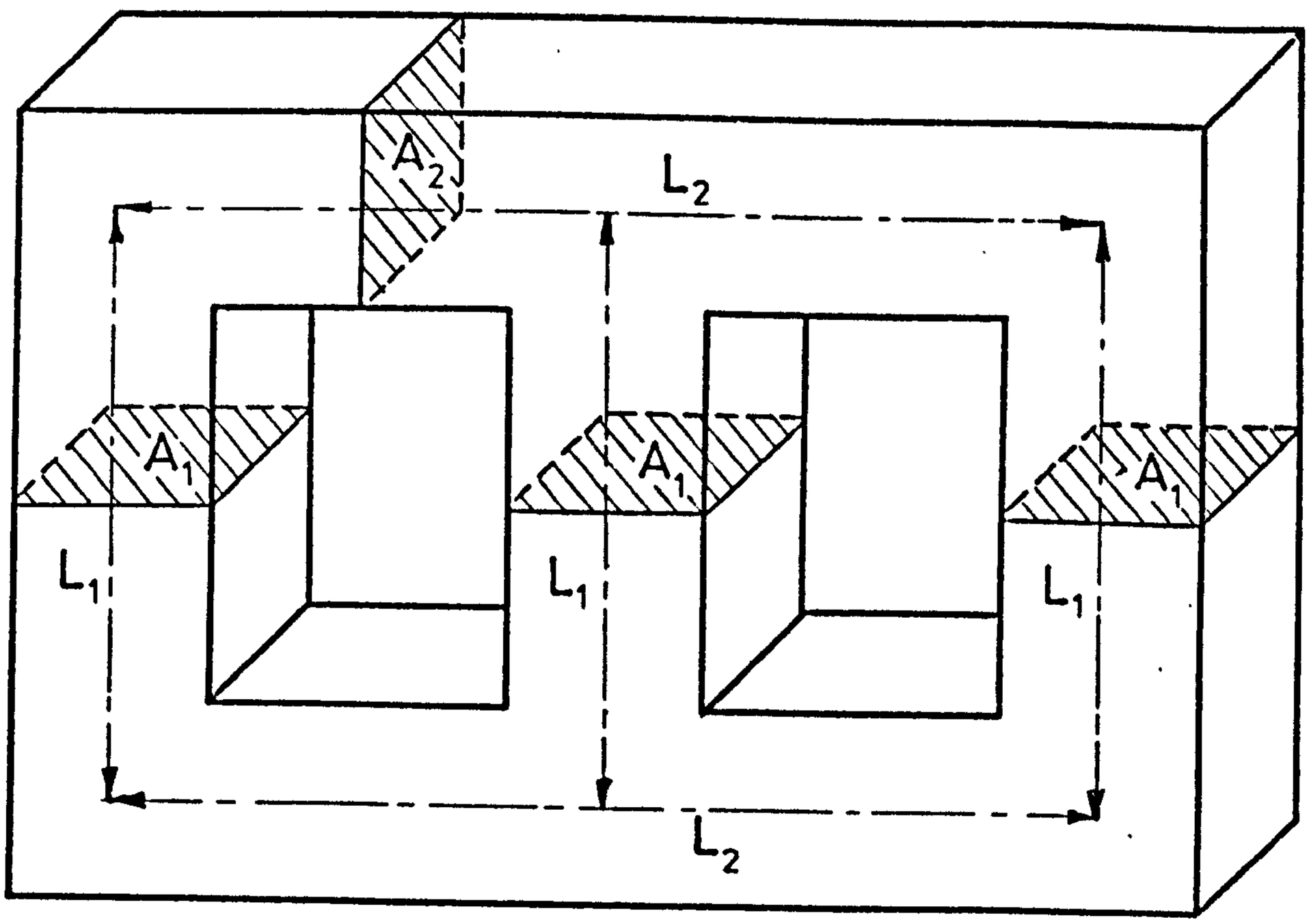

Fig. A1.2 Three-phase transformer construction.

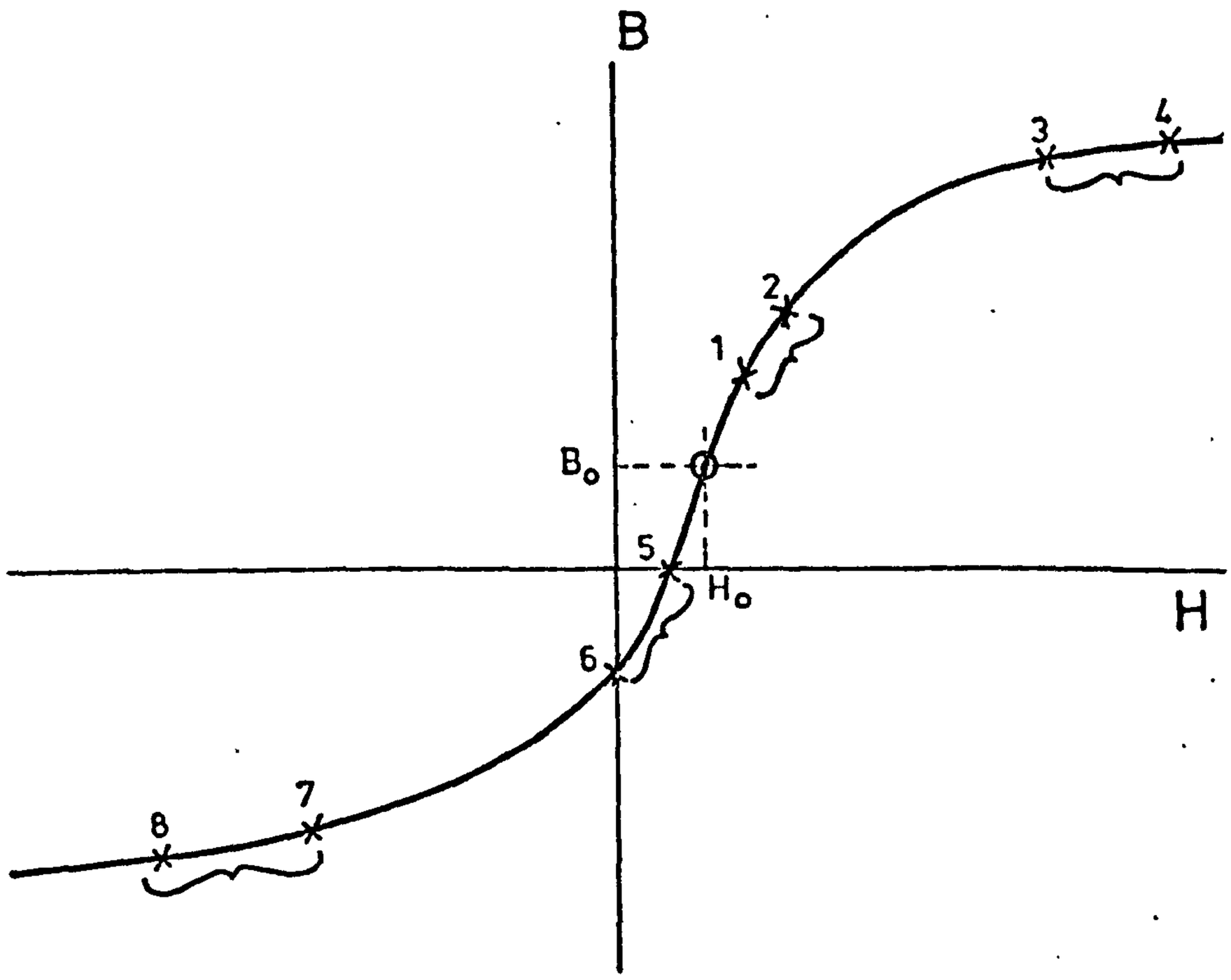

Fig. A2.1 Selection of points on B/H curve for use in evaluating the exponential series coefficients.

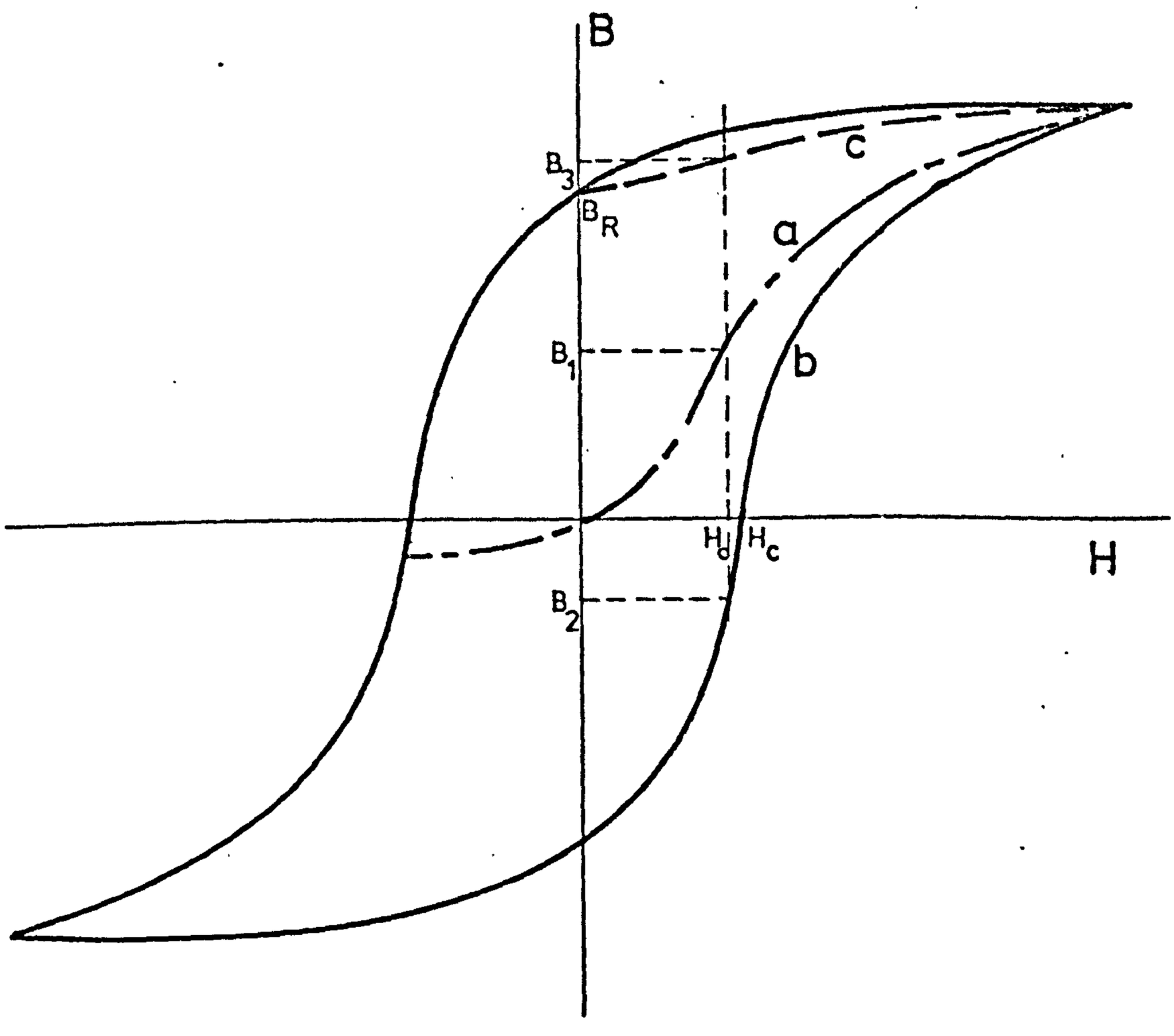

Fig. A3.1 Construction of B/H representation from a single curve.

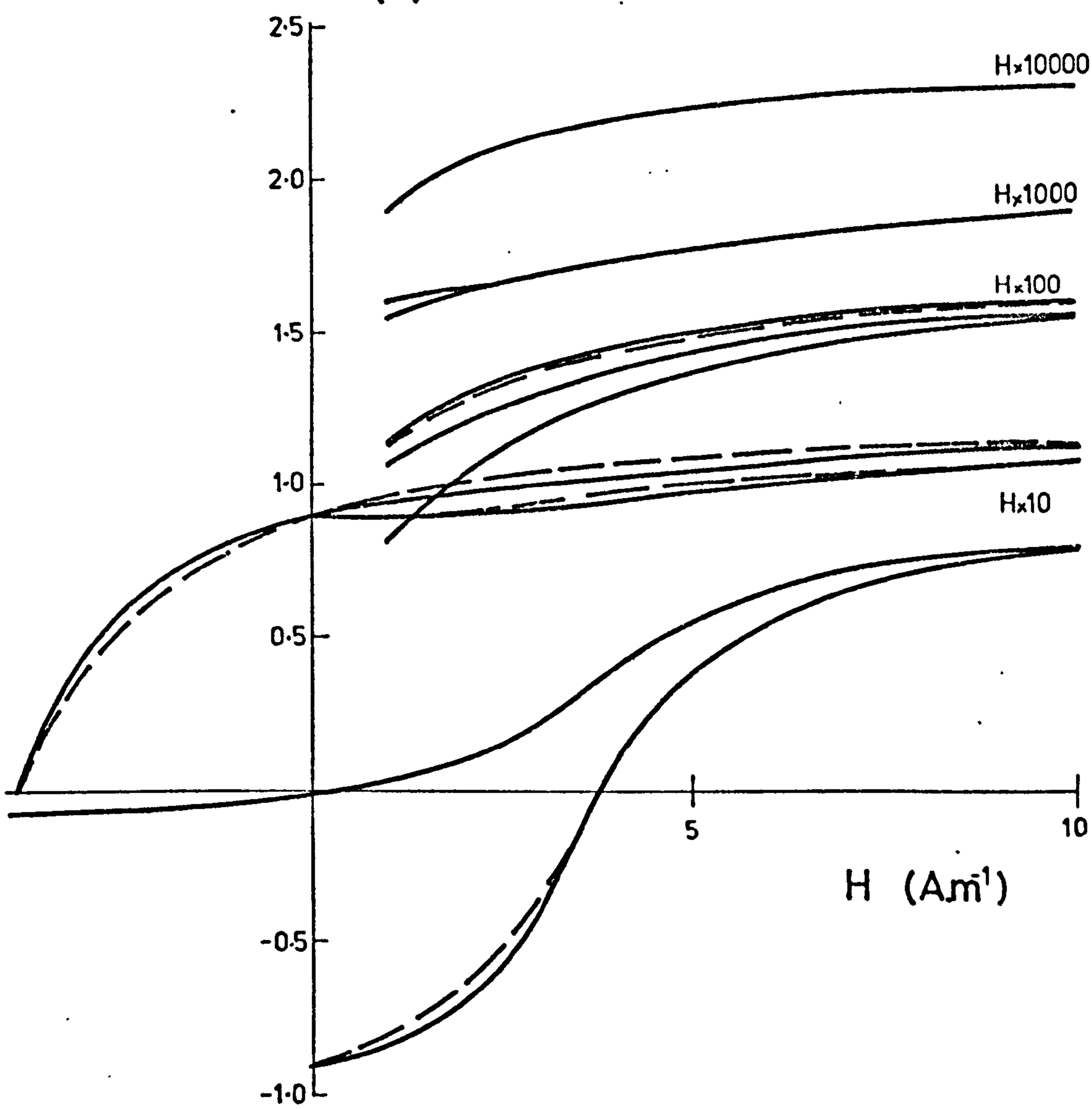

——— complete method

– – – – – representation based on a single curve

Fig. A3.2 Comparison of methods of representing the B/H characteristic. (1-phase transformer).

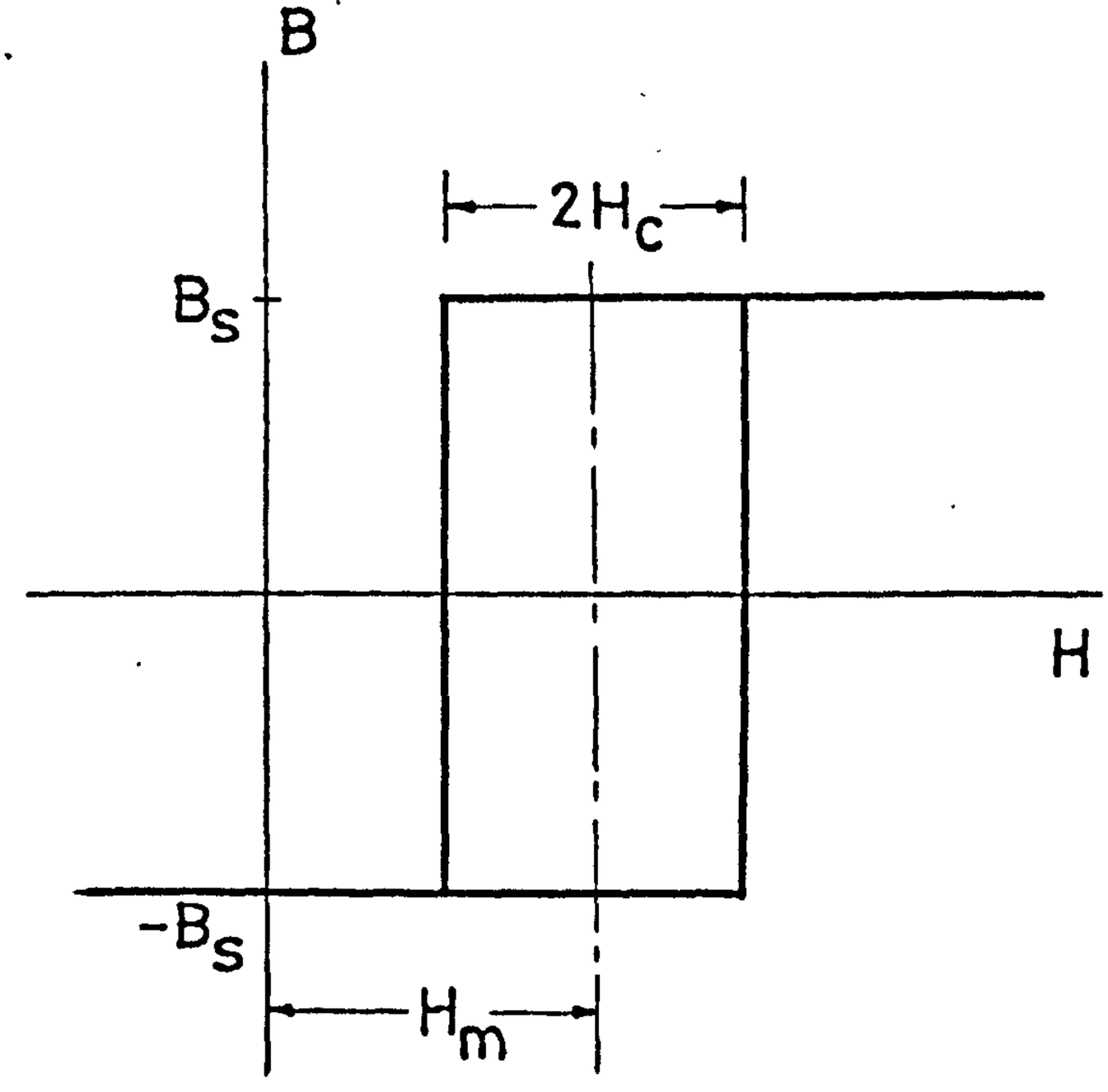

Fig. A4.1 B/H characteristic of elementary dipole.

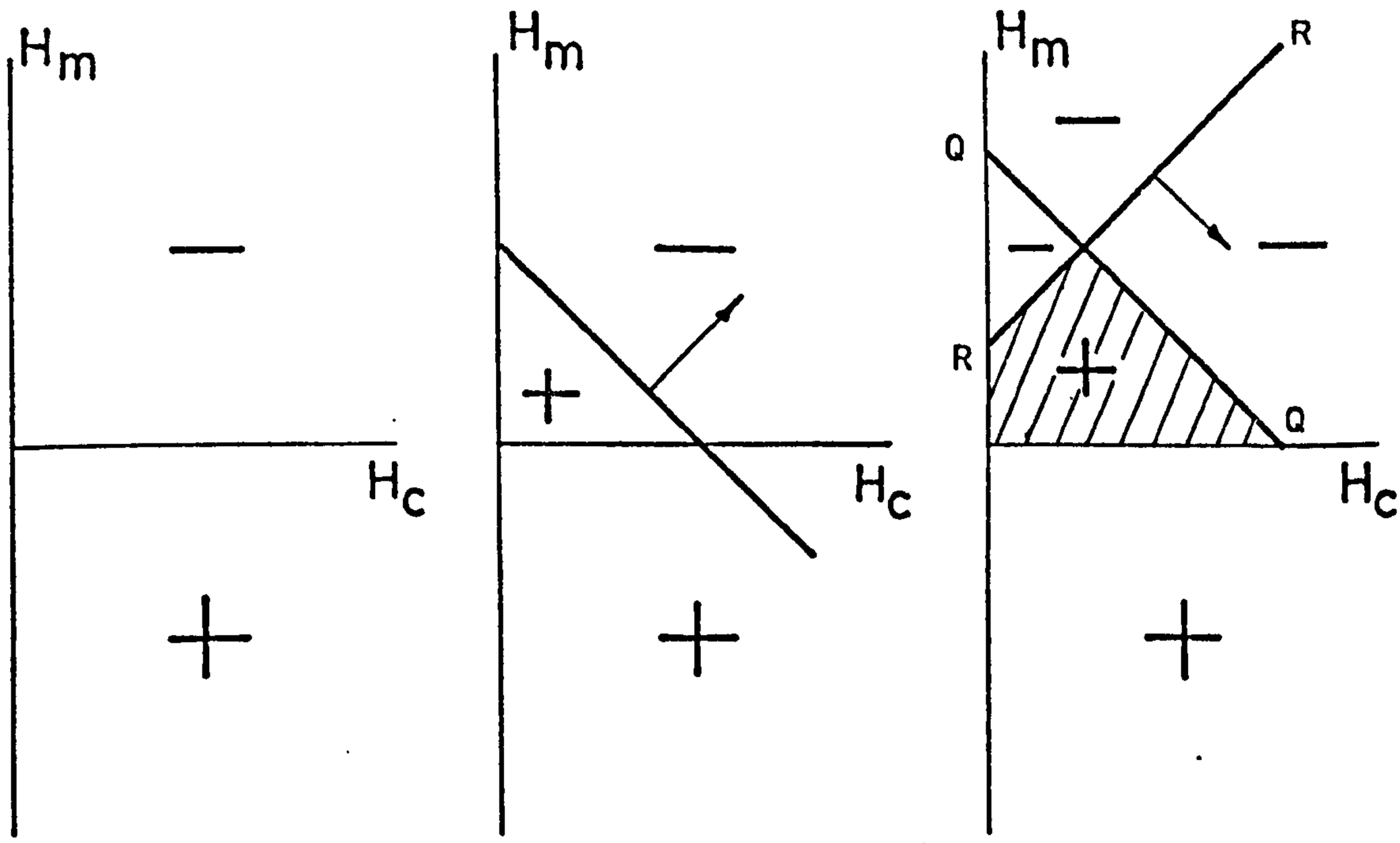

material magnetically neutral

applied field increasing

applied field reducing

Fig. A4.2 Switching of dipoles due to appied field.

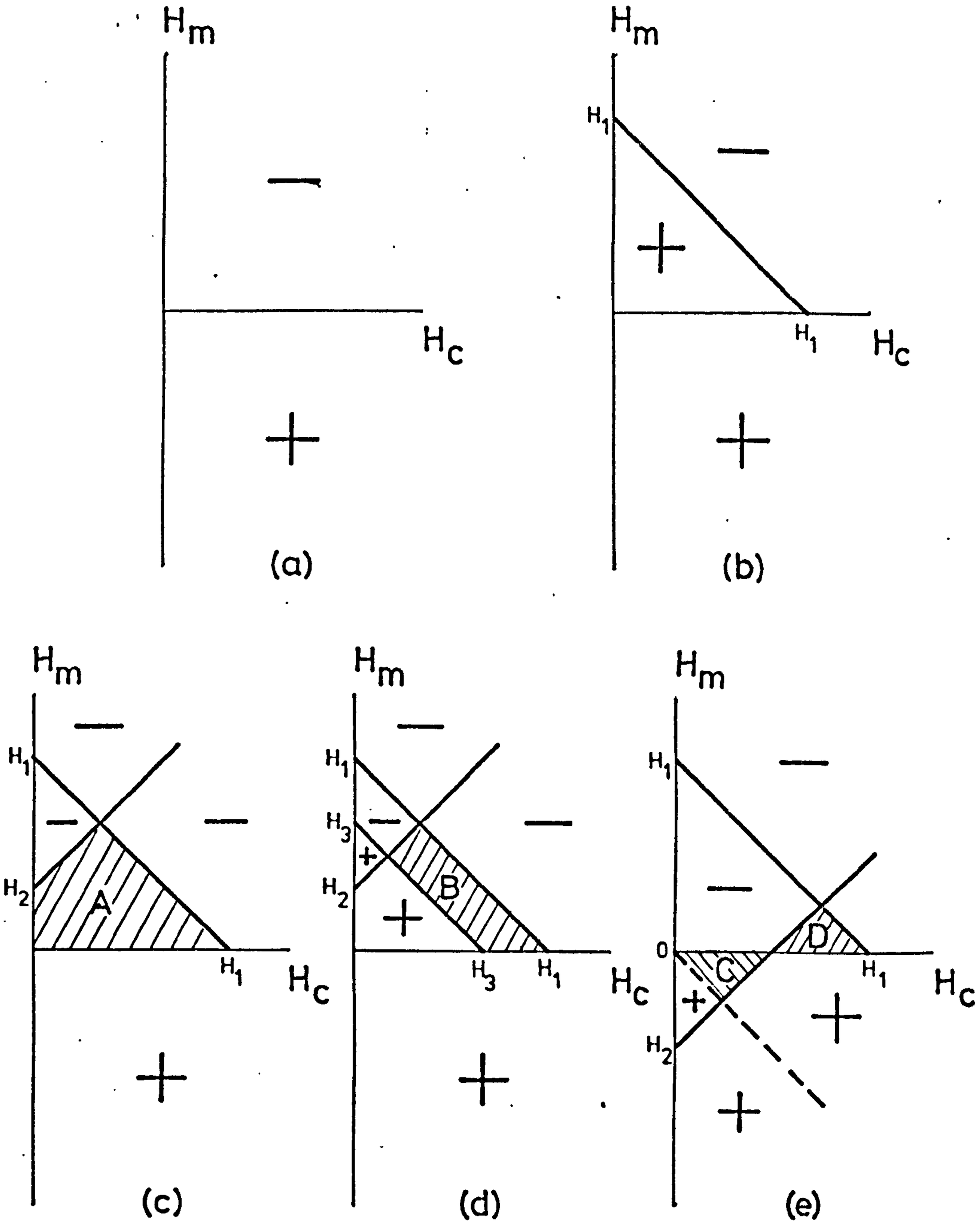

Fig. A4.3 H-plane criteria for the occurrence of cross-overs in the B/H plane.

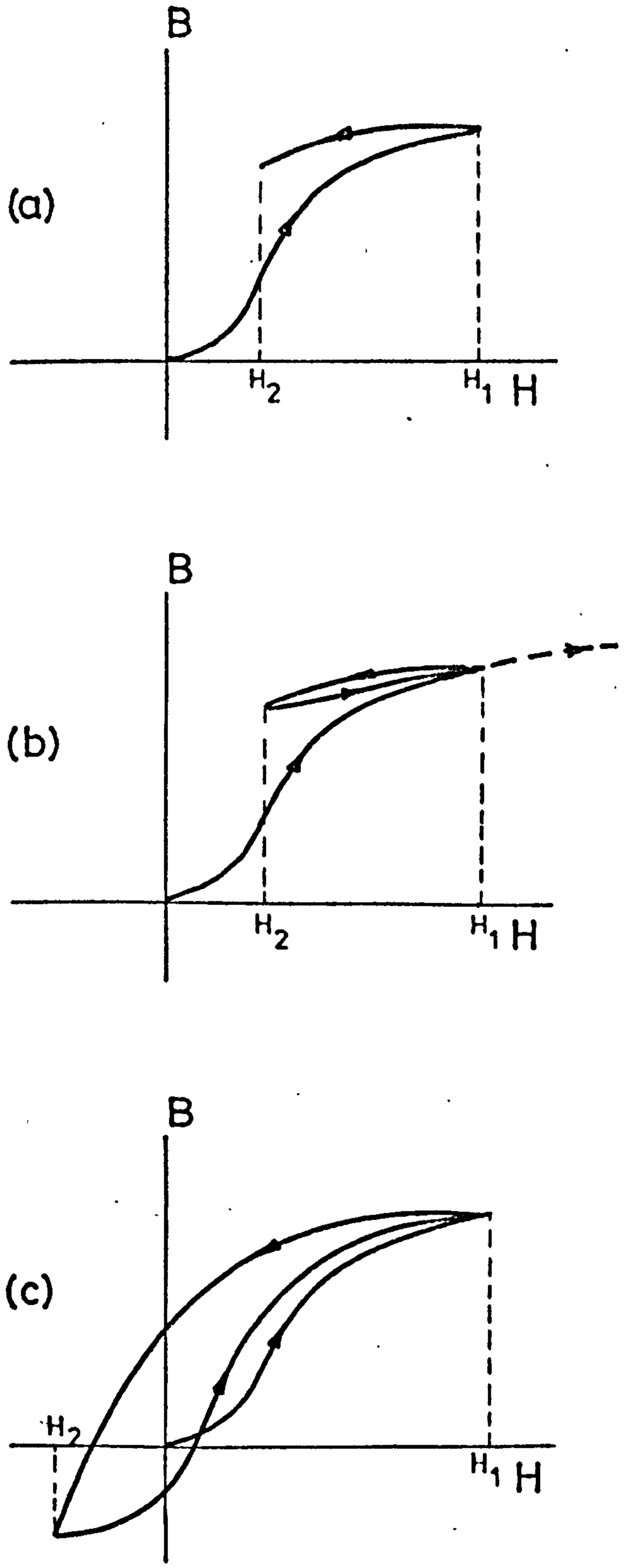

Fig. A4.4 Occurrence of cross-overs in the B/H plane

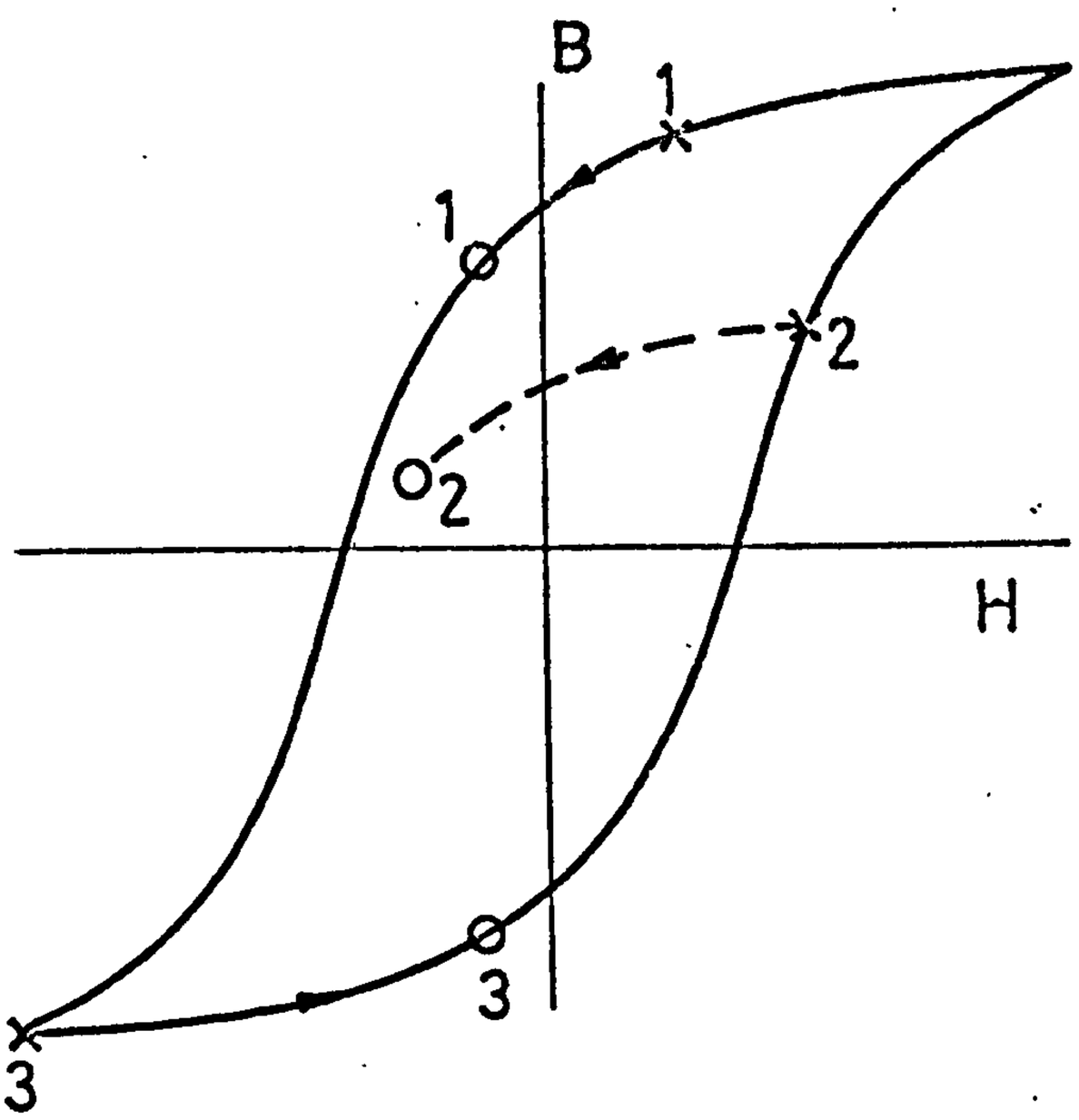

(a) Line Y disconnected first.

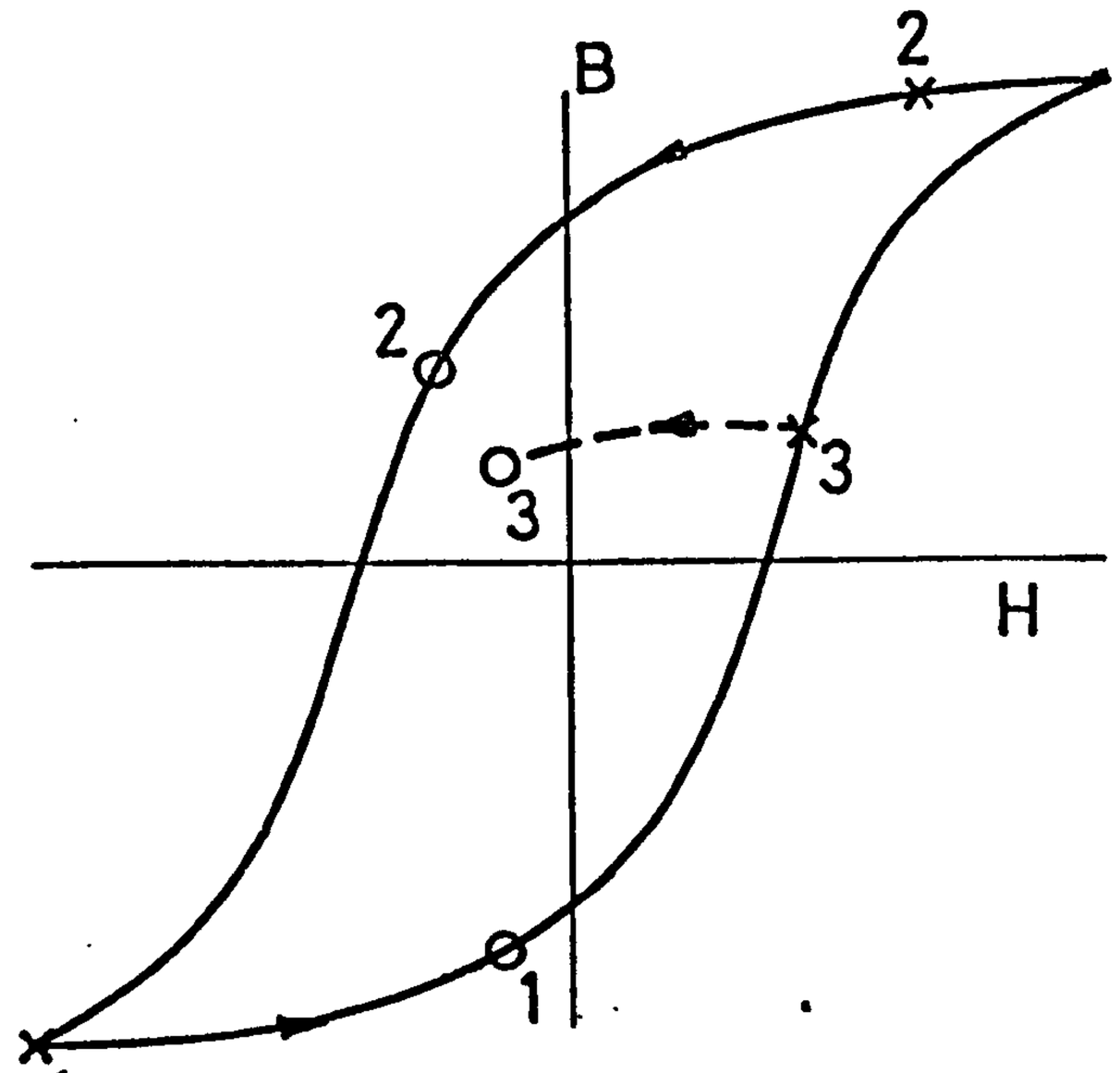

(b) Line Z disconnected first.

Fig. A5.1 Core conditions during disconnection of supply — delta connected primary, no load.

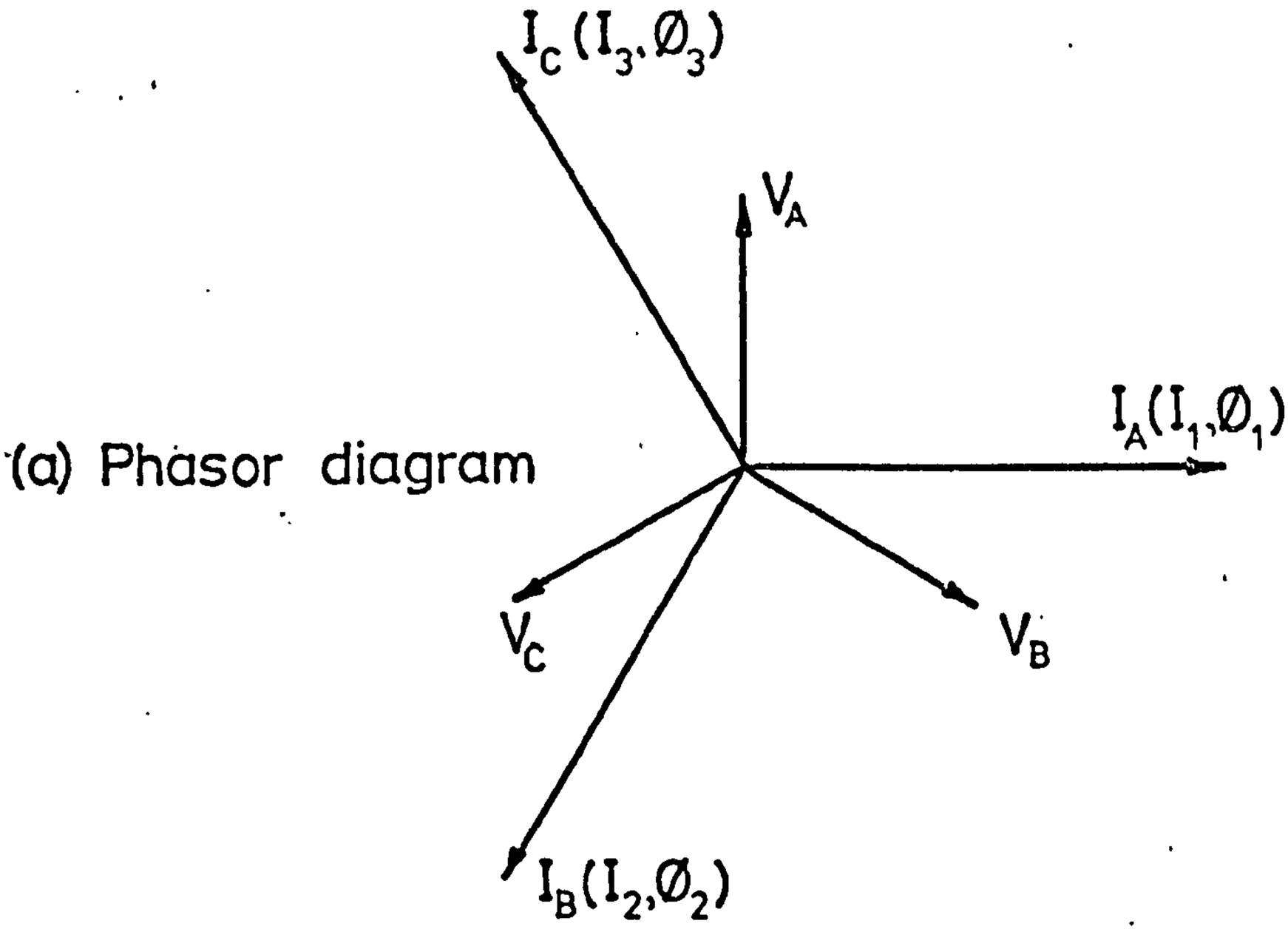

(a) Phasor diagram

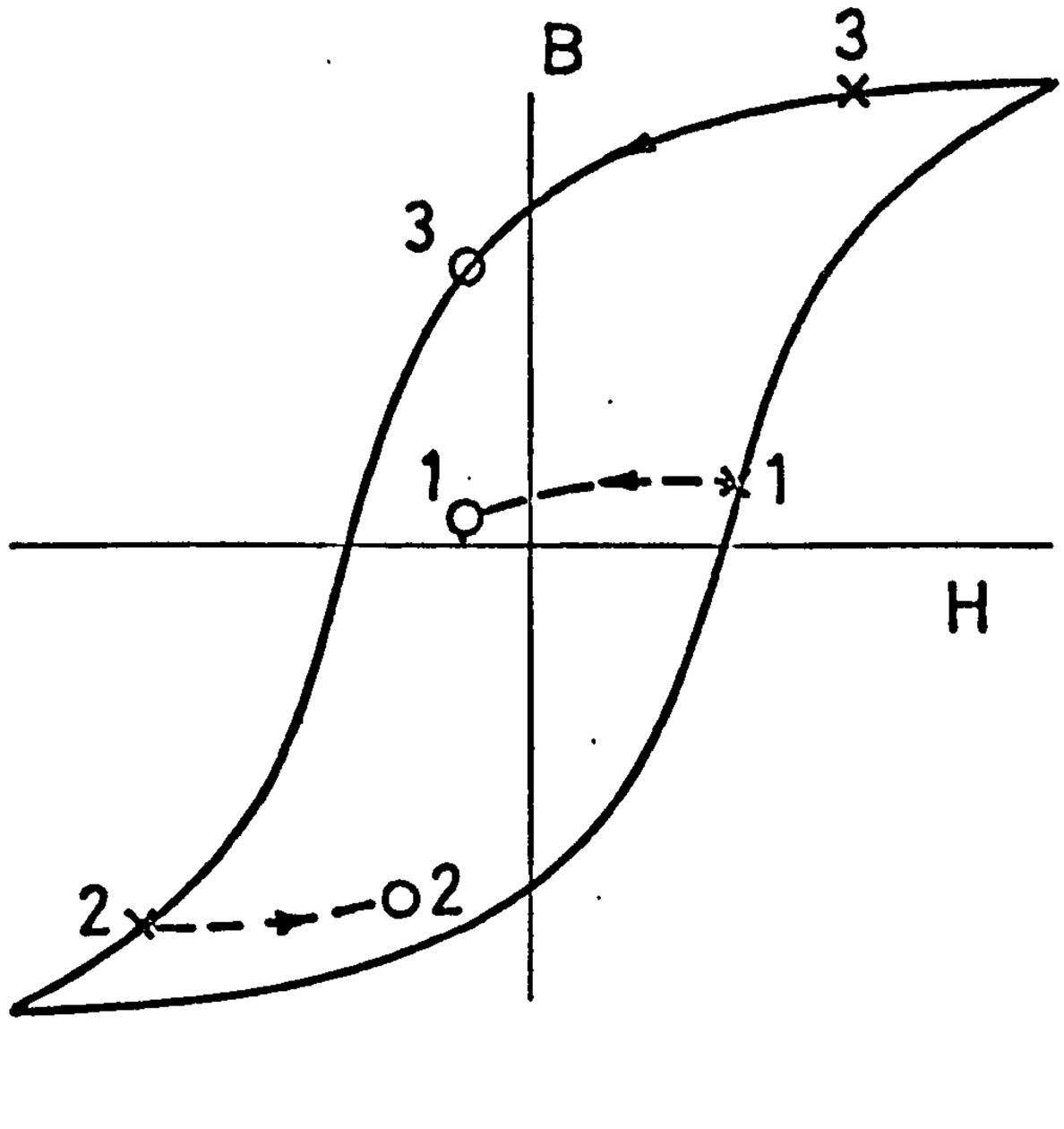

(b) Line A disconnected first.

Fig. A5.2 Disconnection of supply to 3-wire star connected primary, no load.

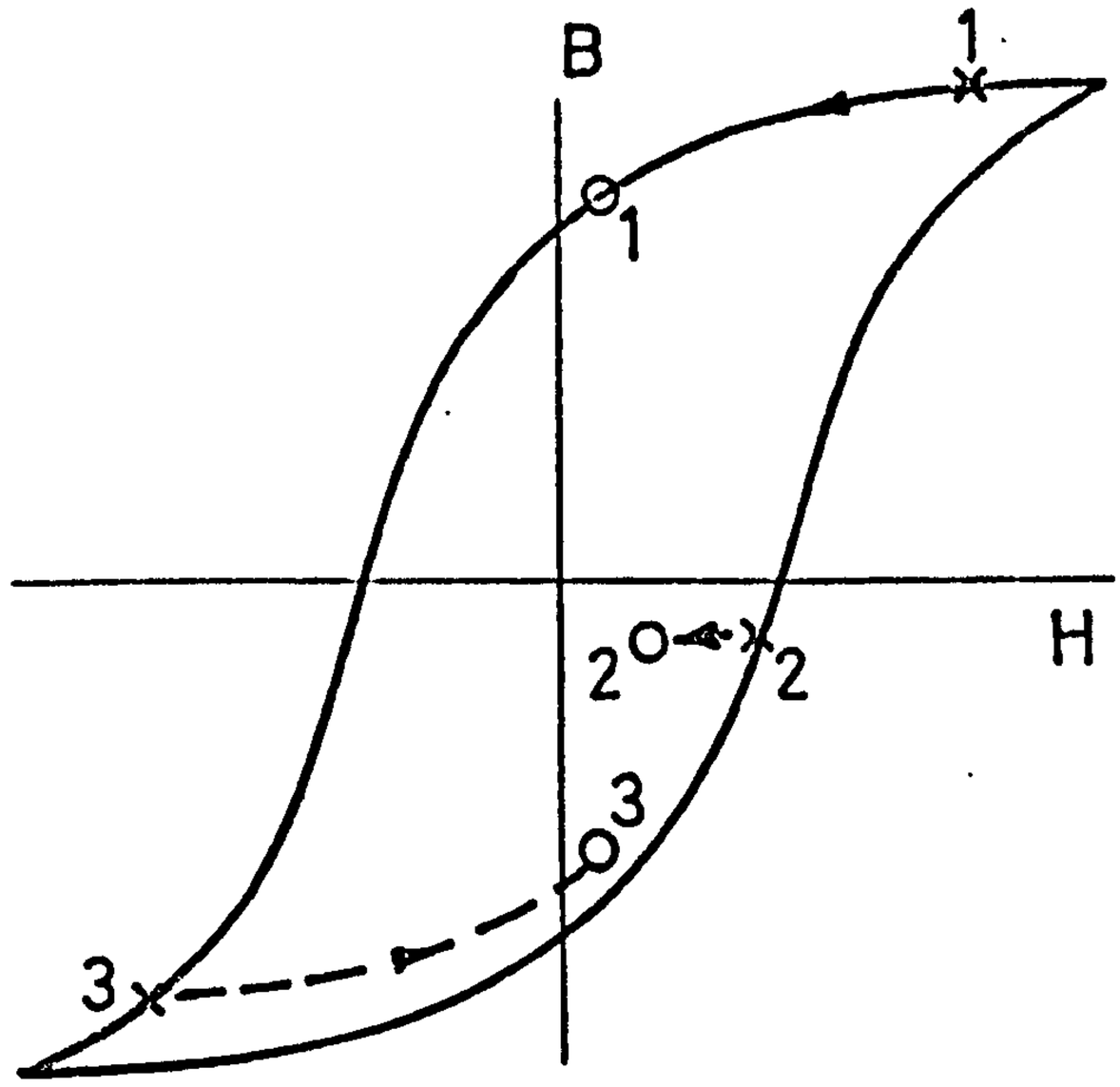

(a) Line B disconnected first.

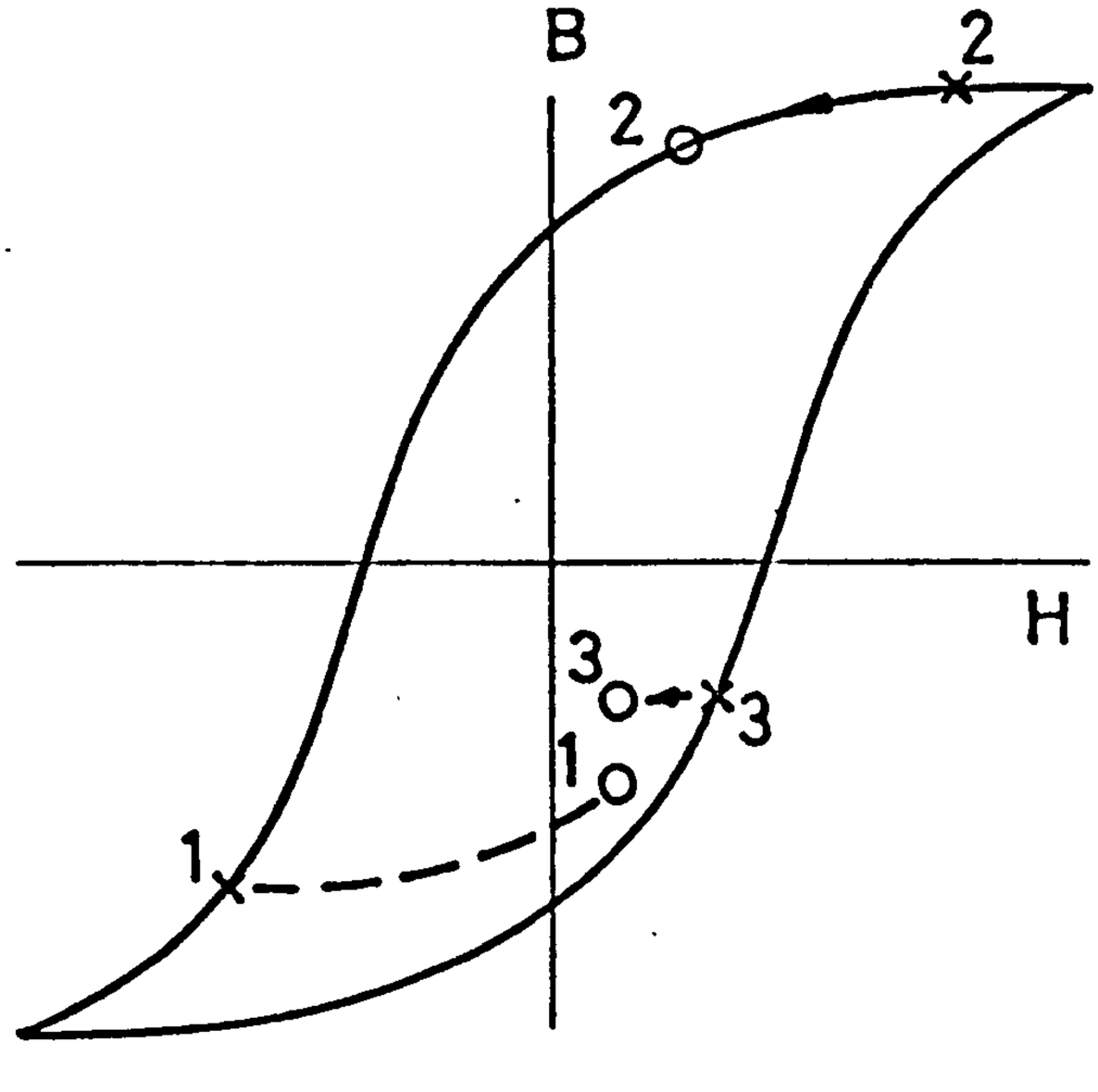

(b) Line C disconnected first.

Fig. A5.3 Disconnection of supply to 3-wire star connected primary, no load.

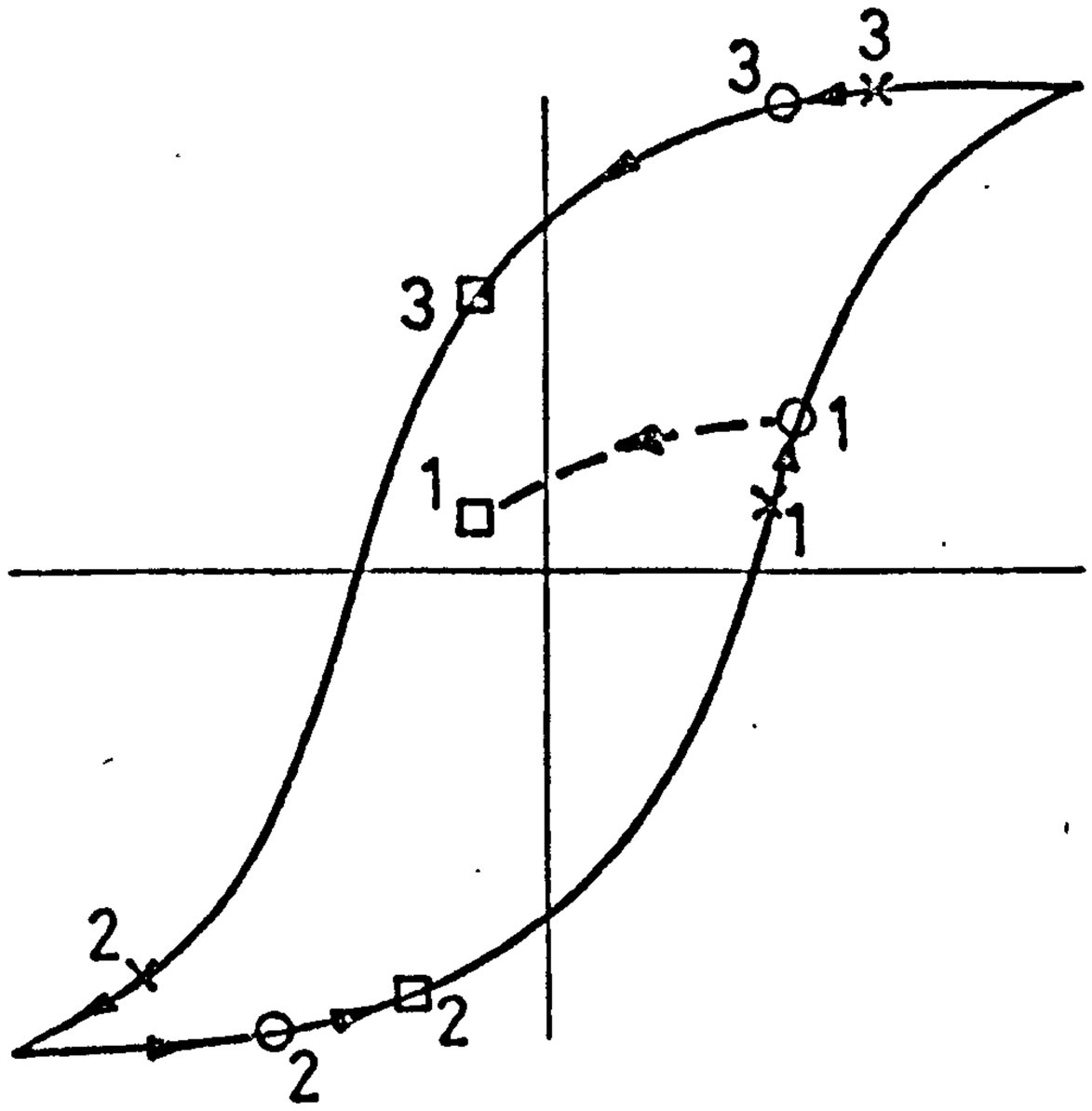

(a) Line A disconnected first.

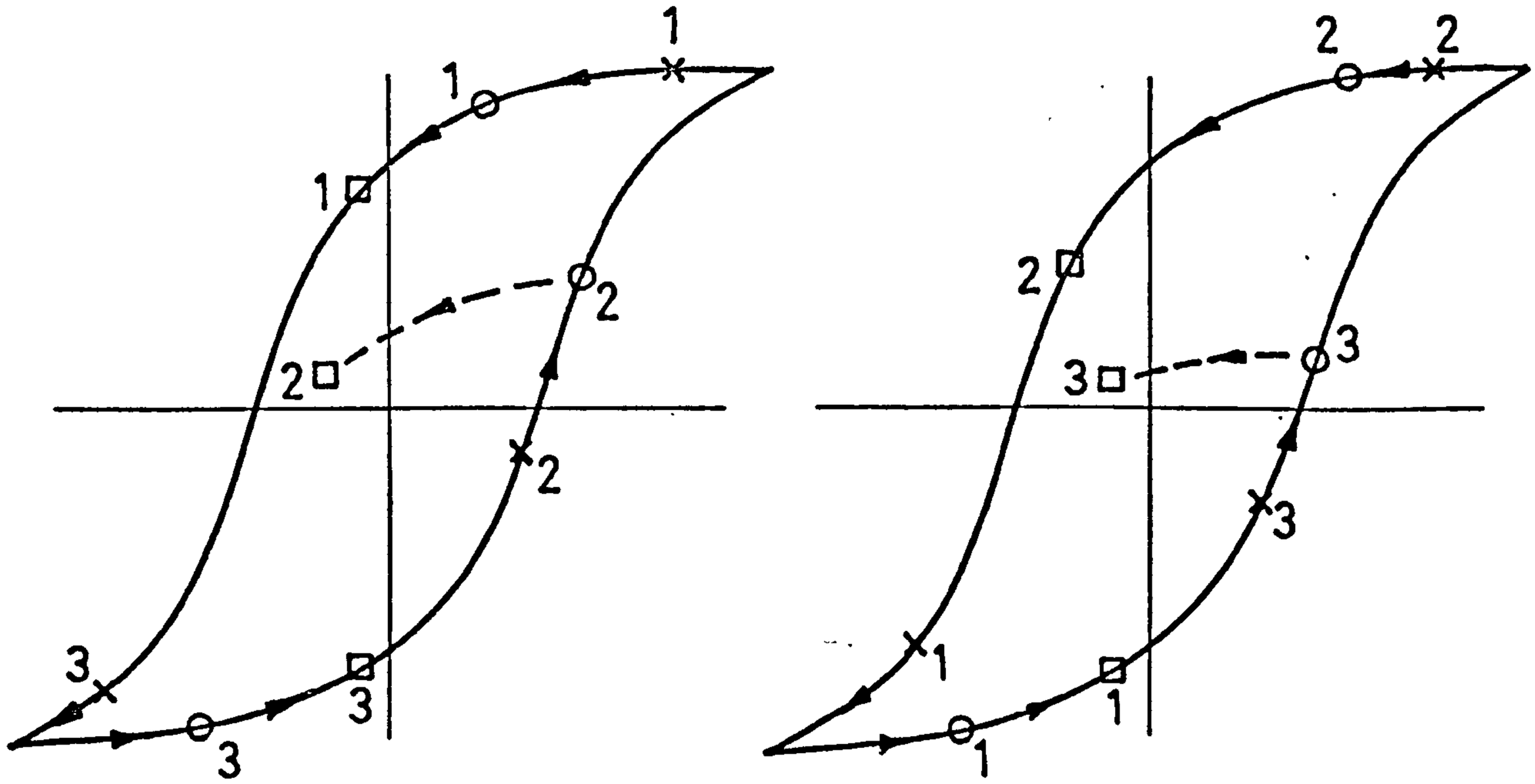

(b) Line B disconnected first. (c) Line C disconnected first.

Fig. A5.4 Core conditions during disconnection of supply — 4-wire star primary, no load.

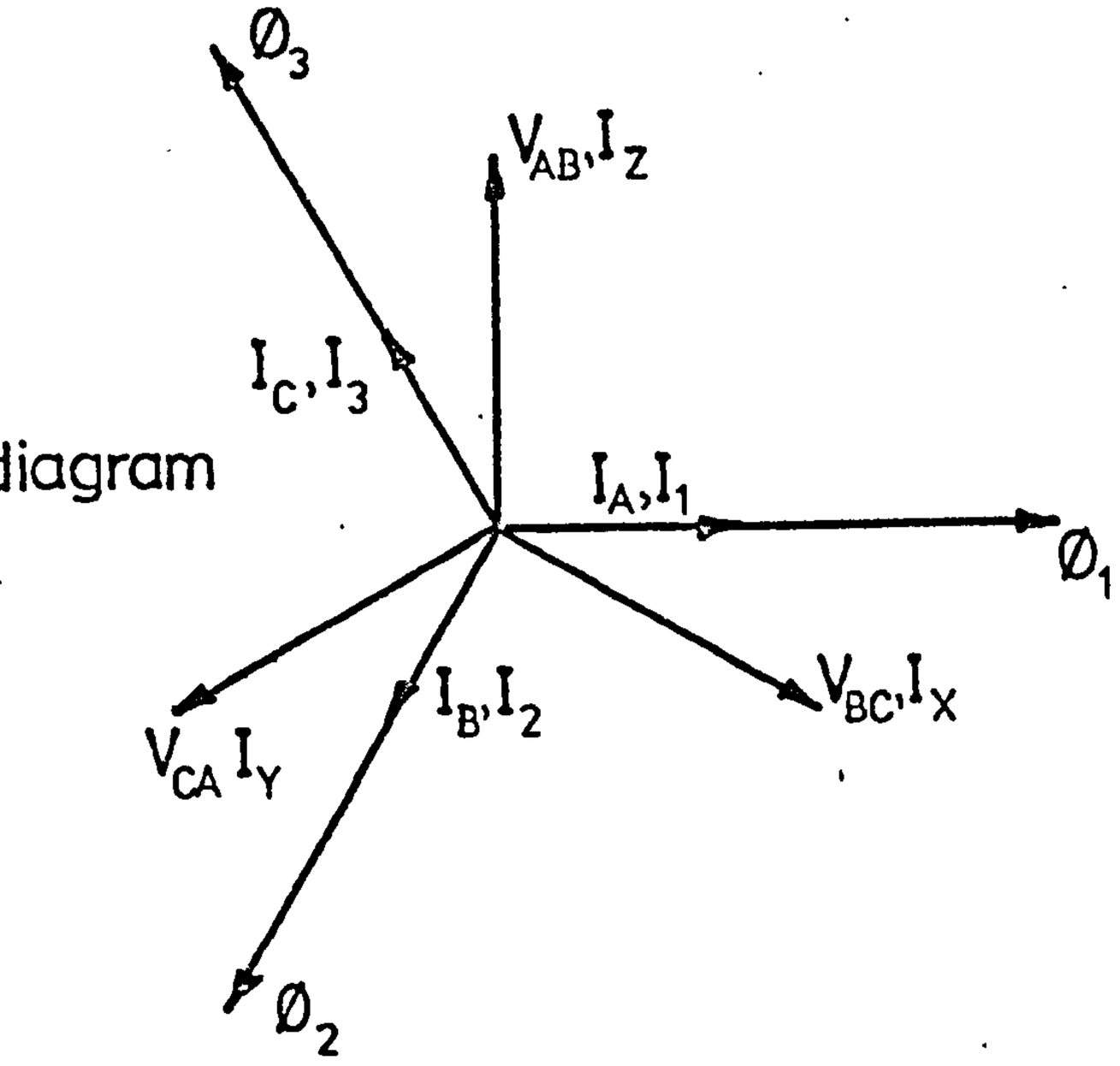

(a) Phasor diagram

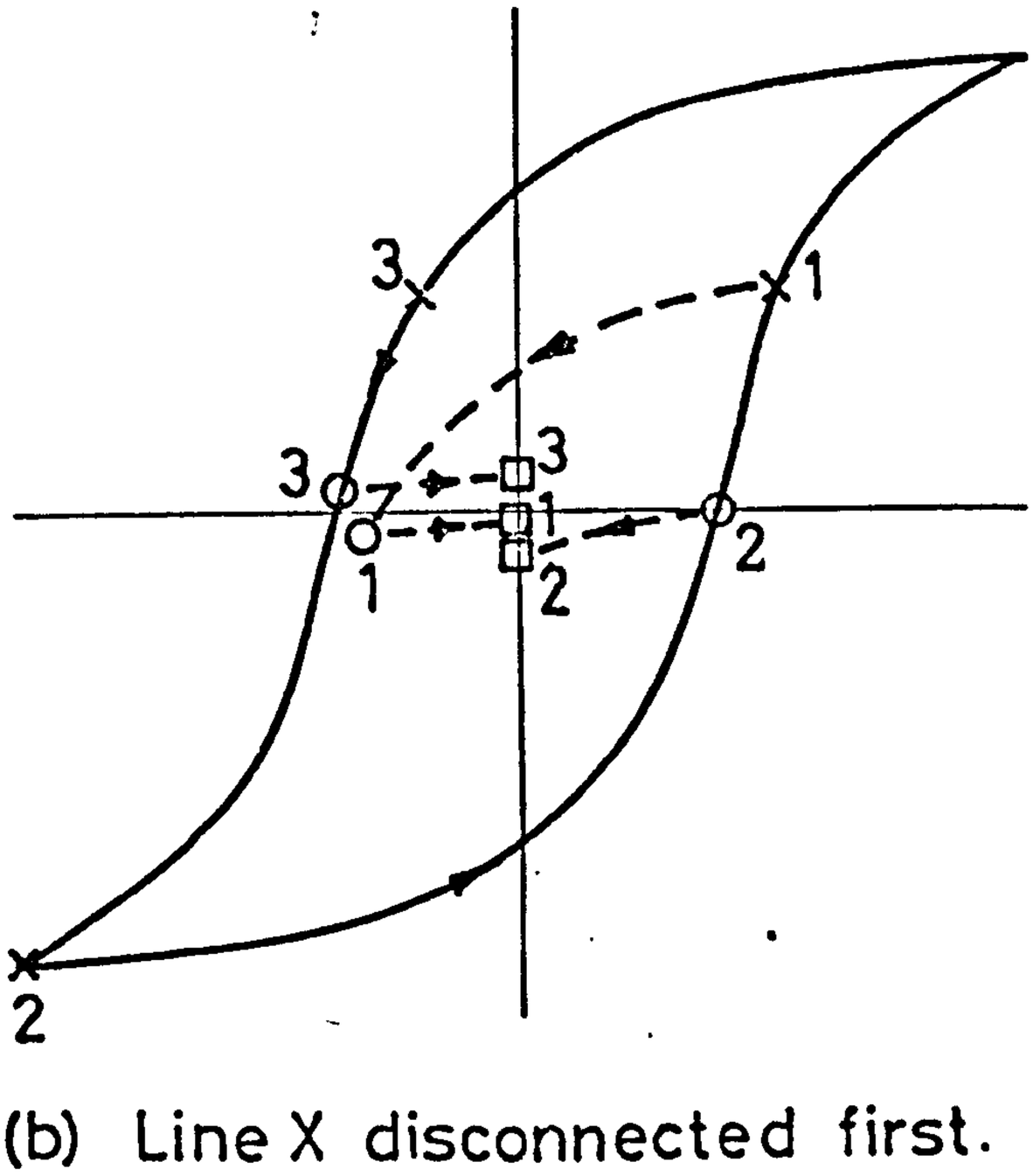

(b) Line X disconnected first.

Fig. A5.5 Disconnection of supply to delta connected primary — 4-wire star connected, zero p.f. inductive load.

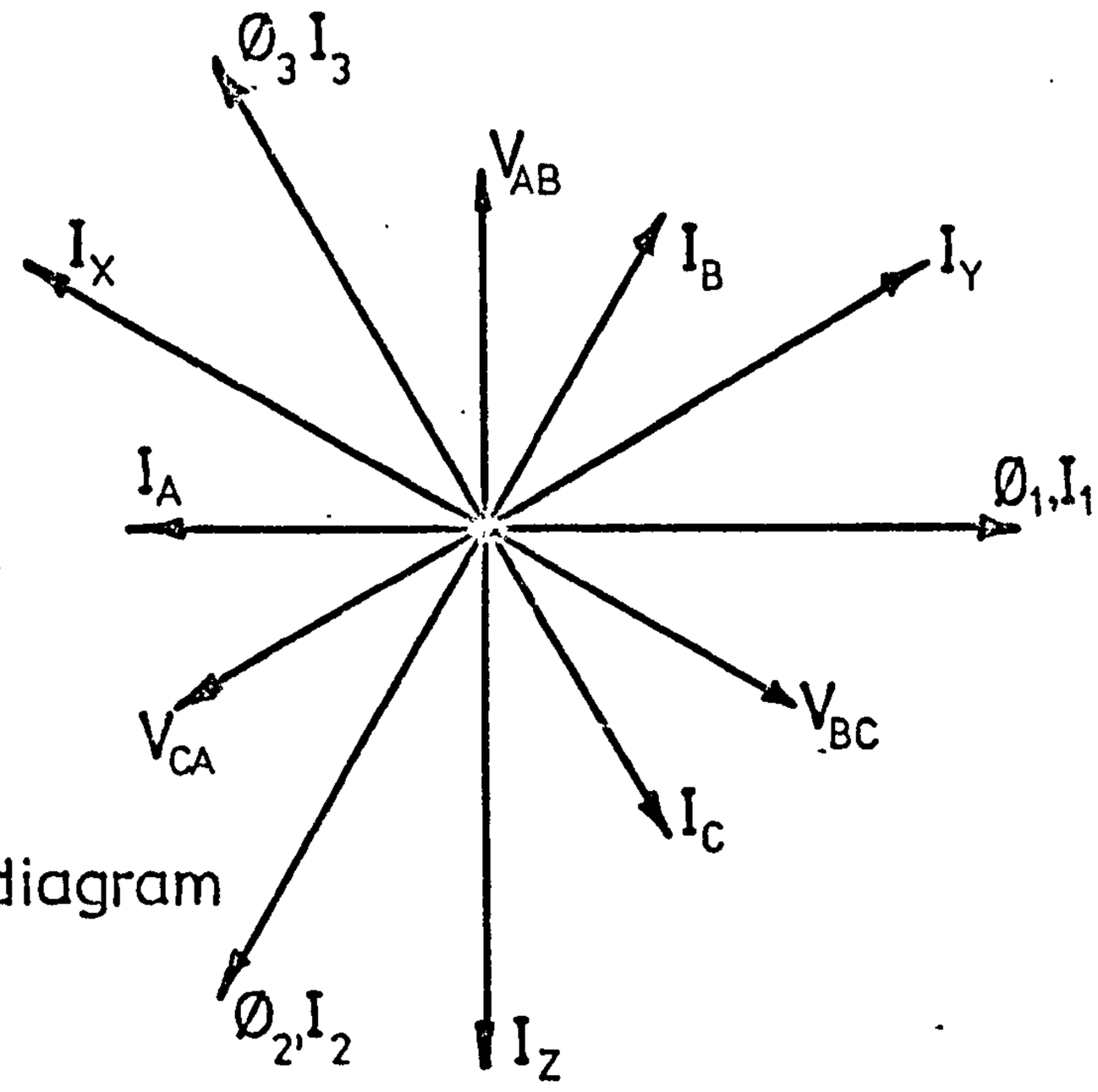

(a) Phasor diagram

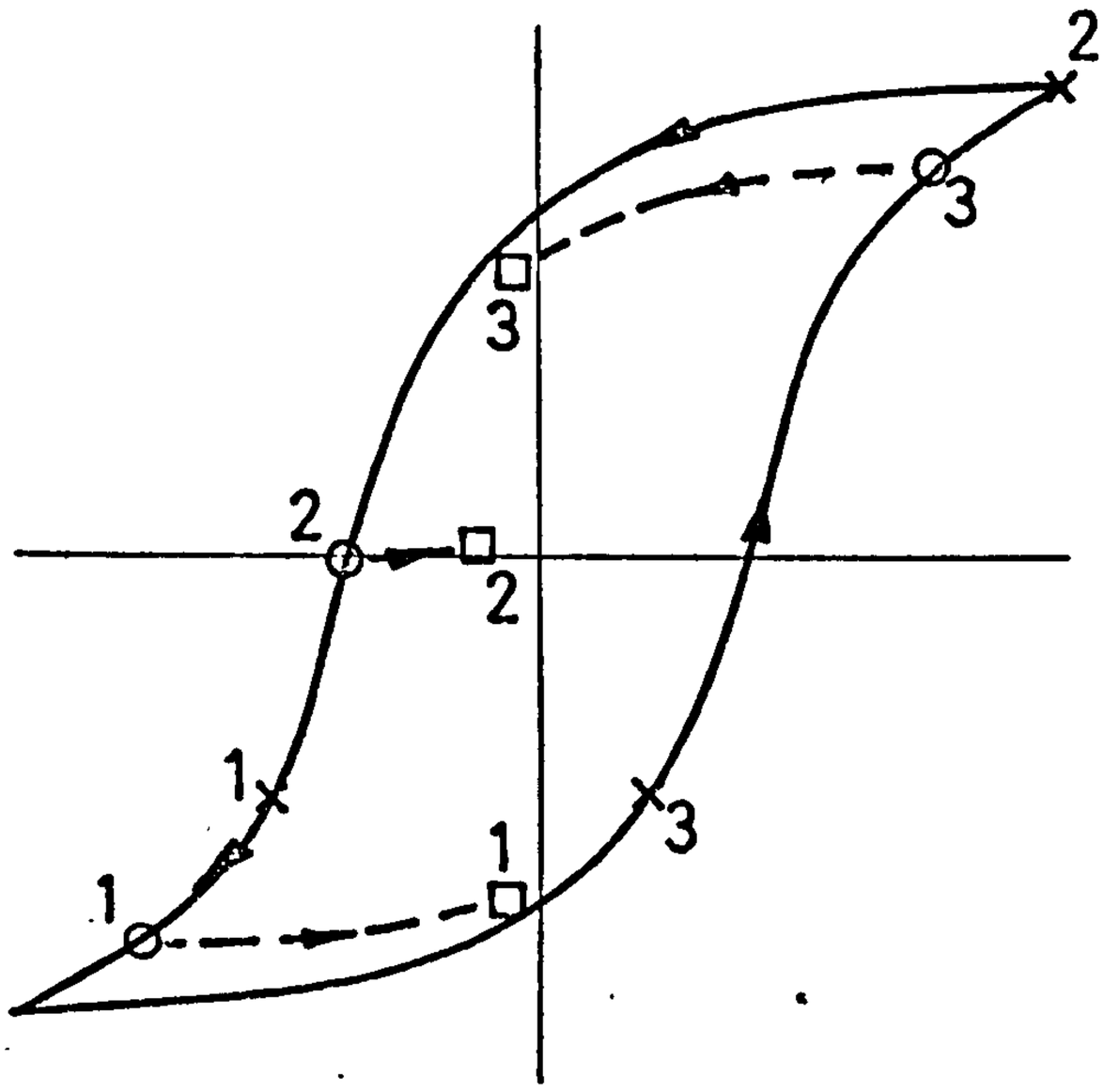

(b) Line X disconnected first.

Fig. A5.6 Disconnection of supply to delta connected primary — 4-wire star connected, zero p.f. capacitive load.